AN ABSTRACT OF THE DISSERTATION OF

Shaun A. Marcott for the degree of Doctor of Philosophy in Geology presented on April 22, 2011.

Title: Late Pleistocene and Holocene Glacier and Climate Change.

Abstract approved: _____

Peter U. Clark

This dissertation presents results from three studies that address major scientific questions in glacial geology and paleoclimatology for the late Pleistocene and Holocene using relatively new geochemical and statistical techniques. Each of the studies attempts to answer a longstanding question in the respective field using geochemical or statistical methods that have not been applied to the problem thus far.

A longstanding question in glaciology is the nature and mechanism of the so-called "Heinrich events" of the last ~60 ka. These massive iceberg discharge events into the North Atlantic from the partial breakup of the Laurentide Ice Sheet are identified from distinct ice rafted debris and detrital carbonate layers in marine sediment cores. The mechanism associated with the initiation of these events is commonly thought to be related to internal ice sheet instabilities. However, Heinrich events consistently occur following a long cooling trend that culminates in an extreme cold event, thus suggesting a possible triggering mechanism by climate. Recent modeling work has proposed an oceanic mechanism associated with ocean warming, but no physical evidence has been made available to date. To test this ocean-warming hypothesis, we measured temperature sensitive trace metals and stable isotopes in benthic foraminifera from a sediment core collected in the western North Atlantic that spans the last six Heinrich events and compared our results to climate model simulations using CCSM3. Our results show subsurface warming occurred prior to or coeval with nearly all of the Heinrich events of the last ~60 ka, thus implicating subsurface ocean warming as the main trigger of these rapid breakups of the Laurentide Ice Sheet.

In the field of glacial geology a longstanding question has been the timing of alpine glacial advances during the Holocene. A number of studies have interpreted several Holocene glacial advances in western North America, but age control is based largely on relative dating techniques, which have been shown to be in error by up to 10,000 yrs in some cases. Based on 124 ^{10}Be surface exposure ages from twenty cirque moraines in ten mountain ranges across western North America, glacier were retreating from moraine positions during the latest Pleistocene or earliest Holocene and not throughout the Holocene epoch as previously assumed, thus requiring a refined interpretation of Holocene glacial activity in western North America and the associated climate forcing.

In the field of paleoclimatology a question regarding how global temperature varied over the entirety of the Holocene epoch has remained to be answered for some time. While many temperature reconstructions exist for the last 2000 years, a full Holocene temperature stack does not exist, despite its potential utility of putting modern climate change into a full interglacial perspective. Based on a global composite of 73 proxy based temperature record, a Holocene temperature stack was constructed and used to demonstrate that a general cooling of ~1°C has occurred from the early to mid Holocene and that centennial and millennial scale variability is modest. We account for both temperature calibration and chronologic uncertainties using a Monte Carlo based approach. Our results are consistent with prior reconstructions of the last 2000 years and now allow for a full Holocene temperature perspective for evaluation with present and future climate change.

Late Pleistocene and Holocene Glacier and Climate Change

by

Shaun A. Marcott

A DISSERTATION

submitted to

Oregon State University

in partial fulfillment of

the requirements for the

degree of

Doctor of Philosophy

Presented April 22, 2011

Commencement June 2011

Doctor of Philosophy dissertation of Shaun A. Marcott presented April 22, 2011.

APPROVED:

Major Professor, representing Geology

Chair of the Department of Geosciences

Dean of the Graduate School

I understand that my dissertation will become part of the permanent collection of Oregon State University libraries. My signature below authorizes release of my dissertation to any reader upon request.

Shaun A. Marcott, Author

ACKNOWLEDGMENTS

No doctoral degree is accomplished alone. Ones dissertation is a collection of ideas and data that comprises an individuals thoughts and hard work, but it is always based on a foundation that was built by others. This dissertation is no exception and so I thank all of those who have helped in this accomplishment.

My advisor and mentor, Peter Clark, has guided me through my PhD. and provided me with enough room to progress on my own and enough foresight to help me along the path. I thank you Peter for taking me as student and for providing me the opportunity to be a part of your group at Oregon State. You have made my tenure here an enjoyable and fruitful experience, and you have been an excellent mentor. Any accomplishments I have or will achieve in the field of science will be because of the foundation that you help me build while working with you. I cannot express in a few typed words what that means to me. Peter, you have given me opportunity, knowledge, aspirations, an excellent education, and friendship. Thank you for the great experience.

Edward Brook provided valuable insight in the systematics of cosmogenic surface exposure dating and ^{10}Be extraction techniques. My laboratory abilities would be wanting had he never taken the time to instruct me and answer my never ending questions. It is a wonder that after spending the better part of 5 years pestering him, to what I can only imagine was near insanity, that he should want me now as a postdoctoral student. However, being keen to hone by laboratory skill set I have selfishly accepted his generous offer. Thank you Ed for our conversations and taking me in on the next phase of my research.

To my other committee members, Joseph Stoner and Steven Hostetler, I thank you for your time spent educating me on all things paleomagnetic and climate modeling. It is rare to have committee members who view their role as one of an additional advisor rather than as a simple title, or even worse a position that only affords them the opportunity to put an annoying student through an intellectual ringer

during their oral and written exams. I also thank Desiree Tullos who served early on as my graduate representative and Frank Chaplen who agreed on short notice to fill the vacant post.

To my other collaborators and teachers, I thank you for your patience and time. Alan Mix was particularly helpful in expanding my knowledge in the field of paleoceanography and statistics. I viewed nearly every minute spent with Alan as an education in something, be it science, history, science fiction, literature, or music. Future generations of students at Oregon State can only hope that Alan lives to 100 and never retires from education and academia. He is an excellent source of information that all students should tap when given the chance. Nicklas Pisias also broadened my understanding of statistics and applying it to questions in paleoclimatology. He was also generous enough to make his statistical codes available to me, for which I am grateful. Conversations with Gary Klinkhammer, Andy Ungerer, Andy Ross, and June Padman also broadened my knowledge of mass spectrometry, proper laboratory technique, and foraminifera identification. Gary was particularly kind in opening up his lab to me and sharing his Matlab code for trace metal analysis from the Haley-O-Matic. Laurence Padman, Anders Carlson, and Thom Davis, who I collaborated with on two of my three projects, shared their deep knowledge in their respective fields. Without them my papers would have lacked substance and not be what they are today. Anders was gracious enough in putting me up for two weeks at WHOI while he was finishing his postdoc. In another life, Anders was also my TA for glacial geology and because of both him and Peter I discovered my passion for glaciers, which I am forever indebted.

My friendships here at Oregon State made life both fulfilling and fun, despite my obstinate personality that could make things “challenging” at times. Thank you all for being part of my life and keeping things very entertaining. You were an excellent group of friends to know and I look forward to working with several of you in the future: Jay Alder, Faron Anslow, Thomas Bauska, Cody Beedlow, Anders Carlson, Jorie Clark, Bre Craig, Josh Cuzzone, Maureen Davies, Lica Ersek, Brent

Goehring, Jon Hornung, Anthony Novak, Summer Praetorius, Julia Rosen, and Sarah Strano.

Finally, I thank the members of my immediate and extended family. Jeremy Shakun started graduate school with me at the same time under Peter and we have become close friends, so close that both my wife and I consider him a part of our family. I was lucky to cross paths with Jeremy. He has taught me much about science and introduced me to a wide variety of subdiscplines in the field of paleoclimatology that I would have not otherwise cared or learned about. His deep understanding and love of his trade is contagious and he has been a catalyst for me. I have learned much from him, but probably the most important has been about life, family, friendship, and integrity. Thank you for the great time over the last five years. I look forward to many more.

My wife, Lennie, has been the most enduring person in my life. She knows me better than I know myself and has supported me throughout my PhD. and sacrificed a great deal of her time and life to my career. Knowing how difficult I can be, it confounds me why she has put up with all of this for so long, but here we are at the end. This degree is as much yours as it is mine.

To my parents and brother, I thank you for instilling in me your work ethic, an argumentative spirit, and the support early on in my life that helped me realize what I wanted from it and how I could attain it. Nearly all of the accomplishments in my life can be traced directly back to the three of you and Lennie. Thank you for being there for me. I never knew how fortunate I was until I left home.

CONTRIBUTIONS OF AUTHORS

Chapter 2 – P.U. Clark co-wrote the manuscript and conceived the project. L. Padman co-wrote the paper and, with S. Springer performed the ice-shelf model simulations. G.P. Klinkhammer performed the Mg/Ca data reduction. Z. Liu, B.L. Otto-Bliesner, F. He, and J. Chen performed the transient model simulations. A.E. Carlson contributed to data analysis and interpretation. A. Ungerer assisted with the Mg/Ca measurements. J. Padman assisted with the oxygen isotope analysis and foraminifera identification. A. Schmittner assisted with model design and implementation.

Chapter 3 – P.U. Clark co-wrote the manuscript, assisted with fieldwork, and helped with the project design. J.D. Shakun assisted with fieldwork and chemical procedures. E.J. Brook assisted with fieldwork and developed the chemical procedures. A.M. Novak assisted with fieldwork and chemical procedures. P.T. Davis assisted with fieldwork and the project design. M.W. Caffee oversaw the AMS procedures and measurements.

Chapter 4 – P.U. Clark co-wrote the manuscript. J.D. Shakun helped conceive the project and assisted with data analysis. A.C. Mix helped develop the statistical methods.

TABLE OF CONTENTS

TABLE OF CONTENTS (continued)

Page

TABLE OF CONTENTS (continued)

Page

TABLE OF CONTENTS (continued)

Page

LIST OF FIGURES

Figure Page

LIST OF FIGURES (continued)

Figure Page

LIST OF FIGURES (continued)

Figure Page

LIST OF FIGURES (continued)

Figure Page

LIST OF TABLES

Table Page

For my daughter, Leah.

May you find happiness and wonder throughout your life.

Somewhere, something incredible is waiting to be known.

Carl E. Sagan

Science is the belief in the ignorance of experts.

Richard P. Feynman

Late Pleistocene and Holocene Glacier and Climate Change

Chapter 1

Introduction

1.1 Forward

Nearly two hundred years have passed since Charles Lyell coined the phrase *"the present is the key to the past"* based on James Hutton's original work on Uniformitarianism from the 18th century. Today, geologists and oceanographers have turned Hutton's idea onto its head and are considering the importance of the past being the key to the present, and even to the future. Notably, a better understanding of the past global climate is a topic of intense interest as anthropogenic forcing of modern climate is pushing it toward a state not experience during modern civilization.

Understanding the climate of the past (paleoclimate) helps to put modern climate into a larger perspective and allows for evaluating natural climate change and climate change under an anthropogenic influence. Additionally, understanding climate of the past during different configurations of the planet and under different climate forcings has proven useful in understanding the sensitivity of climate change. This dissertation addresses three issues related to paleoclimate in an attempt to shed new light on the mechanism and timing of climate and glacier changes in the past.

1.2 Project Objectives

In Chapter 2, the interplay between climate, oceans, and ice sheets is explored and a hypothesis to answer a long-standing question in paleoclimatology and glaciology related to the mechanism of the so-called Heinrich events is put forward. These massive iceberg discharge events into the North Atlantic from the partial

breakup of the Laurentide Ice Sheet have long been thought to be related to internal ice sheet dynamics (MacAyeal, 1993), but their consistent occurrence during extreme cold events suggests that climate somehow plays a causal role (Clark et al., 2007). Using trace metal (Mg/Ca) and stable isotope ($\delta^{18}O$) measurements from benthic foraminifera, which have both shown to be good proxies for temperature, the timing of subsurface ocean conditions in the North Atlantic is determined and its relationship to Laurentide Ice Sheet explored using a sub ice shelf ocean model.

In Chapter 3, the timing of alpine glacial advances in western North America during the late Pleistocene and Holocene is reconstructed to provide insight into the spatial pattern of climate change in western North America. Several studies have interpreted multiple glacial advances occurring in western North America during the Holocene epoch (Burke and Birkeland, 1983; Davis, 1988), but the chronologies of these advances are based largely on relative dating techniques that have proven to be very unreliable (Clark and Gillespie, 1997; Licciardi et al., 2004). Because of the dearth of organic materials in glaciated terrains, radiocarbon dating has proven difficult to utilize. Using surface exposure dating of moraine boulders, which has proven to be a robust method for deriving glacial chronologies (Brook et al., 1993; Gosse et al., 1995; Licciardi, 2001; Licciardi et al., 2004), the timing of glacial advances is reevaluated across the western United States.

In Chapter 4, 73 globally distributed proxy based temperature records that span the Holocene are compiled and averaged together to evaluate the global and hemispheric climate changes of the last 10,000 years. While many temperature reconstructions exist for the last 2000 years (Esper et al., 2002; Moberg et al., 2005; Mann et al., 2008), a full Holocene temperature reconstruction does not exist despite the potential utility of such a record to put modern climate change into a full interglacial perspective. Using a Monte Carlo based technique, temperature and chronologic uncertainties are accounted for during the analysis to improve the robustness of the interpretations being made.

1.3 References

Brook, E. J., Kurz, M. D., Ackert, J. R. P., Denton, G. H., Brown, E. T., Raisbeck, G. M., and Yiou, F. (1993). Chronology of Taylor Glacier advances in Arena Valley, Antarctica, using *in situ* cosmogenic ^{3}He and ^{10}Be. *Quaternary Research* **39,** 11-23.

Burke, R. M., and Birkeland, P. W. (1983). Holocene Glaciation in the Mountain Ranges of the Western United States. *In* "Late Quaternary Environments of the United States." (H. E. Wright, Ed.), pp. 3-11. University of Minnesota Press, Minneapolis.

Clark, D. H., and Gillespie, A. R. (1997). Timing and significance of late-glacial and Holocene cirque glaciation in the Sierra Nevada, California. *Quaternary International* **38/39,** 21-38.

Clark, P. U., Hostetler, S. W., Pisias, N. G., Schmittner, A., and Meissner, K. J. (2007). Mechanisms for an ~7-kyrs climate and sea-level oscillation during Marine Isotope Stage 3. *In* "Ocean Circulation: Mechanisms and Impacts " (A. Schmittner, J. C. H. Chiang, and S. R. Hemming, Eds.), pp. 392. American Geophysical Union, Washington, DC.

Davis, P. T. (1988). Holocene Glacier Fluctuations in the American Cordillera. *Quaternary Science Reviews* **7,** 129-157.

Gosse, J. C., Evenson, E. B., Klein, J., Lawn, B., and Middleton, R. (1995). Precise cosmogenic ^{10}Be measurements in western North America: Support for a global Younger Dryas cooling event. *Geology* **23,** 877-880.

Licciardi, J. M. (2001). Chronology of latest Pleistocene lake-level fluctuations in the pluvial Lake Chewaucan basin, Oregon, USA. *Journal of Quaternary Science* **16,** 545-553.

Licciardi, J. M., Clark, P. U., Brook, E. J., Elmore, D., and Sharma, P. (2004). Variable responses of western U.S. glaciers during the last deglaciation. *Geology* **32,** 81-84.

MacAyeal, D. R. (1993). Binge/purge oscillations of the Laurentide ice sheet as a cause of the North Atlantic's Heinrich events. *Paleoceanography* **8, No. 6,** 775-784.

Chapter 2

Ice-shelf collapse from subsurface warming as a trigger for Heinrich events

Shaun A. Marcott [1], Peter U. Clark [1], Laurie Padman [2], Gary P. Klinkhammer [3], Scott Springer [4], Zhengyu Liu [5], Bette L. Otto-Bliesner [6], Anders E. Carlson [5,7], Andy Ungerer [3], June Padman [3], Feng He [5], Jun Cheng [5], and Andreas Schmittner [3]

[1]Department of Geosciences, Oregon State University, Corvallis, OR 97331, USA

[2]Earth & Space Research, 3350 SW Cascade Ave., Corvallis, OR 97333, USA

[3]College of Oceanic and Atmospheric Sciences, Oregon State University, Corvallis, OR 97331, USA

[4]Earth & Space Research, 2101 Fourth Ave., Suite 1310, Seattle WA 98121, USA

[5]Center for Climatic Research and Department of Atmospheric and Oceanic Sciences, University of Wisconsin, Madison, WI 53706, USA

[6]Climate and Global Dynamics Division, National Center for Atmospheric Research, Boulder, CO 80307, USA

[7]Department of Geoscience, University of Wisconsin, Madison, WI 53706, USA

[8]Key Laboratory of Meteorological Disaster, Nanjing University of Information Science and Technology, Nanjing, 210044, China

Submitted to the Proceedings of the National Academy of Sciences

2.1 Abstract

Episodic iceberg-discharge events from the Hudson Strait Ice Stream (HSIS) of the Laurentide Ice Sheet, referred to as Heinrich events, are commonly attributed to internal ice-sheet instabilities, but their systematic occurrence at the culmination of a large reduction in the Atlantic meridional overturning circulation (AMOC) indicates a climate control. We report Mg/Ca data on benthic foraminifera from an intermediate-depth site in the northwest Atlantic and results from a climate-model simulation that reveal basin-wide subsurface warming at the same time as large reductions in the AMOC, with temperature increasing by ~2°C over a 1-2 kyr interval prior to a Heinrich event. In simulations with an ocean model coupled to a thermodynamically active ice shelf, the increase in subsurface temperature increases basal melt rate under an ice shelf fronting the HSIS by a factor of ~6. By analogy with recent observations in Antarctica, the resulting ice-shelf loss and attendant HSIS acceleration would produce a Heinrich event.

2.2 Introduction

Heinrich events represent the episodic discharge of icebergs from the Hudson Strait Ice Stream (HSIS) of the Laurentide Ice Sheet to the North Atlantic Ocean during late-Pleistocene glaciations (Heinrich, 1988). Although commonly attributed to internal ice-sheet instabilities (MacAyeal, 1993), their occurrence at the culmination of a large reduction in the Atlantic meridional ocean circulation (AMOC) suggests a possible trigger by climate (Zahn et al., 1997; Clark et al., 2007). Models suggest that ocean responses to an AMOC reduction might destabilize the HSIS grounding line and trigger Heinrich events either through dynamic and steric sea-level rise or warming of intermediate-depth (hereafter subsurface) waters causing destabilization of ice shelves and attendant HSIS surging (Shaffer et al., 2004; Clark et al., 2007; Alvarez-Solas et al., 2010). Grounding lines, however, are thought to be stable to the decimeter-scale sea-level rise associated with a reduced AMOC (Alley et

al., 2007a). Moreover, evidence for subsurface warming remains widely debated (Dokken and Jansen, 1999; Rasmussen et al., 2003; Meland et al., 2008), and the relationship between ocean temperature and total ice-shelf mass loss from basal melting is sensitive to the geometry and ocean setting of the specific ice shelf being considered (Holland and Jenkins, 1999).

Our study is based on core EW9302-2JPC (1251 m, 4847.70'N, 45°05.09'W) which, according to climate model simulations, is at a depth and latitude that is ideal for monitoring subsurface warming associated with a reduction in the AMOC (Figure 2.1) (Liu et al., 2009). Previous work on this core identified ice-rafted detrital carbonate layers that represent Heinrich events (Figure 2.2 a), with associated changes in benthic faunas and the $\delta^{18}O$ of their carbonate tests that suggested intrusions of a relatively warm water mass coincident with the events (Rasmussen et al., 2003). However, because the temperature transfer function for the benthic faunas is unknown, and ice-volume and hydrographic changes can mask the temperature signal in the $\delta^{18}O$ of calcite, the inferred temperature changes remain poorly constrained.

To further evaluate variability in bottom water temperature (BWT) at this site, we measured Mg/Ca in benthic foraminiferal calcite associated with the four Heinrich events (H1, H3, H5a, H6) for which sufficient numbers of foraminifera existed in this core. Considering analytical and calibration uncertainties, we calculate an error of 1.3°C for our Mg/Ca-derived BWT reconstructions. Recent work suggests that the CO_3^{2-} ion may also affect Mg/Ca in some benthic foraminifera at temperatures below ~3°C, where the carbonate ion saturation ($\Delta[CO_3^{2-}]$) decreases rapidly with temperature, and at low saturation levels (Elderfield et al., 2006). We used CO2SYS (Lewis and Wallace, 1998) to calculate modern $\Delta[CO_3^{2-}]$ at our site based on values of temperature, pressure, salinity, total alkalinity, total CO_2, phosphate, and silicate retrieved from the WOCE database (WOCE, 2002). The corresponding value (~55 mol/kg) suggests that the site is very weakly affected by the $[CO_3^{2-}]$ effect today (Elderfield et al., 2006). During the last glacial period, the deep Atlantic Ocean was

less saturated in [CO_3^{2-}], decreasing by ~20 μmol/kg due to the intrusion of cold, undersaturated Antarctic Bottom Water (Yu et al., 2008). At intermediate-water depths (1-2 km) such as for our site, however, the glacial North Atlantic was ~20-30 μmol/kg higher in [CO_3^{2-}] than present and Holocene values (Yu et al., 2008), suggesting that our measured Mg/Ca values were not influenced by past Δ[CO_3^{2-}].

2.3 Results

Two independent temperature proxies support our Mg/Ca-derived BWTs. First, our reconstructed BWT at ~19 ka of 0 ± 1.3°C agrees at 1σ with a Last Glacial Maximum temperature of -1.2 ± 0.2°C reconstructed from pore fluids at site 981 on the Feni Drift (2184 m; 55°29'N, 14°39'W) (Adkins et al., 2002). Second, the amplitude and structure of the BWT change during the last deglaciation is in excellent agreement with the temperature change derived from the ice-volume corrected $\delta^{18}O$ ($\delta^{18}O_{IVC}$) measured on benthic fauna from this core assuming a temperature-dependent fractionation of 0.25‰ $°C^{-1}$ for calcite (O'Neil et al., 1969) (Figure 2.2 b) (Appendix A).

The Mg/Ca data from EW9302-2JPC identify several systematic BWT changes that occurred in association with each of the four Heinrich IRD layers for which we have sufficient data (Figure 2.2 b). (1) Temperatures gradually increased prior to the start of each Heinrich layer, with the start of the warming beginning ~1-2 kyr before each Heinrich event on our timescale. This early warming is replicated by the $\delta^{18}O_{IVC}$ (temperature) record associated with H1. (2) The warming trend prior to each Heinrich layer is consistently associated with a temperature oscillation of 3-4°C. (3) Each temperature oscillation occurs around a mean value that is close to the present BWT of ~3.4°C and reaches a maximum BWT of 5-7°C during the Heinrich layer.

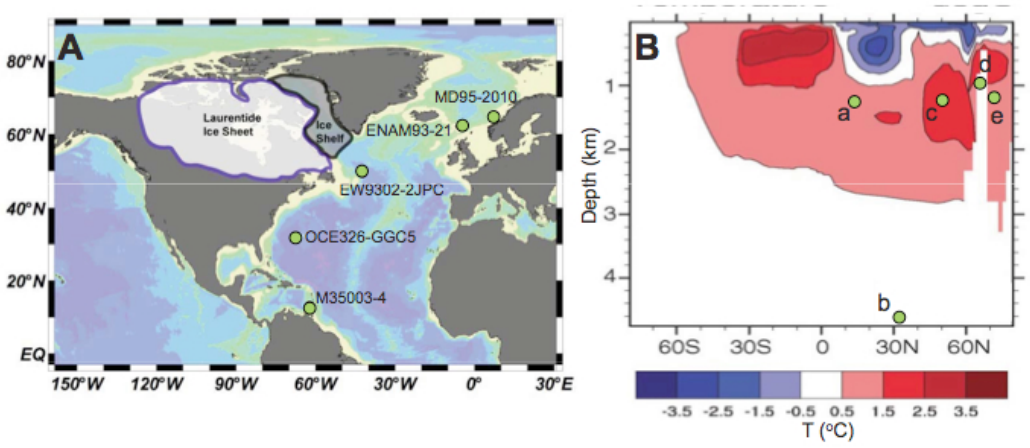

Figure 2.1. Location map of core sites.

(A) Location of core sites with records discussed in text (green dots). Also shown is extent of ice shelf derived from the Hudson Strait Ice Stream as reconstructed in (Hulbe, 1997). (B) Zonal mean temperature anomaly (T °C) in the Atlantic basin for a strongly reduced (~4 Sv) versus active (~13 Sv) AMOC (Liu et al., 2009). Location of core sites also shown: site a is core M35003-4, site b is core OCE326-GGC5, site c is core EW9302-2JPC, site d is core ENAM93-21, and site e is core MD95-2010.

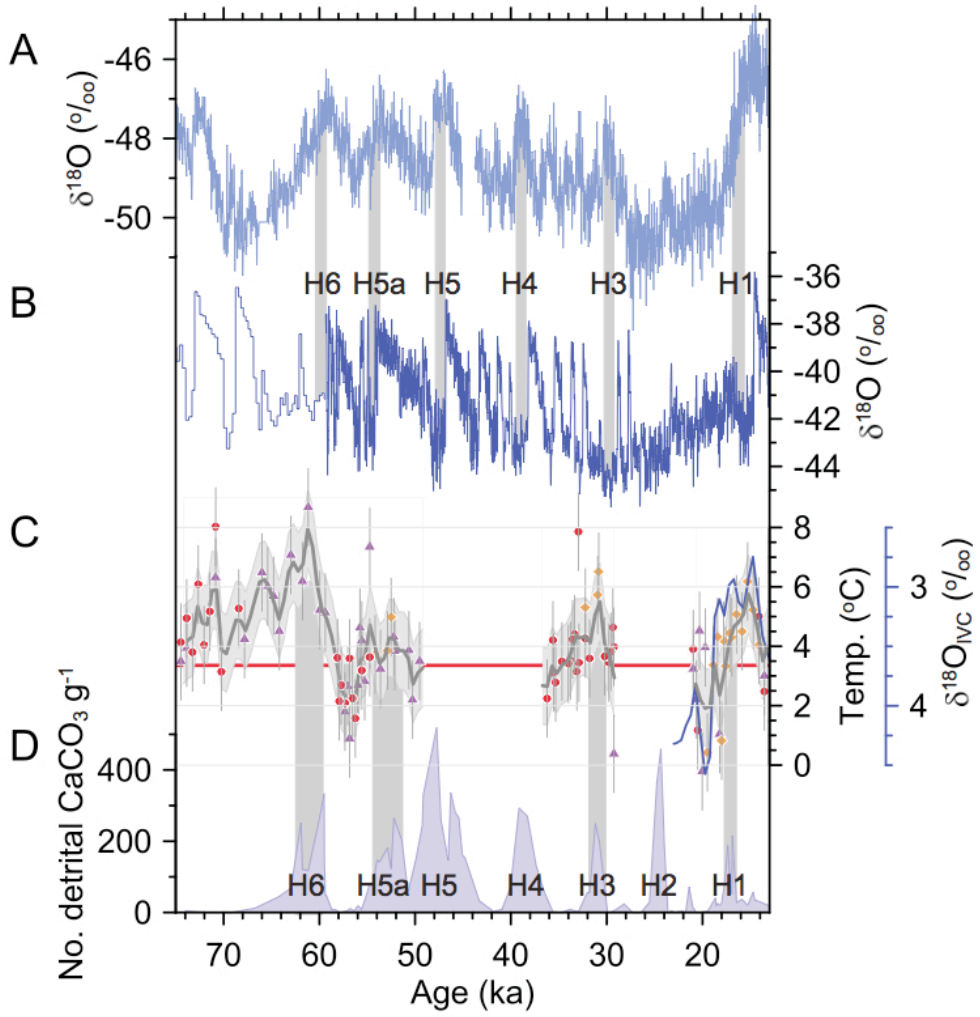

Figure 2.2. Bottom water temperatures and paleoclimate reconstructions. (A) $\delta^{18}O$ record from Antarctic EDML ice core (Jouzel et al., 2007b) on revised age model (Lemieux-Dudon et al., 2010). (B) $\delta^{18}O$ record from Greenland NGRIP ice core(NGRIPmembers, 2004) on revised age model (Lemieux-Dudon et al., 2010) (<60 ka) and from GISP2 ice core (>60 ka) on published age model (Meese, 1997). (C) Mg/Ca-derived bottom water temperatures for core EW9302-2JPC (1251 m, 48o47.70'N, 45o05.09'W). Orange diamonds are measurements on Cibicidoides spp., purple triangles are on Cibicidoides lobulatus, and red circles are on Melonis

barleeanum. To better evaluate the longer term temperature changes, we linearly interpolated our data to a 10-yr interval and then applied a 500-yr Gaussian filter to derive the time series shown (thick gray line), with a 1.3°C error based on analytical uncertainty. Also shown is the ice-volume corrected benthic $\delta^{18}O$ ($\delta^{18}O_{IVC}$) record from this core (blue line) during the last deglaciation (Appendix A). (D) Number of ice-rafted detrital $CaCO_3$ grains g^{-1} of sediment in core EW9302-2JPC, with increases in these grains identifying Heinrich layers 1 through 6 (Appendix A).

A number of proxy records show that the AMOC began to decrease 1-2 kyr prior to Heinrich events (Bond and Lotti, 1995; Zahn et al., 1997; McManus et al., 2004; Gutjahr et al., 2010; Mangini et al., 2010); this decline has been which can be attributed to a climatically induced increase in freshwater fluxes from Northern Hemisphere ice sheets (Clark et al., 2004; Clark et al., 2007). Model simulations indicate that, without an active AMOC and associated cooling of the ocean interior by convection, continued downward mixing of heat at low latitudes warms subsurface waters to a depth of ~2500 m. Some of the heat accumulated in the subsurface is transported poleward, causing a temperature inversion in the northern North Atlantic (Figure 2.1 b) (Shaffer et al., 2004; Liu et al., 2009). We use results from a simulation with the National Center for Atmospheric Research Community Climate System Model version 3 (NCAR CCSM3) (Liu et al., 2009) to evaluate the transient response of the BWT at our core site to a reduction in the AMOC during the last deglaciation. Initial reduction in the AMOC occurs in response to increased freshwater fluxes to the North Atlantic associated with onset of deglaciation from the LGM at ~19 ka (Figure 2.3 a) (Clark et al., 2004; Liu et al., 2009). Here we find that the simulated BWT anomaly at our core site caused by the change in the AMOC is in good agreement with our Mg/Ca derived record, with temperature increasing by ~2°C prior to H1, followed by cooling induced by the resumption of the AMOC at the start of the Bølling interstadial ~14.6 ka (Figure 2.3 c).

Although similar subsurface warming preceding H1 has been inferred in the subtropical (Ruhlemann et al., 1999) and high-latitude (Rasmussen et al., 1996; Rasmussen and Thomsen, 2004) North Atlantic from changes in benthic foraminifera $\delta^{18}O$, the $\delta^{18}O$ changes in the Nordic Seas have alternatively been interpreted as recording increased brine formation beneath expanded sea ice (Dokken and Jansen, 1999; Meland et al., 2008), and thus are largely independent of temperature. Our new Mg/Ca measurements on *C. spp.* (N=1), *C. lobulatus* (N=3) and *M. barleeanum* (N=16) for a core from the Nordic Seas (MD95-2010, 1,226 m depth) (Figure 2.1 b) demonstrate that the 1.5 per mil $\delta^{18}O_{IVC}$ signal at this site can be explained by ~6°C

of warming (Figure 2.4 a), thus supporting subsurface warming rather than brine formation as the cause of the large $\delta^{18}O_{IVC}$ signal. Changes in temperature simulated by the CCSM3 model further suggest that the $\delta^{18}O_{IVC}$ signal at this and other North Atlantic sites represents a dominant temperature control reflecting basin-wide subsurface warming (Figure 2.4). The model also simulated small changes in salinity at intermediate depths as freshwater added to the surface was convected downward through the Labrador Sea in the subpolar gyre, suggesting that the associated advection of light $\delta^{18}O$ water may account for some small fraction of the $\delta^{18}O_{IVC}$ signal (Figure 2.4) (Appendix A).

Our Mg/Ca data also suggest a similar phasing between earlier changes in the AMOC, subsurface temperatures and Heinrich events during marine isotope stage 3 (60-26 ka). In particular, correlation of marine records with synchronized Greenland and Antarctica ice-core temperature records shows that Heinrich events during this interval only occurred when Greenland was at its coldest and Antarctica was at its warmest (Figure 2.2 c,d) (Bond et al., 1993; Blunier and Brook, 2001), which is the maximum expression of a strong reduction in the AMOC and its attendant meridional ocean heat transport (Crowley, 1992). These changes in the AMOC are documented by a variety of proxy records, which show a gradual AMOC reduction prior to, and the near-complete replacement of North Atlantic Intermediate Water with Antarctic Bottom Water in the North Atlantic basin at the times of Heinrich events (Zahn et al., 1997; Robinson et al., 2005; Gutjahr et al., 2010). The 1-2 kyr interval of gradual subsurface warming suggested by our Mg/Ca data that peaks at the same time as H3, H5a, and H6 (Figure 2.2 a) is thus consistent with a response to a maximum reduction in the AMOC at these times as well.

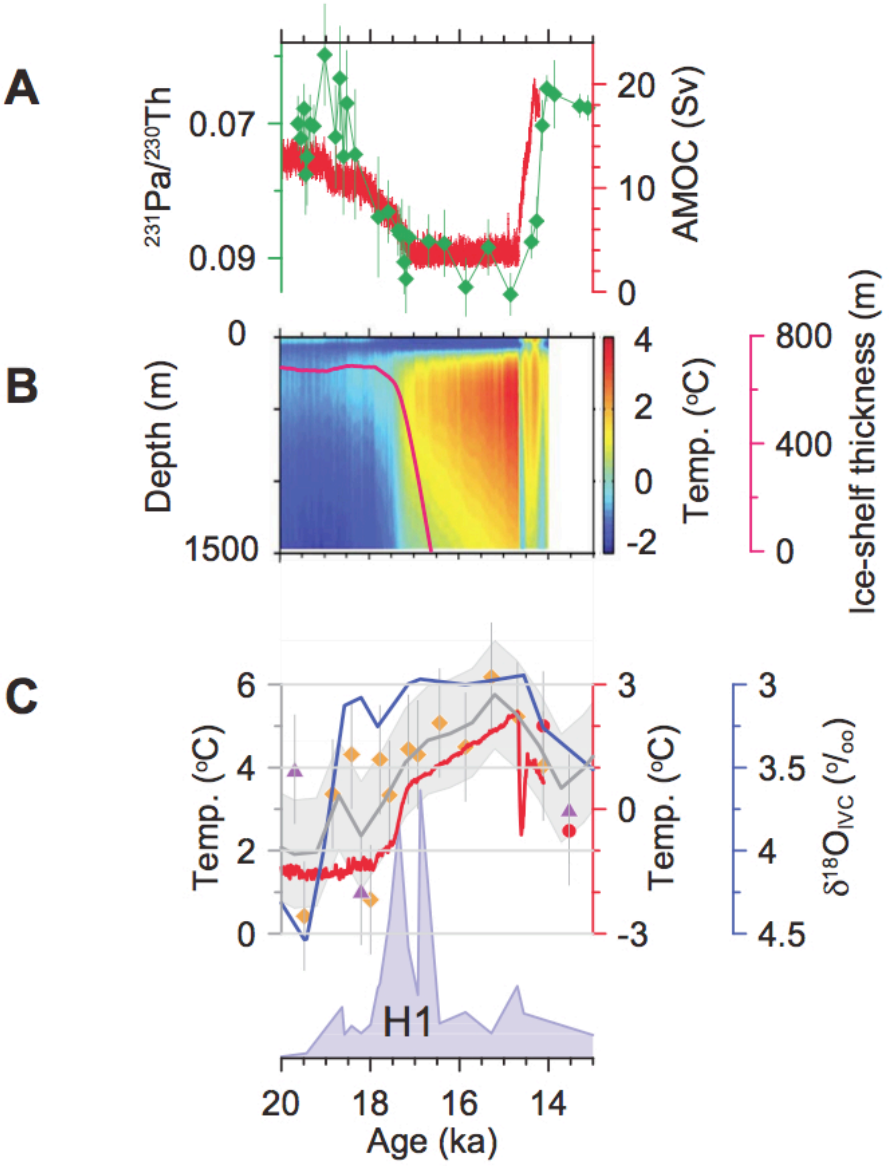

Figure 2.3. Bottom water temperature and modeling results.

(A) Comparison between the $^{231}Pa/^{230}Th$ record from the Bermuda Rise (core OCE326-GGC5), a proxy of AMOC strength (McManus et al., 2004), and strength of the maximum AMOC transport simulated by the NCAR CCSM3 (Liu et al., 2009) during the last deglaciation. (B) Evolution of temperature as a function of time and depth simulated by the NCAR CCSM3 at the location of core EW9302-2JPC. Also

shown is the evolution of computed changes ice-shelf thickness (red line) in response to the temperature evolution (Appendix A). (C) Mg/Ca-derived bottom water temperatures for core EW9302-2JPC. Orange diamonds are measurements on Cibicidoides spp., purple triangles are on Cibicidoides lobulatus, and red circles are on Melonis barleeanum. To better evaluate the longer term temperature changes, we linearly interpolated our data to a 10-yr interval and then applied a 500-yr Gaussian filter to derive the time series shown (thick gray line), with a 1.3°C error based on analytical uncertainty. Also shown is the ice-volume corrected benthic $\delta^{18}O$ ($\delta^{18}O_{IVC}$) record from this core (blue line) and the temperature for the core site simulated by the NCAR CCSM3 (red line). Ice-rafted detrital $CaCO_3$ record of Heinrich event 1 from the core shown by light blue fill pattern.

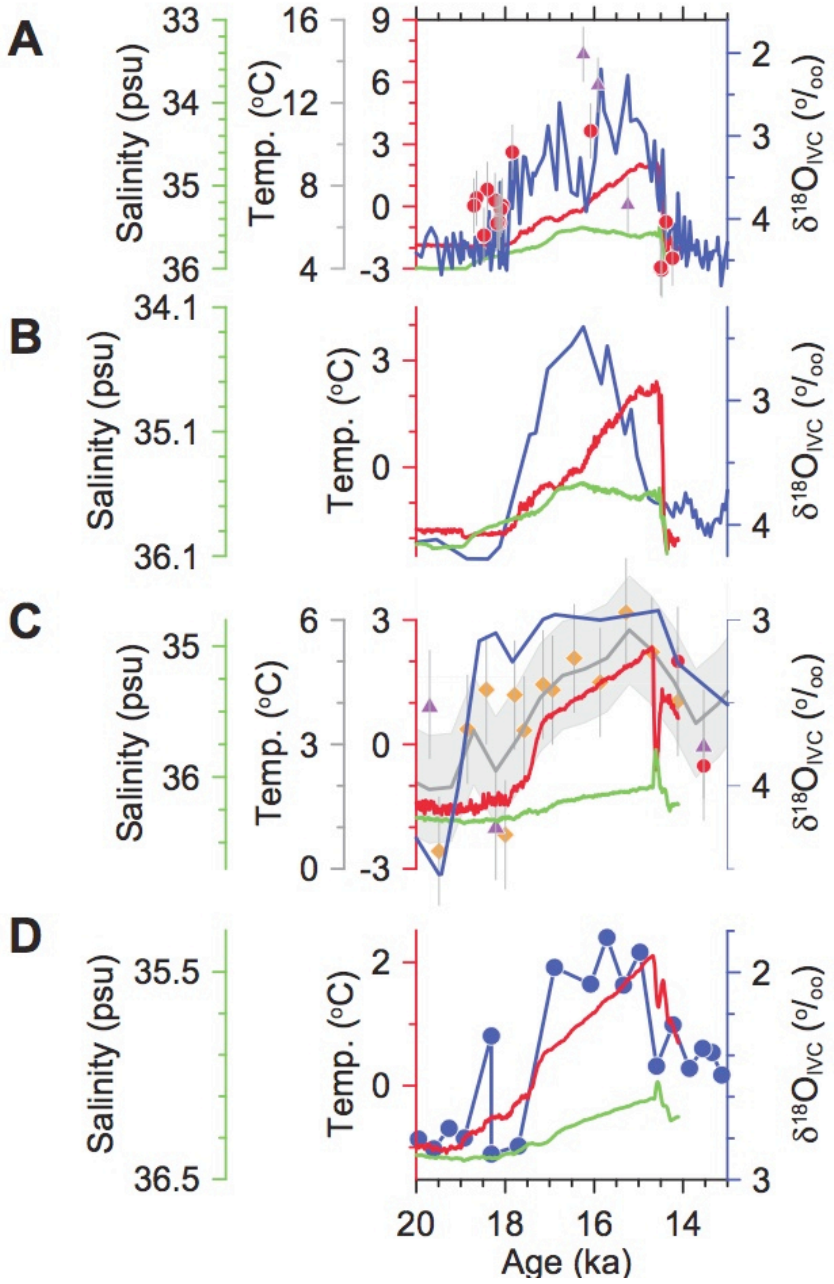

Figure 2.4. $\delta^{18}O$ records from the Atlantic Basin and simulated CCSM3 results. Comparison of $\delta^{18}O_{IVC}$ records from a subtropical North Atlantic site and two sites from the Nordic Seas (Figure 2.1) with changes in temperature and salinity simulated by the CCSM3 model at these sites in response to the decrease in the AMOC shown

in Figure 2.3a. The temperature scale for each plot is equivalent to the associated $\delta^{18}O_{IVC}$ scale assuming a temperature-dependent fractionation of 0.25‰ $°C^{-1}$ for calcite (O'Neil et al., 1969). (A) Ice-volume corrected benthic $\delta^{18}O$ ($\delta^{18}O_{IVC}$) record from core MD95-2010 (1,226 m depth; 66°41.05' N, 04°33.97' E) during the last deglaciation. Also shown is the temperature (red line) and salinity (green line) for the core site simulated by the NCAR CCSM3, and our new Mg/Ca-derived bottom water temperatures, where purple triangles are on C. lobulatus and red circles are on M. barleeanum. (B) As in (A), but for core ENAM93-21 (1,020 m depth; 66°44.3' N, 03°59.92' E) (Rasmussen et al., 1996). (C) Mg/Ca-derived bottom water temperatures for core EW9302-2JPC. Orange diamonds are measurements on Cibicidoides spp., purple triangles are on C. lobulatus, and red circles are on M. barleeanum, with a 3-point weighted average (blue line). Also shown is the temperature (red line) and salinity (green line) for the core site simulated by the NCAR CCSM3. (D) As in (A), but for core M35003-4 (1,299 m depth; 12°05'N, 61°15'W) (Rühlemann et al., 2004).

Because of the complex ocean-ice processes that exist beneath ice shelves (Holland and Jenkins, 1999), the effect of the open-ocean subsurface warming documented here on the stability of an ice shelf fronting the HSIS is unclear. We apply a high-resolution ocean model coupled to a non-evolving but thermodynamically active ice shelf (Figure 2.2, Appendix A) to explore the sensitivity of basal melt rate to subsurface warming for a specified ice shelf filling Baffin Bay and the Labrador Sea (Hulbe, 1997). Initial model hydrography is derived from the CCSM3 simulation of the last deglaciation (Appendix A) (Liu et al., 2009). We refer to an active AMOC, with cold subsurface temperatures, as the "cold state," corresponding to model years 19.5-19.0 ka, and an inactive AMOC, with warm subsurface temperatures, as the "warm state," corresponding to model years 17.0-16.5 ka.

For the cold state, we find that the shelf-averaged basal melt rate is 0.17 m a^{-1}, with the integrated volume loss from the ice shelf by basal melt being ~10% of the estimated flux of ~660 km^3 a^{-1} across the HSIS grounding line (Hulbe, 1997). For the warm state, the averaged basal melt rate is 1.03 m a^{-1}. We also performed three additional intervening simulations with our regional model, for a total of five spanning the interval from 19.5 ka to 16.5 ka, which allows us to derive the relation between ocean temperature T_i at the typical depth of the ice-shelf base (400-800 m), and shelf-averaged melt rate $M_{av} = 0.54 + 0.34.T_i$ (m a^{-1}). Based on the simulated temperature evolution for water depths of 400-800 m, our computed time-history of ice-shelf thinning in response to the warming of intermediate-depth waters indicates a ~1000-year timescale for collapse of the ice shelf (red curve in Figure 2.2 b), although based on modern analogs, it is likely that the ice shelf would collapse before it thinned to zero; we thus expect that our estimate of this timescale is a maximum. Additional factors (rate of grounding line migration, calving rate) may modulate this response, but are unlikely to significantly change the timescale (Appendix A). The model also indicates that maximum melt rates along the deep grounding line of the HSIS increased six-fold, from ~6 m a^{-1} to 35-40 m a^{-1}, comparable to estimates from

empirical models based on modern observations of grounding line melt rates (Rignot and Jacobs, 2002). By analogy with recent studies of Antarctic ice shelves and buttressed ice streams (Joughin et al., 2010), more rapid grounding line thinning would accelerate the HSIS outflow prior to ice-shelf collapse.

2.4 Conclusions

Our data and model results indicate that basin-wide subsurface warming occurred in the North Atlantic in response to a reduction in the AMOC prior to Heinrich events, and that Heinrich events did not occur until the AMOC was at its weakest and subsurface temperatures were near their maximum values. We also find that the open-ocean subsurface warming significantly increases the rate of mass loss from the ice shelf fronting the HSIS. Our results thus support simplified climate modeling results suggesting that a weakened or collapsed ice shelf would trigger an ice-stream surge, producing a Heinrich event (Shaffer et al., 2004; Alvarez-Solas et al., 2010), analogous to the recent response of Antarctic glaciers to the loss of buttressing ice shelves (Rignot et al., 2004). By confirming the significance that subsurface warming played in triggering past ice-sheet instabilities, our results provide important insights into possible future behavior of similarly configured Antarctic ice-sheet sectors, should warmer waters penetrate beneath their large, buttressing ice shelves.

2.5 Methods

We used an automated flow-through system (Haley and Klinkhammer, 2002) which cleans and dissolves the carbonate shells and thus minimizes the effects of secondary calcite and clay contamination (Appendix A). We analyzed the benthic species *Cibicidoides lobulatus* (N=46), *Cibicidoides spp.* (N=23), and *Melonis barleeanum* (N=44), including 15 replicate analyses, and converted Mg/Ca ratios to BWTs following published calibration curves (Appendix A). The age model for

EW9302-2JPC is based on six previously published ^{14}C dates (Rasmussen et al., 2003), a well-dated tephra layer at 408 cm depth (ASH II), an age-to-depth tie point at the midpoint of H6 (Stoner et al., 2000) corresponding to the peak in ice-rafted detrital carbonate at 496 cm depth in EW9302-2JPC, and the marine isotope stage 5/4 boundary (544 cm) based on the $\delta^{18}O$ planktonic foraminifera data from the core (Rasmussen et al., 2003) (Appendix A). We emphasize, however, that the relative timing of changes of any given proxy within the core relative to those of another proxy is established directly from the stratigraphic position of each sample within the core, and is thus insensitive to any uncertainties in numerical chronology.

2.6 Acknowledgements

We thank Ellen Roosen of the WHOI core repository for subsampling of EW9302-2JPC, Trond Dokken for providing samples from MD95-2010, Anne Jennings and Matthew Wolhowe for technical assistance, Tine Rasmussen for sharing data, and Jeremy Shakun, Alan Mix, Edward Brook, Joseph Stoner, and Thomas Bauska for comments. Support was provided by the NSF Paleoclimate Program (P.U.C., G.P.K., A.E.C., Z.L., B.O.-B., and A.S.) and NASA grant NNG05GR58G (L.P.). Computer time was provided by the DOE INCITE program.

2.7 References

Adkins, J. F., McIntyre, K., and Schrag, D. P. (2002). The salinity, temperature, and $d^{18}O$ of the glacial deep ocean. *Science* **298,** 1769-1773.

Alley, R. B., Anandakrishnan, S., Dupont, T. K., Parizek, B. R., and Pollard, D. (2007a). Effect of sedimentation on ice-sheet grounding-line stability. *Science* **315,** 1838-1841.

Alvarez-Solas, J., Charbit, S., Ritz, C., Paillard, D., Ramstein, G., and Dumas, C. (2010). Links between ocean temperature and iceberg discharge during Heinrich events. *Nature Geoscience* **3,** 122-126.

Blunier, T., and Brook, E. J. (2001). Timing of millennial-scale climate change in Antarctica and Greenland during the last glacial period. *Science* **291,** 109-112.

Bond, G., Broecker, W., Johnsen, S., McManus, J., Labeyrie, L., Jouzel, J., and Bonani, G. (1993). Correlations between climate records from North Atlantic sediments and Greenland ice. *Nature* **365,** 143-147.

Bond, G. C., and Lotti, R. (1995). Iceberg discharges into the North Atlantic on millennial time scales during the last glaciation. *Science* **267,** 1005-1010.

Clark, P. U., Hostetler, S. W., Pisias, N. G., Schmittner, A., and Meissner, K. J. (2007). Mechanisms for an ~7-kyrs climate and sea-level oscillation during Marine Isotope Stage 3. *In* "Ocean Circulation: Mechanisms and Impacts - Past and Future Changes of Meridional Overturning." (A. Schmittner, J. C. H. Chiang, and S. R. Hemming, Eds.), pp. 392. American Geophysical Union, Washington, DC.

Clark, P. U., McCabe, A. M., Mix, A. C., and Weaver, A. J. (2004). Rapid rise of sea level 19,000 years ago and its global implications. *Science* **304,** 1141-1144.

Crowley, T. J. (1992). North Atlantic deep water cools the southern hemisphere. *Paleoceanography* **7,** 489-497.

Dokken, T., and Jansen, E. (1999). Rapid changes in the mechanism of ocean convection during the last glacial period. *Nature* **401,** 458-461.

Elderfield, H., Yu, J., Anand, P., Kiefer, K., and Nyland, B. (2006a). Calibrations for benthic foraminiferal Mg/Ca paleothermometry and the carbonate ion hypothesis. *Earth and Planetary Science Letters* **250,** 633-649.

Gutjahr, M., Hoogakker, B. A. A., Frank, M., and McCave, I. N. (2010). Changes in North Atlantic Deep Water strength and bottom water masses during Marine Isotope Stage 3 (45-35 ka BP). *Quaternary Science Review* **29,** 2451-2461.

Haley, B. A., and Klinkhammer, G. P. (2002). Development of a flow-though system for cleaning and dissolving foraminiferal tests. *Chemical Geology* **185,** 51-69.

Heinrich, H. (1988). Origin and consequences of cyclic ice rafting in the Northeast Atlantic ocean during the past 130,000 years. *Quaternary Research* **29,** 142-152.

Holland, D. M., and Jenkins, A. (1999). Modelling thermodynamic ice-ocean interactions at the base of an ice shelf. *Journal of Physical Oceanography* **29,** 1787-1800.

Hulbe, C. L. (1997). An ice shelf mechanism for Heinrich layer production. *Paleoceanography* **12,** 711-717.

Joughin, I., Smith, B. E., and Holland, D. M. (2010). Sensitivity of 21st century sea level to ocean-induced thinning of Pine Island Glacier, Antarctica. *Geophysical Research Letters* **37**.

Jouzel, J., Masson-Delmotte, V., Cattani, O., Dreyfus, G., Falourd, S., Hoffmann, G., Minster, B., Nouet, J., Barnola, J. M., Chappellaz, J., Fischer, H., Gallet, J. C., Johnsen, S., Leuenberger, M., Loulergue, L., Luethi, D., Oerter, H., Parrenin, F., Raisbeck, G., Raynaud, D., Schilt, A., Schwander, J., Selmo, E., Souchez, R., Spahni, R., Stauffer, B., Steffensen, J. P., Stenni, B., Stocker, T. F., Tison, J. L., Werner, M., and Wolff, E. W. (2007). Orbital and millennial Antarctic climate variability over the past 800,000 years. *Science* **317,** 793-796.

Lemieux-Dudon, B., Blayo, E., Petit, J. R., Waelbroeck, C., Svensson, A., Ritz, C., Barnola, J. M., Narcisi, B. M., and Parrenin, F. (2010). Consistent dating for Antarctic and Greenland ice cores. *Quaternary Science Reviews* **29,** 8-20.

Lewis, E., and Wallace, D. W. R. (1998). *CO2 system calculations, ORNL/CDIAC-105 (CO2SYS v.1.05)*.

Liu, Z., Otto-Bliesner, B. L., He, F., Brady, E. C., Tomas, R., Clark, P. U., Carlson, A. E., Lynch-Stieglitz, J., Curry, W., Brook, E. J., Erickson, D., Jacob, R., Kutzbach, J. E., and Cheng, J.

Liu, Z., Otto-Bliesner, B. L., He, F., Brady, E. C., Tomas, R., Clark, P. U., Carlson, A. E., Lynch-Stieglitz, J., Curry, W., Brook, E. J., Erickson, D., Jacob, R., Kutzbach, J. E., and Cheng, J. (2009). Transient simulation of last deglaciation with a new mechanism for Bølling-Allerød warming. *Science* **325,** 310-314.

MacAyeal, D. R. (1993). Binge/purge oscillations of the Laurentide Ice Sheet as a cause of the North Atlantic's Heinrich events. *Paleoceanography* **8,** 775-784.

Mangini, A., Godoy, J. M., Kowsmann, R., Santos, G. M., Ruckelshausen, M., Schroeder-Ritzrau, A., and Wacker, L. (2010). Deep sea corals off Brazil verify a poorly ventilated Southern Pacific Ocean during H2, H1 and the Younger Dryas. *Earth and Planetary Science Letters* **293,** 269-276.

McManus, J. F., Francois, R., Gherardi, J.-M., Keigwin, L. D., and Brown-Leger, S. (2004). Collapse and rapid resumption of Atlantic meridional criculation linked to deglacial climate changes. *Nature* **428,** 834-837.

Meese, D. A. (1997). The Greenland Ice Sheet Project 2 depth-age scale: Methods and results. *J. Geophys. Res.* **102,** 26411-26423.

Meland, M. Y., Dokken, T. M., Jansen, E., and Hevrøy, K. (2008). Water mass properties and exchange between the Nordic seas and the northern North Atlantic during the period 23-6 ka: Benthic oxygen isotopic evidence. *Paleoceanography* **23,** PA1210, doi:10.1029/2007PA001416.

NGRIP members. (2004). High-resolution record of Northern Hemisphere climate extending into the last interglacial period. *Nature* **431,** 147-151.

O'Neil, J. R., Clayton, R. N., and Mayeda, T. K. (1969). Oxygen isotope fractionation in divalent metal carbonates. *Journal of Chemical Physics* **51,** 5547-5558.

Rasmussen, T. L., Oppo, D. W., Thomsen, E., and Lehman, S. J. (2003). Deep sea records from the southeast Labrador Sea: Ocean circulation changes and ice-rafting events during the last 160,000 years. *Paleoceanography* **18,** doi:10.1029/2001PA000736.

Rasmussen, T. L., and Thomsen, E. (2004). The role of the North Atlantic Drift in the millennial timescale glacial climate fluctuations. *Palaeogeography Palaeoclimatology Palaeoecology* **210,** 101-116.

Rasmussen, T. L., Thomsen, E., van Weering, T. C. E., and Labeyrie, L. (1996). Rapid changes in surface and deep water conditions at the Faeroe Margin during the last 58,000 years. *Paleoceanography* **11,** 757-772.

Rignot, E., Casassa, G., P., G., Krabill, W., Rivera, A., and Thomas, A. (2004). Accelerated ice discharge from the Antarctic Peninsula following the collapse of Larsen B ice shelf. *Geophysical Research Letters* **31,** doi:10.1029/2004GL020697.

Rignot, E., and Jacobs, S. S. (2002). Rapid bottom melting widespread near Antarctic Ice Sheet grounding lines. *Science* **296,** 220-2023.

Robinson, L. F., Adkins, J. F., Keigwin, L. D., Southon, J., Fernandez, D. P., Wang, S.-L., and Scheirer, D. S. (2005). Radiocarbon variability in the Western Northt Atlantic during the last deglaciation. *Science* **310,** 1469-1473.

Rühlemann, C., Mulitza, S., Lohmann, G., Paul, A., Prange, M., and Wefer, G. (2004). Intermediate depth warming in the tropical Atlantic related to weakened

thermohaline circulation: Combining paleoclimate data and modeling results for the last deglaciation. *Paleoceanography* **19,** doi:10.1029/2003PA000948.

Ruhlemann, C., Mulitza, S., Muller, P. J., Wefer, G., and Zahn, R. (1999). Warming of the tropical Atlantic Ocean and slowdown of thermohaline circulation during the last deglaciation. *Nature* **402,** 511-514.

Shaffer, G., Olsen, S. M., and Bjerrum, C. J. (2004). Ocean subsurface warming as a mechanism for coupling Dansgaard-Oeschger climate cycles and ice-rafting events. *Geophysical Research Letters* **31,** L24202, doi:10.1029/2004GL020968.

Stoner, J. S., Channell, J. E. T., Hillaire-Marcel, C., and Kissel, C. (2000). Geomagnetic paleointensity and environmental record from Labrador Sea core MD95-2024: global marine sediment and ice core chronostratigraphy for the last 110 kyr. *Earth and Planetary Science Letters* **183,** 161-177.

WOCE. (2002). World Ocean Circulation Experiment, Global Data, Version 3.0. WOCE International Project Office, Southampton, UK.

Yu, J., Elderfield, H., and Pitrowski, A. M. (2008). Seawater carbonate ion-δ13C systematics and application to glacial-interglacial North Atlantic ocean circulation. *Earth and Planetary Science Letters* **271,** 209-220.

Zahn, R., Schönfeld, J., Kudrass, H.-R., Park, M.-H., Erlenkeuser, H., and Grootes, P. M. (1997). Thermohaline instability in the North Atlantic during meltwater events: Stable isotope and ice-rafted detritus records from core SO75-26KL, Portugues margin. *Paleoceanography* **12,** 696-710.

Chapter 3

Late Pleistocene and Holocene Cirque Glaciation, western North America

Shaun A. Marcott [1], Peter U. Clark [1], Jeremy D. Shakun [2], Edward J. Brook [1], Anthony M. Novak [3], P. Thompson Davis [4], and Mark W. Caffee [5]

[1]Department of Geosciences, Oregon State University, Corvallis, OR 97331, USA

[2]Department of Earth Sciences, Boston University, Boston, MA, 02215, USA

[3]Department of Earth Sciences, Dalhousie University, Halifax NS, B3H 4J1, Canada

[4]Department of Natural and Applied Sciences, Bentley University, Waltham, MA 02452, USA

[5]Department of Physics, Purdue University, W. Lafayette, IN 47907, USA

To be submitted to Science

3.1 Abstract

Glaciers are intrinsically linked to climate, and given the sensitivity of small alpine glaciers to climate change, accurate and precise chronologies of their fluctuations are important in elucidating both the temporal and spatial structure of climate variability. Despite nearly a century of research, the timing of late Pleistocene and Holocene alpine glaciation in much of western North America remains poorly constrained. Here we present 124 ^{10}Be ages from twenty cirque moraines in ten mountain ranges across western North America that were previously interpreted to be mid- to late Holocene in age. With the exception of one moraine in western British Columbia, our new ^{10}Be glacial chronology indicates that these moraines were deposited during the latest Pleistocene or earliest Holocene, requiring a refined interpretation of Holocene glacial activity in western North America and the associated climate forcing. Although alpine glaciers may have continued to fluctuate during the Holocene, they did not advance beyond their Little Ice Age maxima. Rather, cirque glacier activity in western North America has followed in near step with late Pleistocene high latitude climate and the associated forcing.

3.2 Introduction

Precise glacial chronologies are a key component in developing an understanding of large climate shifts during the Holocene epoch (Jansen et al., 2007). Although it has recently been shown that glacial advances in both the northern and southern hemisphere may be synchronous when forced by CO_2 or other large scale climate forcings (Schaefer et al., 2006) (see (Clark et al., 2009) for a modified perspective), it is still unclear whether glacial advances during the Holocene were in fact globally synchronous (Licciardi et al., 2009; Schaefer et al., 2009).

In western North America, Holocene glacial fluctuations were first documented in the 1920s (Matthes, 1929) and further refined in the 1960s (Richmond, 1960; Birkeland, 1964; Crandell, 1969) with the advent of radiocarbon

dating and relative dating techniques. Porter and Denton (1967) summarized the evidence for Holocene glacial activity in western North America and introduced the term Neoglaciation, which referred to glacial advances over the past 5000 years including the most recent advance, the Little Ice Age (LIA). While some studies have shown that the LIA represents the culmination of the Neoglacial advances, several others have suggested that older advances represented more-extensive glaciation during the Holocene epoch (Davis, 1988). To address this issue, we collected samples for cosmogenic surface exposure dating (^{10}Be) from ten mountain ranges in western North America where prior detailed glacial mapping has been conducted. Because the numerical dating controls on the majority of the glacial deposits in western North America is sparse, our new chronology fills a large gap in the glacial database and allows for a better comparison between glacial advances and climate change in western North America.

3.3 Methods

We sampled boulders from cirque moraines in the western United States and one site in southern British Columbia (Figure 3.1) that are inset to large Pleistocene moraines and just distal to the glacial deposits associated with the LIA (Appendix B). The majority of these well-preserved moraines have been interpreted as Neoglacial or early Holocene in age based on a number of numerical and relative dating techniques and are well suited for cosmogenic surface exposure dating with ^{10}Be because of the quartz-bearing lithologies that primarily make up the deposits. Large boulders exist on all of the moraine crests and were the primary targets for deriving the glacial chronologies. Six to eight ^{10}Be exposure dates were obtained from the majority of the moraines to derive mean ages of the deposits. Of the 124 derived ages, we identified ten outliers (8%) using Chauvenet's criterion (Appendix B). We interpret the surface exposure ages of the glacial deposits to represent the timing of moraine depositional cessation and retreat of the glaciers from the deposit. Individual moraine ages are reported as the arithmetic mean and the standard error uncertainty. Other

uncertainties associated with the production of ^{10}Be at our sites, age calculations and errors, and the full dataset can be found in Appendix B.

3.4 Results

Our results demonstrate that with the exception of one site in southwestern British Columbia (Clague et al., in preparation), all the sampled moraines were deposited during the latest Pleistocene or earliest Holocene (Figure 3.2), in contrast to previous interpretations (Davis, 1988) which interpreted the majority of these deposits as middle or late Holocene in age based on poor numerical control or the relative dating techniques with large uncertainties. Our data from nearly all of the sampled locations (19 of 20 moraines) clearly demonstrate that glaciers in the American West did not reach positions more extensive than the LIA during the Neoglacial, a conclusion that is likely true for all of western North America accept in those instances that may not be climatically driven and instead are related to local factors such as debris cover or local shading. This finding is in good agreement with our current understand of Holocene climate where Northern Hemisphere temperatures were generally warmer in the early and middle Holocene, and thus not conducive for major glacial growth until the LIA (Marcott et al., in review).

3.5 Discussion

From the glacial chronologies of these ten mountain ranges and the existing data from other studies (Figure 3.3) a scenario of alpine glacial activity in western North America can be derived. Following the local LGM (Clark et al., 2009), glaciers across western North America began retreating from the large Pleistocene moraines 15-30 km downvalley from the cirque headwalls. By ~15 kyr these glacier had reached new equilibrium positions 1-2 km from the cirque peaks, and by 15-13 ka warmer and/or drier conditions across western North America caused further retreat (Whitlock and Bartlein, 1997; Hendy and Kennett, 2000; Barron et al., 2003; Asmerom et al., 2010; Wagner et al., 2010). Cooler and/or wetter conditions

beginning at ~13 kyr (Whitlock and Bartlein, 1997; Hendy and Kennett, 2000; Barron et al., 2003; MacDonald et al., 2008) likely caused the alpine glaciers to begin readvancing to new equilibrium positions until 12-11 ka when a return to warmer conditions caused some glaciers to retreat. By 11-8 ka the remaining cirque glaciers across western North America began to retreat once again and likely completely disappeared until the next major glacial phase in western North America some 7-10 kyr later culminating during the LIA, which was the final, major moraine building phase in western North America. While glaciers may have waxed and waned from 8 kyrs to the LIA, they never advanced beyond the LIA moraines except in few isolated locations (Clague et al., in preparation).

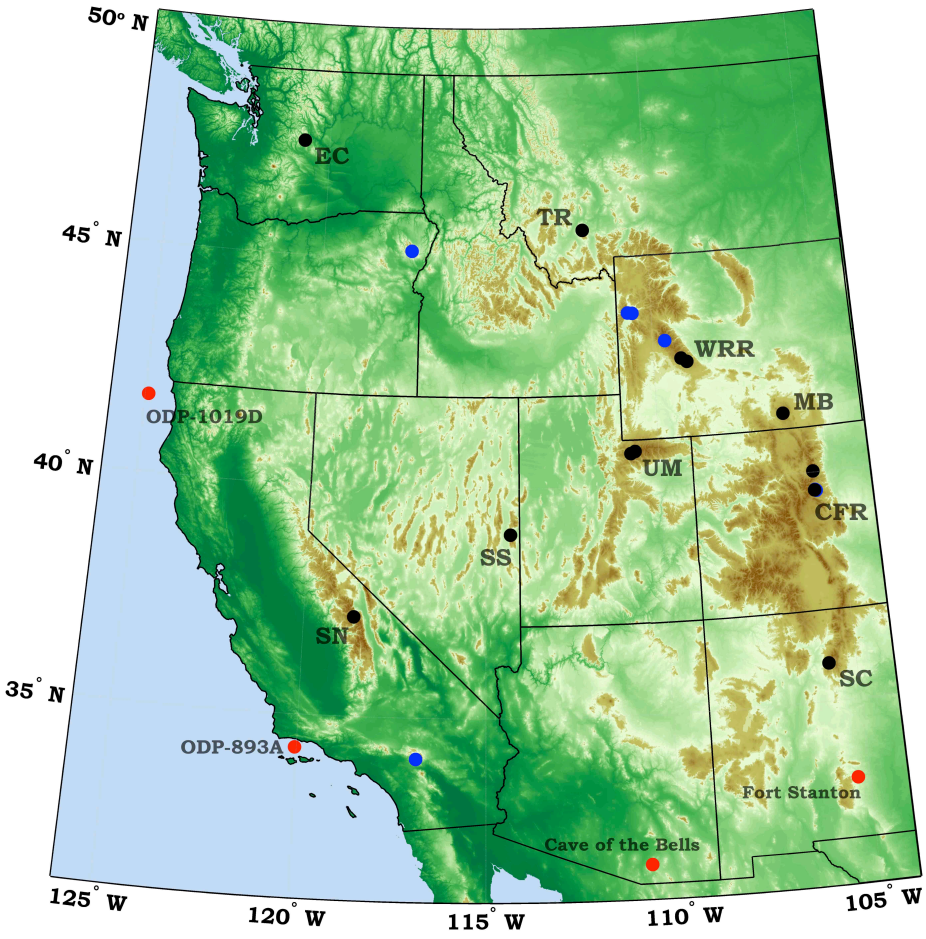

Figure 3.1. Shaded relief map of western North America.
Black circles with labels indicate field site locations from this study, blue circles are other locations referenced in text where ^{10}Be based cirque chronologies exist, and red circles are locations of paleoclimate data referenced in the text and plotted in Fig. 3. EC – Enchantment Lakes Basin, North Cascade Range; TR – Tobacco Root Range; WRR – Wind River Range; MB – Medicine Bow Mountains; UM – Uinta Mountains; CFR – Colorado Front Range; SS – South Snake Range; SN – Sierra Nevada Range; SC – Sangre de Cristo Mountains.

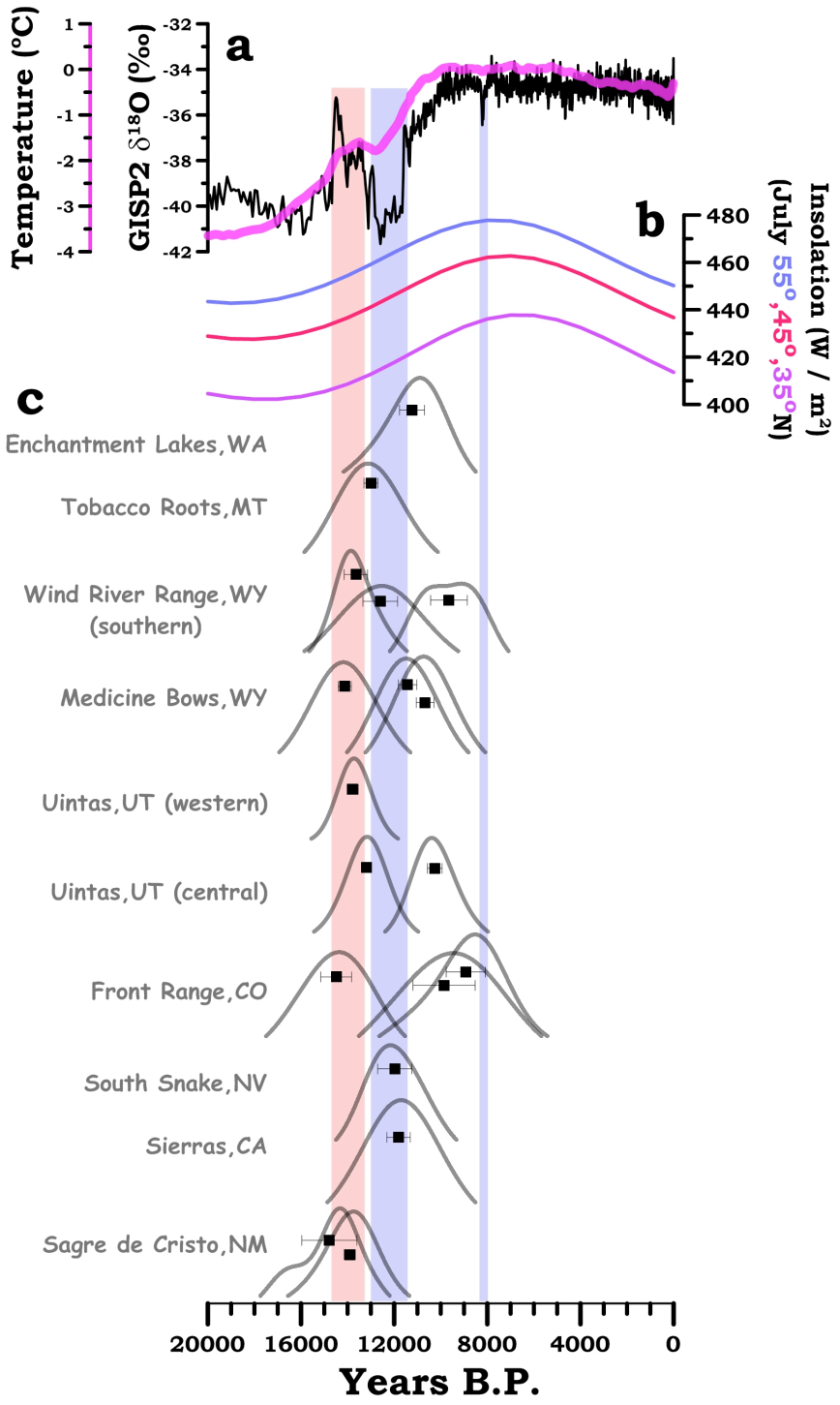

Figure 3.2. Timing of glacial retreat from cirque moraines in western North America, global and hemispheric temperature reconstructions, and high latitude forcings.

a. Oxygen isotopes from summit Greenland (Stuiver and Grootes, 2000) and a global temperature reconstruction (Marcott et al., in review; Shakun et al., in review). **b.** July insolation for 35°, 45°, and 55°N (Laskar et al., 2004). **c.** Probability density function with normalized y-axis (black line) and arithmetic mean and standard error (2σ) (black square) of surface exposure dates for moraines in the referenced mountain ranges and U.S. state locations.

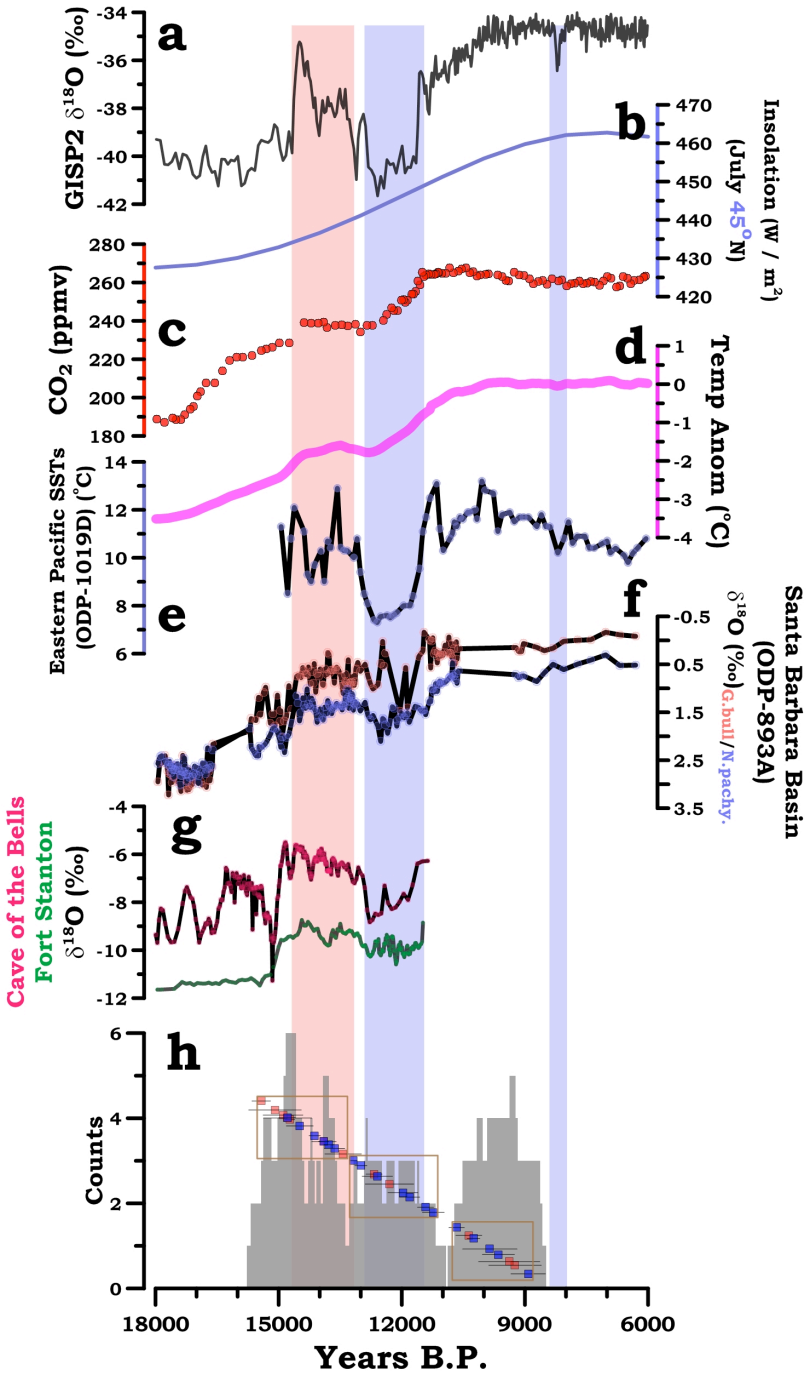

Figure 3.3. Comparing climate reconstructions and their potential forcings with cirque glacial advances across western North America.

a. Oxygen isotopes from summit Greenland (Stuiver and Grootes, 2000). **b.** July insolation for 45°N (Laskar et al., 2004). **c.** Concentrations of carbon dioxide in the atmosphere as recorded in an Antarctic ice core (Monnin et al., 2001; Lemieux-Dudon et al., 2009). **d.** Temperature reconstruction from a globally stacked record (Marcott et al., in review; Shakun et al., in review). **e.** Sea surface temperature reconstruction from the eastern Pacific off the northern California coast (Barron et al., 2003). **f.** Oxygen isotopes from planktonic foraminifera in the Santa Barbara Basin off the southern California coast (Hendy and Kennett, 2000). **g.** Oxygen isotopes from stalagmite deposits from two caves in the southwestern United States (Asmerom et al., 2010; Wagner et al., 2010). **h.** ^{10}Be based surface exposure ages from cirque moraines in western North America from this study (blue squares with 1σ standard error) and others (Gosse et al., 1995; Owen et al., 2003; Licciardi et al., 2004; Benson et al., 2007; Licciardi and Pierce, 2008) (red squares with error) and histogram of cumulative mean moraine ages (±1σ) from this study and others (gray line and fill) binned into 50 year increments.

The timing of glacial advances in western North America can be understood in the context of millennial and orbital scale climate variability over the last 15 ka. Work from this study combined with others (Figure 3.3) show that the timing of alpine glaciation in western North America following the LGM was primarily controlled by climate change, though non-climatic processes (e.g. glacier hypsometry, debris cover, glacier aspect) may have influenced glacier area and account for some of the scatter in the moraine ages. Glacial retreat occurred in three broad time intervals for the latest Pleistocene and earliest Holocene. The first from 15-13 ka was associated with abrupt warming of the Northern Hemisphere (Bølling-Allerød), the second phase from approximately 13-11 ka was associated with the Younger Dryas cooling in the North Atlantic, and the final phase of glacial retreat between 11-8 ka was in response to high latitude maximum summer insolation and near peak interglacial warming (Marcott et al., in review) where most climate records in the western United States indicate warmer temperatures than the previous 3-4 ka and a return to more Bølling-Allerød like conditions (Figure 3.3).

Our new ^{10}Be based chronology from western North America provides evidence that Holocene glacial advances culminated sometime during the LIA and not during multiple intervals throughout the interglacial as previously proposed. It also supports evidence that latest Pleistocene advances in western North America were regionally variable (Clark and Gillespie, 1997), but that the general pattern of glaciation followed in near step with high latitude forcings from the North Atlantic.

3.6 Acknowledgements

We thank P. Birkeland, J. Clague, J. Clark, D. Dahms, V. Ersek, B. Goehring, G. Osborn, and B. Menounos for assistance with fieldwork; G. Baker, H. Basagic, A. Fountain, B. Goehring, S. Hostetler, B. Laabs, J. Licciardi, G. Osborn, and G. Stock for discussions; S. Ma at PRIME Labs for assistance in AMS sample preparation; J.Cuzzone, L. Farmer, C. Carlson-Ham, and K. Zahnle-Hostetler for lab assistance; and the National Parks and Forest Service for permissions and access to the field

sites. This work was supported by National Science Foundation grants to S.A.M., P.U.C., P.T.D., and E.J.B., a Geological Society of America student research grant to S.A.M., and student scholarships to S.A.M. and A.M.N. from Oregon State University.

3.7 References

Asmerom, Y., Polyak, V. J., and Burns, S. J. (2010). Variable winter moisture in the southwestern United States linked to rapid glacial climate shifts. *Nature Geoscience* **3,** 114-117.

Barron, J. A., Heusser, L., Herbert, T., and Lyle, M. (2003). High resolution climatic evolution of coastal northern California during the past 16,000 years. *Paleoceanography* **18,** 20-1 to 20-14.

Benson, L., Madole, R. F., Kubik, P., and McDonald, R. (2007). Surface-exposure ages of Front Range moraines that may have formed during the Younger Dryas, 8.2 cal ka, and Little Ice Age events. *Quaternary Science Review* **26,** 1638-1649.

Birkeland, P. W. (1964). Pleistocene glaciation of the northern Sierra Nevada, north of Lake Tahoe, California. *Journal of Geology* **72**.

Clague, J., Marcott, S. A., Menounos, B., Osborn, G., Novak, A. M., and Clark, P. U. (in preparation).

Clark, D. H., and Gillespie, A. R. (1997). Timing and significance of late-glacial and Holocene cirque glaciation in the Sierra Nevada, California. *Quaternary International* **38/39,** 21-38.

Clark, P. U., Dyke, A. S., Shakun, J. D., Carlson, A. E., Clark, J., Wohlfarth, B., Hostetler, S. W., Mitrovica, J. X., and McCabe, A. M. (2009). The Last Glacial Maximum. *Science* **325,** 710-714.

Crandell, D. R. (1969). Surficial geology of Mount Rainier National Park, Washington. *U.S. Geological Survey Bulletin 1288*.

Davis, P. T. (1988). Holocene Glacier Fluctuations in the American Cordillera. *Quaternary Science Reviews* **7,** 129-157.

Gosse, J. C., Evenson, E. B., Klein, J., Lawn, B., and Middleton, R. (1995). Precise cosmogenic ^{10}Be measurements in western North America: Support for a global Younger Dryas cooling event. *Geology* **23,** 877-880.

Hendy, I., and Kennett, J. (2000). Dansgaard/Oeschger cycles and the California Current System; Planktonic foraminiferal response. *Paleoceanography* **15,** 30-42.

Jansen, E., Overpeck, J., Briffa, K. R., Duplessy, J.-C., Joos, F., Masson-Delmotte, V., Olago, D., Otto-Bliesner, B. L., Peltier, W. R., Rahmstorf, S., Ramesh, R., Raynaud, D., Rind, D., Solomina, O., Villalba, R., and Zhang, D. (2007). Paleoclimate. *In* "Climate Change 2007: The Physical Science Basis. Contribution of Working Group I to the Fourth Assessment Report of the Intergovernmental Panel on Climate Change." (S. Solomon, D. Qin, M. Manning, Z. Chen, M. Marquis, K. B. Averyt, M. Tignor, and H. L. Miller, Eds.). Cambridge University Press, Cambridge.

Laskar, J., Robutel, P., Joutel, F., Gastineau, M., Correia, A. C. M., and Levrard, B. (2004). A long term numerical solution for the insolation quantities of the Earth. *Astronomy and Astrophysics* **428,** 261-285.

Lemieux-Dudon, B., Blayo, E., Petit, J.-R., Waelbroeck, C., Svensson, A., Ritz, C., Barnola, J.-M., Narcisi, B. M., and Parrenin, F. (2009). Consistent dating of Antarctica and Greenland ice cores. *Quaternary Science Review* **29,** 8-20.

Licciardi, J. M., Clark, P. U., Brook, E. J., Elmore, D., and Sharma, P. (2004). Variable responses of western U.S. glaciers during the last deglaciation. *Geology* **32,** 81-84.

Licciardi, J. M., and Pierce, K. L. (2008). Cosmogenic exposure-age chronologies of Pinedale and Bull Lake glaciations in greater Yellowstone and the Teton Range, U.S.A. *Quaternary Science Review* **27,** 814-831.

Licciardi, J. M., Schaefer, J. M., Taggart, J. R., and Lund, D. C. (2009). Holocene glacier fluctuations in the Peruvian Andes indicate northern climate linkage. *Science* **325,** 1677-1679.

MacDonald, G. M., Moser, K., Bloom, A. M., Porinchu, D. F., Potito, A. P., Wolfe, B. B., Edwards, T. W. D., Petel, A., Orme, A. R., and Orme, A. J. (2008). Evidence of temperature depression and hydrological variations in the eastern Sierra Nevada during the Younger Dryas stade. *Quaternary Research* **70,** 131-140.

Marcott, S. A., Shakun, J. D., Clark, P. U., and Mix, A. C. (in review). Holocene Temperature Variations.

Matthes, F. E. (1929). Multiple glaciations in the Sierra Nevada. *Science* **70,** 75-76.

Monnin, E., Indermuhle, A., Dallenbach, A., Fluckiger, J., Stauffer, B., and Stocker, T. F. (2001). Atmospheric CO2 concentrations over the last glacial termination. *Science* **291,** 112-114.

Owen, L. A., Finkel, R. C., Minnich, R. A., and Perez, A. E. (2003). Extreme southwestern margin of late Quaternary glaciation in North America: Timing and controls. *Geology* **31,** 729-732.

Porter, S. C., and Denton, G. H. (1967). Chronology of Neoglaciation in the North American Cordillera. *Amer. Jour. of Sci* **265,** 177-210.

Richmond, G. M. (1960). Glaciation of the east slope of Rocky Mountain National Park, Colorado. *Geological Society of America Bulletin* **71,** 1371-1382.

Schaefer, J. M., Denton, G. H., Barrell, D. J. A., Ivy-Ochs, S., Kubik, P. W., Andersen, B. G., Phillips, F. M., Lowell, T. V., and Schluchter, C. (2006). Near-Synchronous Interhemispheric Termination of the Last Glacial Maximum in Mid-Latitudes. *Science* **312,** 1510-1513.

Schaefer, J. M., Denton, G. H., Kaplan, M., Putnam, A., Finkel, R. C., Barrell, D. J. A., Andersen, B. G., Schwartz, R., Mackintosh, A., Chinn, T., and Schluchter, C. (2009). High-frequency Holocene glacier fluctuations in New Zealand differ from the northern signature. *Science* **324,** 622-625.

Shakun, J. D., Clark, P. U., He, F., Liu, Z., Otto-Bleisner, B., Marcott, S. A., Mix, A. C., Schmittner, A., and Bard, E. (in review). CO2 forcing of global climate during the last deglaciation.

Stuiver, M., and Grootes, P. M. (2000). GISP2 oxygen isotope ratios. *Quaternary Research* **53,** 277-284.

Wagner, J. D. M., Cole, J. E., Beck, J. W., Patchett, P. J., Henderson, G. M., and Barnett, H. R. (2010). Moisture variability in the southwestern United States linked to abrupt glacial climate change. *Nature Geoscience* **3,** 110-113.

Whitlock, C., and Bartlein, P. J. (1997). Vegetation and climate change in northwest America during the past 125 kyr. *Nature* **388,** 57-61.

Chapter 4

A Reconstruction of Holocene Temperature

Shaun A. Marcott [1], Peter U. Clark [1], Jeremy D. Shakun [2], Alan C. Mix [3]

[1]Department of Geosciences, Oregon State University, Corvallis, OR 97331, USA

[2]Department of Earth Sciences, Boston University, Boston, MA, 02215, USA

[3]College of Oceanic and Atmospheric Sciences, Oregon State University, Corvallis, OR 97331, USA

To be submitted to Nature

4.1 Abstract

The global and northern hemispheric climate of the past 2000 years has been well documented in several temperature reconstructions (Esper et al., 2002; Moberg et al., 2005; Ammann and Wahl, 2007; Mann et al., 2008), which place modern climate change into a longer term perspective. By comparison, however, global temperature changes throughout the entire Holocene interglaciation remain poorly understood. Here we reconstruct a global temperature stack for the past 11,000 years from a globally distributed dataset with decadal-to-centennial resolution. We account for calibration and chronological uncertainties are accounted for using a Monte Carlo based approach. Our new reconstruction shows a general cooling trend of ~1°C since an early to mid Holocene temperature maximum, driven primarily by northern mid and high latitude records. Centennial and millennial scale variability is modest when compared to records from the last deglacial, but consistent with multi-centennial variability from reconstructions of the past 2000 years. The resolution of our reconstruction limits our ability to determine if the recent warming of the past few decades has reached maximum interglacial values; however, from model-based projections of 21st-century climate we infer that the mean global temperature will rise well above the warmest levels of the current interglaciation by 2100.

4.2 Introduction

Present and future global climate change is of great concern to society as well as governments agencies as they plan to mitigate emissions and adapt to climate change (Alley et al., 2007b). Placing present climate into a historical perspective beyond the instrumental record is thus important for distinguishing anthropogenic influences on climate from natural variability that inherently exists in the climate system (Jansen et al., 2007). Previous proxy based studies have reconstructed temperature changes of the last 2000 years and have shown that climate of the last few decades is likely anomalous compared to the past two millennia (Esper et al.,

2002; Moberg et al., 2005; Ammann and Wahl, 2007; Mann et al., 2008). However, a comparable global temperature reconstruction does not exist for the entirety of the present interglaciation (the Holocene, past 11,500 years). Reconstructing a complete Holocene temperature record represents a significant challenge for several reasons: most temperature reconstructions spanning the majority of the Holocene do not reliably go through the instrumental calibration period (A.D. 1850s-1990s) making it difficult to tie them directly to present climate; they are low resolution compared to annually and decadally resolved climate archives of the last 2000 years; and most have dating uncertainties greater than 100 years.

4.3 Results

Here we combine 73 proxy based temperature records from across the globe (Figure 4.1) and develop a globally stacked Holocene temperature reconstruction. The datasets that comprise this reconstruction are based on a number of paleoclimatic archives (Appendix C) with sampling resolutions ranging from 1 to 400 years. The records span the majority of the Holocene and are calibrated to temperature following established proxy based methods. Chronologic and temperature calibration uncertainty are both accounted for through a Monte Carlo based randomization scheme (see Methods). In order to compare our globally stacked record directly with modern climatology, we mean shift our temperature record to a common period of overlap with a reconstruction for the past 2000 years (Mann et al., 2008) (Figure 4.2), which is itself reported as an anomaly from the A.D. 1961-1990 period and is cross validated with the Climate Research Unit (University of East Anglia) instrumental surface-air temperature dataset (Brohan et al., 2006). Shifting the mean of our record to that of Mann et al. (2008), preserves the general shape of the temperature anomaly time series and acts to quantify the temperature anomalies from a different reference point (i.e. 4,500-5,500 yr BP vs. A.D. 1960-1990).

Our reconstruction shows a warming of ~0.6°C from the early Holocene, 11,000 yr BP, to a mid Holocene temperature plateau extending from 5,500 – 9,500

yr BP. This temperature plateau is followed by a long-term cooling trend of 0.6 – 1.0°C until 200 yr BP (Figure 4.2). Multi centennial variability is generally modest in our reconstructions and no apparent underlying multi-millennial scale oscillation exists in the temperature stack as has been previously demonstrated in records from the North Atlantic (Bond, 1997). However, some structure does exist, notably a warm interval centered at approximately 1200 yr BP possibly associated with the Medieval Climate Anomaly (Bradley et al., 2003), and a cool period centered at 250 yr BP referred to as the Little Ice Age (LIA) (Matthes, 1942). At the multi-centennial scale, our temperature reconstruction is in excellent agreement with the global CRU-EIV composite mean temperature of Mann et al. (2008) for the last 1500 years, and within our temperature uncertainties they are indistinguishable (Figure 4.2 a-b). The difference between our two methods of reconstructing the temperature time series is most apparent for the last 500 years where the RegEM algorithm (Schneider, 2001) has infilled a significant portion of the absent data points, which likely explains the ~0.2°C difference. Over the remaining portion of the Holocene our two methods replicate one another very well (Figure 4.2 c-d) making reference to either interchangeable.

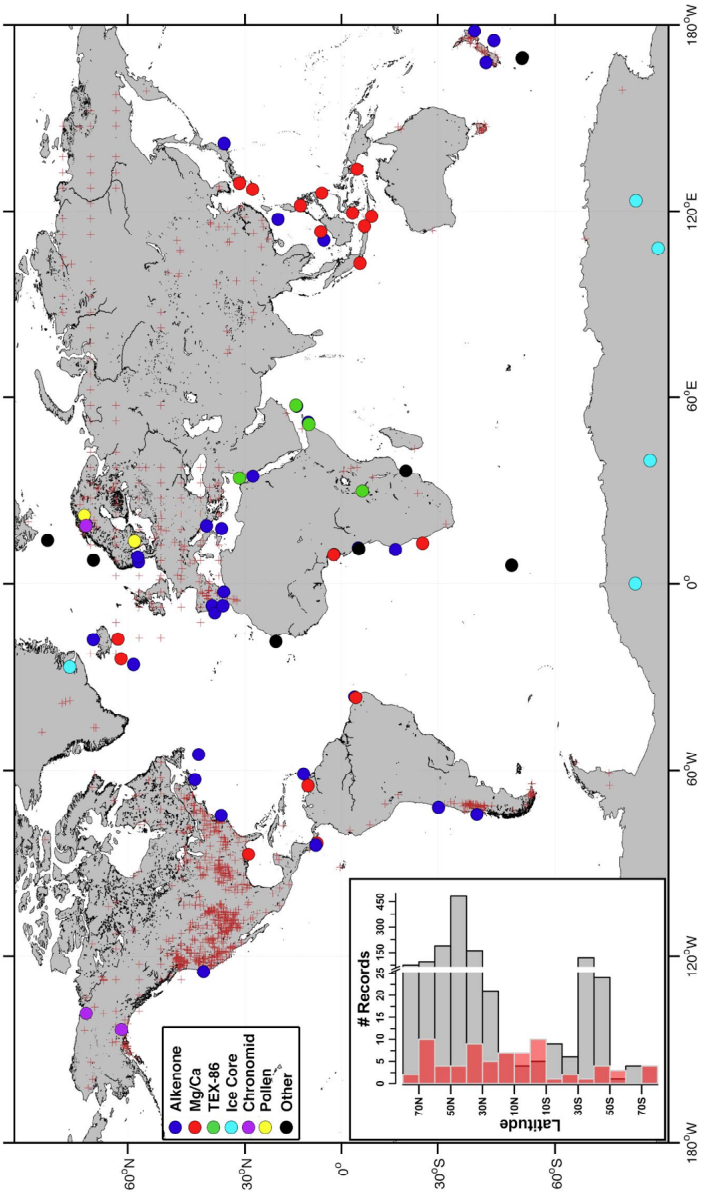

Figure 4.1. Location map and latitudinal distribution of proxy based temperature datasets.

Map of temperature datasets from this study separated by temperature proxy (dots) and datasets used in Mann et al. (2008) (crosses). (Inset) Latitudinal distribution of data from this study (red) and Mann et al. (2008) (gray). Note break in y-axis at 25.

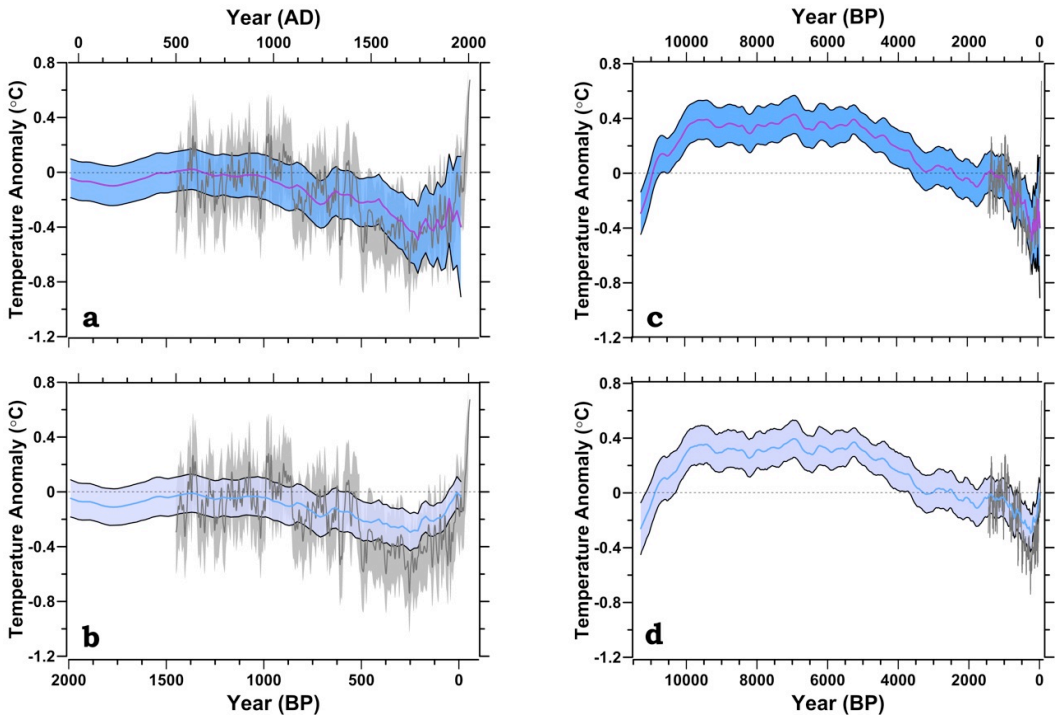

Figure 4.2. Time series of globally stacked temperature anomalies.
a, Mean of globally stacked temperature anomalies for arithmetic mean calculation (purple) with 1σ error (blue band) and Mann et al.'s (2008) global CRU-EIV composite mean temperature (dark gray) with error (light gray) for last two millennia. **b,** Mean of globally stacked temperature records for the RegEM (Schneider, 2001) calculation with 2σ error (purple band) and Mann et al.'s (2008) global CRU-EIV composite mean temperature with error (Mann et al., 2008). **c, d,** Same as a and b but extended through the last 11,300 years. Note that the error of Mann et al. (2008) was removed for clarity. Mean temperature values for the globally stacked temperature records have been mean shifted by +0.3°C to match Mann et al. (2008) for a common period of overlap (490-1450 yr BP).

To test the reproducibility of our two methods for reconstructing the temperature stack, we experimented with various ways of calculating the globally stacked temperature anomalies (Figure 4.3 a,e). We divided the records into 10° latitudinal bins and weighted them by their cosine of latitude to test the sensitivity of our datasets being skewed toward the northern hemisphere. A jack-knife technique, where for each of the Monte Carlo simulations 50% of the records were randomly excluded, was also implemented to determine the sensitivity of the global stack to any one record or group of records. While some differences exist at the centennial scale amongst the various methods (Figure 4.3 a), they are very small (<0.2°C) for most of the reconstruction, well within the uncertainties of our stacked temperature record, and do not affect the long-term trend in the reconstruction, demonstrating the robustness of our record at the multi-centennial and multi-millennial scale.

4.4 Discussion

Our temperature reconstruction of the last 2000 years is in general agreement with prior work at the centennial and millennial time scale (Huang, 2004; Moberg et al., 2005; Ammann and Wahl, 2007; Mann et al., 2008) (Figure 4.3 b,f). A common concern with most paleoclimate reconstructions of the last 2000 years has been that at the 100- to 1000-year frequencies climate archives, such as tree rings, do not accurately capture the long-term variability in the climate system (von Storch et al., 2004). Based on the agreement between our low-resolution global temperature stack and the higher-resolution data, we find that prior temperature reconstructions of the last two millennia do well at capturing climate variability at the lower-frequencies. This is consistent with prior studies that addressed this problem, albeit with datasets that were much more temporally limited than ours (Moberg et al., 2005; Wahl et al., 2006; Mann et al., 2007; Wahl and Ammann, 2007).

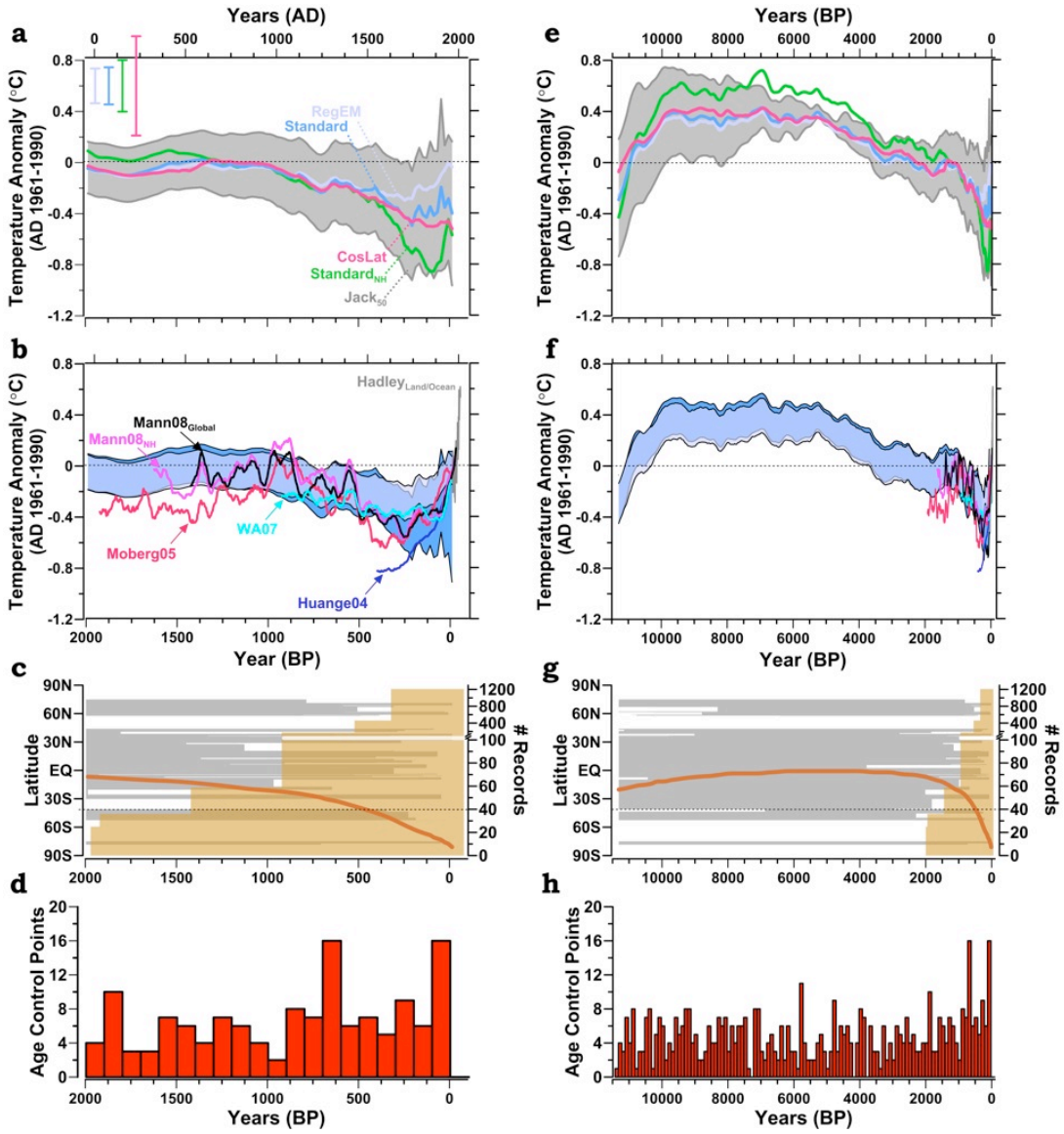

Figure 4.3. Comparison of different methods and reconstructions of global and hemispheric temperature anomalies.

a, Mean values of our global and hemispheric temperature anomalies using several methods (Standard – Arithmetic mean calculation; $Standard_{NH}$ – Arithmetic mean calculation of Northern Hemisphere records only; CosLat – Arithmetic mean calculation, cosine of latitude weighted; RegEM – Mean calculation using RegEM). The gray shading ($Jack_{50}$) represents the 1σ band when randomly leaving 50% of the

records out during each Monte Carlo mean calculation. **b,** Published temperature anomaly reconstructions that have been smoothed with a 51 point running average, $Mann08_{Global}$ (Mann et al., 2008), $Mann08_{NH}$ (Mann et al., 2008), Moberg05 (Moberg et al., 2005), WA07 (Ammann and Wahl, 2007), Huange04 (Huang, 2004), $Hadley_{Land/Ocean}$ (Brohan et al., 2006), and plotted with our global temperature stacks (Blue/Purple bands same as in Figure 4.2). The temperature anomalies for all the records are referenced to the 1961-1990 instrumental period from Mann et al. (2008). **c,** Number of records used to construct the global temperature stack through time for our reconstruction (orange line) and Mann et al. (2008) (gold bars). Note y-axis break at 100. Latitudinal distribution of our records (gray bars) through time. **d,** Number of age control points (e.g. ^{14}C dates) that constrain the time series through time. **e-h,** Same as **a-d** but extended through the last 11,300 years.

The agreement among our temperature reconstruction and others of the last 2000 years (Figure 4.3 b) demonstrates the fidelity of our record and provides confidence that we are replicating the global temperature throughout the entire Holocene interglacial (Figure 4.3 f). Based on our globally stacked temperature reconstruction, we conclude that temperatures of the last few decades are 'likely' (Moss and Schneider, 2000; Manning et al., 2004) anomalous compared to the present interglacial period. Mean annual global temperature in the next two decades will be ~1°C higher than pre-industrial values and by A.D. 2100 it will increase by another degree (Meehl et al., 2007). Assuming a business-as-usual progression of future greenhouse gas emissions, this will 'very likely' (Moss and Schneider, 2000) place modern climate outside the natural variability of the present interglacial in the next few decades and is 'virtually certain' to place it outside by the end of the century. Additionally, we find no evidence that present global warming is part of a longer period millennial oscillation not captured in the shorter temperature reconstruction of the last two millennia, and we demonstrate good agreement between our low-resolution, longer term record with the high-resolution, shorter term records over the period of overlap (Mann et al., 2008). This work highlights the anomalousness of present climate change by putting it in a full Holocene perspective, emphasizing the concerns already addressed in the last report by the IPCC (Solomon et al., 2007).

4.5 Methods

4.5.1 Temperature and Chronologic Uncertainties

In order to incorporate the full range of error associated with both the proxy calibrated temperatures and the age control points used to construct the time series, we implemented a Monte Carlo based approach. 10,000 Monte Carlo simulations were performed for each of the datasets that incorporated both the temperature calibration and chronologic uncertainties (Appendix C). The temperature records

used in this study were derived from multiple proxy-based methods, including $U^{K'}_{37}$, TEX_{86}, Mg/Ca, chronomids, pollen, ice cores, and biomass assemblages (e.g., foraminifera, diatoms, radiolaria). The uncertainty associated with each of the proxies was randomly varied following a normal distribution and errors were assumed to not correlate through time in order to maximize the temperature uncertainties. All $U^{K'}_{37}$ based alkenone records were converted to temperature following the global core top calibration of Müller et al. (1998). TEX_{86}, Mg/Ca, and all biomass assemblage records were converted to temperature following the original publication from where the data were obtained (Apendix C). Chronomid based temperatures errors (±1.7°C) were derived from the average root mean squared error (RMSE) of several studies. Pollen temperature errors followed the RMSE of Seppä et al. (2005) (±1.7°C). Ice core based temperature error was conservatively assumed to be ±30%.

Chronologic errors were accounted for by varying the 543 age control points (e.g. calibrated ^{14}C date) within their uncertainty and by allowing error between age control points to follow a random walk, after Huybers and Wunch (2004), with a jitter (J) value of 200. Chronologic error was assumed to be autocorrelated and was modeled as a first order autoregressive process. All radiocarbon based ages were recalibrated with CALIB 6.0.1 using INTCAL09 and its protocol (Reimer, 2009) for the site-specific locations and materials. Marine reservoir ages were taken from the originally published manuscripts. Ice core chronologic uncertainty was assumed to be ±1% for Greenland and ±2% for Antarctica.

4.5.2 Globally Stacked Temperature Calculation

To calculate the global temperature stack from the 73 records, each record was linearly interpolated to a common time step of 20 years. While the majority of the records have a sampling resolution of >100 years, 20 years was chosen in order to capture the majority of the variability in both the low and high resolution records.

However, our temperature stack only can be used to address changes at the low frequency (>100 yrs) because of the resolution of the datasets that comprise the global stack and therefore cannot be used to compare with the annual and decadal variability of higher-frequency records. All of the datasets were originally converted to temperature anomalies from the mean temperature value between 4500-5500 yrs BP, which is the common period of overlap for all of the records. The temperature records for each of the 10,000 Monte Carlo simulations were globally stacked using two methods: a simple arithmetic mean calculation and a data infilling regularized expectation maximization algorithm (RegEM) (Schneider, 2001) for constructing complete time series with missing values. For the RegEM method, we did not modify the original code and applied the default values and methods (Schneider, 2001).

4.6 Acknowledgements

Discussions with multiple individuals helped improve the quality of this work. We thank E.J. Brook, V. Erserk, S.W. Hostetler, and N.G. Pisias for providing invaluable insight and helpful discussion. The excellent datasets graciously provided by T. Barrows, J.-H. Kim, Y. Kubota, I. Larocque, G. Leduc, M. McGlone, T. Rodrigues, C. Rühlemann, J. Sachs, R. Schneider, H. Seppä, J. Tierney, M. Yamamoto, B. Vinther, and C. Waelbrock, as well as the datasets compiled from the NOAA NGDC and PANGAEA databases, made this research possible. Funding for this work was provided by the NSF Paleoclimate Program for the Paleovar Project.

4.7 References

Alley, R. B., Berntsen, T., Bindoff, N. L., Chen, Z., Chidthaisong, A., Friedlingstein, P., Gregory, J. M., Hegerl, G. C., Heimann, M., Hewitson, B., Hoskins, B. J., Joos, F., Jouzel, J., Kattsov, V., Lohmann, U., Manning, M., Matsuno, T., Molina, M., Nicholls, N., Overpeck, J., Qin, D., Raga, G., Ramaswamy, V., Ren, J., Rusticucci, M., Solomon, S., Somerville, R., Stocker, T. F., Stott, P. A., Stouffer, R. J., Whetton,

P., Wood, R. A., and Wratt, D. (2007b). Summary for Policymakers. *In* "Climate Change 2007: The Physical Science Basis. Contribution of Working Group I to the Fourth Assessment Report of the Intergovernmental Panel on Climate Change." (S. Solomon, D. Qin, M. Manning, Z. Chen, M. Marquis, K. B. Averyt, M. Tignor, and H. L. Miller, Eds.). Cambridge University Press, Cambridge.

Ammann, C. M., and Wahl, E. R. (2007). The importance of the geophysical context in statistical evaluations of climate reconstruction procedures. *Climate Change* **85,** 71-88.

Bond, G. (1997). A pervasive millennial-scale cycle in North Atlantic Holocene and Glacial climates. *Science* **278,** 1257-1266.

Bradley, R. S., Hughes, M. K., and Diaz, H. F. (2003). Climate in Medieval Time. *Science* **302,** 404-405.

Brohan, P., Kennedy, J. J., Haris, I., Tett, S. F. B., and Jones, P. D. (2006). Uncertainty estimates in regional and global observed temperature changes: A new dataset from 1850. *Journal of Geophysical Research* **111,** D12106, doi:10.1029/2005JD006548

Esper, J., Cook, E. R., and Schweingruber, F. H. (2002). Low-Frequency Signals in Long Tree-Ring Chronologies for Reconstructing Past Temperature Variability. *Science* **295,** 2250-2253.

Huang, S. (2004). Merging information from different resources for new insights into climate change in the past and future. *Geophysical Research Letters* **31,** L13205, doi:10.1029/2004GL019781.

Huybers, P., and Wunch, C. (2004). A depth-derived Pleistocene age model: Uncertainty estimates, sedimentation variability, and nonlinear climate change. *Paleoceanography* **19,** PA1028, doi:10.1029/2002PA000857.

Jansen, E., Overpeck, J., Briffa, K. R., Duplessy, J.-C., Joos, F., Masson-Delmotte, V., Olago, D., Otto-Bliesner, B. L., Peltier, W. R., Rahmstorf, S., Ramesh, R., Raynaud, D., Rind, D., Solomina, O., Villalba, R., and Zhang, D. (2007). Paleoclimate. *In* "Climate Change 2007: The Physical Science Basis. Contribution of Working Group I to the Fourth Assessment Report of the Intergovernmental Panel on Climate Change." (S. Solomon, D. Qin, M. Manning, Z. Chen, M. Marquis, K. B. Averyt, M. Tignor, and H. L. Miller, Eds.). Cambridge University Press, Cambridge.

Mann, M. E., Rutherford, S., Wahl, E., and Ammann, C. (2007). Robustness of proxy-based climate field reconstruction methods. *Journal of Geophysical Research* **112,** D12109, doi: 10.1029/2006JD008272.

Mann, M. E., Zhang, Z., Hughes, M. K., Bradley, R. S., Miller, S. K., Rutherford, S., and Ni, F. (2008). Proxy-based reconstructions of hemispheric and global surface temperature variations over the past two millennia. *Proceedings of the National Academy of Sciences* **105,** 13252-13257.

Manning, M. R., Petit, M., Easterling, D., Murphy, J., Patwardhan, A., Rogner, H.-H., Swart, R., and Yohe, G. (2004). *In* "IPCC Workshop on Describing Scientific Uncertainties in Climate Change to Support Analysis of Risk and of Options: Workshop report." Intergovernmental Panel on Climate Change, Geneva.

Matthes, F. E. (1942). Report of Committee on Glaciers, 1941-1942. *Amer. Geophys. Union Trans.* **23,** 374-392.

Meehl, G. A., Stocker, T. F., Collins, W. D., Friedlingstein, P., Gaye, A. T., Gregory, J. M., Kitoch, A., Knutti, R., Murphy, J. M., Noda, A., Raper, S. C. B., Watterson, I. G., Weaver, A. J., and Zhao, Z.-C. (2007). Global Climate Projections. *In* "Climate Change 2007: The Physical Science Basis. Contribution of Working Group I to the Fourth Assessment Report of the Intergovernmental Panel on Climate Change." (S.

Solomon, D. Qin, M. Manning, Z. Chen, M. Marquis, K. B. Averyt, M. Tignor, and H. L. Miller, Eds.). Cambridge University Press, Cambridge.

Moberg, A., Sonechkin, D. M., Holmgren, K., Datsenko, N. M., Karlén, W., and Laureitzen, S. E. (2005). Highly variable Northern Hemisphere temperatures reconstructed from low- and high-resolution proxy data. *Nature* **433,** 613-617.

Moss, R., and Schneider, S. (2000). Uncertainties, in Guidance Papers on the Cross Cutting Issues of the Third Assessment Reprot of the IPCC. *In* "Intergovernmental Panel on Climate Change (IPCC)." (R. Pachauri, T. Taniguchi, and K. Tanaka, Eds.), Geneva.

Müller, P. J., Kirst, G., Ruthland, G., von Storch, I., and Rosell-Melé, A. (1998). Calibration of the alkenone paleotemperature index UK'37 based on core-tops from the eastern South Atlantic and the global ocean (60N-60S). *Geochimica et Cosmochimica Acta* **62,** 1757-1772.

Reimer, P. J., Baillie, M. G. L., Bard, E., Bayliss, A., Beck, J. W., Blackwell, P. G., Bronk Ramsey, C., Buck, C. E., Burr, G. S., Edwards, R. L., Friedrich, M., Grootes, P. M., Guilderson, T. P., Hajdas, I., Heaton, T. J., Hogg, A. G., Hughen, K. A., Kaiser, K. F., Kromer, B., McCormac, F. G., Manning, S. W., Reimer, R. W., Richards, D. A., Southon, J. R., Talamo, S., Turney, C. S. M., van der Plicht, J., and Weyhenmeyer, C.E. (2009). INTCAL 09 and MARINE09 radiocarbon age calibration curves, 0-50,000 years Cal BP. *Radiocarbon* **51,** 1111-1150.

Schneider, T. (2001). Analysis of incomplete climate data: Estimation of mean values and covariance matrices and imputation of missing values. *Journal of Climate* **14,** 853-871.

Seppä, H., Hammarlund, D., and Antonsson, K. (2005). Low-frequency and high-frequency changes in temperature and effective humidity during the Holocene in

south-central Sweden: implications for atmospheric and oceanic forcings of climate. *Climate Dynamics* **25,** 285-297.

Solomon, S., Qin, D., Manning, M., Chen, Z., Marquis, M., Averyt, K. B., Tignor, M., and Miller, H. L. (2007). Contribution of Working Group II to the Fourth Assessment Report of the Intergovernmental Panel on Climate Change, 2007. *In* "Contribution of Working Group II to the Fourth Assessment Report of the Intergovernmental Panel on Climate Change, 2007." Cambridge University Press, New York.

von Storch, H., Zorita, E., Jone, J. M., Dimitriev, Y., González-Rouco, F., and Tett, S. F. B. (2004). Reconstructing past climate from noisy data. *Science* **306,** 679-682.

Wahl, E. R., and Ammann, C. M. (2007). Robustness of the Mann, Bradley, Hughes reconstruction of Northern Hemisphere surface temperatures: Examination of criticisms based on the nature and processing of proxy climate evidence. *Climate Change* **85,** 33-69.

Wahl, E. R., Ritson, D. M., and Ammann, C. M. (2006). Comment on "Reconstructing Past Climate from Noisy Data". *Science* **312,** 529b.

Chapter 5

Conclusions

This dissertation is a compilation of three studies that address major scientific questions in glacial geology and paleoclimatology for the late Pleistocene and Holocene using geochemical and statistical techniques. Each of the studies addresses longstanding questions in the field of paleoclimatology using geochemical and/or statistical methods.

5.1 Chapter Summaries

Chapter 2 uses temperature sensitive chemical tracers in benthic foraminifera and climate and ice shelf modeling results to explore the interplay between climate, oceans, and ice sheets over the past 60 kyr in the North Atlantic. The study also addresses the mechanism associated with the episodic iceberg-discharge events from the Hudson Strait Ice Stream (HSIS) of the Laurentide Ice Sheet, commonly referred to as Heinrich events. The data and model results indicate that basin-wide subsurface warming occurred in the North Atlantic in response to a reduction in the AMOC prior to Heinrich events, and that Heinrich events did not occur until the AMOC was at its weakest and subsurface temperatures were near their maximum values. It was also found that the open-ocean subsurface warming significantly increases the rate of mass loss from the ice shelf fronting the HSIS. The results thus support simplified climate modeling results suggesting that a weakened or collapsed ice shelf would trigger an ice-stream surge, producing a Heinrich event (Shaffer et al., 2004; Alvarez-Solas et al., 2010), analogous to the recent response of Antarctic glaciers to the loss of buttressing ice shelves (Rignot et al., 2004). By providing evidence of the significance that subsurface warming played in triggering past ice-sheet instabilities,

the results provide important insights into possible future behavior of similarly configured Antarctic ice-sheet sectors, should warmer waters penetrate beneath their large, buttressing ice shelves.

In Chapter 3, the timing of alpine glacial advances in western North America during the late Pleistocene and Holocene is reconstructed to provide insight into the spatial pattern of climate change in western North America. Based on 124 ^{10}Be ages from twenty cirque moraines in ten mountain ranges across western North America, Holocene glacial advances culminated sometime during the Little Ice Age and not during multiple intervals throughout the interglacial as previously purported. It also supports evidence that latest Pleistocene advances in western North America were regionally variable, but that the general pattern of glaciation followed high latitude forcings from the North Atlantic. This new ^{10}Be glacial chronology requires a refined interpretation of Holocene glacial activity in western North America and the associated climate forcing. While alpine glaciers may have continued to fluctuate during the Holocene, they never advanced beyond their Little Ice Age maximum. Instead, cirque glacier activity in western North America has followed in near step with late Pleistocene high latitude climate and the associated forcing, emphasizing their utility in deriving climate information.

In Chapter 4, a globally distributed dataset of 73 proxy based temperature records that span the Holocene were compiled and averaged together to evaluate the global and hemispheric climate changes of the last 10,000 years. Statistical techniques were also applied to the dataset to account for chronologic and temperature calibration uncertainties using a Monte Carlo based approach. Based on a global temperature stack for the past 11,000 years, a general cooling trend of ~1°C since an early to mid Holocene temperature maximum was defined, driven primarily by northern mid and high latitude records. Centennial and millennial scale variability was modest when compared to records from the last deglacial, but consistent with most multi-centennial variability from reconstructions of the past 2000 years. Based on the study, recent warming of the past few decades has reached near maximum

interglacial values and has 'likely' (Moss and Schneider, 2000; Manning et al., 2004) exceeded them within the 1σ uncertainty band. Based on future projections provided by the most recent IPCC report (Meehl et al., 2007) global mean temperatures will rise well above the warmest levels of the current interglacial by 2100 and possibly within a matter of decades. Additionally, no evidence is found that present global warming is part of a longer period millennial oscillation not captured in the shorter temperature reconstruction of the last two millennia, and it is demonstrated that good agreement exist between this low-resolution, longer term record and the high-resolution, shorter term records over the period of overlap (Mann et al., 2008). This study highlights the anomalousness of present climate change by putting it in a full Holocene perspective, emphasizing the concerns already addressed in the last report by the IPCC (Solomon et al., 2007).

5.2 References

Alvarez-Solas, J., Charbit, S., Ritz, C., Paillard, D., Ramstein, G., and Dumas, C. (2010). Links between ocean temperature and iceberg discharge during Heinrich events. *Nature Geoscience* **3,** 122-126.

Mann, M. E., Zhang, Z., Hughes, M. K., Bradley, R. S., Miller, S. K., Rutherford, S., and Ni, F. (2008). Proxy-based reconstructions of hemispheric and global surface temperature variations over the past two millennia. *Proceedings of the National Academy of Sciences* **105,** 13252-13257.

Manning, M. R., Petit, M., Easterling, D., Murphy, J., Patwardhan, A., Rogner, H.-H., Swart, R., and Yohe, G. (2004). *In* "IPCC Workshop on Describing Scientific Uncertainties in Climate Change to Support Analysis of Risk and of Options: Workshop report." Intergovernmental Panel on Climate Change, Geneva.

Meehl, G. A., Stocker, T. F., Collins, W. D., Friedlingstein, P., Gaye, A. T., Gregory, J. M., Kitoch, A., Knutti, R., Murphy, J. M., Noda, A., Raper, S. C. B., Watterson, I.

G., Weaver, A. J., and Zhao, Z.-C. (2007). Global Climate Projections. *In* "Climate Change 2007: The Physical Science Basis. Contribution of Working Group I to the Fourth Assessment Report of the Intergovernmental Panel on Climate Change." (S. Solomon, D. Qin, M. Manning, Z. Chen, M. Marquis, K. B. Averyt, M. Tignor, and H. L. Miller, Eds.). Cambridge University Press, Cambridge.

Moss, R., and Schneider, S. (2000). Uncertainties, in Guidance Papers on the Cross Cutting Issues of the Third Assessment Reprot of the IPCC. *In* "Intergovernmental Panel on Climate Change (IPCC)." (R. Pachauri, T. Taniguchi, and K. Tanaka, Eds.), Geneva.

Rignot, E., Casassa, G., P., G., Krabill, W., Rivera, A., and Thomas, A. (2004). Accelerated ice discharge from the Antarctic Peninsula following the collapse of Larsen B ice shelf. *Geophysical Research Letters* **31,** doi:10.1029/2004GL020697.

Shaffer, G., Olsen, S. M., and Bjerrum, C. J. (2004). Ocean subsurface warming as a mechanism for coupling Dansgaard-Oeschger climate cycles and ice-rafting events. *Geophysical Research Letters* **31,** L24202, doi:10.1029/2004GL020968.

Solomon, S., Qin, D., Manning, M., Chen, Z., Marquis, M., Averyt, K. B., Tignor, M., and Miller, H. L. (2007). Contribution of Working Group II to the Fourth Assessment Report of the Intergovernmental Panel on Climate Change, 2007. *In* "Contribution of Working Group II to the Fourth Assessment Report of the Intergovernmental Panel on Climate Change, 2007." Cambridge University Press, New York.

Appendices

Appendix A - Ice-shelf collapse from subsurface warming as a trigger for Heinrich events

A.1 Mg/Ca measurements

Only three species in our core have Mg/Ca temperature calibrations (*Melonis barleeanum*, *Cibicidoides lobatulus,* and *Cibicidoides spp.*), and these species only occurred in sufficient numbers for measurements to bracket the four Heinrich events H1, H3, H5a, H6. Moreover, because the species composition varies downcore, no one species was always available for each depth. At 15 depths, however, we replicated multi-species Mg/Ca measurements, of which 13 replicate at 1σ and the other two replicate at 2σ (Table A1). Mg/Ca ratios (mmol/mol) were converted to bottom water temperatures (BWT) using calibrations developed in the North Atlantic Ocean near Iceland for *M. barleeanum* (Kristjánsdóttir et al., 2007) [Mg/Ca = 0.658 * exp(0.137 * BWT)] and *C. lobatulus* (Quillman et al., 2008) (Mg/Ca = 1.10 + 0.129 * BWT). Mg/Ca ratios were converted to BWT for *Cibicidoides spp.* [Mg/Ca = 0.90 * exp(0.11 * BWT)] using a global calibration (Elderfield et al., 2006). The automated flow-through system has an average standard deviation of 0.08 mmol/mol for duplicate Mg/Ca samples (Klinkhammer et al., 2004); combined with the temperature calibration error for the individual benthic species (Elderfield et al., 2006; Kristjánsdóttir et al., 2007; Quillman et al., 2008) the range of propagated uncertainty is 1.0 – 1.5 °C. Our Mg/Ca BWT error (~1.3°C) is in agreement with previous work where replicate foraminifera analysis, species calibration and the carbonate ion ($[CO_3^{2-}]$) effect uncertainties are considered (Lear et al., 2002; Kristjánsdóttir et al., 2007; Quillman et al., 2008).

We measured 111 samples from core EW9302-2JPC and 20 samples from core MD95-2010 (Tables A1, A2). We also made Mg/Ca measurements on two core-top samples, one on *Cibicidoides* spp. and one on *M. barleeanum*. Based on 17 hydrographic profiles within 50 km of our core, the range of BWT for depths 1000-

1500 m is 3.29-3.86 (3.43 $\pm$ 0.28 at 2σ) °C. Our core-top measurements are 4.9 $\pm$ 2.6 and 6.3 $\pm$ 2.6 °C (2σ), which overlap at 2σ. Based on the existing age model, however, it is unlikely that the core top is modern; extrapolating our age model from the two youngest age constraints (Vedde Ash (=12.2 ka) at 16 cm, calibrated ^{14}C age (=16.9 ka) at 32 cm) would suggest the core top sample (1.5 cm) is ~7.5 ka.

A.2 Age Model

The age model for EW9302-2JPC is based on previously published ^{14}C dates, tephra layers at 16 cm (Vedde Ash) and 408 cm depth (ASH II), and tie points at 496 cm (peak of H6) to the age of peak of H6 determined by correlation to Greenland ice cores (Stoner et al., 2000) and at 544 cm depth to the age of the marine isotope stage 5/4 boundary (Rasmussen et al., 2003) (Table A3). The age model for MD95-2010 is based on previously published ^{14}C dates (Dokken and Jansen, 1999) that were recalibrated using Calib 6.0 (Hughen et al., 2004) (Table A2).

Table A1. Mg/Ca data for core EW9302-2JPC.

Subsampling for Mg/Ca measurements was done in 1cm intervals.

Depth (cm) Midpoint	Age (yrs)	Mg/Ca (mmol/mol)	Species
1.5	0	1.798	Cib. Spp
1.5	0	1.283	M.barl.
12.5	11208	1.321	Cib. Spp
18.5	12954	1.556	Cib. Spp
20.5	13536	1.491	Cib. Lobt
20.5	13536	0.924	M. barl
22.5	14118	1.403	Cib. Spp
22.5	14118	1.306	M. barl
24.5	14700	1.599	Cib. Spp
26.5	15282	1.776	Cib. Spp
28.5	15864	1.476	Cib. Spp
30.5	16446	1.573	Cib. Spp
32.5	16935	1.446	Cib. Spp
34.5	17148	1.467	Cib. Spp
38.5	17573	1.299	Cib. Spp
40.5	17786	1.427	Cib. Spp
42.5	17999	0.985	Cib. Spp
44.5	18212	1.238	Cib. Lobt
46.5	18424	1.447	Cib. Spp
50.5	18850	1.303	Cib. Spp
56.5	19488	0.943	Cib. Spp
58.5	19701	1.611	Cib. Lobt
61.5	20020	1.073	Cib. Lobt
64.5	20309	1.683	Cib. Lobt
68.5	20494	0.772	M.barl.
71.5	20632	1.385	Cib. Lobt
78.5	20955	1.518	Cib. Lobt
78.5	20955	1.123	M.barl.
203.5	29245	1.149	Cib. Lobt
203.5	29245	1.135	M. barl
205.5	29351	1.241	M. barl
209.5	29563	1.109	M. barl
213.5	29775	1.056	M. barl
221.5	30199	1.086	M. barl
233.5	30835	1.842	Cib. Spp

235.5	30941	1.69	Cib. Spp
245.5	31789	1.076	M. barl
249.5	32232	1.613	Cib. Spp
249.5	32232	1.179	M. barl
255.5	32897	1.055	M.barl.
256	32952	1.93	M.barl.
257.5	33118	1.013	M.barl.
259.5	33340	1.203	M. barl
261.5	33561	1.175	M.barl.
263.5	33783	1.065	M. barl
265.5	34004	1.05	M. barl
271.5	34669	1.061	M. barl
277.5	35333	0.963	M. barl
279.5	35555	1.009	M. barl
280	35610	1.17	M.barl.
285.5	36219	0.894	M. barl
325.5	40649	1.89	Cib. Lobt
327.5	40871	1.194	Cib. Lobt
328	40926	1.36	Cib. Lobt
335.5	41757	1.258	Cib. Lobt
351.5	44694	1.462	Cib. Lobt
357.5	45810	1.951	Cib. Spp
359.5	46182	1.503	Cib. Lobt
363.5	46925	1.339	Cib. Lobt
377.5	49529	1.555	Cib. Lobt
381.5	50272	1.387	Cib. Lobt
383.5	50644	1.602	Cib. Lobt
391.5	52132	1.598	Cib. Lobt
392	52225	1.66	Cib. Lobt
393.5	52504	1.557	Cib. Spp
395.5	52876	1.375	Cib. Spp
399.5	53619	1.521	Cib. Lobt
402.5	54177	1.356	Cib. Spp
405.5	54735	2.307	Cib. Lobt
405.5	54735	1.791	Cib. Lobt
405.5	54735	1.082	M.barl.
409.5	55273	1.467	Cib. Lobt
415.5	55566	1.645	Cib. Lobt
415.5	55566	1.0175	M. barl
419.5	55762	1.7	Cib. Lobt
423.5	55957	1.458	Cib. Lobt

424	55982	1.45	Cib. Lobt
429.5	56251	0.816	M. barl
435.5	56544	0.895	M. barl
441.5	56837	1.218	Cib. Lobt
441.5	56837	1.076	M.barl.
445.5	57032	1.446	Cib. Lobt
451.5	57326	1.335	Cib. Lobt
451.5	57326	0.875	M. barl
459.5	57716	0.951	M. barl
463.5	57912	0.883	M. barl
467.5	58107	1.079	M. barl
493.5	59378	1.766	Cib. Lobt
497.5	59953	1.777	Cib. Lobt
501.5	61161	2.223	Cib. Lobt
503.5	61766	1.902	Cib. Lobt
507.5	62974	2.016	Cib. Lobt
511.5	64182	1.685	Cib. Lobt
513.5	64786	1.838	Cib. Lobt
515.5	65391	1.88	Cib. Lobt
517.5	65995	1.94	Cib. Lobt
523.5	67807	1.65	Cib. Lobt
525.5	68411	1.354	M. barl
531.5	70224	1.012	M.barl.
533.5	70828	1.915	Cib. Lobt
533.5	70828	1.976	M.barl.
535.5	71432	1.336	M.barl.
537.5	72036	1.145	M.barl.
539.5	72641	1.514	M.barl.
541.5	73245	1.107	M.barl.
543.5	73849	1.609	Cib. Lobt
543.5	73849	1.295	M.barl.
545.5	74453	1.551	Cib. Lobt
545.5	74453	1.159	M.barl.
547.5	75057	1.289	Cib. Lobt
547.5	75057	1.11	M.barl.
549.5	75662	2.085	Cib. Lobt
549.5	75662	1.603	M.barl.

Table A2. Data for core MD95-2010.

Subsampling for Mg/Ca measurements was done in 1cm intervals except where indicated.

Depth (cm) Midpoint	Age (yrs)	Mg/Ca (mmol/mol)	Species	BWT (deg C)	Notes
54.5	***12549***	-	-	-	Calibrated ^{14}C Age
123.5	14236	1.22	M.barl.	4.505	
129.5	14382	1.549	M.barl.	6.249	
133.5	14479	1.128	M.barl.	3.934	
134.5	14504	1.149	M.barl.	4.069	
134.5	14504	1.62	Cib Lobat	4.031	
136.5	***14540***	-	-	-	Calibrated ^{14}C Age
146.5	15242	1.96	Cib.spp	7.075	
156.5	15911	2.758	Cib Lobat	12.853	
159	16079	2.828	M.barl.	10.643	Sample interval: 158-160cm
161.5	16246	2.95	Cib Lobat	14.341	
173.5	***17015***	-	-	-	Calibrated ^{14}C Age
192.5	17841	2.457	M.barl.	9.617	
197.5	***18032***	-	-	-	Calibrated ^{14}C Age
199.5	18063	1.726	M.barl.	7.039	
202.5	18100	1.684	M.barl.	6.859	
204.5	18125	1.54	M.barl.	6.207	
206.5	18150	1.557	M.barl.	6.287	
209	18181	1.535	M.barl.	6.183	Sample interval: 208-210cm
213	18231	1.787	M.barl.	7.293	Sample interval: 212-214cm
226.5	18399	3.673	Cib Lobat		Suspect value; not included
227	18405	1.922	M.barl.	7.824	Sample interval: 226-228cm
233	18479	1.419	M.barl.	5.61	Sample interval: 232-234cm
246	18641	1.814	M.barl.	7.402	Sample interval: 245-247cm
251	18703	1.725	M.barl.	7.035	Sample interval: 250-252cm

300.5	***19312***	-	-	-	Calibrated ^{14}C Age

A.3 Ice-rafted debris

Because the resolution (8 cm) of the original published detrital carbonate (DC) record from core EW9302-2JPC (Rasmussen et al., 2003) is at a lower resolution than our temperature data, we generated new DC data for the Heinrich layers where we have temperature data from Mg/Ca. We duplicated the original counting protocols and then counted DC from several of the original intervals to demonstrate replication (Figure A1).

A.4 Oxygen Isotopes

We made six new $\delta^{18}O$ measurements on *C.lobatulus*, *C.wuellerstorfi* (each with 0.64 per mil correction for fractionation) and *M. barleeanum* (0.4 per mil correction) from core EW9302-2JPC at the OSU Stable Isotope Laboratory for the deglacial interval (20-13 ka) to supplement those already published (Rasmussen et al., 2003). Prior to stable isotope measurements, benthic species were carefully selected so as to not incorporate "dirty" samples into the analysis. Otherwise, all samples followed previous procedures (Benway et al., 2006b). Sediment samples were cleaned and sieved with deionized water and calgon, and dried at 40°C. One to six specimens of *C.lobatulus*, *C.wuellerstorfi*, or *M. barleeanus* were used for each stable isotope measurement. All benthic foraminifera samples were sonicated in deionized water and methanol. Samples were then dried at room temperature (~25°C) for 24 hours, and then analyzed at Oregon State University on a Finnigan-MAT 252 stable isotope ratio mass spectrometer equipped with a Kiel-III carbonate device. Samples were reacted at 70°C in phosphoric acid, and all data are reported relative to the Pee Dee Belemnite standard through our internal standard, which is regularly calibrated against NBS-19.

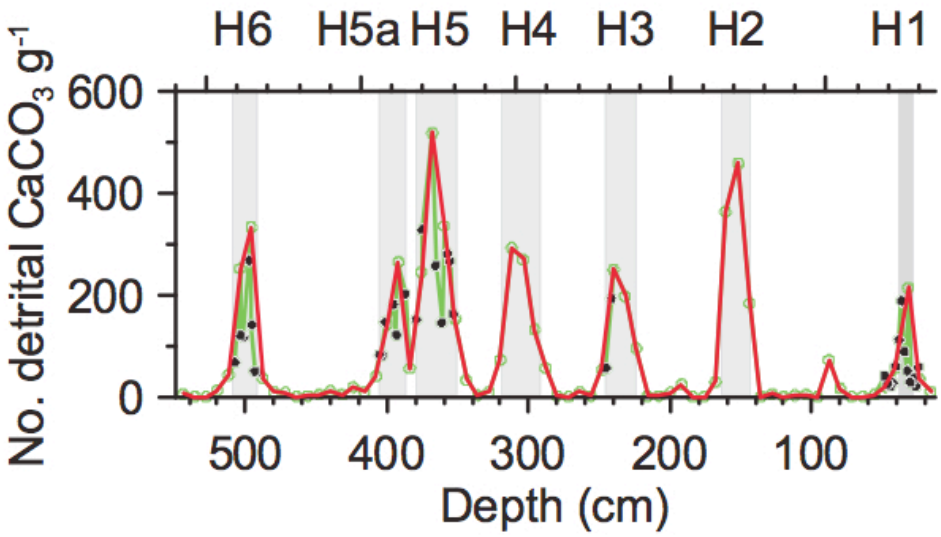

Figure A1. Detrital carbonate counts from EW9302-2JPC.

The original record (Rasmussen et al., 2003) (red line) is compared to our higher resolution record (green line, with original data shown by green dots and our new data shown by black dots), showing replication of original samples as well as new DC counts.

We calculated the ice-volume corrected benthic $\delta^{18}O$ ($\delta^{18}O_{IVC}$) record for cores EW9302-2JPC and MD95-2010 during the last deglaciation where sufficient independent sea-level constraints exist. To calculate $d^{18}O_{IVC}$, we used a eustatic sea-level record (Bassett et al., 2005) to subtract changes in seawater $d^{18}O$ from the published $\delta^{18}O$ record, assuming a relation of 1‰ change in seawater $\delta^{18}O$ is equivalent to 130 m sea-level (Schrag et al., 2002).

We calculated the change in intermediate water depth $\delta^{18}O$ due to the salinity decrease by assuming a meltwater end-member salinity of 0 psu and $\delta^{18}O$ of -25‰ to -35‰ (Remenda et al., 1994; Aharon, 2003). We used the freshwater flux from Liu et al. (2009) and solved for the ocean flux to match the change in salinity following Carlson (2009). Substitution of the $\delta^{18}O$ end member values (-25‰ to -35‰ for meltwater, +1‰ for ocean water) determines the change in $\delta^{18}O$. The modeled ~0.5 psu decrease in the Norwegian Sea equates to a ~0.4-0.5‰ decrease (-25‰ and -35‰, respectively). The modeled ~0.3 psu decrease in the southeast Labrador Sea and in the Caribbean equates to a ~0.2-0.3‰ decrease (-25‰ and-35‰, respectively).

5. Possible Contamination of Samples by Dolomite

Because Heinrich layers contain dolomite, negative $\delta^{18}O$ excursions in foraminifera associated with Heinrich layers may be due to contamination by fine dolomitic particles (Hodell and Curtis, 2008); similar contamination issues may apply to our Mg/Ca data. Because the flow-through method that we used for Mg/Ca measurements sequentially dissolves foram calcite from the surface inwards, it allows us to evaluate any possible sources of contamination, which is its acknowledged strength in making Mg/Ca measurements. In particular, these data (Figure A2) unequivocally demonstrate that there is no contamination of our forams by detrital dolomite, and thus this is not an issue for our $\delta^{18}O$ or Mg/Ca data. For example, Hodell and Curtiss (2008) found increases in Ca/Sr associated with detrital carbonate in the Heinrich layers, suggesting that if our samples were contaminated by detrital carbonate, we should see increases in Ca/Sr of our forams. The absence of this signal thus demonstrates that there is no such contamination, indicating that it is not an issue

for our $\delta^{18}O$ data. Similarly, the absence of a Mg signal in the outer part of our forams unequivocally demonstrates that there is no contamination of any surface coatings by dolomite, although we emphasize that the significance of the flow-through method is to remove any such our coating on the shell before collecting data from the inner part of the foram shell which used in our study. Finally, we saw no evidence of dissolution of forams or lithic carbonate grains, indicating that there are no dissolution effects.

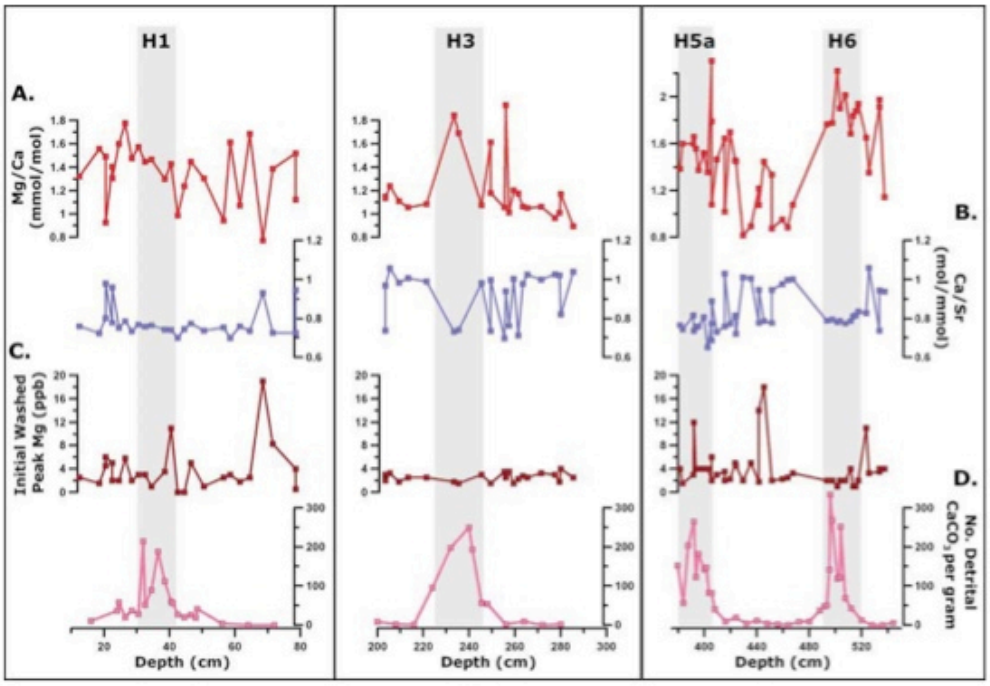

Figure A2. Elemental information from EW9302-2JPC.

(A) Mg/Ca data, (B) Ca/Sr data from the entire foram, (C) Mg from the initial outer dissolved part of the foram, and (D) carbonate IRD.

A.5 Ocean Model with Ice-Shelf Thermodynamic Coupling

The ocean model is based on the Regional Ocean Modeling System (ROMS) version 3.0 (Shchepetkin and McWilliams, 2003; Shchepetkin and McWilliams, 2005). ROMS is a free-surface, hydrostatic ocean model that solves the 3D primitive equations for a finite-difference lateral grid and a terrain-following vertical coordinate. For a recent application of ROMS with coupling to a thermodynamically active ice shelf, see Dinniman et al. (2007).

The model was formulated on the domain shown in Figure A3. The horizontal grid spacing is $\Delta x \approx 10$ km and there are 25 vertical levels. Minimum thickness of the water column (ice base to seabed) is set to 200 m. Model bathymetry was based on TOPO12.1 (http://topex.ucsd.edu/marine_topo/mar_topo.html), an updated version of the global gridded bathymetry dataset first reported by Smith and Sandwell (1997). The TOPO12.1 grid includes the International Bathymetric Chart of the Arctic Ocean (Jakobsson et al., 2008).

The ice-shelf geometry follows Hulbe (1997): the ice shelf fills Baffin Bay and grounds across Davis Strait, cutting off the northern portion of Baffin Bay which is then excluded from our model. Ice draft (required for the model) is obtained from 0.85 times the modeled steady-state ice thickness in Hulbe (1997).

The bathymetry grid was first smoothed to 10 km to match the final model grid spacing, then smoothed further to reduce errors that arise in the baroclinic pressure gradient calculation in models that use terrain-following vertical coordinate systems (Beckmann and Haidvogel, 1993). See Padman et al. (2009) for details on numerical requirements for smoothing, and smoothing methodology. The ice-shelf draft fields digitized from Hulbe (1997) were already sufficiently smooth.

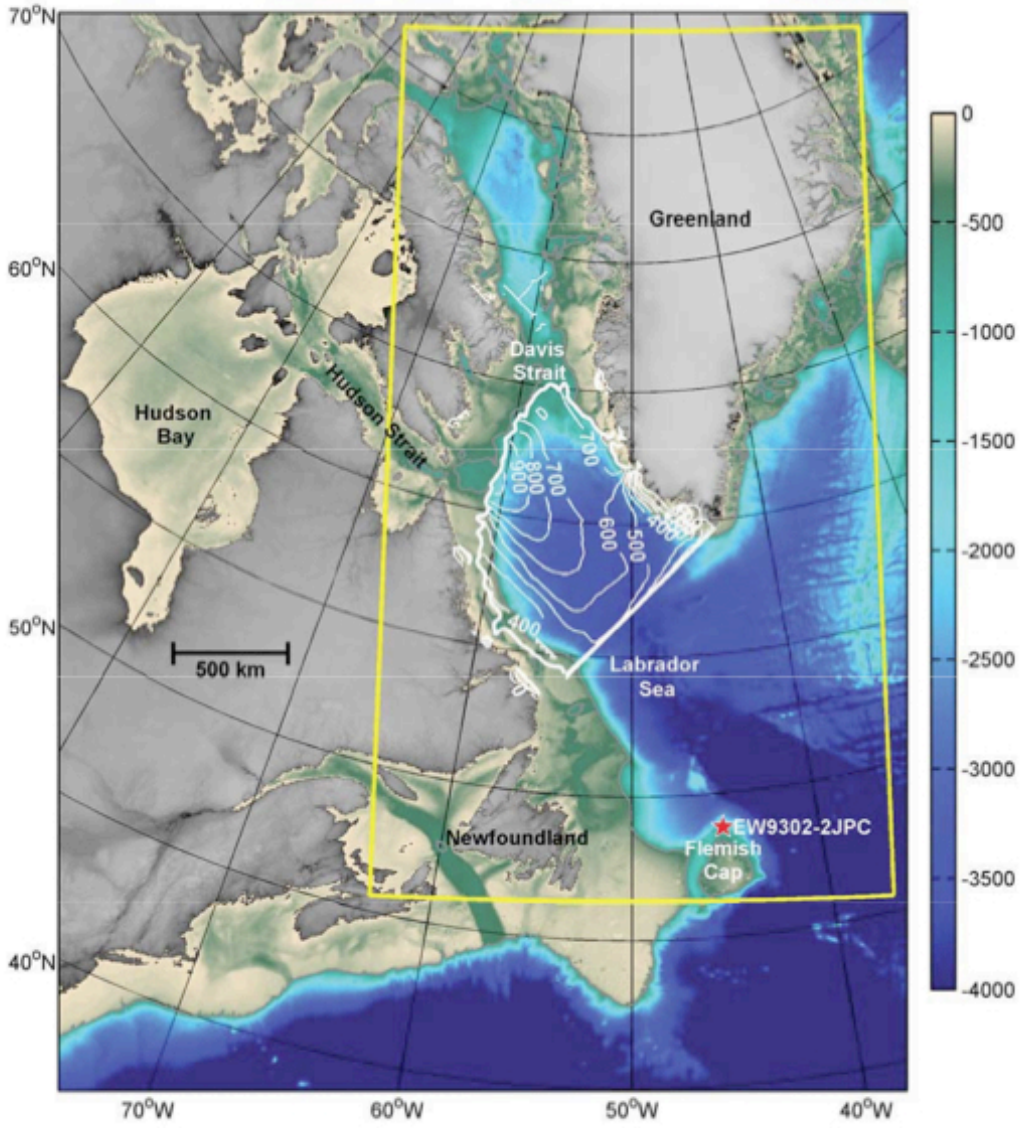

Figure A3. Modern bathymetry in m (color scale on right) from TOPO12.1. White annotated contours show ice-shelf draft (m). Bold white contour outlines edge of model ice shelf: Baffin Bay north of the ice shelf grounding line in Davis Strait is treated as land. Yellow outline shows domain of ocean model with coupled ice-shelf thermodynamics.

Model hydrography is derived from a simulation with the National Center for Atmospheric Research Community Climate System Model version 3 (NCAR CCSM3) (Liu et al., 2009). As initial conditions we use profiles, averaged over 500 yr, taken from near the center of the ice-shelf front (Figure A4), and assume horizontal homogeneity. We ran five states: a "cold" state (model years 19.5-19.0 ka), three intermediate states (18.5-18.0 ka, 18.0-17.5 ka, 17.5-17.0) and a "warm" state (17.0-16.5 ka). The approximate values of subsurface temperature from CCSM3 for these five periods, each averaged over the 400-800 m depth range corresponding to ice-shelf draft, are T_i=-1.1°C, -1.1°C, -0.8°C, +0.6°C, and +1.7°C, respectively.

The model was forced by barotropic tides (tide height and currents) at the open boundaries. Tides were recalculated for a larger-domain model of the North Atlantic Ocean, using open boundary conditions from the modern global barotropic tide model TPXO7.2 (Egbert and Erofeeva, 2004). Geometry in the Labrador Sea and Baffin Bay was modified to reflect the presence of the specified ice shelf. We assume that the effect of tides of the change in geometry due to the ice shelf does not extend to the boundaries of the larger-domain model. The addition of tides to the circulation that would develop independently through buoyancy fluxes at the ice-shelf base speeds up model equilibration but, for this case, has little effect on the steady-state basal melt rate distribution.

We use the three-equation formulation of ice/ocean thermodynamic exchange described by Holland and Jenkins (1999) as applied in ROMS by Dinniman et al. (2007). In our application, the friction velocity is calculated at each time step, and so explicitly includes the effects of time-varying tidal currents as well as the thermohaline circulation, or "plume flow", associated with basal melt.
Vertical mixing elsewhere in the model was parameterized by the Mellor-Yamada level 2.5 turbulence closure scheme (Mellor and Yamada, 1982). Benthic stress was modeled as quadratic drag with c_d=0.003. We used a Laplacian ("harmonic") formulation for the horizontal mixing of momentum and tracers, with coefficients of the lateral viscosity A_H and diffusivity K_H both set to 5 $m^2 s^{-1}$.

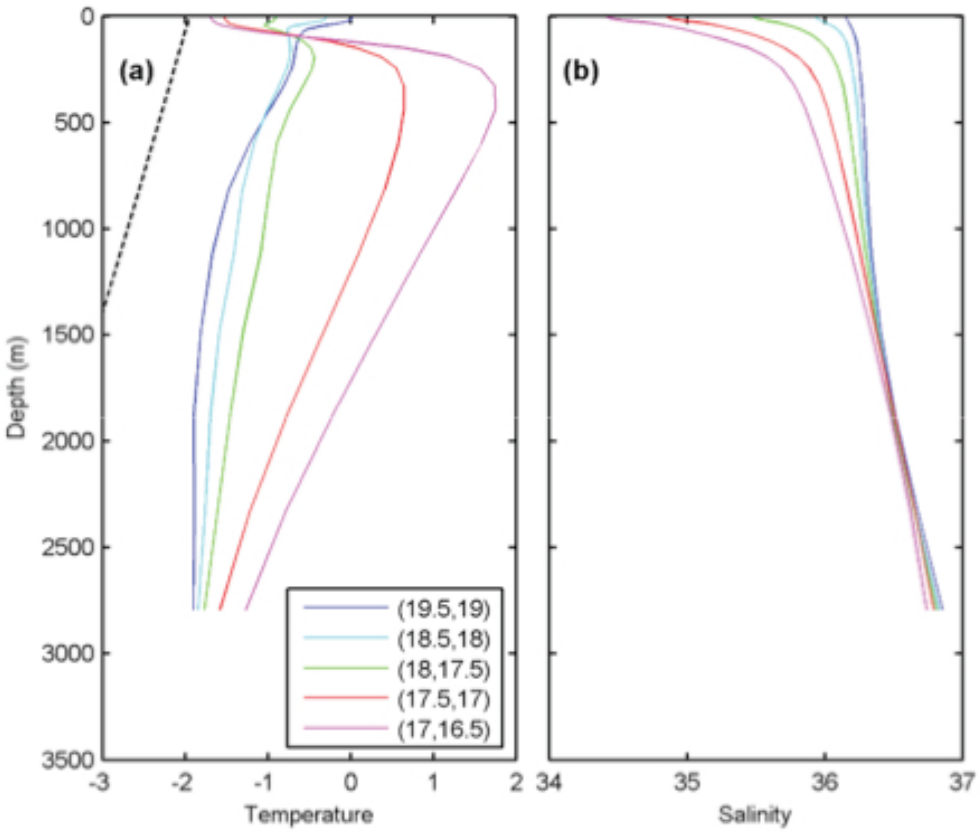

Figure A4. Profile temperatures from CCSM3.

(A) Solid lines show profiles of temperature from NCAR CCSM3 for a model node near the center of the paleo-ice-front at 56°N, 47.5°W. Temperatures have been averaged over the 500-year time intervals (years BP) listed in the legend. Dashed lines show *in situ* freezing temperature for a salinity of 35.5. (B) As in A, for salinity.

Maps of predicted basal melt rate M_b (Figure A4) for the cold (19.5-19 ka) and warm (17-16.5 ka) states show similar structure, with highest rates along southwest Greenland where the inflowing water first meets deeply grounded ice and at the deep grounding line of the Hudson Strait Ice Stream. However, the magnitude of M_b for the warm state is about six times higher than for the cold state so that the difference map $\Delta M_b = M_b(\text{warm}) - M_b(\text{cold})$ (Figure A5, right panel) looks similar to M_b(warm).

Modern ice shelves tend to lose ~1/2 of their mass through basal melting and 1/2 through calving. The Hulbe model (Hulbe, 1997) assumed that, at steady-state, ice volume input across the HSIS grounding line (~660 $km^3\ a^{-1}$) was balanced entirely by calving at a specified ice front (Figure A2). The shelf-integrated mass loss due to modeled mean basal melt (~0.17 m a^{-1}) in the cold state corresponds to ~70 $km^3\ a^{-1}$, or ~10% of the total mass loss. The linear relationship between ice-front CCSM3 temperature T_i and shelf-averaged basal melt rate M_{av} from our five simulations is:

$$M_{av} = 0.54 + 0.34.T_i \quad (\text{m } a^{-1})$$

From this equation and the time series of T_i at the original temporal resolution of the model output (10 yr), we estimate a time history of shelf-integrated mass loss corresponding to the excess melt rate relative to the cold state value (assumed to represent a steady-state ice shelf). Mass loss begins near 18 ka. Integration of this mass loss in time leads to total removal of the ice shelf near 16.7 ka.

This estimate of collapse time requires several assumptions: (*i*) calving rate remains constant throughout the transition to the warm state; (*ii*) the HSIS ice-volume flux remains constant even as the ice shelf thins; (*iii*) area-averaged basal melt rate follows the above linear relationship to T_i even as the ice-shelf draft decreases by excess melt; (*iv*) the opening of northern Baffin Bay (north of Davis Strait) as the ice shelf thins has no impact on subsequent circulation or melt rate of the modeled portion of the ice shelf; and (*v*) net surface accumulation of mass (snowfall) directly

on the ice shelf is an insignificant term in the ice-shelf mass budget under all experienced climate states, or can be incorporated as a revision to the calving flux of ~590 km^3 a^{-1}. Violation of any of these assumptions will change the integrated mass loss and collapse time in ways that cannot be quantified without fully coupled ocean, glaciological and atmospheric models

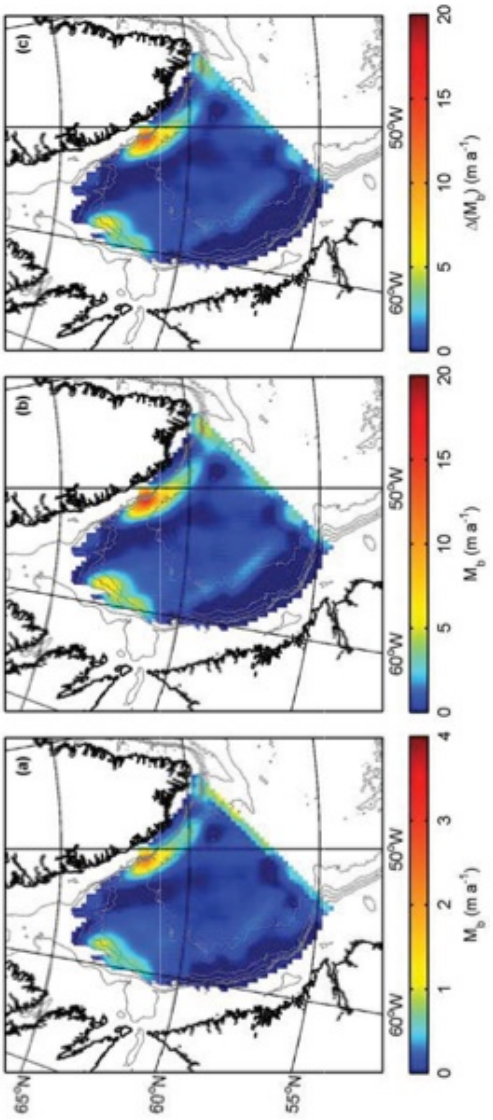

Figure A5. Basal melt rate from sub ice shelf model.

(A) Modeled basal melt rate M_b (m a^{-1}) for cold state 19.5-19 ka. (B) Same as A, for warm state 17-16.5 ka. (C) Difference between warm-state and cold-state basal melt rates, ΔM_b. Note smaller color range for map of cold-state M_b.

A.6 References

Aharon, P. (2003). Meltwater flooding events in the Gulf of Mexico revisited: implications for rapid climate change during the last deglaciation. *Paleoceanography* **18,** doi:10.1029/2002PA0000840.

Bassett, S. E., Milne, G. A., Mitrovica, J. X., and Clark, P. U. (2005). Ice sheet and solid earth influences on far-field sea-level histories. *Science* **309,** 925-928.

Beckmann, A., and Haidvogel, D. B. (1993). Numerical simulation of flow around a tall isolated seamount. Part I: Problem formulation and model accuracy. *Journal of Physical Oceanography* **23,** 1736-1753.

Benway, H. M., Mix, A. C., Haley, B. A., and Klinkhammer, G. P. (2006). Eastern Pacific Warm Pool paleosalinity and climate variability: 0-30 kyr. *Paleoceanography* **21**.

Carlson, A. E. (2009). Geochemical constraints on the Laurentide Ice Sheet contribution to Meltwater Pulse 1A. *Quaternary Science Review* **28,** 1625-1630.

Dinniman, M. S., Klinck, J. M., and Smith, W. W., Jr. (2007). The influence of sea ice cover and icebergs on circulation and water mass formation in a numerical circulation model of the Ross Sea, Antarctica. *Journal of Geophysical Research* **112,** C11013. doi:10.1029/2006JC004036.

Dokken, T., and Jansen, E. (1999). Rapid changes in the mechanism of ocean convection during the last glacial period. *Nature* **401,** 458-461.

Egbert, G. D., and Erofeeva, S. Y. (2004). Efficient inverse modeling of barotropic ocean tides. *Journal of Oceanic and Atmospheric Technology* **19,** 183-204.

Elderfield, H., Yu, J., Anand, P., Kiefer, T., and Nyland, B. (2006). Calibrations for benthic foraminiferal Mg/Ca paleothermometry and the carbonate ion hypothesis. *Earth and Planetary Science Letters* **250,** 633-649.

Hodell, D. A., and Curtis, J. H. (2008). Oxygen and carbon isotopes of detrital carbonate in North Atlantic Heinrich Events. *Marine Geology* **256,** 30-35.

Holland, D. M., and Jenkins, A. (1999). Modelling thermodynamic ice-ocean interactions at the base of an ice shelf. *Journal of Physical Oceanography* **29,** 1787-1800.

Hughen, K. A., Baillie, M. G. L., Bard, E., Beck, J. W., Bertrand, C. J. H., Blackwell, P. G., Buck, C. E., Burr, G. S., Cutler, K. B., Damon, P. E., Edwards, R. L., Fairbanks, R. G., Friedrich, M., Guilderson, T. P., Kromer, B., McCormac, G., Manning, S., Ramsey, C. B., Reimer, P. J., Reimer, R. W., Remmele, S., Southon, J. R., Stuiver, M., Talamo, S., Taylor, F. W., van der Plicht, J., and Weyhenmeyer, C. E. (2004). Marine04 marine radiocarbon age calibration, 0-26 cal kyr BP. *Radiocarbon* **46,** 1059-1086.

Hulbe, C. L. (1997). An ice shelf mechanism for Heinrich layer production. *Paleoceanography* **12,** 711-717.

Jakobsson, M., Macnab, R., Mayer, L., Anderson, R., Edwards, M., Hatzky, J., Schenke, H. W., and Johnson, P. (2008). An improved bathymetric portrayal of the Arctic Ocean: Implications for ocean modeling and geological, geophysical and oceanographic analyses. *Geophysical Research Letters* **35**.

Klinkhammer, G. P., Haley, B. A., Mix, A. C., Benway, H. M., and Cheseby, M. (2004). Evaluation of automatd flow-through time-resolved analysis of foraminifera for Mg/Ca paleothermometry. *Paleoceanography* **19,** PA4030, doi:10.1029/2004PA001050.

Kristjánsdóttir, G. B., Lea, D. W., Jennings, A. E., Pak, D. K., and Belanger, C. L. (2007). New spatial Mg/Ca-temperature calibrations for three Arctic, benthic foraminifera and reconstruction of north Iceland shelf temperature for the past 4000 years. *Geochemistry, Geophysics, and Geosystems* **8,** Q03P21, doi:10.1029/2006GC001425.

Lear, C. H., Rosenthal, Y., and Slowey, N. (2002). Benthic foraminifera Mg/Ca-paleothermometry: A revised core-top calibration. *Geochimica et Cosmochimica Acta.* **66,** 3375-3387.

Liu, Z., Otto-Bliesner, B. L., He, F., Brady, E. C., Tomas, R., Clark, P. U., Carlson, A. E., Lynch-Stieglitz, J., Curry, W., Brook, E. J., Erickson, D., Jacob, R., Kutzbach, J. E., and Cheng, J. (2009). Transient simulation of last deglaciation with a new mechanism for Bølling-Allerød warming. *Science* **325,** 310-314.

Mellor, G. L., and Yamada, T. (1982). Development of a turbulence closure model for geophysical fluid problems. *Reviews of Geophysics and Space Physics* **20,** 851-875.

Padman, L., Howard, S. L., Orsi, A., and Muench, R. D. (2009). Tides of the northwestern Ross Sea and their impact on dense outflows of Antarctic Bottom Water. *Deep Sea Research, Part II* **56,** 818-834.

Quillman, U., Marchitto, T. M., Andrews, J. T., Jennings, A. E., and Dean, W. E. (2008). *38th International Arctic Workshop, Abstracts and Programs*.

Rasmussen, T. L., Oppo, D. W., Thomsen, E., and Lehman, S. J. (2003). Deep sea records from the southeast Labrador Sea: Ocean circulation changes and ice-rafting events during the last 160,000 years. *Paleoceanography* **18,** doi:10.1029/2001PA000736.

Remenda, V. H., Cherry, J. A., and Edwards, T. W. D. (1994). Isotopic composition of old ground water from Lake Agassiz: implications for Late Pleistocene climate. *Science* **266,** 1975-1978.

Schrag, D. P., Adkins, J. F., McIntyre, K., Alexander, J. L., Hodell, D. A., Charles, C. D., and McManus, J. F. (2002). The oxygen isotopic composition of seawater during the Last Glacial Maximum. *Quaternary Science Reviews* **21,** 331-342.

Shchepetkin, A. F., and McWilliams, J. C. (2003). A method for computing horizontal pressure-gradient force in an oceanic model with a nonaligned vertical coordinate. *Journal of Geophysical Research* **108(C3),** 3090, doi:10.1029/2001JC001047.

Shchepetkin, A. F., and McWilliams, J. C. (2005). The Regional Oceanic Modeling System (ROMS): a split explicit, free-surface, topography-following-coordinate oceanic model. *Ocean Modelling* **9,** 347-404.

Smith, W. H. F., and Sandwell, D. T. (1997). Global sea floor topography from satellite altimetry and ship depth soundings. *Science* **277,** 1956-1962.

Sosdian, S., and Rosenthal, Y. (2009). Deep-Sea temperature and ice volume changes across the Pliocene-Pleistocene climate transition. *Science* **325,** 306-310.

Stoner, J. S., Channell, J. E. T., Hillaire-Marcel, C., and Kissel, C. (2000). Geomagnetic paleointensity and environmental record from Labrador Sea core MD95-2024: global marine sediment and ice core chronostratigraphy for the last 110 kyr. *Earth and Planetary Science Letters* **183,** 161-177.

Appendix B – Late Pleistocene and Holocene Cirque Glaciation, western North America

B.1 Field Methods

Samples for ^{10}Be exposure dating were collected from the tops of boulders resting on moraine crests at all of the field site locations using hammers and chisels. Special care was made to select "ideal" boulders for cosmogenic dating do to potential age discrepancies amongst boulders arising from poor selection protocol. We selected boulders approximately ~0.5 meters or taller to limit the potential for excessive snow cover, prior exhumation and/or burial; boulders resting on moraine crests which were least likely to be affected by overturning or toppling during moraine degradation; boulders with little to no surface erosion or exfoliation features; and boulders with flat tops and/or simple surface geometries to limit uncertainties made for shielding calculations. Approximately 1-3 kg were collected from the top 2-4 cm of each boulder for cosmogenic chemistry. Shielding measurements were made in the field using a Suunto clinometer and surface slopes were measured using a Brunton compass. Latitude, longitude, and elevation information for each boulder was collected using a handheld GPS and crosschecked with topographic maps. Geometries of each boulder were also measured in the field and each boulder was sketched and photographed as an archive for future evaluation.

B.2 Laboratory Methods

To isolate ^{10}Be from each sample we followed the methods of Licciardi (2000) and Rinterknecht (2003) with the modifications of Goehring (2006) at Oregon State University. The top 1-2 cm of each sample were crushed in a Bico disk mill and sieved to the 250 – 710 μm size fraction. The magnetic fraction of each sample was then removed using a Frantz Isodynamic Mineral Separator. All samples were first

leached for 24 – 48 hours in 5 – 10% HNO_3 and then for 24 – 72 hours in a 1% HNO_3 + 1% HF solution while sitting in warm ultrasonic baths to remove all non-quartz minerals and meteoric ^{10}Be from the quartz surfaces. Samples were then measured by inductively coupled plasma-optical spectroscopy (ICP-OES) to determine if sufficient quartz purities were obtained by way of measuring Al, Ca, Fe, K, Mg, Na, and Ti in each sample. After sufficient purities were obtained, 20 – 50 g of sample together with ~0.25μg of Be carrier (Table B1) were added to Teflon beakers and dissolved in concentrated HF. The HF was then evaporated and several $HClO_4$ and HCl evaporations were preformed to drive off the remaining fluorides and convert the samples to chloride form. Following the evaporation steps, the samples were run through cation and anion exchange columns to isolate the Be. After the chromatography was completed, the pH of each sample was brought up to 5 to precipitate any Ti remaining in the sample. The samples were then centrifuged for 15 minutes and the precipitated Ti was separated from the samples. Following the Ti-removal, the pH of each sample was brought up to 8 with NH_4OH to precipitate $Be(OH)_2$ and then washed three times in ultrapure water with a pH of 8 to remove any possible boron. The samples were transferred to acid cleaned quartz crucibles and evaporated at 80 – 90°C in a laminar flow HEPA hood. The $Be(OH)_2$ was then converted to BeO by heating the covered crucibles in a rapid mineralizer for 60 minutes at 999°C. Finally, samples were packed into targets in the laminar flow hood for AMS analysis following the procedures of PRIME Labs.

B.3 Exposure Age Calculations

After correcting for the system blank, beryllium ratios ($^{10}Be/^{9}Be$) were converted to ^{10}Be atoms and then to ^{10}Be atoms per gram of quartz (Table B1). Following the methods and online program of the CHRONUS Calculator v.2.2 (Balco et al., 2008; Balco et al., 2009), shielding corrections and exposure ages were calculated for each individual moraine boulder (Table B2-B4). All raw $^{10}Be/^{9}Be$

were calibrated against the Revised ICN standard (07KNSTD) following the protocol outlined by PRIME Lab. Cosmogenic exposure ages were calculated using multiple scaling models and production rates (Table B3 & B4). The ages reported in this publication were derived using the scaling scheme of Lifton et al. (2005) and the production rates from northeastern North America calibration dataset (Balco et al., 2009). Because recent work (Lifton et al., 2009) has shown that the local production rate in the western United States closely matches new calibration work from both eastern North America (Balco et al., 2009) and New Zealand (Putnam et al., 2010), we choose to use the sea level high latitude production rate of 4.50 ± 0.22 atom g^{-1} yr^{1} (Balco et al., 2009). However, for completeness and for future and present researchers we provide all of the scaling and production schemes available to date (Tables B3 & B4).

To calculate the moraine age and uncertainties, we take the arithmetic mean of the boulder exposure ages and the standard error. Outliers in a set of boulder ages from a single moraine are initially defined as being greater than 4 standard deviations from the mean value of the other boulder exposure ages. This method of identifying outliers accounts for 6 of the 10 identified from this dataset. We then use Chavenet's criterion (Taylor, 1997) to identify any remaining outlier, which were four in total (Table B3 & B4).

Because the majority of the boulders sampled had pristine surfaces that showed no clear erosional features and were generally glacially striated, we do not apply an erosion correction to our surface exposure ages. We do not apply a snow correction to our surface exposure ages, as no correlation between boulder height and surface exposure age is distinguishable. Additionally, we consider our boulder sampling sites, which are from the exposed moraine ridges, to be generally wind swept through the year. However, assuming our boulder ages were covered by half a meter of snow (ρ = 0.3 g cm^{-3}) for 4 months of the year, a correction of ~3% would be necessary (Gosse and Phillips, 2001), which is well within the age uncertainties from the scaling and production calculations. Because both snow cover and surface

weathering would decrease the apparent exposure age, we consider our surface exposure dates a minimum limiting ages of moraine abandonment.

Table B1. Processing and sample information for determining ^{10}Be concentrations and uncertainties.

Sample ID	Qtz. Mass (g)	^{9}Be Carrier (g)*	^{10}Be / ^{9}Be (10^{-15})	1σ (10^{-15})	^{10}Be (atoms/ g) (10^{5})	1σ (10^{5})
LL-MB-01	51.8690	0.2450	2171.0	46.01	6.84053	0.14527
LL-MB-03	50.3300	0.2450	1995.0	51.11	6.47720	0.16630
LL-MB-04	51.4200	0.2650	1855.0	50.79	6.37629	0.17495
LL-MB-06	61.6900	0.2400	2404.0	101.70	6.23967	0.26441
LL-MB-07	53.7270	0.2500	2121.0	89.41	6.58351	0.27803
LL-MB-08	55.3300	0.2490	2170.0	69.01	6.51452	0.20756
DPI-MB-01	53.2410	0.2500	1592.0	55.06	4.98374	0.17281
DPI-MB-03	55.4950	0.2500	1616.0	49.19	4.85357	0.14812
DPI-MB-04	42.9339	0.2520	1236.0	52.45	4.83345	0.20577
DPI-MB-05	41.8060	0.2400	1191.0	52.03	4.55415	0.19965
DPI-MB-08	41.2580	0.2470	1742.0	70.87	6.95394	0.28356
DP0-MB-01	38.5830	0.2450	1148.0	49.87	4.85526	0.21167
DP0-MB-02	35.6540	0.2370	1149.0	37.62	5.08643	0.16720
DP0-MB-03	35.6450	0.2450	1179.0	36.05	5.39783	0.16567
DP0-MB-04	36.8970	0.2460	1232.0	39.52	5.47214	0.17615
DP0-MB-05	35.7200	0.2510	1133.0	43.22	5.30283	0.20302
DP0-MB-06	35.9630	0.2500	1151.0	39.48	5.32956	0.18348
SBO-SFF-01	34.9510	0.2495	1431.0	59.68	6.80513	0.28481
SBO-SFF-02	35.1620	0.2502	1349.0	44.56	6.39343	0.21204
SBO-SFF-03	35.5850	0.2508	1421.0	57.34	6.67172	0.27018

SBO-SFF-04	35.6570	0.2508	1422.0	41.28	6.66295	0.19420
SBO-SFF-05	36.1910	0.2508	1432.0	42.75	6.61095	0.19813
SBO-SFF-06	36.0810	0.2515	1413.0	26.20	6.56117	0.12231
SBO-SFF-07	38.1060	0.2490	1465.0	26.59	6.37761	0.11636
SBI-01	47.0129	0.2563	1828.0	24.90	6.64704	0.09073
SBI-02	45.5939	0.2525	1877.0	24.62	6.93344	0.09113
SBI-03	46.4218	0.2507	1730.0	33.63	6.23066	0.12138
SBI-04	41.6438	0.2538	422.0	9.90	1.70470	0.04038
SBI-06	48.5866	0.2505	2304.0	34.49	7.92584	0.11884
SBI-07	49.5200	0.2545	2112.0	44.65	7.24144	0.15335
BLI-WP-01	40.8351	0.2500	1086.0	43.76	4.42486	0.17917
BLI-WP-02	39.9985	0.2518	1262.0	42.71	5.29044	0.17982
BLI-WP-04	39.8360	0.2501	1233.0	25.44	5.15437	0.10698
BLI-WP-05	39.8132	0.2473	1190.0	31.60	4.92089	0.13137
BLI-WP-08	39.8703	0.2502	1054.0	30.27	4.40139	0.12715
BLI-WP-09	43.9415	0.2484	1277.0	33.60	4.80712	0.12710
BL-01	48.4565	0.2558	1850.0	27.33	6.51401	0.09642
BL-02	47.3202	0.2536	1846.0	26.56	6.59864	0.09513
BL-03	44.7177	0.2534	1802.0	67.09	6.81054	0.25405
BL-05	42.5665	0.2550	1617.0	23.53	6.45941	0.09421
BL-07	43.9988	0.2525	1667.0	36.44	6.37948	0.13975
BL-08	43.6797	0.2532	1712.0	22.57	6.61825	0.08745
DHO-UM-01	52.8050	0.2573	1741.0	37.57	5.62680	0.13553
DHO-UM-02	47.5340	0.2605	1412.0	76.86	5.12424	0.31143
DHO-UM-03	61.9320	0.2556	2048.0	34.82	5.61229	0.10643

DHO-UM-04	65.0920	0.2582	2264.0	34.38	5.96704	0.10100
DHI-UM-01	52.7076	0.2481	1654.0	65.41	5.16048	0.22769
DHI-UM-02	53.0260	0.2488	1588.0	53.57	4.93715	0.18594
DHI-UM-03	60.6070	0.2480	1746.0	65.97	4.73761	0.19963
DHI-UM-04	53.5100	0.2460	1646.0	31.81	5.01514	0.10837
DHI-UM-05	61.0294	0.2470	1983.0	34.80	5.32666	0.10432
DHI-UM-06	52.8942	0.2471	1604.0	35.49	4.96529	0.12279
DHM-UM-01	43.1800	0.2569	1619.0	40.67	6.38523	0.17910
DHM-UM-02	64.5510	0.2570	2246.0	75.26	5.94104	0.22155
DHM-UM-03	51.9670	0.2631	1961.0	63.26	6.59166	0.23684
DHM-UM-04	47.5380	0.2570	1743.0	68.42	6.25010	0.27352
DHM-UM-05	66.9440	0.2565	2512.0	39.33	6.39851	0.11155
DHM-UM-06	49.3273	0.2583	1860.0	32.50	6.46348	0.12607
DHM-UM-07	53.9480	0.2584	1978.0	30.94	6.28986	0.10981
SCM-WRR-01	29.2750	0.2555	901.5	17.72	5.18187	0.11521
SCM-WRR-02	50.6950	0.2565	1358.0	33.12	4.54770	0.12413
SCM-WRR-03	47.6980	0.2571	1139.0	31.57	4.05606	0.12608
SCM-WRR-04	46.1220	0.2557	1399.0	48.34	5.13476	0.19828
SCM-WRR-05	41.2370	0.2546	1266.0	23.74	5.16938	0.10881
SCM-WRR-06	47.5440	0.2546	1186.0	29.75	4.19736	0.11808
SCM-WRR-07	45.0060	0.2550	1161.0	40.31	4.34645	0.16906
SCO-WRR-001	42.2840	0.2496	1377.0	58.56	5.37918	0.25567
SCO-WRR-002	41.2420	0.2452	1603.0	79.93	6.31479	0.35136
SCO-WRR-003	40.4550	0.2555	1586.0	36.75	6.63862	0.17186
SCO-WRR-004	45.1230	0.2540	1646.0	77.33	6.14231	0.32185

SCO-WRR-005	42.7290	0.2471	1694.0	73.00	6.49432	0.31216
SCO-WRR-006	47.3750	0.2460	1714.0	41.87	5.90055	0.16093
SCO-WRR-007	42.3750	0.2493	1425.0	52.46	5.54982	0.22832
TLO-WRR-01	41.2053	0.2477	1641.0	33.03	6.53805	0.14711
TLO-WRR-02	41.8268	0.2475	1757.0	51.33	6.89433	0.22471
TLO-WRR-03	41.3950	0.2485	1662.0	49.12	6.61352	0.21817
TLO-WRR-04	33.0890	0.2465	1312.0	32.79	6.46421	0.18099
TLO-WRR-05	51.9010	0.2529	1911.0	64.01	6.17971	0.23066
TLO-WRR-06	43.5720	0.2499	1357.0	46.88	5.14986	0.19895
TLO-WRR-07	48.2110	0.2482	1750.0	74.50	5.97434	0.28360
TLO-WRR-08	41.7840	0.2484	1573.0	74.00	6.19574	0.32529
CFR-01	46.4800	0.2620	1828.0	85.94	6.87480	0.35805
CFR-02	59.0850	0.2550	1606.0	202.10	4.62320	0.64464
CFR-03	51.9464	0.2586	1502.0	86.74	4.98694	0.31915
CFR-04	44.5256	0.2630	1092.0	39.48	4.29898	0.17240
CFR-05	47.9000	0.2540	1112.0	139.10	3.92989	0.54515
CFR-06	53.0280	0.2579	1540.0	255.80	4.99547	0.91945
APO-01	41.1370	0.2570	513.6	148.90	2.13202	0.68752
APO-02	41.0050	0.2555	1393.0	323.30	5.78788	1.48882
APO-03	45.6483	0.2637	967.6	117.80	3.72423	0.50295
APO-04	44.7600	0.2460	1441.0	288.30	5.28105	1.17104
APO-05	43.4430	0.2530	1483.0	76.92	5.75974	0.33110
APO-06	46.2914	0.2565	1203.0	66.23	4.44352	0.27125
APO-07	42.9424	0.2570	1246.0	74.34	4.97139	0.32884
UCL-CFR-01	54.2300	0.2540	2379.0	55.28	7.40497	0.19152

UCL-CFR-03	42.7551	0.2534	1874.0	61.59	7.37003	0.26996
UCL-CFR-05	43.6186	0.2584	2036.0	60.33	8.00898	0.26432
UCL-CFR-06	42.1611	0.2560	2020.0	62.90	8.14348	0.28245
UCL-CFR-07	42.0980	0.2566	2008.0	50.44	8.12605	0.22745
BL-BG-03	46.8370	0.2574	879.9	43.02	3.22067	0.15798
BL-BG-04	48.6130	0.2567	826.6	21.50	2.90647	0.08399
BL-BG-05	47.2094	0.2602	838.0	48.97	3.07582	0.19951
BL-BG-06	49.8820	0.2545	923.6	34.82	3.13887	0.13135
BL-BG-07	37.4710	0.2625	605.5	19.56	2.82119	0.10139
TR-01	48.5963	0.2567	1313.0	62.43	4.62435	0.24375
TR-02	48.9428	0.2600	1323.0	39.03	4.68627	0.15328
TR-03	49.1390	0.2615	1330.0	40.44	4.71944	0.15910
TR-06	47.0700	0.2562	1127.0	33.55	4.08848	0.13502
TR-07	53.2090	0.2538	1398.0	59.31	4.44657	0.20911
TR-08	50.9210	0.2510	1446.0	40.49	4.75310	0.14755
SNV-01	41.2085	0.2610	1323.0	120.80	5.58728	0.56548
SNV-02	43.5204	0.2558	661.6	19.68	2.58709	0.08560
SNV-03	45.7310	0.2567	1466.0	55.62	5.48799	0.23078
SNV-04	40.3580	0.2568	1186.0	56.27	5.03050	0.26466
SNV-05	40.3757	0.2557	1177.0	54.23	4.96861	0.25387
SNV-06	43.4650	0.2581	1249.0	54.59	4.94459	0.23961
SNV-07	40.8000	0.2582	1227.0	37.00	5.17658	0.17311
SNV-08	46.3725	0.2585	935.1	41.58	3.47250	0.17135
**DPI-Blank	-	0.2470	3.837	1.2810	-	-
**LL-Blank	-	0.2520	3.549	1.1190	-	-

**TGO-Blank	-	0.2518	4.864	1.8250	-	-
**SBO-Blank	-	0.2478	5.521	2.5080	-	-
**BLI-Blank	-	0.2498	2.818	0.9725	-	-
**SBI-Blank	-	0.2560	2.782	0.4642	-	-
**BL-Blank	-	0.2531	3.649	0.5391	-	-
**LGRL-Blank	-	0.2580	1.851	0.8166	-	-
**BG-Blank	-	0.2635	5.030	1.1910	-	-
**TR-Blank	-	0.2580	1.572	0.7707	-	-
**SNV-Blank	-	0.2577	2.730	1.5330	-	-
**APO-Blank	-	0.2445	3.326	1.1820	-	-
**Blank-1	-	0.2443	20.660	4.6060	-	-
**Blank-2	-	0.2463	17.720	2.4480	-	-
**Blank-3	-	0.2586	2.076	0.6889	-	-

** - ^{9}Be carrier concentration is 1000ppm.*
*** - System blanks (Average ^{10}Be / ^{9}Be Ratio: 5.466 x 10^{-15}).*

Table B2. Sample information for age calculations with CHRONUS calculator (Balco et al., 2008).

	Sample ID	Latitude (DD)	Longitude (DD)	Elevation (m)	Density (g/cm^3)	Shielding	Be (atom / g)	1σ (atom/g)
Medicine Bow Mt., WY Lookout Lake	LL-MB-01	41.34	-106.32	3251	2.7	0.978	684053	14527
	LL-MB-03	41.34	-106.32	3253	2.7	0.978	647720	16630
	LL-MB-04	41.34	-106.32	3253	2.7	0.979	637629	17495
	LL-MB-06	41.34	-106.32	3260	2.7	0.989	623967	26441
	LL-MB-07	41.34	-106.32	3260	2.7	0.988	658351	27803
	LL-MB-08	41.34	-106.32	3253	2.7	0.986	651452	20756
Medicine Bow Mt., WY Disaster Peak inner	DPI-MB-01	41.34	-106.33	3267	2.7	0.967	498374	17281
	DPI-MB-03	41.34	-106.33	3276	2.7	0.958	485357	14812
	DPI-MB-04	41.34	-106.33	3276	2.7	0.956	483345	20577
	DPI-MB-05	41.34	-106.33	3276	2.7	0.955	455415	19965
	DPI-MB-08	41.34	-106.33	3265	2.7	0.967	695394	28356
Medicine Bow Mt., WY Disaster Peak outer	DP0-MB-01	41.34	-106.32	3261	2.7	0.979	485526	21167
	DP0-MB-02	41.34	-106.32	3272	2.7	0.980	508643	16720
	DP0-MB-03	41.34	-106.32	3272	2.7	0.980	539783	16567

	DP0-MB-04	41.34	-106.32	3270	2.7	0.978	547214	17615
	DP0-MB-05	41.34	-106.32	3270	2.7	0.980	530283	20302
	DP0-MB-06	41.34	-106.32	3277	2.7	0.983	532956	18348
Sangre de Cristos, NM Lake Katherine outer	SBO-SFF-01	35.83	-105.75	3590	2.65	0.974	680513	28481
	SBO-SFF-02	35.83	-105.75	3590	2.65	0.974	639343	21204
	SBO-SFF-03	35.83	-105.75	3590	2.65	0.974	667172	27018
	SBO-SFF-04	35.83	-105.75	3590	2.65	0.974	666295	19420
	SBO-SFF-05	35.83	-105.75	3590	2.65	0.974	661095	19813
	SBO-SFF-06	35.83	-105.75	3590	2.65	0.974	656117	12231
	SBO-SFF-07	35.83	-105.75	3590	2.65	0.974	637761	11636
Sangre de Cristos, NM Lake Katherine inner	SBI-01	35.84	-105.75	3605	2.65	0.963	664704	9073
	SBI-02	35.84	-105.75	3605	2.65	0.963	693344	9113
	SBI-03	35.84	-105.75	3605	2.65	0.963	623066	12138
	SBI-04	35.84	-105.75	3605	2.65	0.963	170470	4038
	SBI-06	35.84	-105.75	3598	2.65	0.962	792584	11884
	SBI-07	35.84	-105.75	3598	2.65	0.963	724144	15335
South Snake Range, NV Wheerler	BLI-WP-01	39.00	-114.30	3190	2.7	0.983	442486	17917
	BLI-WP-02	39.00	-114.30	3190	2.7	0.984	529044	17982

Peak								
	BLI-WP-04	39.00	-114.30	3190	2.7	0.984	515437	10698
	BLI-WP-05	39.00	-114.30	3180	2.7	0.985	492089	13137
	BLI-WP-08	39.00	-114.30	3180	2.7	0.984	440139	12715
	BLI-WP-09	39.00	-114.30	3180	2.7	0.985	480712	12710
Uinta Mts., UT (west) Blue Lake	BL-01	40.71	-110.81	3351	2.7	0.994	651401	9642
	BL-02	40.71	-110.81	3351	2.7	0.996	659864	9513
	BL-03	40.71	-110.81	3351	2.7	0.996	681054	25405
	BL-05	40.71	-110.81	3355	2.7	0.974	645941	9421
	BL-07	40.70	-110.81	3351	2.7	0.996	637948	13975
	BL-08	40.70	-110.81	3351	2.7	0.992	661825	8745
Uinta Mts., UT (central) Deadhorse Lake outer	DHO-UM-01	40.75	-110.68	3387	2.7	0.987	562680	13553
	DHO-UM-02	40.75	-110.68	3387	2.7	0.987	512424	31143
	DHO-UM-03	40.75	-110.68	3387	2.7	0.982	561229	10643
	DHO-UM-04	40.75	-110.68	3377	2.7	0.970	596704	10100
Uinta Mts., UT (central) Deadhorse Lake inner	DHI-UM-01	40.75	-110.69	3402	2.7	0.979	516048	22769
	DHI-UM-02	40.75	-110.69	3402	2.7	0.979	493715	18594
	DHI-UM-03	40.75	-110.69	3402	2.7	0.978	473761	19963
	DHI-UM-04	40.75	-110.69	3402	2.7	0.970	501514	10837
	DHI-UM-05	40.75	-110.69	3424	2.7	0.978	532666	10432

	DHI-UM-06	40.75	-110.69	3424	2.7	0.977	496529	12279
Uinta Mts., UT (central) Deadhorse Lake middle	DHM-UM-01	40.74	-110.68	3389	2.7	0.986	638523	17910
	DHM-UM-02	40.74	-110.68	3389	2.7	0.987	594104	22155
	DHM-UM-03	40.74	-110.68	3389	2.7	0.987	659166	23684
	DHM-UM-04	40.74	-110.68	3389	2.7	0.983	625010	27352
	DHM-UM-05	40.75	-110.68	3382	2.7	0.987	639851	11155
	DHM-UM-06	40.75	-110.68	3382	2.7	0.987	646348	12607
	DHM-UM-07	40.75	-110.68	3382	2.7	0.986	628986	10981
Wind River Range, WY Stough Creek middle	SCM-WRR-01	42.64	-109.02	3370	2.65	0.937	518187	11521
	SCM-WRR-02	42.64	-109.02	3370	2.65	0.937	454770	12413
	SCM-WRR-03	42.64	-109.02	3370	2.65	0.935	405606	12608
	SCM-WRR-04	42.64	-109.02	3370	2.65	0.937	513476	19828
	SCM-WRR-05	42.64	-109.02	3370	2.65	0.937	516938	10881
	SCM-WRR-06	42.64	-109.02	3370	2.65	0.936	419736	11808
	SCM-WRR-07	42.64	-109.02	3370	2.65	0.937	434645	16906
Wind River Range, WY Stough Creek outer	SCO-WRR-001	42.64	-109.02	3347	2.65	0.946	537918	25567
	SCO-WRR-002	42.64	-109.02	3355	2.65	0.946	631479	35136
	SCO-WRR-003	42.64	-109.02	3355	2.65	0.946	663862	17186
	SCO-WRR-004	42.64	-109.02	3355	2.65	0.943	614231	32185

	SCO-WRR-005	42.64	-109.02	3355	2.65	0.946	649432	31216
	SCO-WRR-006	42.64	-109.02	3355	2.65	0.946	590055	16093
	SCO-WRR-007	42.64	-109.02	3363	2.65	0.946	554982	22832
Wind River Range, WY Temple Lake	TLO-WRR-01	42.72	-109.18	3253	2.65	0.981	653805	14711
	TLO-WRR-02	42.72	-109.18	3253	2.65	0.987	689433	22471
	TLO-WRR-03	42.72	-109.18	3253	2.65	0.985	661352	21817
	TLO-WRR-04	42.72	-109.18	3253	2.65	0.988	646421	18099
	TLO-WRR-05	42.72	-109.18	3253	2.65	0.988	617971	23066
	TLO-WRR-06	42.72	-109.18	3253	2.65	0.984	514986	19895
	TLO-WRR-07	42.72	-109.18	3253	2.65	0.987	597434	28360
	TLO-WRR-08	42.72	-109.18	3253	2.65	0.987	619574	32529
Front Range, CO Triple Lakes Inner	CFR-01	40.03	-105.63	3480	2.65	0.980	687480	35805
	CFR-02	40.03	-105.63	3480	2.65	0.980	462320	64464
	CFR-03	40.03	-105.63	3480	2.65	0.980	498694	31915
	CFR-04	40.03	-105.63	3480	2.65	0.980	429898	17240
	CFR-05	40.03	-105.63	3480	2.65	0.980	392989	54515
	CFR-06	40.03	-105.63	3480	2.65	0.980	499547	91945
Front Range, CO Triple Lakes Outer	APO-01	40.03	-105.63	3470	2.65	0.980	213202	68752
	APO-02	40.03	-105.63	3470	2.65	0.980	578788	148882
	APO-03	40.03	-105.63	3470	2.65	0.980	372423	50295

	APO-04	40.03	-105.63	3470	2.65	0.980	528105	117104
	APO-05	40.03	-105.63	3470	2.65	0.980	575974	33110
	APO-06	40.03	-105.63	3470	2.65	0.980	444352	27125
	APO-07	40.03	-105.63	3470	2.65	0.980	497139	32884
Front Range, CO	UCL-CFR-01	39.61	-105.64	3613	2.65	0.969	740497	19152
Upper Chicago Lake	UCL-CFR-03	39.61	-105.64	3625	2.65	0.967	737003	26996
	UCL-CFR-05	39.61	-105.64	3616	2.65	0.967	800898	26432
	UCL-CFR-06	39.61	-105.64	3613	2.65	0.967	814348	28245
	UCL-CFR-07	39.61	-105.64	3613	2.65	0.967	812605	22745
Cascades, WA	BL-BG-03	47.48	-120.81	2315	2.65	0.980	322067	15798
Brisingamen	BL-BG-04	47.48	-120.81	2310	2.65	0.980	290647	8399
	BL-BG-05	47.48	-120.81	2310	2.65	0.980	307582	19951
	BL-BG-06	47.48	-120.81	2310	2.65	0.980	313887	13135
	BL-BG-07	47.48	-120.81	2310	2.65	0.980	282119	10139
Tobacco Roots, MT	TR-01	45.60	-112.00	2765	2.65	0.980	462435	24375
Hollowtop	TR-02	45.60	-112.00	2765	2.65	0.980	468627	15328
	TR-03	45.60	-112.00	2765	2.65	0.980	471944	15910
	TR-06	45.60	-112.00	2765	2.65	0.980	408848	13502
	TR-07	45.60	-112.00	2765	2.65	0.980	444657	20911
	TR-08	45.60	-112.00	2765	2.65	0.980	475310	14755
Sierra Nevada, CA	SNV-01	37.17	-118.62	3390	2.65	0.980	558728	56548

Baboon Lakes	SNV-02	37.17	-118.62	3390	2.65	0.980	258709	8560
	SNV-03	37.17	-118.62	3390	2.65	0.980	548799	23078
	SNV-04	37.17	-118.62	3380	2.65	0.980	503050	26466
	SNV-05	37.17	-118.62	3380	2.65	0.980	496861	25387
	SNV-06	37.17	-118.62	3390	2.65	0.980	494459	23961
	SNV-07	37.17	-118.62	3390	2.65	0.980	517658	17311
	SNV-08	37.17	-118.62	3390	2.65	0.980	347250	17135

- Left most column is the Mount Range, U.S. state abbreviation, and moraine name given either by previous authors or in this manuscript.
- 07KNSTD was the ^{10}Be standard for all samples; No erosion correction was applied to the samples; All samples were cut to 2cm thicknesses or less.

Table B3. Age calculations with CHRONUS v.2.2 calculator (Balco et al., 2008) for multiple scaling methods.
Below each column of dates is the arithmetic mean and standard error at 2σ in kyr (Lal, 1991; Dunai, 2000; Stone, 2000; Dunai, 2001; Desilets and Zreda, 2003; Lifton et al., 2005; Desilets et al., 2006).

		Desilets and others (2003,2006)		Dunai (2001)		Lifton and others (2005)		Time-dependent (Lal (1991) / Stone (2000))		Lal (1991) / Stone (2000)	
Sample ID	1σ* (yr)	Exposure Age (yr)	1σ** (yr)	Exposure Age (yr)	1σ** (yr)	Exposure Age (yr)	1σ** (yr)	Exposure Age (yr)	1σ** (yr)	Exposure Age (yr)	1σ** (yr)
LL-MB-01	*332*	*14404*	*1732*	*14313*	*1714*	*13992*	*1416*	*15364*	*1341*	*15595*	*1400*
LL-MB-03	380	13639	1652	13563	1635	13238	1353	14554	1287	14747	1341
LL-MB-04	400	13424	1631	13353	1615	13028	1337	14327	1274	14511	1327
LL-MB-06	595	12948	1628	12886	1613	12558	1352	13828	1309	13996	1357
LL-MB-07	626	13657	1716	13581	1700	13255	1426	14581	1380	14776	1432
LL-MB-08	471	13614	1669	13539	1652	13213	1373	14528	1314	14720	1367
		13.46 ± 0.27		**13.38 ± 0.26**		**13.06 ± 0.26**		**14.36 ± 0.28**		**14.55 ± 0.29**	
DPI-MB-01	396	10517	1296	10500	1289	10169	1065	11220	1025	11374	1067
DPI-MB-03	340	10279	1255	10266	1248	9934	1028	10970	986	11123	1027
DPI-MB-04	474	10256	1289	10243	1282	9912	1067	10944	1036	11098	1076
DPI-MB-05	460	9674	1220	9672	1215	9331	1009	10314	982	10464	1021
DPI-MB-08	*651*	*14663*	*1836*	*14567*	*1817*	*14243*	*1525*	*15655*	*1472*	*15903*	*1532*
		10.18 ± 0.36		**10.17 ± 0.35**		**9.84 ± 0.36**		**10.86 ± 0.39**		**11.01 ± 0.39**	

DP0-MB-01	480	10164	1281	10154	1275	9822	1061	10833	1031	10985	1071
DP0-MB-02	377	10561	1296	10543	1289	10212	1064	11271	1023	11426	1064
DP0-MB-03	373	11208	1369	11178	1360	10849	1123	11980	1078	12129	1121
DP0-MB-04	398	11393	1397	11360	1387	11032	1147	12179	1102	12328	1146
DP0-MB-05	458	11024	1370	10998	1362	10668	1131	11776	1093	11927	1136
DP0-MB-06	411	10991	1354	10965	1345	10636	1113	11746	1073	11898	1115
		10.89 ± 0.37		**10.87 ± 0.36**		**10.54 ± 0.36**		**11.63 ± 0.40**		**11.78 ± 0.40**	
SBO-SFF-01	629	13746	1726	13695	1712	13288	1428	14617	1381	14972	1449
SBO-SFF-02	468	12917	1587	12881	1576	12483	1302	13751	1250	14063	1312
SBO-SFF-03	597	13478	1686	13432	1673	13030	1393	14338	1346	14677	1412
SBO-SFF-04	429	13460	1640	13414	1628	13013	1342	14320	1282	14658	1348
SBO-SFF-05	437	13355	1630	13312	1618	12911	1334	14211	1276	14543	1341
SBO-SFF-06	270	13255	1588	13214	1576	12813	1289	14107	1222	14433	1287
SBO-SFF-07	257	12884	1542	12849	1531	12451	1252	13716	1187	14027	1249
		13.30 ± 0.24		**13.26 ± 0.23**		**12.86 ± 0.23**		**14.15 ± 0.25**		**14.48 ± 0.26**	
SBI-01	201	13460	1603	13414	1591	13012	1299	14334	1228	14673	1295
SBI-02	202	14037	1671	13980	1657	13567	1354	14935	1279	15308	1350
SBI-03	269	12614	1512	12583	1502	12191	1229	13447	1167	13751	1228

SBI-04	*89*	*3844*	*463*	*3921*	*470*	*3784*	*384*	*3976*	*348*	*3753*	*338*
SBI-06	265	16021	1912	15905	1890	15493	1551	17034	1464	17581	1556
SBI-07	341	14699	1767	14624	1751	14216	1438	15626	1363	16052	1441
		14.17 ± 1.15		**14.10 ± 1.12**		**13.70 ± 1.12**		**15.08 ± 1.21**		**15.47 ± 1.30**	
BLI-WP-01	449	10403	1300	10423	1298	10087	1078	10892	1021	11067	1064
BLI-WP-02	451	12440	1531	12423	1523	12079	1263	13050	1190	13226	1238
BLI-WP-04	268	12117	1455	12107	1448	11757	1188	12708	1107	12881	1154
BLI-WP-05	331	11630	1410	11628	1404	11284	1156	12192	1081	12363	1127
BLI-WP-08	320	10402	1266	10423	1263	10087	1039	10884	972	11058	1015
BLI-WP-09	320	11356	1376	11358	1371	11019	1128	11903	1055	12074	1100
		11.39 ± 0.70		**11.39 ± 0.68**		**11.05 ± 0.68**		**11.94 ± 0.74**		**12.11 ± 0.74**	
BL-01	209	12979	1547	12929	1535	12590	1259	13896	1193	14072	1244
BL-02	206	13127	1564	13074	1551	12736	1273	14054	1206	14235	1258
BL-03	550	13542	1681	13480	1666	13145	1390	14495	1341	14693	1394
BL-05	210	13208	1574	13153	1561	12816	1281	14144	1214	14328	1266
BL-07	302	12694	1527	12650	1515	12312	1247	13591	1188	13761	1237
BL-08	190	13212	1573	13158	1559	12821	1279	14145	1211	14329	1263
		13.13 ± 0.23		**13.07 ± 0.22**		**12.74 ± 0.23**		**14.05 ± 0.25**		**14.24 ± 0.25**	
DHO-UM-01	290	11020	1330	11007	1323	10667	1085	11826	1040	11984	1083
DHO-UM-02	664	10031	1334	10036	1330	9695	1125	10743	1119	10902	1159
DHO-UM-03	228	11041	1322	11027	1315	10688	1076	11850	1027	12007	1071
DHO-UM-	221	11964	1429	11933	1419	11588	1162	12835	1107	12994	1154

04											
		11.01 ± 0.79		**11.00 ± 0.77**		**10.66 ± 0.77**		**11.81 ± 0.85**		**11.97 ± 0.85**	
DHI-UM-01	486	10090	1274	10094	1269	9753	1056	10820	1032	10980	1073
DHI-UM-02	397	9655	1198	9668	1195	9317	985	10346	958	10504	997
DHI-UM-03	426	9266	1163	9287	1161	8928	959	9933	938	10088	976
DHI-UM-04	233	9891	1189	9900	1184	9557	967	10603	925	10763	966
DHI-UM-05	220	10273	1231	10273	1226	9931	1000	11037	958	11200	1000
DHI-UM-06	259	9589	1158	9603	1155	9248	942	10291	906	10449	946
		9.79 ± 0.30		**9.80 ± 0.29**		**9.46 ± 0.30**		**10.51 ± 0.32**		**10.66 ± 0.33**	
DHM-UM-01	383	12503	1520	12461	1509	12123	1246	13425	1197	13594	1245
DHM-UM-02	*473*	*11616*	*1441*	*11590*	*1432*	*11250*	*1189*	*12476*	*1153*	*12634*	*1198*
DHM-UM-03	506	12899	1595	12848	1582	12510	1316	13851	1273	14028	1323
DHM-UM-04	586	12279	1549	12241	1538	11901	1287	13185	1256	13349	1303
DHM-UM-05	239	12576	1504	12533	1492	12195	1224	13497	1166	13667	1215
DHM-UM-06	270	12707	1524	12661	1511	12323	1242	13638	1184	13810	1234
DHM-UM-07	236	12379	1480	12340	1469	12002	1205	13285	1147	13451	1196
		12.56 ± 0.18		**12.51 ± 0.18**		**12.18 ± 0.18**		**13.48 ± 0.20**		**13.65 ± 0.20**	
SCM-WRR-	249	10281	1237	10259	1229	9919	1005	11048	966	11175	1005

01											
SCM-WRR-02	268	9020	1094	9019	1089	8660	888	9686	860	9804	895
SCM-WRR-03	273	8049	984	8065	981	7711	798	8621	776	8760	810
SCM-WRR-04	429	10189	1267	10168	1260	9828	1043	10947	1018	11073	1055
SCM-WRR-05	235	10257	1232	10235	1224	9895	1000	11021	960	11148	999
SCM-WRR-06	255	8318	1010	8329	1007	7975	819	8921	794	9053	828
SCM-WRR-07	365	8612	1072	8618	1068	8262	877	9246	860	9369	894
		9.25 ± 0.74		**9.24 ± 0.73**		**8.89 ± 0.73**		**9.93 ± 0.80**		**10.05 ± 0.80**	
SCO-WRR-001	555	10727	1367	10698	1358	10360	1137	11516	1118	11644	1156
SCO-WRR-002	760	12524	1638	12461	1624	12127	1377	13477	1366	13613	1409
SCO-WRR-003	372	13160	1594	13085	1578	12750	1303	14162	1253	14314	1302
SCO-WRR-004	698	12220	1582	12163	1568	11826	1324	13149	1309	13279	1352
SCO-WRR-005	675	12877	1645	12808	1630	12472	1372	13859	1349	14002	1395
SCO-WRR-006	348	11703	1421	11655	1409	11317	1161	12592	1119	12717	1161

SCO-WRR-007	491	10952	1371	10917	1362	10580	1133	11780	1108	11905	1148
		12.02 ± 0.71		**11.97 ± 0.69**		**11.63 ± 0.69**		**12.93 ± 0.77**		**13.07 ± 0.77**	
TLO-WRR-01	325	13344	1607	13273	1592	12937	1312	14255	1248	14403	1297
TLO-WRR-02	494	13964	1714	13881	1697	13541	1411	14914	1353	15086	1405
TLO-WRR-03	480	13438	1651	13366	1635	13030	1359	14356	1304	14507	1353
TLO-WRR-04	397	13105	1593	13039	1579	12701	1306	14001	1248	14140	1295
TLO-WRR-05	506	12534	1555	12477	1542	12142	1284	13387	1238	13515	1282
TLO-WRR-06	*438*	*10485*	*1304*	*10464*	*1297*	*10125*	*1075*	*11174*	*1039*	*11294*	*1077*
TLO-WRR-07	623	12128	1546	12079	1534	11739	1288	12952	1257	13073	1298
TLO-WRR-08	714	12577	1628	12520	1615	12184	1365	13434	1338	13563	1381
		13.01 ± 0.48		**12.95 ± 0.47**		**12.61 ± 0.47**		**13.90 ± 0.51**		**14.04 ± 0.52**	
CFR-01	*743*	*12933*	*1673*	*12880*	*1659*	*12531*	*1401*	*14007*	*1393*	*14209*	*1444*
CFR-02	1334	8636	1580	8664	1583	8309	1422	9367	1530	9544	1572
CFR-03	661	9350	1257	9370	1256	9006	1061	10120	1074	10297	1114
CFR-04	357	8011	1000	8049	1000	7700	821	8674	811	8874	851

CFR-05	1127	7319	1335	7367	1341	7058	1203	7899	1285	8110	1330
CFR-06	1903	9367	2052	9386	2054	9022	1888	10138	2057	10315	2105
		8.54 ± 0.79		**8.57 ± 0.78**		**8.22 ± 0.76**		**9.24 ± 0.86**		**9.43 ± 0.85**	
APO-01	*1427*	*4325*	*1487*	*4412*	*1516*	*4216*	*1423*	*4569*	*1525*	*4420*	*1478*
APO-02	3102	10937	3103	10925	3097	10578	2921	11844	3216	12023	3274
APO-03	1046	7000	1257	7053	1264	6762	1132	7513	1198	7728	1243
APO-04	2439	9974	2511	9981	2511	9634	2343	10786	2566	10967	2619
APO-05	690	10884	1432	10872	1425	10525	1204	11785	1206	11964	1250
APO-06	564	8342	1110	8375	1110	8025	932	9036	943	9224	982
APO-07	685	9382	1271	9401	1270	9038	1075	10146	1090	10322	1130
		9.42 ± 1.25		**9.43 ± 1.23**		**9.09 ± 1.22**		**10.19 ± 1.37**		**10.37 ± 1.36**	
UCL-CFR-01	378	13123	1589	13058	1575	12711	1299	14315	1267	14549	1323
UCL-CFR-03	530	12989	1609	12926	1595	12578	1327	14184	1308	14412	1363
UCL-CFR-05	522	14178	1742	14088	1724	13745	1434	15449	1404	15742	1468
UCL-CFR-06	559	14441	1781	14343	1762	14006	1469	15729	1439	16040	1506

UCL-CFR-07	450	14405	1752	14308	1733	13971	1436	15690	1399	15999	1466
		13.83 ± 0.64		**13.74 ± 0.62**		**13.40 ± 0.63**		**15.07 ± 0.68**		**15.35 ± 0.72**	
BL-BG-03	558	11408	1461	11460	1462	10993	1214	11446	1119	11343	1135
BL-BG-04	298	10349	1260	10405	1261	9954	1025	10368	926	10269	942
BL-BG-05	707	10942	1477	10996	1479	10538	1247	10970	1170	10869	1181
BL-BG-06	465	11163	1401	11216	1402	10754	1155	11195	1056	11092	1072
BL-BG-07	359	10051	1242	10108	1244	9661	1016	10065	924	9967	939
		10.78 ± 0.51		**10.84 ± 0.50**		**10.38 ± 0.50**		**10.81 ± 0.52**		**10.71 ± 0.51**	
TR-01	677	12382	1604	12371	1597	11960	1341	12807	1277	12806	1305
TR-02	426	12546	1540	12533	1532	12120	1262	12979	1177	12978	1208
TR-03	442	12634	1554	12620	1546	12205	1275	13071	1190	13070	1222
TR-06	*375*	*10958*	*1346*	*10961*	*1340*	*10563*	*1101*	*11315*	*1027*	*11318*	*1055*
TR-07	581	11911	1517	11904	1510	11496	1259	12314	1192	12312	1220
TR-08	410	12723	1556	12708	1548	12291	1274	13163	1186	13164	1218
		12.44 ± 0.29		**12.43 ± 0.28**		**12.01 ± 0.28**		**12.87 ± 0.30**		**12.87 ± 0.30**	
SNV-01	1314	12084	1883	12100	1881	11705	1658	12721	1681	12941	1731
SNV-02	*198*	*5808*	*712*	*5873*	*717*	*5699*	*593*	*5969*	*541*	*5982*	*557*
SNV-03	536	11865	1490	11885	1486	11491	1235	12493	1180	12710	1230
SNV-04	618	10934	1416	10967	1415	10598	1187	11493	1145	11713	1193
SNV-05	593	10799	1391	10834	1391	10467	1165	11350	1122	11569	1169
SNV-06	556	10678	1365	10716	1364	10350	1140	11230	1095	11448	1142
SNV-07	402	11181	1374	11209	1372	10837	1131	11771	1070	11987	1119
SNV-08	*397*	*7436*	*952*	*7508*	*958*	*7231*	*798*	*7795*	*763*	*8033*	*804*

		11.26 ± 0.48	**11.29 ± 0.47**	**10.91 ± 0.46**	**11.84 ± 0.51**	**12.06 ± 0.51**

[*] *Internal Uncertainty (1σ)*

[**] *External Uncertainty (1σ)*

Note: Underlined and italicized sample id and numbers are outliers as defined in text and are not included in the mean moraine age calculation.

Table B4. Age calculations with CHRONUS v.2.2 calculator (Balco et al., 2008) for multiple scaling methods using the NE North America calibration set (Balco et al., 2009).

Below each column of dates is the arithmetic mean and standard error at 2σ in kyr.

		Desilets and others (2003,2006)		Dunai (2001)		Lifton and others (2005)		Time-dependent (Lal (1991) / Stone (2000))		Lal (1991) / Stone (2000)	
Sample ID	1σ* (yr)	Exposure Age (yr)	1σ** (yr)	Exposure Age (yr)	1σ** (yr)	Exposure Age (yr)	1σ** (yr)	Exposure Age (yr)	1σ** (yr)	Exposure Age (yr)	1σ** (yr)
LL-MB-01	*379*	*15338*	*819*	*15199*	*813*	*15111*	*806*	*17304*	*919*	*17789*	*938*
LL-MB-03	434	14533	804	14411	798	14315	791	16398	903	16820	920
LL-MB-04	456	14300	803	14183	797	14085	790	16137	902	16540	918
LL-MB-06	679	13802	895	13694	889	13588	880	15589	1007	15958	1026
LL-MB-07	715	14557	942	14433	935	14337	927	16432	1060	16858	1082
LL-MB-08	537	14501	848	14379	842	14283	834	16362	953	16782	971
		14.34 ± 0.28		**14.22 ± 0.28**		**14.12 ± 0.28**		**16.18 ± 0.31**		**16.59 ± 0.34**	
DPI-MB-01	451	11223	673	11169	671	11023	661	12716	760	12970	771
DPI-MB-03	388	10966	633	10918	631	10767	620	12431	714	12682	724
DPI-MB-04	540	10944	710	10896	708	10744	697	12405	803	12655	815
DPI-MB-05	525	10323	679	10288	677	10124	665	11688	766	11934	778
DPI-MB-08	*743*	*15613*	*996*	*15465*	*988*	*15379*	*980*	*17633*	*1122*	*18142*	*1148*

		10.86 ± 0.38		**10.82 ± 0.37**		**10.66 ± 0.38**		**12.31 ± 0.44**		**12.56 ± 0.44**	
DP0-MB-01	548	10843	711	10798	709	10644	697	12277	803	12524	815
DP0-MB-02	430	11266	664	11212	662	11067	652	12771	750	13026	760
DP0-MB-03	426	11965	691	11896	688	11759	679	13554	780	13826	791
DP0-MB-04	454	12170	713	12098	710	11968	700	13784	805	14062	816
DP0-MB-05	522	11766	732	11701	728	11562	718	13331	826	13598	838
DP0-MB-06	469	11735	702	11670	699	11531	689	13304	793	13571	804
		11.62 ± 0.4		**11.56 ± 0.39**		**11.42 ± 0.4**		**13.17 ± 0.45**		**13.43 ± 0.46**	
SBO-SFF-01	718	14646	945	14543	939	14361	925	16447	1057	17076	1092
SBO-SFF-02	534	13783	816	13702	812	13513	799	15497	913	16038	940
SBO-SFF-03	681	14368	914	14274	909	14092	895	16141	1023	16739	1056
SBO-SFF-04	489	14350	818	14257	814	14074	801	16121	915	16717	943
SBO-SFF-05	499	14242	818	14152	814	13968	801	16001	915	16586	943
SBO-SFF-	308	14139	741	14052	737	13864	725	15886	828	16461	851

06											
SBO-SFF-07	293	13749	718	13669	715	13480	703	15461	803	15998	825
		14.18 ± 0.24		**14.09 ± 0.24**		**13.91 ± 0.24**		**15.94 ± 0.27**		**16.52 ± 0.29**	
SBI-01	229	14341	729	14247	725	14064	713	16127	815	16724	838
SBI-02	230	14937	757	14825	753	14643	741	16787	846	17448	872
SBI-03	307	13456	709	13382	706	13194	694	15161	795	15672	815
SBI-04	*101*	*4070*	*221*	*4137*	*225*	*4056*	*220*	*4426*	*239*	*4276*	*229*
SBI-06	302	17034	873	16849	864	16687	853	19175	977	20054	1014
SBI-07	389	15629	834	15495	828	15322	816	17562	933	18296	964
		15.08 ± 1.21		**14.96 ± 1.17**		**14.78 ± 1.18**		**16.96 ± 1.36**		**17.64 ± 1.48**	
BLI-WP-01	513	11100	705	11084	705	10925	694	12347	782	12617	795
BLI-WP-02	514	13269	791	13208	789	13075	779	14735	875	15080	890
BLI-WP-04	306	12931	687	12878	686	12739	676	14365	760	14691	771
BLI-WP-05	377	12414	692	12372	691	12228	681	13790	765	14090	777
BLI-WP-08	365	11102	631	11086	631	10928	620	12341	698	12610	709
BLI-WP-09	365	12127	675	12091	674	11943	664	13472	746	13763	757
		12.16 ± 0.74		**12.12 ± 0.73**		**11.97 ± 0.74**		**13.51 ± 0.82**		**13.81 ± 0.84**	
BL-01	239	13839	708	13742	704	13626	696	15666	797	16050	810
BL-02	235	13989	714	13888	710	13774	702	15832	803	16227	817
BL-03	627	14423	889	14313	883	14207	874	16321	1002	16750	1023
BL-05	239	14078	719	13976	715	13864	707	15937	810	16338	823
BL-07	345	13534	726	13445	722	13325	714	15329	818	15690	831
BL-08	217	14087	714	13986	710	13873	702	15942	804	16344	817

		13.99 ± 0.24		**13.89 ± 0.24**		**13.78 ± 0.24**		**15.84 ± 0.27**		**16.23 ± 0.29**	
DHO-UM-01	330	11757	641	11704	639	11554	629	13383	727	13658	736
DHO-UM-02	758	10703	836	10674	834	10507	820	12181	950	12434	966
DHO-UM-03	261	11787	618	11733	617	11583	607	13415	700	13691	709
DHO-UM-04	252	12769	661	12695	658	12563	649	14506	747	14822	757
		11.75 ± 0.84		**11.7 ± 0.83**		**11.55 ± 0.84**		**13.37 ± 0.95**		**13.65 ± 0.98**	
DHI-UM-01	554	10762	710	10730	708	10565	696	12262	806	12517	819
DHI-UM-02	452	10297	636	10276	635	10102	623	11720	721	11974	733
DHI-UM-03	486	9893	639	9880	639	9698	626	11248	724	11500	737
DHI-UM-04	266	10555	564	10528	564	10359	553	12024	640	12275	648
DHI-UM-05	251	10964	578	10927	577	10765	566	12515	656	12775	665
DHI-UM-06	296	10232	561	10211	560	10035	549	11662	636	11918	646
		10.45 ± 0.32		**10.43 ± 0.31**		**10.25 ± 0.32**		**11.91 ± 0.37**		**12.16 ± 0.37**	
DHM-UM-01	437	13339	753	13252	749	13130	740	15156	852	15508	866

DHM-UM-02	*539*	*12405*	*764*	*12339*	*761*	*12202*	*750*	*14113*	*866*	*14411*	*879*
DHM-UM-03	577	13751	836	13653	831	13536	822	15613	945	15995	963
DHM-UM-04	669	13100	861	13019	857	12891	847	14888	976	15224	993
DHM-UM-05	273	13409	697	13321	693	13199	685	15226	787	15582	799
DHM-UM-06	308	13544	714	13452	710	13332	701	15375	806	15741	819
DHM-UM-07	269	13198	686	13115	682	12990	674	14992	775	15332	786
		13.39 ± 0.19		**13.3 ± 0.19**		**13.18 ± 0.19**		**15.21 ± 0.21**		**15.56 ± 0.23**	
SCM-WRR-01	284	10963	589	10906	587	10746	577	12514	669	12739	676
SCM-WRR-02	306	9633	540	9602	539	9411	526	10963	611	11176	619
SCM-WRR-03	311	8591	498	8579	498	8364	484	9789	565	9986	573
SCM-WRR-04	489	10864	678	10809	675	10647	663	12399	771	12623	780
SCM-WRR-05	268	10937	582	10880	580	10720	570	12484	661	12709	668
SCM-WRR-06	291	8888	501	8870	501	8659	488	10122	569	10324	576

SCM-WRR-07	417	9201	575	9178	574	8974	560	10473	652	10680	662
		9.87 ± 0.78		**9.83 ± 0.77**		**9.65 ± 0.79**		**11.25 ± 0.9**		**11.46 ± 0.91**	
SCO-WRR-001	633	11440	781	11374	777	11224	766	13043	888	13275	900
SCO-WRR-002	867	13352	991	13247	984	13125	973	15208	1126	15522	1145
SCO-WRR-003	424	14025	777	13906	771	13790	763	15962	880	16321	894
SCO-WRR-004	797	13033	936	12935	930	12808	919	14849	1064	15144	1080
SCO-WRR-005	770	13725	943	13612	936	13494	926	15626	1071	15965	1089
SCO-WRR-006	397	12485	700	12398	696	12264	686	14232	794	14500	804
SCO-WRR-007	560	11683	747	11610	744	11462	733	13332	850	13573	861
		12.82 ± 0.75		**12.73 ± 0.74**		**12.6 ± 0.75**		**14.61 ± 0.85**		**14.9 ± 0.88**	
TLO-WRR-01	371	14214	766	14100	761	13986	753	16061	861	16418	874
TLO-WRR-02	563	14876	876	14749	869	14638	861	16808	986	17212	1003
TLO-WRR-03	548	14317	846	14201	840	14087	831	16177	952	16541	968
TLO-WRR-	453	13962	788	13852	783	13733	774	15778	886	16117	899

04											
TLO-WRR-05	577	13358	823	13259	818	13136	808	15105	927	15405	940
TLO-WRR-06	*499*	*11186*	*698*	*11130*	*695*	*10974*	*684*	*12661*	*787*	*12881*	*796*
TLO-WRR-07	710	12933	883	12843	878	12713	867	14629	996	14906	1010
TLO-WRR-08	815	13405	964	13306	957	13182	947	15158	1087	15461	1104
		13.87 ± 0.51		**13.76 ± 0.5**		**13.64 ± 0.5**		**15.67 ± 0.57**		**16.01 ± 0.6**	
CFR-01	*847*	*13791*	*987*	*13689*	*981*	*13564*	*970*	*15782*	*1127*	*16201*	*1152*
CFR-02	1521	9243	1369	9243	1369	9038	1338	10615	1571	10881	1609
CFR-03	753	9985	805	9971	805	9786	789	11462	923	11739	942
CFR-04	407	8563	542	8574	543	8364	529	9861	622	10116	634
CFR-05	1285	7807	1150	7832	1154	7614	1122	8983	1323	9245	1360
CFR-06	2171	10002	1909	9987	1907	9803	1871	11482	2192	11759	2243
		9.12 ± 0.85		**9.12 ± 0.83**		**8.92 ± 0.84**		**10.48 ± 0.96**		**10.75 ± 0.97**	
APO-01	*1627*	*4583*	*1496*	*4660*	*1522*	*4524*	*1477*	*5108*	*1668*	*5038*	*1645*
APO-02	3538	11678	3066	11625	3053	11466	3010	13410	3522	13707	3599
APO-03	119	7440	1070	7471	1075	7271	1046	8537	1227	8809	1265

	2										
APO-04	2781	10645	2423	10616	2417	10443	2377	12228	2784	12503	2846
APO-05	787	11619	878	11567	875	11409	862	13345	1007	13640	1025
APO-06	644	8926	699	8931	700	8722	682	10255	801	10515	819
APO-07	781	10018	825	10003	825	9819	808	11491	945	11768	965
		10.05 ± 1.34		**10.04 ± 1.32**		**9.86 ± 1.33**		**11.54 ± 1.54**		**11.82 ± 1.55**	
UCL-CFR-01	431	13994	775	13878	770	13757	761	16123	889	16590	908
UCL-CFR-03	605	13854	848	13741	842	13617	832	15980	974	16437	997
UCL-CFR-05	595	15100	892	14955	885	14851	877	17388	1024	17956	1051
UCL-CFR-06	637	15369	923	15217	915	15118	907	17697	1059	18289	1088
UCL-CFR-07	513	15338	866	15186	858	15087	850	17661	993	18250	1019
		14.73 ± 0.67		**14.6 ± 0.65**		**14.49 ± 0.66**		**16.97 ± 0.76**		**17.5 ± 0.82**	
BL-BG-03	636	12161	844	12184	846	11894	824	12941	895	12927	890
BL-BG-04	339	11028	627	11058	629	10774	612	11718	663	11702	658
BL-BG-05	806	11662	949	11688	952	11402	927	12403	1007	12386	1003
BL-BG-06	531	11899	767	11924	769	11636	749	12656	813	12641	808
BL-BG-07	409	10709	650	10741	653	10458	634	11373	688	11358	683
		11.49 ± 0.54		**11.52 ± 0.54**		**11.23 ± 0.54**		**12.22 ± 0.59**		**12.2 ± 0.59**	

TR-01	772	13200	951	13154	948	12938	931	14467	1040	14601	1045
TR-02	486	13374	788	13325	786	13109	771	14657	860	14797	863
TR-03	504	13467	801	13417	799	13201	784	14759	874	14902	878
TR-06	*428*	*11685*	*690*	*11656*	*689*	*11440*	*675*	*12804*	*753*	*12903*	*754*
TR-07	662	12700	863	12659	861	12444	845	13920	943	14038	947
TR-08	468	13561	786	13511	785	13293	770	14863	858	15009	861
		13.26 ± 0.3		**13.21 ± 0.3**		**13 ± 0.3**		**14.53 ± 0.33**		**14.67 ± 0.34**	
SNV-01	1499	12892	1453	12866	1450	12676	1428	14372	1618	14753	1659
SNV-02	*226*	*6110*	*361*	*6167*	*364*	*6048*	*357*	*6627*	*389*	*6817*	*398*
SNV-03	612	12663	818	12641	817	12451	803	14123	909	14490	928
SNV-04	705	11671	840	11667	840	11472	825	13026	935	13353	954
SNV-05	676	11523	816	11521	817	11330	802	12864	909	13188	928
SNV-06	634	11394	785	11394	786	11203	772	12728	875	13050	893
SNV-07	459	11942	708	11935	709	11737	695	13327	787	13665	802
SNV-08	*453*	*7939*	*552*	*7996*	*556*	*7803*	*542*	*8864*	*614*	*9156*	*632*
		12.01 ± 0.51		**12.00 ± 0.50**		**11.81 ± 0.50**		**13.41 ± 0.56**		**13.75 ± 0.58**	

[*] *Internal Uncertainty (1σ)*

[**] *External Uncertainty (1σ)*

Note: Underlined and italicized sample id and numbers are outliers as defined in text.

B.4 Prior Work

All exposure dates from other studies mentioned in the text were recalculated using the CHRONUS Calculator v.2.2 (Balco et al., 2008; Balco et al., 2009). All of the information used for the calculations was derived from the original literature (e.g. location information, shielding corrections, rock densities, etc) including snow corrections when available (Table B5 – B7). Outliers were identified using the same criterion as previously described where they were initially defined as being greater than 4 standard deviations from the mean value of the other boulder exposure ages. We then use Chavenet's criterion (Taylor, 1997) to identify any remaining outlier, which were five in total (Table B6 & B7).

B.4.1 Medicine Bow Mountains (Snowy Range), Wyoming.

Oviatt (1977) differentiated the age of cirque deposits using relative dating methods (lichens, weathering rinds, soil characteristics) inferring a Neoglacial age for the inner most moraines, Disaster Peak deposits, and a type 'Temple Lake' age for the outer moraines, Lookout Lake deposits. He subsequently revised the inferred age for Disaster Peak deposits as being early Holocene or latest Pleistocene, with no record of Neoglaciation though this is based on no additional data or numerical constraints (pers. comm., in (Davis, 1988)).

B.4.2 Sangre de Cristos, New Mexico.

Using relative dating techniques (weather rinds, soil profiles), Wesling (1988) mapped two cirque moraines in the vicinity of Lake Katherine that he assigned late Pleistocene to early Holocene age for the outermost moraine and a late Holocene age for the innermost based on a single radiocarbon date (3700 ^{14}C yr BP) from charcoal

underlying a till deposit. Subsequent work by Armour et al. (2002) combined results from a sediment core from a bog downvalley of the high alpine cirques with the mapped moraines from the Lake Katherine cirque to argue for glacier advances during the Younger Dryas and Neoglaciation. Our new data show that both the inner and outer moraines mapped separately by Wesling (1988) are coeval in age.

B.4.3 South Snake Range (Wheeler Peak – Great Basin National Park), Nevada.

Osborn and Bevis (2001) summarized evidence for three latest Pleistocene/Holocene glaciations in Nevada. They inferred the youngest advances to be LIA and mid- Neoglacial in age based largely on their positions relative to cirque headwalls. The older glacial advance occurred during the latest Pleistocene or early Holocene (pre-Hypsithermal) as inferred from Mazama tephra deposits on moraine slopes and weathering rinds of boulders on moraines. The outer of three recessional moraines, Angel Lake depsosits, in the Ruby Range in northwestern Nevada are dated greater than 13,000±900 ^{14}C yr BP. At Wheeler Peak in Great Basin National Park near the Utah-Nevada border, Osborn and Beavis mapped three end moraines between the Wheeler Peak rock glacier that is late Holocene in age and the large Angel Lake moraines, which they inferred some to be latest Pleistocene in age though no relative or numerical dates were used.

B.4.4 Wind River Range (Stough Creek), Wyoming.

Dahms (2002) mapped four glacial deposit in the Stough Creek Basin of the Wind River Range directly upslope of Bigfoot Lake. The innermost deposits he correlated to the Gannett Peak deposits in the Colorado Front Range and just distal to this deposit he mapped a moraine, which he termed the Black Joe formation, and

assigned an age of late Holocene to it based on lichen and soil development. We have since reinterpreted his Black Joe 'moraine' to be a rock glacier deposit most likely correlative with his Gannett Peak deposits. Based on the morphology (steeper sloped on the downfacing side and less steep on the upfacing slope) and the sorting of the deposit (typically angular boulders with little to no soil deposits) we make our interpretation. Downslope from these deposits toward Bigfoot Lake, Dahms (2002) mapped two additional moraines, which he termed and correlated to the type Alice Lake and Temple Lake advances. He assigned ages to these moraines of 4,000 – 6000 yrs and 10,000 – 12,000 yrs, respectively.

B.4.5 Uinta Mountains (Deadhorse Lake), Utah.

Munroe (2002) mapped several cirque moraines near Deadhorse Lake that he dated with lichenometry as mid- to late Neoglaciation (~1,300–3,000 yr BP). ^{14}C ages of 8,570±80 and 8,950±70 ^{14}C yr BP on organic material from bogs behind cirque moraines in nearby valleys suggest possible latest Pleistocene glaciers extending 1-2 km beyond present cirque headwalls (Munroe, 2002). Of the three moraines mapped in this study, one was out of stratigraphic order (DHO-UM), which we attribute to exhumation during moraine deflation (Figure B25). We did not include this moraine in our western North American compilation and data analysis, but we do include the ages and information regarding this moraine here in the Appendix.

B.4.6 Wind River Range (Temple Lake), Wyoming.

Based on relative weathering of deposits in the Temple Lake area in the southern Wind River Range, Moss (1951) suggested that moraines that lie about 3 km from the modern glacier margin are about 10,000 years old. In contrast, Richmond

(1965) considered these moraines to be Neoglacial in age (1,000-4,000 yrs) and subsequently named them Temple Lake stade. In 1974 Currey (1974) dated organic material from a bog on the inner type Temple Lake moraine to 6500 ± 230 ^{14}C yr BP and assigned a pre-Neoglcial age to the deposits. Miller and Birkeland (1974) concurred with Currey's pre-Neoglacial age assessment of the type Temple Lake, but still recognized three ages of Neoglacial deposits in the area. Zielinski and Davis (1987) ^{14}C-dated lake sediment cores in Temple Lake valley, which demonstrated that the type Temple Lake moraines were possibly late Pleistocene.

B.4.7 Colorado Front Range (Triple Lakes), Colorado.

In Arapaho cirque on the east side of the Colorado Front Range (CFR), Benedict (1973) used lichenometry, rock weathering, soils, and ^{14}C dating to distinguish three periods of Neoglacial activity, in which he introduced the term Triple Lakes stade as correlative to the Temple Lake stade in Wyoming. Benedict (1973) suggested that the earliest of the Triple Lakes advances occurred about 4485 ± 100 ^{14}C yr BP, based on a sediment sample obtained outside the outer type Triple Lakes moraine, and that the middle of the three advances occurred about 3865 ± 100 ^{14}C yr BP, based on a sample of proglacial lake sediment exposed in a former drainage channel across the inner type Triple Lakes moraine. However, Davis (1988) obtained a sediment core from the small pond that is impounded by the inner type Triple Lakes moraine and dated near-basal sediments to 10,410 ± 520 and 9915 ± 380 ^{14}C yr BP from detrital organic material. The most recent of the Triple Lakes glacier advances is represented only by a rock glacier in Arapaho cirque, which Benedict (1973) dated by lichenometry to approximately 3000 ^{14}C yr BP.

B.4.8 Colorado Front Range (Chicago Lakes), Colorado.

Benson et al. (2007) dated samples from three sites in the Colorado Front Range by ^{10}Be. Six samples from LIA moraines fronting Isabelle Glacier, just north of Arapaho cirque suggest up to 1,500 – 3,000 yrs BP of ^{10}Be inheritance, 12 samples from Butler Gulch cirque, ~25 km south-southwest of Arapaho cirque, suggest moraines were formed during the early Holocene, and 8 of 9 samples from near Lower Chicago Lake, ~45 km south of Arapaho cirque, suggest moraines were formed during the Younger Dryas. However, there is much scatter in the data, especially for the Butler Gulch samples, suggesting issues with inheritance, but also perhaps shielding and sample quality. The production choice used by Benson et al. (2007) is also questionable and likely too high. When calculated with the CHRONUS online calculator, the Lower Chicago Lakes moraine is 1,000 – 2000 years older (Table B7).

B.4.9 Cascade Range (Enchantment Lakes Basin), Washington.

Waitt et al. (1982) distinguished two moraines in the Enchantment Lakes Basin based on tephra deposits, rock weathering and moraine morphology. The youngest moraine was thought to represent a LIA advance, whereas the older was interpreted to be early Holocene (>7,700 yrs BP). However, Bilderback (2004) reinterpreted the age of this older moraine to be >11,300 yrs BP based on limiting ^{14}C ages from bulk sediments in a core collected from Lake Viviane down valley of the moraine. Based on an increase in rock flour in the cores, Bilderback (2004) recognized the LIA advance and also interpreted that a Neoglacial advance occurred ~2,800 – 3,300 ^{14}C ka B.P.

B.4.10 Tobacco Root Range, Montana.

In the Tobacco Root Range, Hall and Heiny (1983) mapped moraines about 2 km from cirque headwalls that they correlated to the type Temple Lake based on rock weathering and soils. Hall and Heiny (1983) also recognized three sets of moraines closer to cirque headwalls that they interpreted to be early, mid-, and late Neoglacial in age.

B.4.11 Sierra Nevada (Baboon Lakes), California.

Birman (1964) proposed three late-Holocene glaciations for the Sierra Nevada: the older Hilgard, the Recess Peak, and the younger Matthes glaciation. The Matthes glaciation is thought to have occurred during the LIA. Zreda and Phillips (1995) inferred the age of the Hilgard glaciation to be middle Holocene from surface exposure ages (^{36}Cl) from moraines in the Little McGee Creek basin (7,000–8,000 yr B.P.), but Clark and Gillespie (1997) argued that it is a recessional phase from the late Pleistocene Tioga glaciation. The Recess Peak glaciation was originally thought to date between 2,000 and 5,000 yr BP (Curry, 1969; Yount et al., 1979), but Clark and Gillespie (1997) used limiting ^{14}C ages from multiple lake sediment cores throughout the Sierra to demonstrate that the advance must have occurred >13,000 yrs BP, though the timing of glaciation after ~13,000 years comes from a single ^{14}C age from organic silt in the Baboon Lakes (11,190 ± 70 ^{14}C ; core BL-2 from 115-116cm). Subsquent work by Phillips et al (2009) based on surface exposure dating with ^{36}Cl have yielded an average age of 12,500 ± 700 yrs BP for the Recess Peak moraines near Baboon Lakes with an oldest boulder age of 13,500 yr BP the latter age being taken as their best estimate of the moraine deposition.

Table B5. Sample information for age calculations with CHRONUS calculator (Balco et al., 2008) of other sites not from this study with ^{10}Be chronologies.

	Sample ID	Lat. (DD)	Long. (DD)	Elev. (m)	Thickness (cm)	Density (g/cm^3)	Shield.	Be (atom/g)	1σ (atom/g)	Be Std
(Gosse et al., 1995) Inner Titcomb Lakes	WY-92-140	43.120	-109.640	3231	8	2.65	0.9668	476000	14280	KNSTD
	WY-92-139	43.120	-109.640	3231	4	2.65	0.9668	591000	17730	KNSTD
	WY-93-333	43.120	-109.640	3231	3	2.65	0.9668	596600	17898	KNSTD
	WY-93-339	43.120	-109.640	3231	4	2.65	0.9668	623900	18717	KNSTD
	WY-92-138	43.120	-109.640	3231	4	2.65	0.9668	627000	18810	KNSTD
	WY-93-338	43.120	-109.640	3231	5	2.65	0.9668	625100	18753	KNSTD
	WY-93-335	43.120	-109.640	3231	8	2.65	0.9668	615700	18471	KNSTD
	WY-93-337	43.120	-109.640	3231	9	2.65	0.9668	624700	18741	KNSTD
	WY-93-336	43.120	-109.640	3231	3	2.65	0.9668	656600	19698	KNSTD

	WY-93-334	43.120	-109.640	3231	7	2.65	0.9668	669700	20091	KNSTD
(Licciardi and Pierce, 2008) Burned Ridge moraine	BR-11	43.752	-110.580	2162	2.25	2.7	1	364700	9000	KNSTD
	BR-3	43.752	-110.615	2126	1	2.7	1	364700	9000	KNSTD
Outer Jenny Lake moraine	OJEN-3	43.766	-110.711	2094	1.5	2.7	1	337700	8000	KNSTD
	OJEN-10	43.783	-110.730	2115	2	2.7	0.992	340700	8000	KNSTD
	OJEN-1	43.766	-110.710	2102	2.25	2.7	1	354700	6000	KNSTD
	OJEN-5	43.766	-110.711	2092	1.5	2.7	1	361700	8000	KNSTD
	OJEN-8	43.765	-110.711	2095	1.5	2.7	1	364700	9000	KNSTD
	OJEN-2	43.766	-110.711	2094	2.5	2.7	1	374700	9000	KNSTD
	OJEN-11	43.784	-110.729	2100	2	2.7	0.992	375700	14000	KNSTD
	OJEN-7	43.765	-110.710	2099	2	2.7	1	380700	9000	KNSTD
	OJEN-9	43.765	-110.711	2095	2	2.7	1	383700	9000	KNSTD
	OJEN-6	43.765	-110.710	2102	1.5	2.7	1	389700	9000	KNSTD
	OJEN-7D	43.765	-110.710	2099	2	2.7	1	391700	11000	KNSTD

Inner Jenny Lake moraine	IJEN-5	43.778	-110.722	2110	2	2.7	1	296700	7000	KNSTD
	IJEN-2	43.780	-110.725	2097	1.75	2.7	1	318700	9000	KNSTD
	IJEN-7	43.767	-110.714	2093	2	2.7	1	324700	8000	KNSTD
	IJEN-1	43.781	-110.726	2113	1.75	2.7	1	337700	8000	KNSTD
	IJEN-3	43.780	-110.723	2108	2	2.7	1	355700	8000	KNSTD
	IJEN-13	43.758	-110.717	2090	1.5	2.7	1	356700	8000	KNSTD
	IJEN-6	43.775	-110.719	2103	1.75	2.7	1	359700	9000	KNSTD
	IJEN-11	43.758	-110.716	2084	2	2.7	1	374700	9000	KNSTD
	IJEN-4	43.779	-110.722	2105	2	2.7	1	438700	13000	KNSTD
	IJEN-12	43.757	-110.716	2085	1.5	2.7	1	449700	8000	KNSTD
(Licciardi et al., 2004) Glacier Lake moraine	GL-3	45.159	-117.284	2509	1.5	2.8	0.9821	301000	12000	KNSTD
	GL-5	45.160	-117.285	2504	2.5	2.8	0.9852	324000	20000	KNSTD
	GL-7C	45.160	-117.284	2502	1	2.8	0.9852	344000	32000	KNSTD
	GL-7B	45.160	-117.284	2502	1	2.8	0.9852	351000	19000	KNSTD
	GL-5C	45.160	-117.285	2504	2.5	2.8	0.9846	348000	19000	KNSTD
	GL-1	45.158	-117.283	2512	1.5	2.8	0.944	363000	15000	KNSTD
	GL-6C	45.160	-117.285	2503	1.5	2.8	0.9852	426000	35000	KNSTD

(Owen et al., 2003)	SG44	34.108	-116.847	3121	5	2.7	0.9594	292923	10497	KNSTD
San Bernadino Mts	SG43	34.108	-116.847	3128	5	2.7	0.9591	313451	11278	KNSTD
Little Draw	SG42	34.108	-116.847	3126	5	2.7	0.9366	335301	11213	KNSTD
	SG41	34.108	-116.847	3123	5	2.7	0.96	398245	13581	KNSTD
North Fork	SG29	34.105	-116.823	3157	5	2.7	0.9614	408038	10834	KNSTD
	SG32	34.105	-116.824	3166	5	2.7	0.9692	439130	11580	KNSTD
	SG31	34.105	-116.824	3167	5	2.7	0.9692	496404	12813	KNSTD
	SG30	34.105	-116.823	3160	5	2.7	0.9614	499585	14190	KNSTD
Big Draw 1	SG49	34.110	-116.845	3049	5	2.7	0.9691	440894	13387	KNSTD
	SG50	34.110	-116.845	3045	5	2.7	0.9711	470939	14409	KNSTD
	SG48	34.110	-116.845	3048	5	2.7	0.9673	494655	28256	KNSTD
Big Draw 2	SG16	34.109	-116.838	3018	5	2.7	0.9776	451488	11886	KNSTD
	SG17	34.109	-116.838	3016	5	2.7	0.9777	476375	12673	KNSTD
	SG18	34.109	-116.838	3011	5	2.7	0.9777	493580	13488	KNSTD
	SG15	34.108	-116.838	3037	5	2.7	0.9782	503736	13151	KNSTD
	SG19	34.109	-116.838	3019	5	2.7	0.9775	324403	9465	KNSTD
Dollar Lake	SG21	34.123	-116.855	2886	5	2.7	0.9812	440836	11728	KNSTD

	SG23	34.123	-116.852	2964	5	2.7	0.9781	480477	12583	KNSTD
	SG24	34.123	-116.852	2847	5	2.7	0.982	475828	11941	KNSTD
	SG22	34.124	-116.853	2848	5	2.7	0.9791	501659	13043	KNSTD
(Benson et al., 2007)	CL03-4	39.620	-105.630	3488	3	2.7	0.982	709100	39710	S555
Chicago Lake	CL03-5	39.620	-105.630	3487	2	2.7	0.982	775200	41861	S555
	CL03-9	39.620	-105.630	3512	4	2.7	0.982	790000	79790	S555
	CL03-6	39.620	-105.630	3496	4	2.7	0.982	802000	44110	S555
	CL03-8	39.620	-105.630	3517	5	2.7	0.982	805300	33823	S555
	CL03-7	39.620	-105.630	3503	3	2.7	0.982	831300	39071	S555
	CL03-1	39.620	-105.630	3476	3	2.7	0.982	840200	39489	S555
	CL03-2	39.620	-105.630	3476	4	2.7	0.982	838300	41915	S555
	CL03-3	39.620	-105.630	3500	4	2.7	0.982	1208000	41072	S555
Bulter Gulch	BG03-1	39.600	-105.600	3663	5	2.7	0.982	622700	31135	S555
	BG03-2	39.600	-105.600	3664	4	2.7	0.982	465300	23265	S555
	BG03-3	39.600	-105.600	3657	2	2.7	0.982	331600	16580	S555
	BG03-4	39.600	-105.600	3655	5	2.7	0.982	401400	20070	S555
	BG03-5	39.600	-105.600	3659	3	2.7	0.982	670800	33540	S555
	BG03-6	39.600	-105.600	3615	3	2.7	0.982	438500	21925	S555
	BG03-7	39.600	-105.600	3666	2.5	2.7	0.982	734300	36715	S555

	BG03-8	39.600	-105.600	3673	2	2.7	0.982	656000	32800	S555
	BG03-9	39.600	-105.600	3671	4	2.7	0.982	726800	36340	S555
	BG03-10	39.600	-105.600	3662	5	2.7	0.982	671900	33595	S555
- No erosion corrections were applied to any of the samples.										

Table B6. Age calculations with CHRONUS v.2.2 calculator (Balco et al., 2008) for multiple scaling methods.

Below each column of dates is the arithmetic mean and standard error at 2σ in kyr.

			Desilets and others (2003,2006)		Dunai (2001)		Lifton and others (2005)		Time-dependent (Lal (1991) / Stone (2000))		Lal (1991) / Stone (2000)	
	Sample ID	1σ* (yr)	Exposure Age (yr)	1σ** (yr)	Exposure Age (yr)	1σ** (yr)	Exposure Age (yr)	1σ** (yr)	Exposure Age (yr)	1σ** (yr)	Exposure Age (yr)	1σ** (yr)
Gosse et al, 1995b	*WY-92-140*	*304*	*9428*	*1150*	*9425*	*1145*	*9064*	*936*	*10018*	*899*	*10119*	*932*
Inner Titcomb Lakes	WY-92-139	366	11315	1381	11281	1371	10938	1130	12067	1083	12170	1122
	WY-93-333	367	11329	1382	11295	1372	10952	1131	12083	1084	12185	1123
	WY-93-339	387	11947	1458	11902	1446	11555	1194	12743	1144	12849	1185
	WY-92-138	389	12006	1465	11961	1453	11613	1200	12806	1149	12913	1190
	WY-93-338	391	12067	1473	12021	1461	11674	1206	12872	1155	12979	1197
	WY-93-335	394	12177	1486	12128	1474	11783	1218	12990	1166	13098	1208

	WY-93-337	403	12452	1520	12399	1507	12057	1246	13285	1193	13398	1235
	WY-93-336	404	12467	1522	12413	1509	12071	1247	13302	1194	13415	1237
	WY-93-334	426	13128	1603	13064	1588	12718	1315	14012	1258	14136	1304
			12.1 ± 0.38		**12.05 ± 0.37**		**11.71 ± 0.37**		**12.91 ± 0.4**		**13.02 ± 0.41**	
Licciardi et al., 2008	BR-11	344	13882	1678	13860	1668	13524	1379	13861	1221	13907	1260
Burned Ridge moraine	BR-3	349	14105	1705	14083	1695	13748	1402	14061	1239	14108	1278
			13.99 ± 0.22		**13.97 ± 0.22**		**13.64 ± 0.22**		**13.96 ± 0.2**		**14.01 ± 0.2**	
Outer Jenny Lake moraine	OJEN-3	319	13441	1622	13426	1613	13100	1332	13368	1174	13405	1211
	OJEN-10	318	13507	1629	13491	1620	13162	1338	13449	1181	13488	1218
	OJEN-1	239	14110	1687	14088	1677	13754	1380	14048	1212	14093	1251
	OJEN-5	319	14397	1733	14374	1723	14039	1423	14330	1253	14381	1294

	OJEN-8	358	14482	1751	14458	1740	14121	1440	14417	1271	14471	1311
	OJEN-2	362	14999	1812	14972	1801	14625	1489	14937	1314	15004	1357
	OJEN-11	562	15023	1865	14995	1854	14647	1549	14966	1384	15033	1426
	OJEN-7	359	15116	1825	15087	1813	14739	1499	15059	1323	15130	1367
	OJEN-9	360	15275	1843	15245	1832	14895	1515	15216	1336	15292	1381
	OJEN-6	357	15365	1853	15335	1842	14983	1522	15312	1343	15392	1389
	OJEN-7D	439	15537	1891	15506	1879	15151	1559	15482	1381	15569	1427
			14.66 ± 0.44		**14.63 ± 0.44**		**14.29 ± 0.43**		**14.6 ± 0.44**		**14.66 ± 0.45**	
Inner Jenny Lake moraine	IJEN-5	277	11730	1415	11731	1409	11412	1160	11653	1023	11689	1055
	IJEN-2	358	12690	1544	12682	1536	12360	1271	12613	1125	12645	1159
	IJEN-7	320	12995	1570	12984	1562	12660	1290	12917	1138	12950	1173
	IJEN-1	315	13279	1602	13265	1594	12939	1316	13218	1161	13254	1197
	IJEN-3	317	14055	1693	14034	1683	13699	1390	13997	1225	14041	1264

	IJEN-13	320	14227	1714	14205	1704	13871	1407	14157	1239	14204	1279
	IJEN-6	357	14232	1722	14210	1712	13875	1416	14172	1250	14220	1290
	IJEN-11	363	15050	1818	15022	1807	14675	1494	14981	1318	15048	1361
	IJEN-4	517	17254	2107	17212	2093	16813	1738	17213	1544	17368	1601
	IJEN-12	321	17864	2140	17820	2125	17407	1751	17809	1541	17986	1602
			14.34 ± 1.23		**14.32 ± 1.22**		**13.97 ± 1.2**		**14.27 ± 1.24**		**14.34 ± 1.27**	
Licciardi et al, 2004 Glacier Lake moraine	GL-3	354	8753	1092	8798	1093	8404	895	8846	827	8865	849
	GL-5	596	9510	1269	9547	1269	9155	1067	9624	1008	9628	1028
	GL-7C	942	9973	1502	10006	1502	9622	1307	10100	1271	10105	1289
	GL-7B	560	10173	1323	10204	1322	9819	1107	10306	1035	10311	1058
	GL-5C	567	10208	1330	10239	1329	9855	1113	10344	1041	10350	1065
	GL-1	460	10931	1369	10955	1367	10568	1132	11095	1044	11101	1071
	GL-6C	*1036*	*12363*	*1782*	*12375*	*1778*	*11977*	*1541*	*12567*	*1484*	*12568*	*1507*
			9.92 ± 0.6		**9.96 ± 0.59**		**9.57 ± 0.6**		**10.05 ± 0.62**		**10.06 ± 0.62**	

Owen et al, 2003	SG44	289	7579	936	7667	943	7405	778	7743	711	8058	759
San Bernadino Mts	SG43	310	8102	1001	8187	1007	7890	830	8279	760	8592	810
Little Draw	SG42	316	8936	1098	9021	1104	8680	905	9132	830	9422	879
	SG41	374	10435	1284	10500	1287	10127	1059	10648	971	10944	1024
			8.76 ± 1.25		**8.84 ± 1.24**		**8.53 ± 1.19**		**8.95 ± 1.27**		**9.25 ± 1.26**	
North Fork	SG29	292	10448	1266	10515	1269	10138	1037	10684	947	10983	1000
	SG32	309	11100	1345	11158	1346	10759	1101	11358	1006	11667	1062
	SG31	341	12576	1523	12620	1522	12173	1244	12867	1138	13186	1199
	SG30	383	12819	1560	12859	1558	12404	1276	13106	1169	13432	1232
			11.74 ± 1.15		**11.79 ± 1.13**		**11.37 ± 1.1**		**12 ± 1.17**		**12.32 ± 1.18**	
Big Draw 1	SG49	382	12045	1471	12088	1470	11660	1206	12230	1099	12535	1157
	SG50	411	12883	1574	12915	1572	12473	1291	13076	1176	13396	1238
	SG48	808	13555	1782	13574	1778	13123	1500	13758	1406	14103	1471
			12.83 ± 0.87		**12.86 ± 0.86**		**12.42 ± 0.85**		**13.02 ± 0.88**		**13.34 ± 0.91**	

Big Draw 2	SG16	342	12483	1513	12518	1511	12092	1237	12650	1120	12961	1180
	SG17	366	13191	1600	13215	1596	12774	1308	13362	1185	13692	1248
	SG18	390	13708	1665	13723	1660	13273	1362	13882	1234	14230	1300
	SG15	375	13749	1666	13765	1661	13310	1362	13946	1235	14297	1301
	SG19	*272*	*8880*	*1081*	*8959*	*1086*	*8630*	*889*	*9009*	*805*	*9300*	*854*
			13.28 ± 0.59		**13.31 ± 0.58**		**12.86 ± 0.57**		**13.46 ± 0.6**		**13.8 ± 0.62**	
Dollar Lake	SG21	364	13240	1606	13252	1600	12830	1314	13305	1180	13628	1242
	SG23	374	13749	1666	13758	1660	13315	1362	13883	1230	14229	1295
	SG24	379	14621	1769	14600	1759	14171	1446	14661	1294	15049	1366
	SG22	415	15408	1868	15365	1854	14933	1528	15455	1368	15906	1448
			14.25 ± 0.96		**14.24 ± 0.93**		**13.81 ± 0.93**		**14.33 ± 0.94**		**14.7 ± 0.99**	
Benson et al, 2007	*CL03-4*	*761*	*12341*	*1616*	*12299*	*1604*	*11953*	*1359*	*13347*	*1355*	*13546*	*1405*
Chicago Lake	CL03-5	797	13387	1742	13322	1727	12979	1463	14466	1453	14698	1509
	CL03-9	1523	13652	2127	13579	2110	13236	1874	14774	1951	15022	2009
	CL03-6	850	13998	1828	13917	1810	13572	1537	15123	1528	15388	1588

	CL03-8	649	13985	1757	13904	1739	13559	1458	15133	1430	15399	1491
	CL03-7	744	14315	1824	14227	1805	13888	1522	15471	1499	15758	1562
	CL03-1	763	14705	1873	14608	1854	14271	1564	15859	1536	16168	1603
	CL03-2	817	14792	1901	14693	1881	14355	1592	15951	1569	16267	1637
	CL03-3	*792*	*20688*	*2552*	*20419*	*2508*	*20058*	*2102*	*22379*	*2045*	*23171*	*2174*
			14.12 ± 0.39		**14.04 ± 0.38**		**13.69 ± 0.39**		**15.25 ± 0.41**		**15.53 ± 0.44**	
Bulter Gulch	BG03-1	551	9854	1265	9855	1260	9511	1054	10787	1060	10987	1104
	BG03-2	407	7243	929	7284	931	6986	773	7904	776	8132	817
	BG03-3	286	5365	688	5429	694	5229	579	5735	563	5718	574
	BG03-4	356	6423	824	6475	827	6230	690	6922	679	7106	713
	BG03-5	585	10469	1344	10457	1338	10114	1121	11464	1127	11668	1173
	BG03-6	391	6995	897	7043	900	6761	748	7575	744	7804	784
	BG03-	636	11370	1460	11338	1451	10994	1218	12475	1226	12675	1274

	7											
	BG03-8	563	10063	1292	10059	1287	9716	1076	11027	1084	11229	1129
	BG03-9	635	11360	1459	11328	1449	10984	1217	12469	1226	12669	1274
	BG03-10	595	10644	1367	10627	1360	10284	1140	11662	1146	11864	1193
			8.98 ± 1.41		**8.99 ± 1.39**		**8.68 ± 1.36**		**9.8 ± 1.58**		**9.99 ± 1.61**	

[*] *Internal Uncertainty (1s)*

[**] *External Uncertainty (1s)*

Note: Underlined and italicized sample id and numbers are outliers as defined in text.

Table B7. Age calculations of other sites not from this study with CHRONUS v.2.2 calculator (Balco et al., 2008) for multiple scaling methods using the NE North America calibration set (Balco et al., 2009).

Below each column of dates is the arithmetic mean and standard error at 2σ in kyr.

			Desilets and others (2003,2006)		Dunai (2001)		Lifton and others (2005)		Time-dependent (Lal (1991) / Stone (2000))		Lal (1991) / Stone (2000)	
	Sample ID	1σ* (yr)	Exposure Age (yr)	1σ** (yr)	Exposure Age (yr)	1σ** (yr)	Exposure Age (yr)	1σ** (yr)	Exposure Age (yr)	1σ** (yr)	Exposure Age (yr)	1σ** (yr)
Gosse et al, 1995b	*WY-92-140*	*347*	*10054*	*577*	*10020*	*576*	*9836*	*564*	*11339*	*648*	*11536*	*655*
Inner Titcomb Lakes	WY-92-139	418	12074	693	12003	690	11853	680	13649	780	13876	788
	WY-93-333	418	12089	694	12018	691	11869	681	13666	781	13894	789
	WY-93-339	441	12740	732	12656	728	12516	718	14398	823	14651	832
	WY-92-138	443	12803	735	12717	731	12578	721	14468	827	14724	837
	WY-93-338	446	12868	739	12781	735	12643	725	14541	832	14799	841

	WY-93-335	450	12984	746	12895	742	12758	732	14671	839	14935	849
	WY-93-337	460	13275	763	13181	758	13048	749	14998	858	15276	868
	WY-93-336	461	13292	763	13197	759	13064	749	15017	859	15296	869
	WY-93-334	486	13992	804	13884	799	13756	789	15796	904	16119	916
			12.90 ± 0.40		**12.81 ± 0.39**		**12.68 ± 0.40**		**14.58 ± 0.45**		**14.84 ± 0.47**	
Licciardi et al., 2008 Burned Ridge moraine	BR-11	393	14781	811	14722	809	14607	800	15628	853	15849	859
	BR-3	398	15018	824	14958	822	14844	813	15850	865	16078	871
			14.90 ± 0.24		**14.84 ± 0.24**		**14.73 ± 0.24**		**15.74 ± 0.22**		**15.96 ± 0.23**	
Outer Jenny Lake moraine	OJEN-3	363	14318	779	14266	777	14156	769	15085	817	15276	821
	OJEN-10	362	14387	781	14334	780	14221	771	15174	820	15370	825
	OJEN-1	273	15022	778	14964	776	14851	768	15835	816	16060	821

	OJEN-5	364	15326	824	15265	822	15152	813	16150	864	16389	870
	OJEN-8	409	15416	846	15354	843	15240	835	16248	887	16491	894
	OJEN-2	412	15962	871	15896	869	15778	860	16827	914	17099	922
	OJEN-11	641	15987	985	15921	982	15801	972	16858	1035	17132	1046
	OJEN-7	409	16086	875	16019	873	15900	864	16963	918	17242	927
	OJEN-9	411	16255	883	16187	881	16066	872	17140	927	17427	935
	OJEN-6	407	16351	886	16282	883	16160	874	17248	930	17541	939
	OJEN-7D	500	16534	934	16464	931	16340	922	17441	981	17742	991
			15.60 ± 0.46		**15.54 ± 0.46**		**15.42 ± 0.46**		**16.45 ± 0.49**		**16.71 ± 0.52**	
Inner Jenny Lake moraine	IJEN-5	315	12508	680	12475	679	12355	670	13180	713	13320	715
	IJEN-2	408	13523	765	13479	763	13365	755	14248	802	14409	806
	IJEN-7	365	13846	759	13798	757	13686	749	14584	796	14757	799
	IJEN-1	359	14147	770	14096	768	13985	760	14918	808	15104	812

	IJEN-3	361	14964	806	14906	804	14792	796	15778	846	16001	852
	IJEN-13	364	15146	816	15087	814	14975	806	15957	855	16186	861
	IJEN-6	407	15152	834	15093	831	14979	823	15974	875	16205	881
	IJEN-11	414	16016	874	15950	872	15832	863	16875	916	17149	925
	IJEN-4	589	18366	1053	18281	1049	18137	1038	19402	1107	19794	1122
	IJEN-12	367	19019	992	18929	989	18782	978	20076	1041	20499	1055
			15.27 ± 1.30		**15.21 ± 1.29**		**15.09 ± 1.29**		**16.10 ± 1.38**		**16.34 ± 1.44**	
Licciardi et al, 2004 Glacier Lake moraine	GL-3	404	9339	590	9358	591	9119	575	10020	630	10104	632
	GL-5	679	10134	799	10144	801	9923	782	10882	856	10974	861
	GL-7C	1075	10628	1119	10633	1120	10419	1097	11422	1201	11518	1209
	GL-7B	638	10841	792	10844	793	10632	776	11657	849	11753	853
	GL-5C	646	10879	799	10882	799	10670	783	11700	857	11796	860
	GL-1	524	11652	747	11645	747	11440	733	12552	802	12652	804
	GL-6C	*1181*	*13176*	*1263*	*13153*	*1261*	*12953*	*1241*	*14198*	*1359*	*14326*	*1368*
			10.58 ± 0.64		**10.58 ± 0.63**		**10.37 ± 0.64**		**11.37 ± 0.70**		**11.47 ± 0.70**	

Owen et al, 2003	SG44	330	8111	492	8177	496	8016	485	8811	532	9183	551
San Bernadino Mts	SG43	353	8675	527	8740	531	8559	519	9437	571	9791	589
Little Draw	SG42	360	9575	567	9632	572	9435	558	10361	612	10736	630
	SG41	427	11142	665	11174	667	10957	653	12072	717	12473	737
			9.38 ± 1.32		**9.43 ± 1.31**		**9.24 ± 1.28**		**10.17 ± 1.42**		**10.55 ± 1.43**	
North Fork	SG29	333	11155	621	11189	624	10968	610	12113	671	12516	689
	SG32	352	11863	660	11890	662	11648	647	12874	712	13297	731
	SG31	389	13418	743	13420	744	13168	728	14521	800	15029	822
	SG30	436	13671	774	13668	775	13414	758	14781	833	15309	857
			12.53 ± 1.21		**12.54 ± 1.20**		**12.30 ± 1.18**		**13.57 ± 1.29**		**14.04 ± 1.35**	
Big Draw 1	SG49	435	12858	741	12863	742	12628	727	13828	793	14286	814
	SG50	469	13738	793	13726	794	13486	778	14747	848	15268	873
	SG48	922	14437	1088	14409	1087	14172	1067	15486	1164	16074	1204
			13.68 ±0.91		**13.67 ± 0.89**		**13.43 ± 0.89**		**14.69 ± 0.96**		**15.21 ±1.03**	
Big Draw	SG16	390	13319	740	13314	741	13082	726	14285	791	14771	812

2												
	SG17	417	14062	784	14042	784	13805	768	15060	836	15605	860
	SG18	445	14595	819	14560	818	14328	803	15619	872	16219	900
	SG15	427	14637	813	14603	812	14367	796	15688	867	16295	894
	SG19	*310*	*9518*	*542*	*9570*	*546*	*9381*	*534*	*10228*	*580*	*10597*	*597*
			14.15 ± 0.61		**14.13 ± 0.60**		**13.90 ± 0.60**		**15.16 ± 0.65**		**15.72 ± 0.71**	
Dollar Lake	SG21	415	14112	787	14080	786	13864	772	14997	832	15530	856
	SG23	426	14637	813	14597	812	14372	797	15620	864	16217	890
	SG24	432	15545	856	15468	853	15266	839	16472	902	17151	933
	SG22	473	16370	908	16267	904	16068	890	17355	958	18128	994
			15.17 ± 1.00		**15.10 ± 0.96**		**14.89 ± 0.97**		**16.11 ± 1.03**		**16.76 ± 1.13**	
Benson et al, 2007 Chicago Lake	*CL03-4*	*868*	*13169*	*981*	*13082*	*975*	*12950*	*964*	*15065*	*1120*	*15446*	*1144*
	CL03-5	909	14270	1042	14156	1034	14042	1024	16290	1187	16761	1216
	CL03-9	1738	14546	1637	14423	1624	14311	1610	16631	1871	17131	1924
	CL03-6	969	14906	1100	14772	1091	14666	1081	17018	1253	17547	1287
	CL03-8	741	14893	962	14759	954	14652	945	17029	1097	17561	1125

	CL03-7	848	15240	1036	15099	1027	14998	1019	17410	1180	17970	1213
	CL03-1	871	15649	1064	15497	1054	15401	1046	17846	1210	18438	1245
	CL03-2	932	15740	1104	15585	1094	15490	1085	17951	1255	18551	1292
	CL03-3	*905*	*22007*	*1315*	*21661*	*1296*	*21628*	*1291*	*25141*	*1497*	*26430*	*1565*
			15.03 ± 0.41		**14.90 ± 0.40**		**14.79 ± 0.41**		**17.17 ± 0.46**		**17.71 ± 0.50**	
Bulter Gulch	BG03-1	628	10518	736	10482	735	10311	721	12232	854	12528	871
	BG03-2	465	7719	540	7738	542	7528	526	8993	628	9272	644
	BG03-3	326	5659	396	5706	399	5577	390	6370	444	6518	453
	BG03-4	406	6796	475	6831	478	6659	465	7810	545	8102	563
	BG03-5	667	11177	783	11126	780	10964	767	12999	908	13305	925
	BG03-6	446	7435	520	7459	522	7269	508	8612	601	8898	618
	BG03-7	725	12150	851	12079	847	11928	835	14112	986	14453	1006
	BG03-	642	10742	752	10701	750	10532	737	12504	873	12804	890

	8											
	BG03-9	725	12139	850	12068	846	11917	834	14106	986	14446	1005
	BG03-10	679	11363	796	11308	793	11149	780	13216	923	13529	941
			9.57 ± 1.52		**9.55 ± 1.50**		**9.38 ± 1.50**		**11.10 ± 1.80**		**11.39 ± 1.83**	

[*] *Internal Uncertainty (1σ)*

[**] *External Uncertainty (1σ)*

Note: Underlined and italicized sample id and numbers are outliers as defined in text.

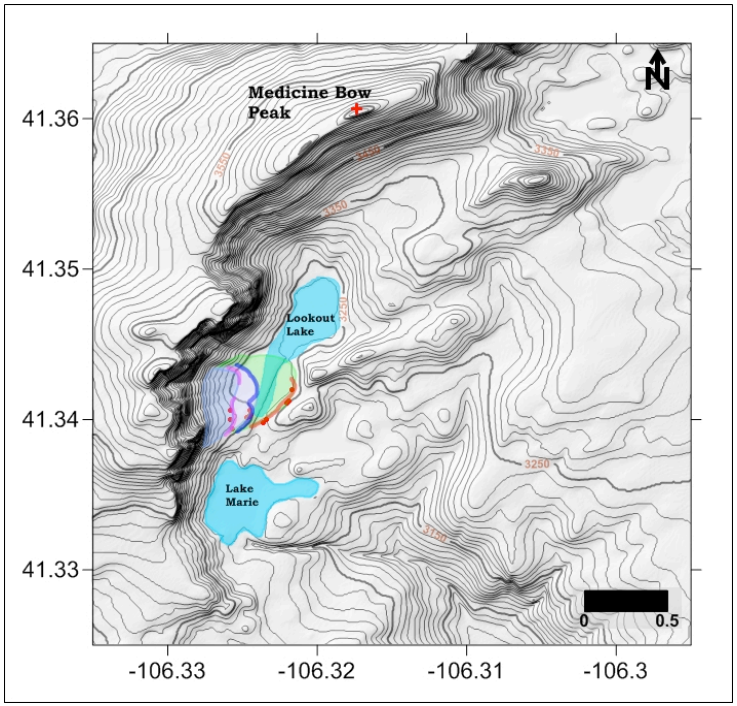

Figure B1. Location map for exposure dating in the Medicine Bows Mountains.

Sampling sites for surface exposure dating (red circles), moraine crests (colored lines), and approximate glacier outlines (transparent, transparent, colored polygons) in the Medicine Bow Mountains. Brown line = LL-MB moraine; Blue line = DPO-MB moraine; Magenta line = DPI-MB moraine. Scale bar is in kilometers.

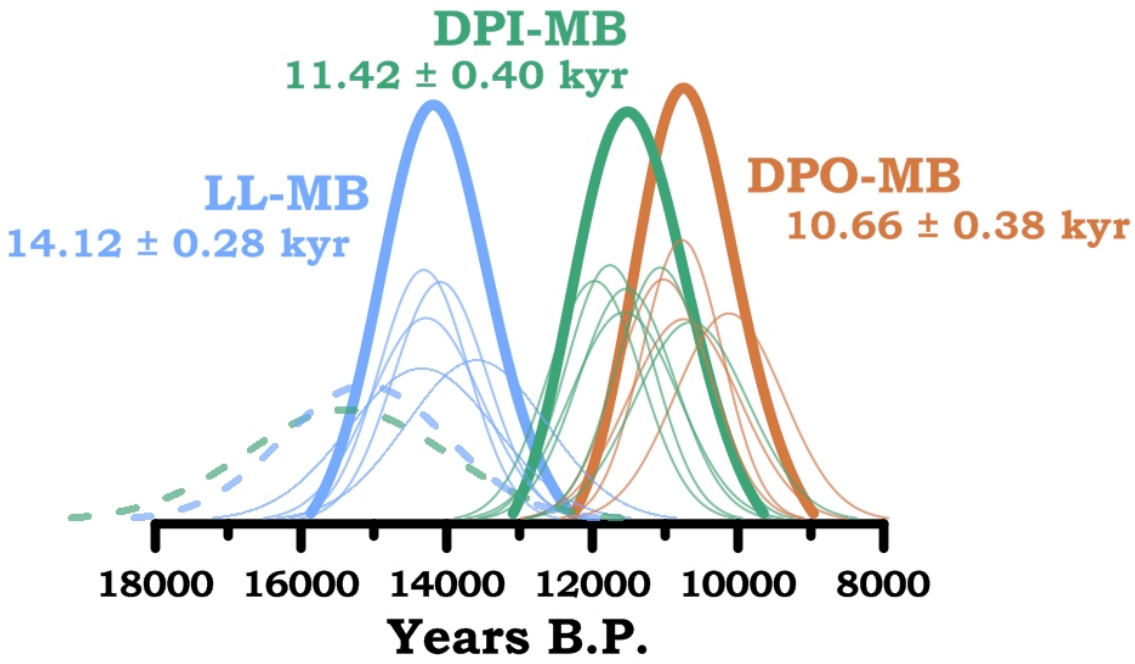

Figure B2. Probability density functions for the Medicine Bows Mountains.

Probability density functions of individual (lines) and summed (bold line) surface exposure ages and mean age and standard error values from Table S4 (Lifton et al. scaling) for the Medicine Bow Mountain moraines. Dashed lines are outlier as defined in text.

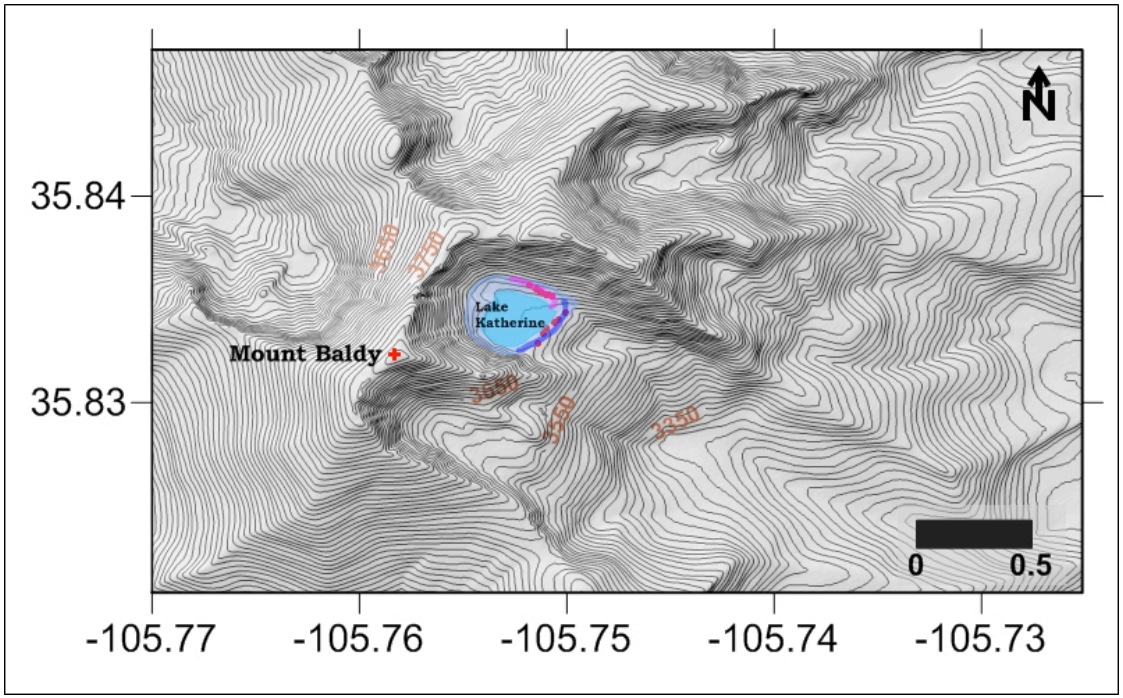

Figure B3. Location map for exposure dating in the Sangre de Cristo Mountains.

Sampling sites for surface exposure dating (red circles), moraine crests (colored lines), and approximate glacier outlines (transparent, transparent, colored polygons) in the Sangre de Cristo Mountains. Blue line = SBO-SFF moraine; Magenta line = SBI moraine. Scale bar is in kilometers.

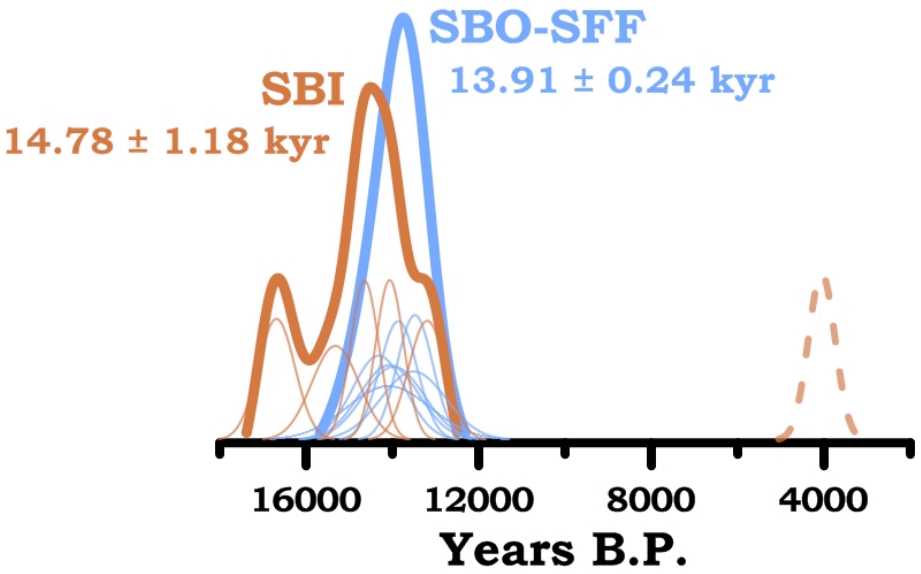

Figure B4. Probability density functions for the Sangre de Cristo Mountains.

Probability density functions of individual (lines) and summed (bold line) surface exposure ages and mean age and standard error values from Table S4 (Lifton et al. scaling) for the Sangre de Cristo Mountains. Dashed lines are outlier as defined in text.

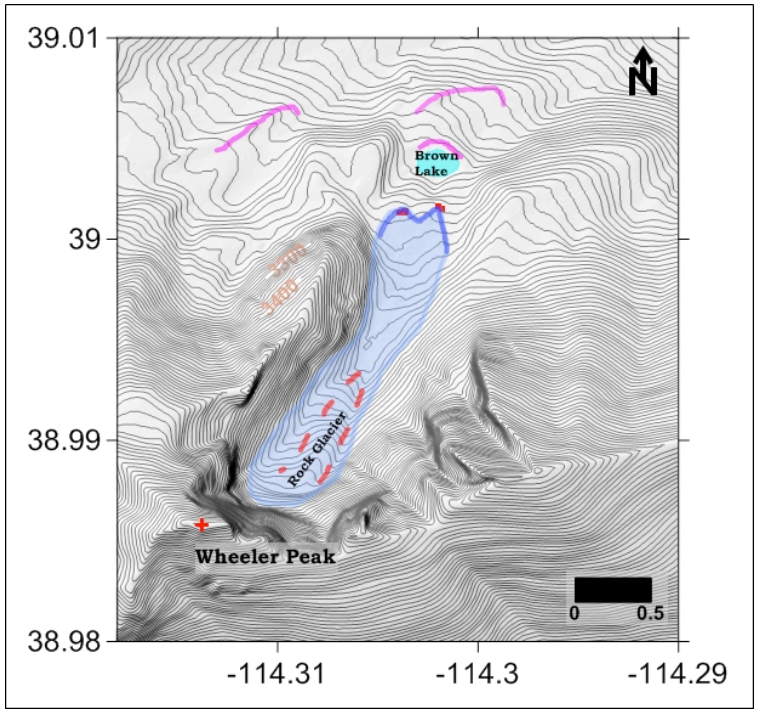

Figure B5. Location map for exposure dating in the South Snake Range.

Sampling sites for surface exposure dating (red circles), moraine crests (colored lines), and approximate glacier outlines (transparent, colored polygons) in the South Snake Range. Red dashed line = rock glacier outline; Blue line = BLI-WP moraine; Magenta line = other moraines as mapped by Osborn and Bevis. Scale bar is in kilometers.

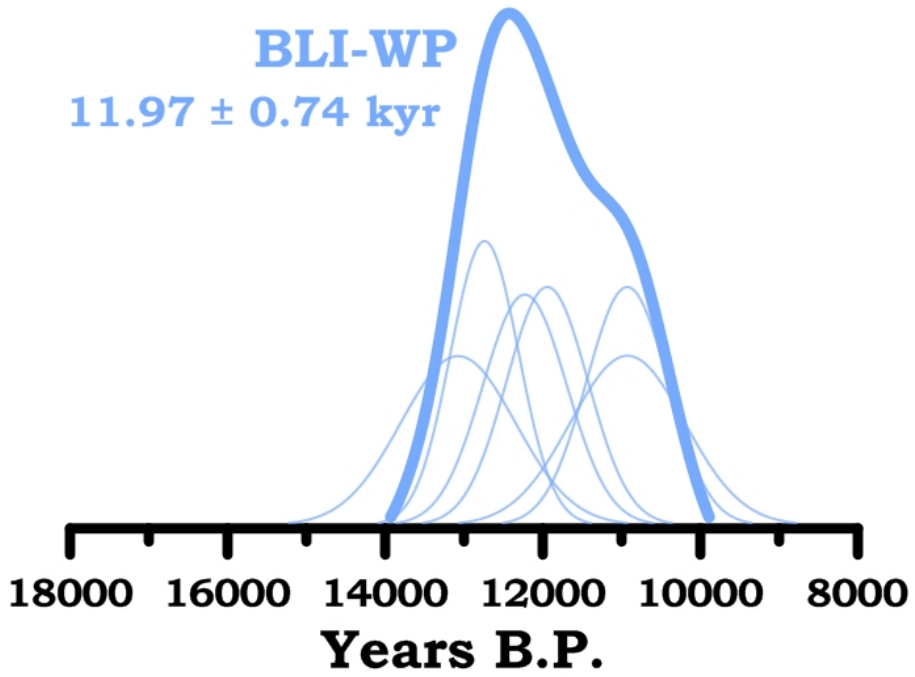

Figure B6. Probability density functions for the South Snake Range.

Probability density functions of individual (lines) and summed (bold line) surface exposure ages and mean age and standard error values from Table S4 (Lifton et al. scaling) for the South Snake Range.

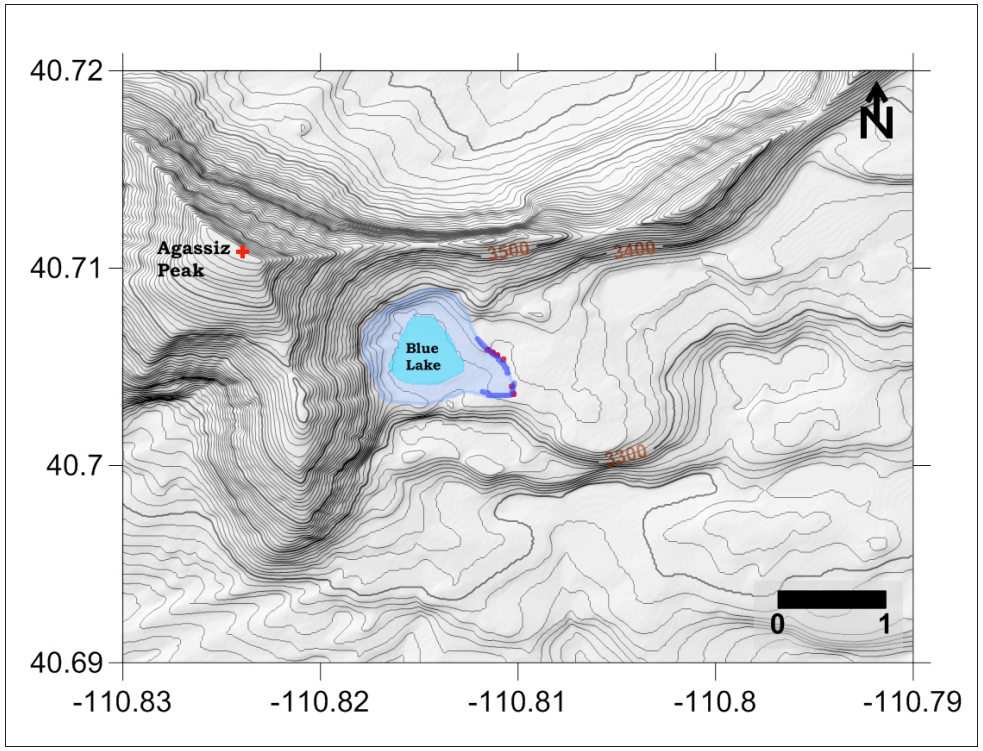

Figure B7. Location map for exposure dating in the Uinta Mountains.

Sampling sites for surface exposure dating (red circles), moraine crests (colored lines), and approximate glacier outlines (transparent, colored polygons) in the Uinta Mountains near Blue Lake. Blue line = BL moraine. Scale bar is in kilometers.

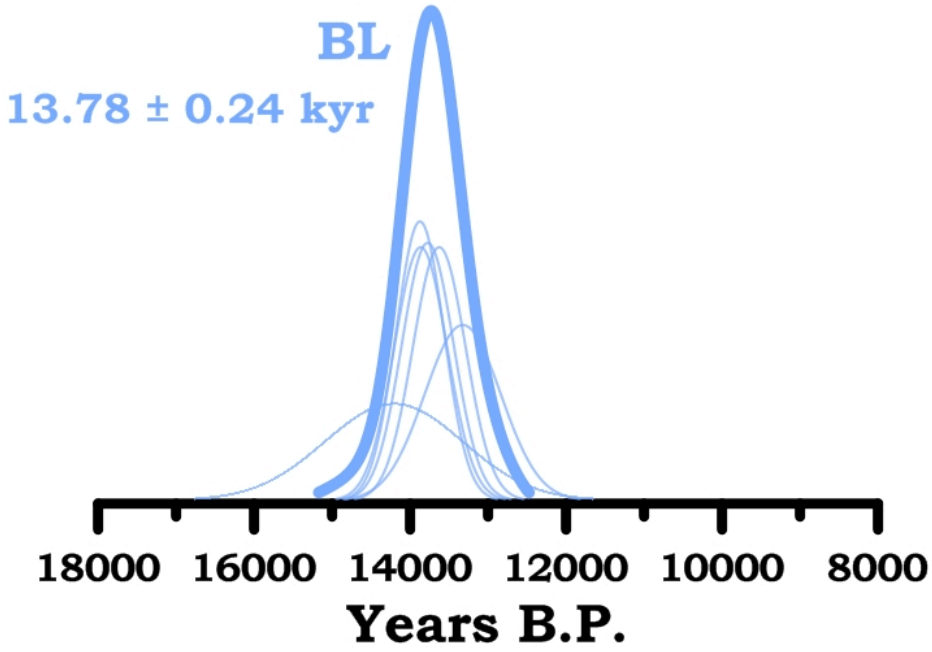

Figure B8. Probability density functions for the Uinta Mountains.

Probability density functions of individual (lines) and summed (bold line) surface exposure ages and mean age and standard error values from Table S4 (Lifton et al. scaling) for the Uinta Mountains near Blue Lake.

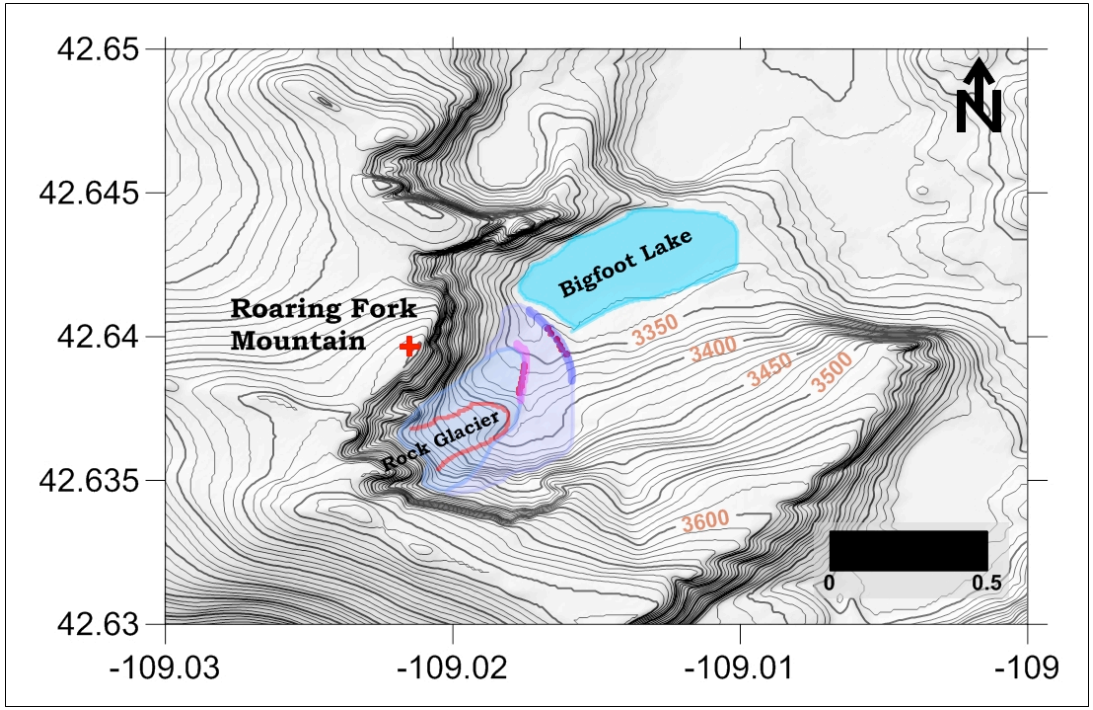

Figure B9. Location map for exposure dating in the Wind River Range.

Sampling sites for surface exposure dating (red circles), moraine crests (colored lines), and approximate glacier outlines (transparent, colored polygons) in the Wind River Range in the Stough Creek Drainage. Red line = rock glacier outline; Blue line = SCM-WRR moraine; Magenta line = SCO-WRR moraine. Scale bar is in kilometers.

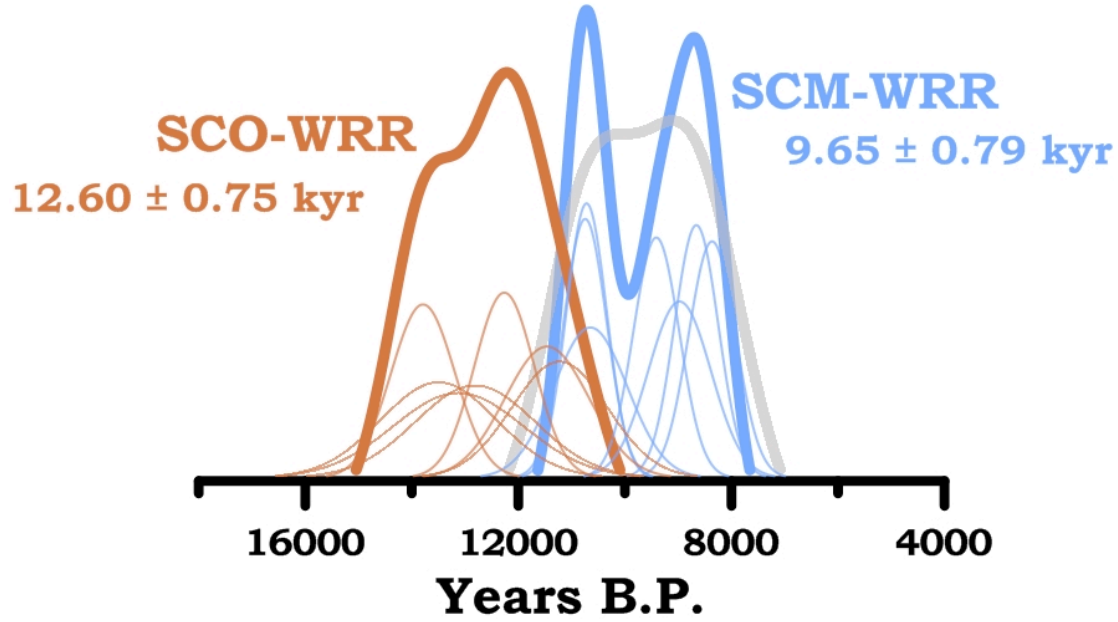

Figure B10. Probability density functions for the Wind River Range.

Probability density functions of individual (lines) and summed (bold line) surface exposure ages and mean age and standard error values from Table S4 (Lifton et al. scaling) for the Wind River Range in the Stough Creek Drainage. The gray line is the 2σ derived probability density function for SCM-WRR.

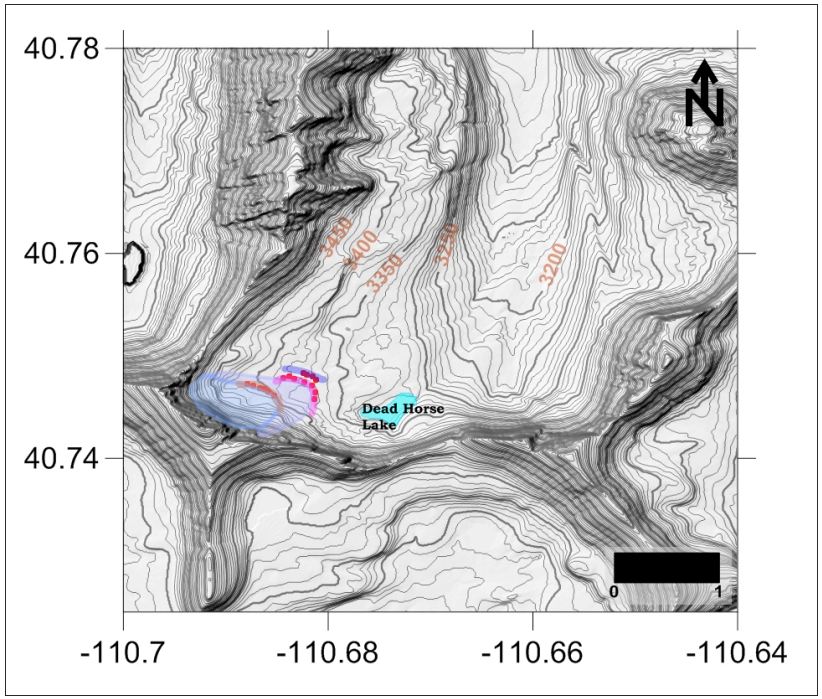

Figure B11. Location map for exposure dating in the Uinta Mountains.

Sampling sites for surface exposure dating (red circles), moraine crests (colored lines), and approximate glacier outlines (transparent, colored polygons) in the Uinta Mountains near Deadhorse Lake. Brown line = DHI-UM moraine; Magenta line = DHM-UM moraine; Blue line = DHO-UM moraine. Scale bar is in kilometers.

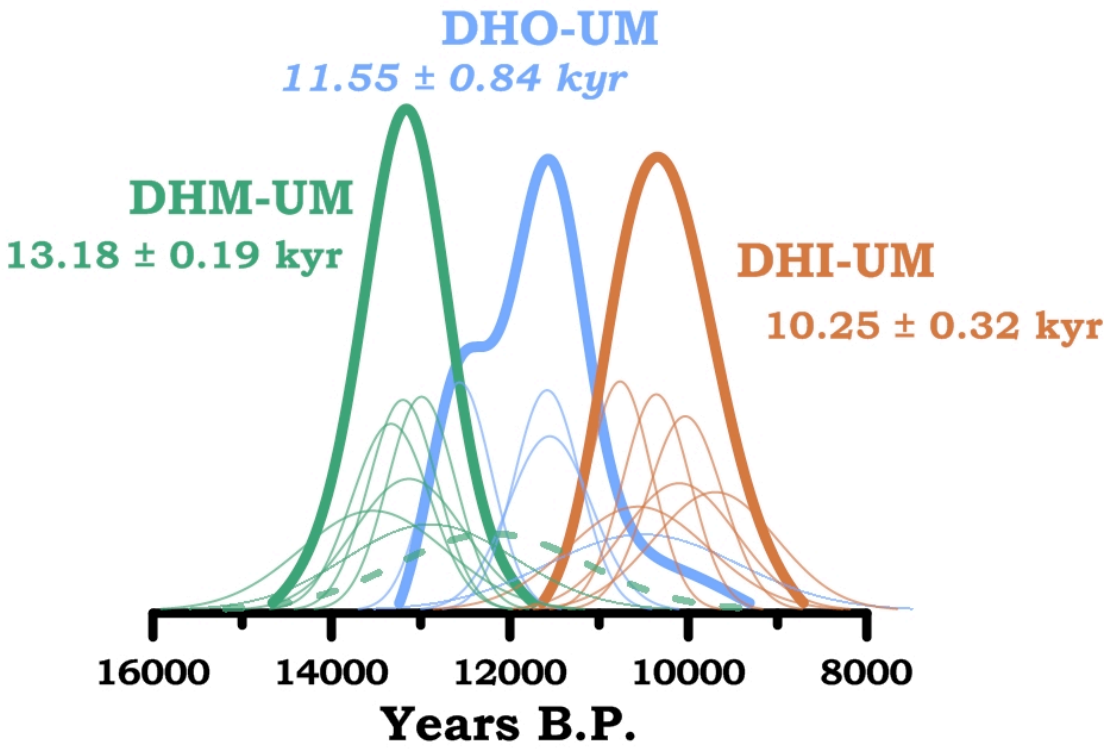

Figure B12. Probability density functions for the Uinta Mountains.

Probability density functions of individual (lines) and summed (bold line) surface exposure ages and mean age and standard error values from Table S4 (Lifton et al. scaling) for the Uinta Mountains near Deadhorse Lake.

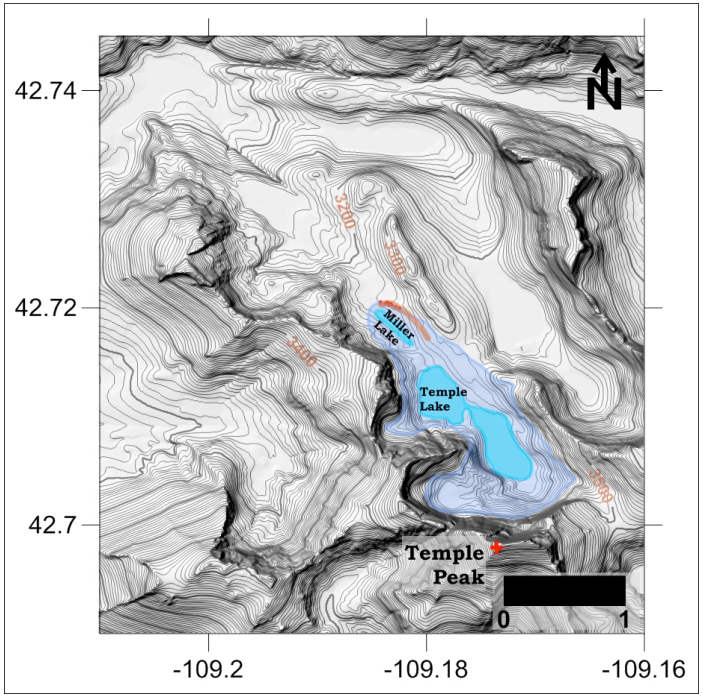

Figure B13. Location map for exposure dating in the Wind River Range.

Sampling sites for surface exposure dating (red circles), moraine crests (colored lines), and approximate glacier outlines (transparent, colored polygons) in the Wind River Range near Temple Lake. Brown line = TLO-WRR moraine; Scale bar is in kilometers.

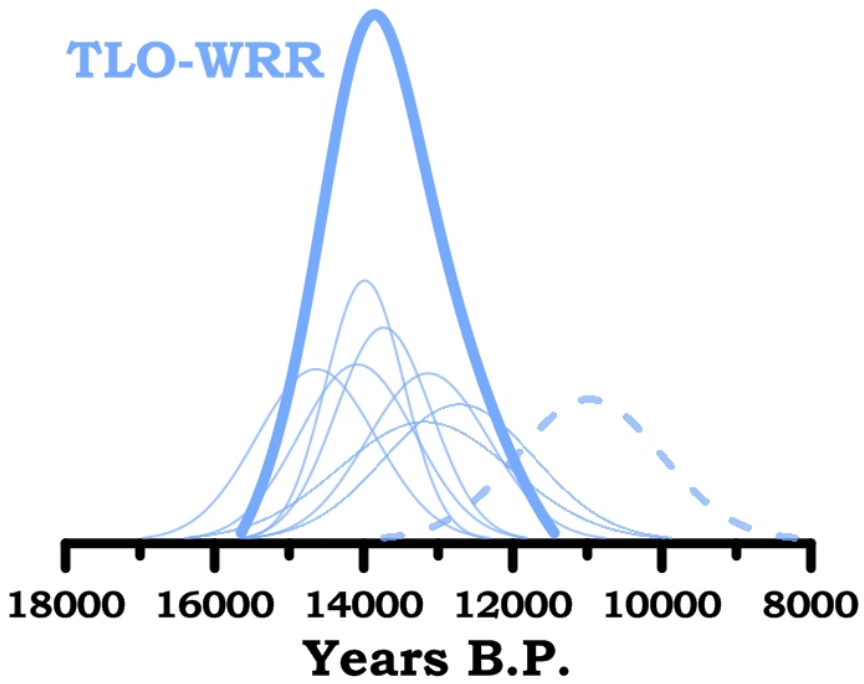

Figure B14. Probability density functions for the Wind River Range.

Probability density functions of individual (lines) and summed (bold line) surface exposure ages and mean age and standard error values from Table S4 (Lifton et al. scaling) for the Wind River Range near Temple Lake. Dashed lines are outlier as defined in text.

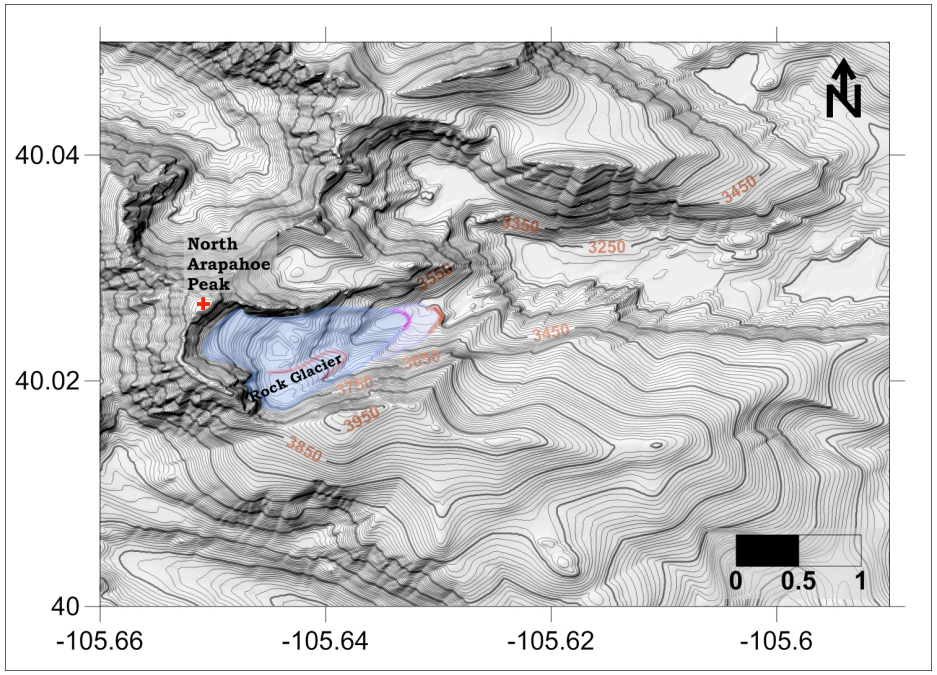

Figure B15. Location map for exposure dating in the Front Range.

Sampling sites for surface exposure dating (red circles), moraine crests (colored lines), and approximate glacier outlines (transparent, colored polygons) in the Colorado Front Range in the Arapahoe Cirque drainage near Triple Lakes. Brown line = APO moraine; Magenta line = CFR moraine; Pink line = outline of rock glacier. Scale bar is in kilometers.

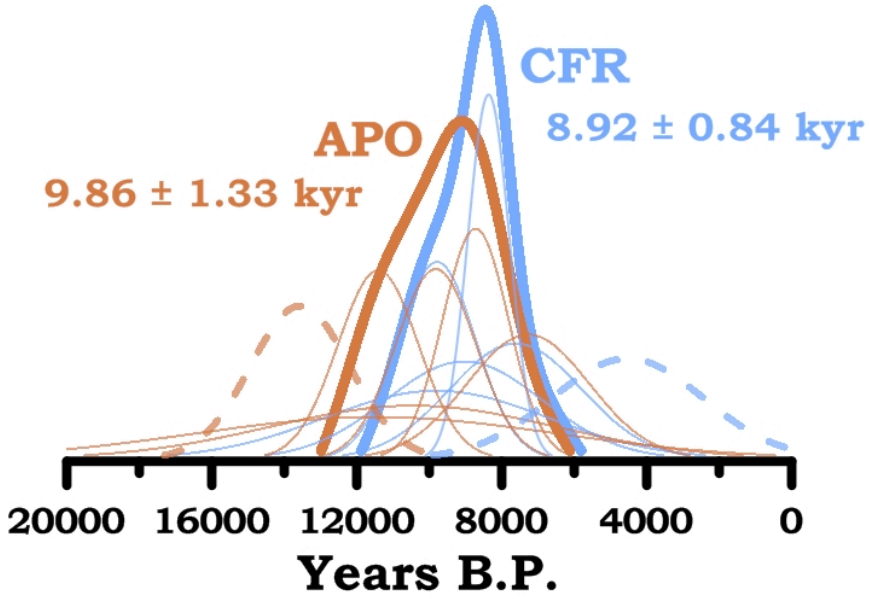

Figure B16. Probability density functions for the Colorado Front Range.

Probability density functions of individual (lines) and summed (bold line) surface exposure ages and mean age and standard error values from Table S4 (Lifton et al. scaling) for the Colorado Front Range in the Arapahoe Cirque drainage near Triple Lakes. Dashed lines are outlier as defined in text.

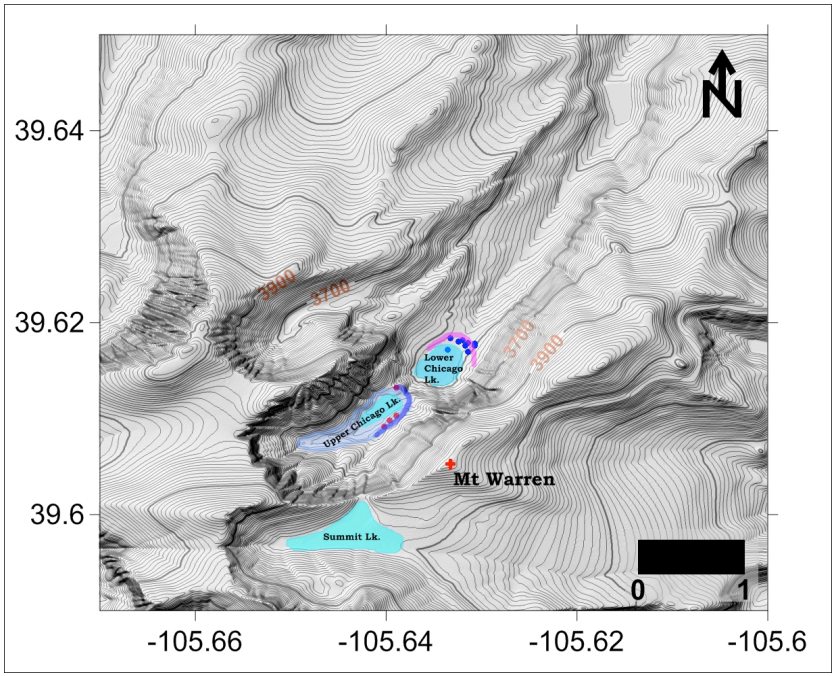

Figure B17. Location map for exposure dating in the Front Range.

Sampling sites for surface exposure dating (red circles), moraine crests (colored lines), and approximate glacier outlines (transparent, colored polygons) in the Colorado Front Range near Upper and Lower Chicago lakes. Blue line = UCL-CFR moraine; Magenta line = Lower Chicago Lake moraine as mapped and dated by Benson et al. Scale bar is in kilometers.

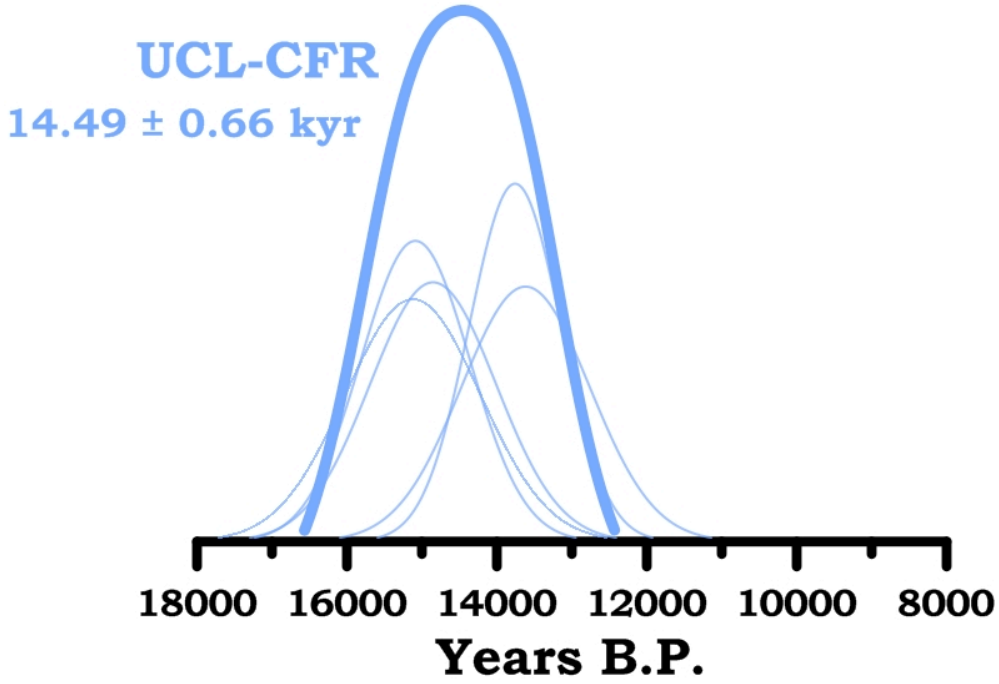

Figure B18. Probability density functions for the Colorado Front Range.

Probability density functions of individual (lines) and summed (bold line) surface exposure ages and mean age and standard error values from Table S4 (Lifton et al. scaling) for the Colorado Front Range near Upper and Lower Chicago lakes.

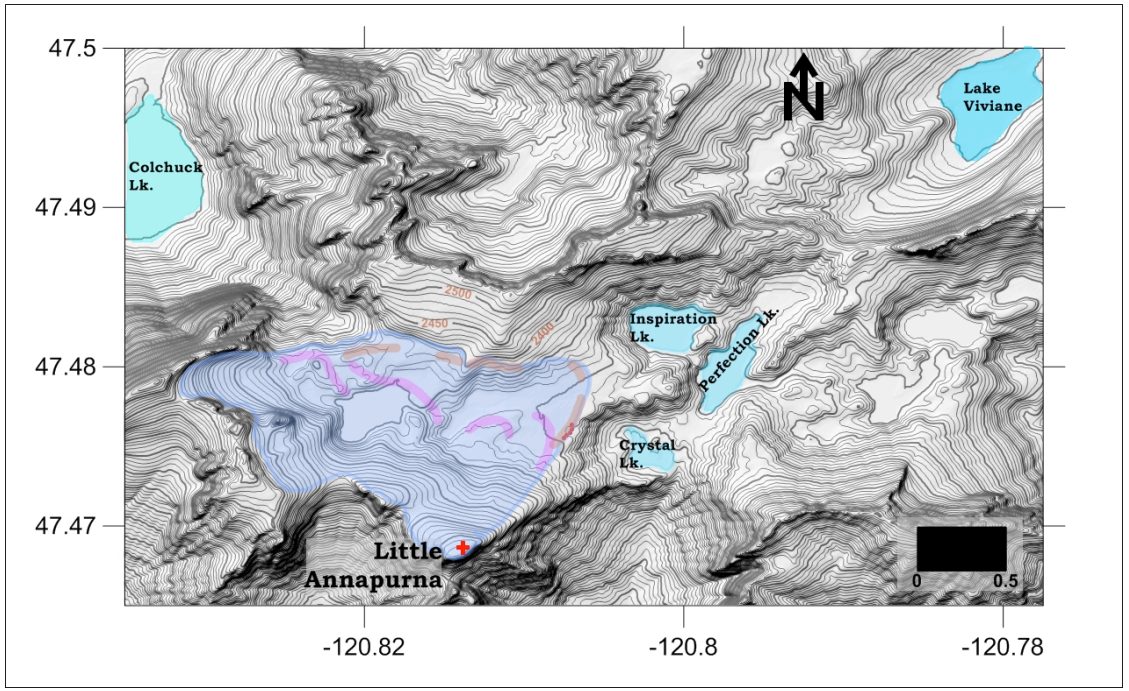

Figure B19. Location map for exposure dating in the Cascade Range.

Sampling sites for surface exposure dating (red circles), moraine crests (colored lines), and approximate glacier outlines (transparent, colored polygons) in the Cascade Range in the Enchantment Lakes Basin. Brown line = BL-BG moraine; Magenta line = moraines as mapped by Bilderback and Waitt et al. Scale bar is in kilometers.

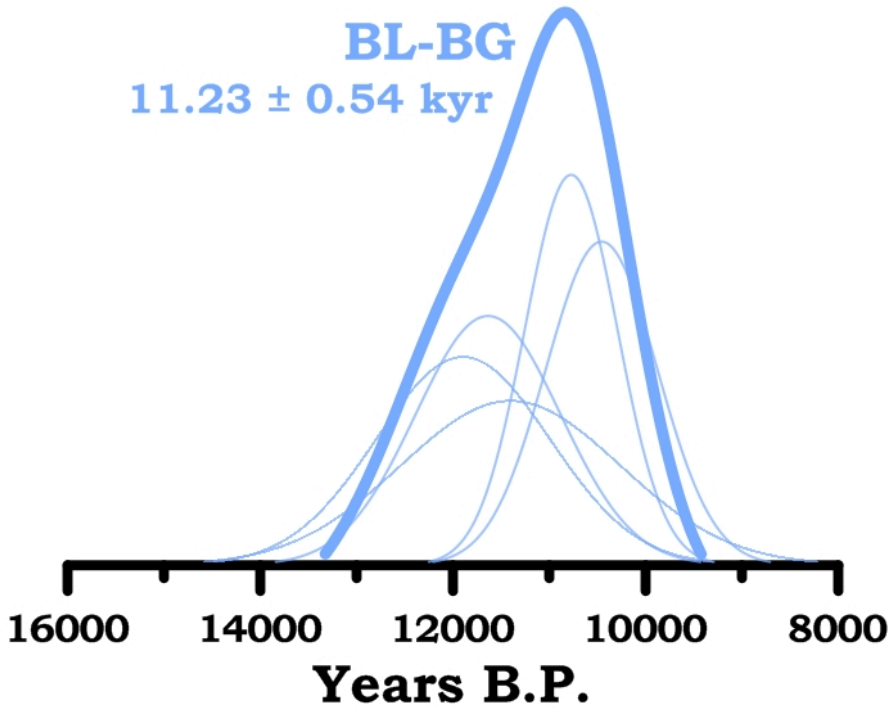

Figure B20. Probability density functions for the Medicine Bows Mountains.

Probability density functions of individual (lines) and summed (bold line) surface exposure ages and mean age and standard error values from Table S4 (Lifton et al. scaling) for the Cascade Range in the Enchantment Lakes Basin.

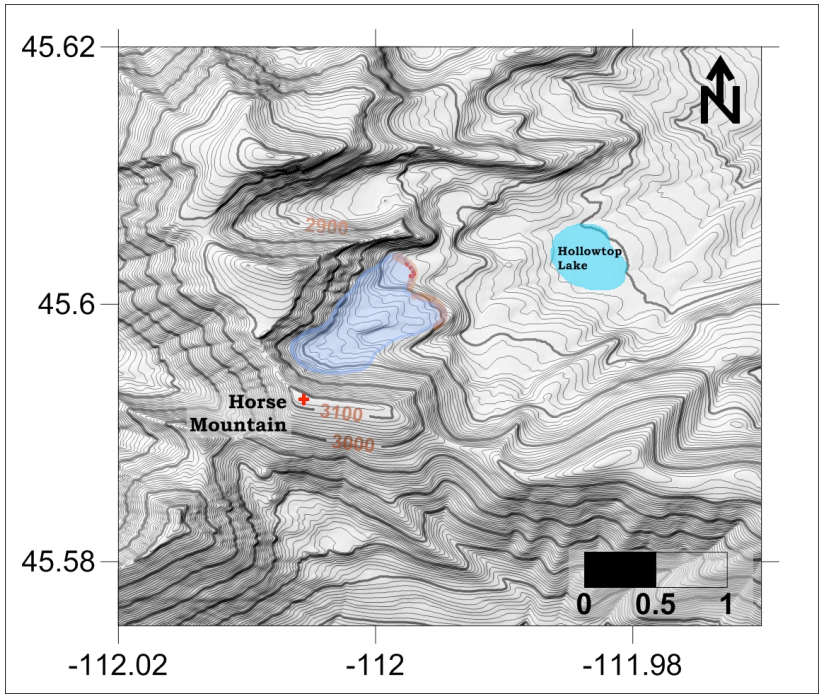

Figure B21. Location map for exposure dating in the Tobacco Root Range.

Sampling sites for surface exposure dating (red circles), moraine crests (colored lines), and approximate glacier outlines (transparent, colored polygons) in the Tobacco Root Range near Hollowtop Lake. Brown line = TR moraine; Scale bar is in kilometers.

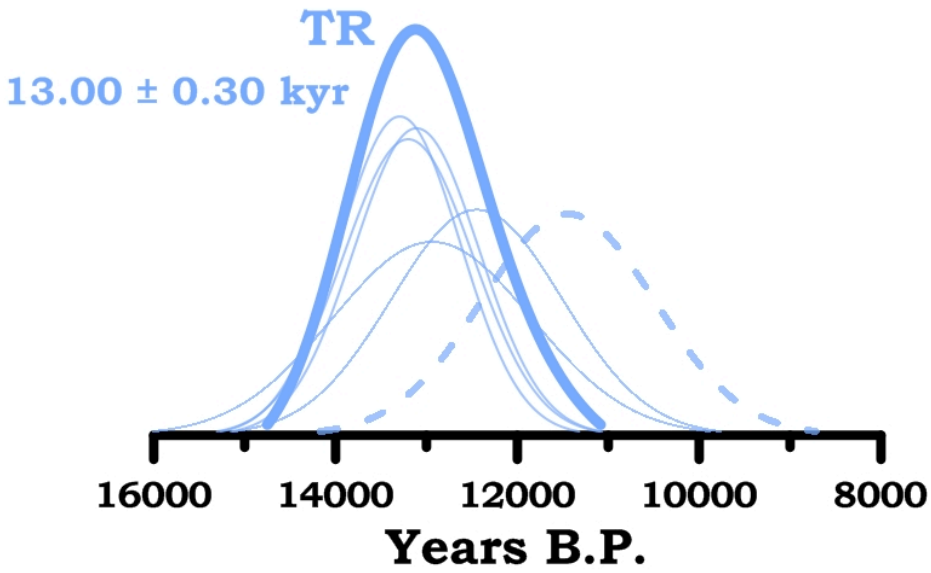

Figure B22. Probability density functions for the Tobacco Root Range.

Probability density functions of individual (lines) and summed (bold line) surface exposure ages and mean age and standard error values from Table S4 (Lifton et al. scaling) for the Tobacco Root Range near Hollowtop Lake. Dashed lines are outlier as defined in text.

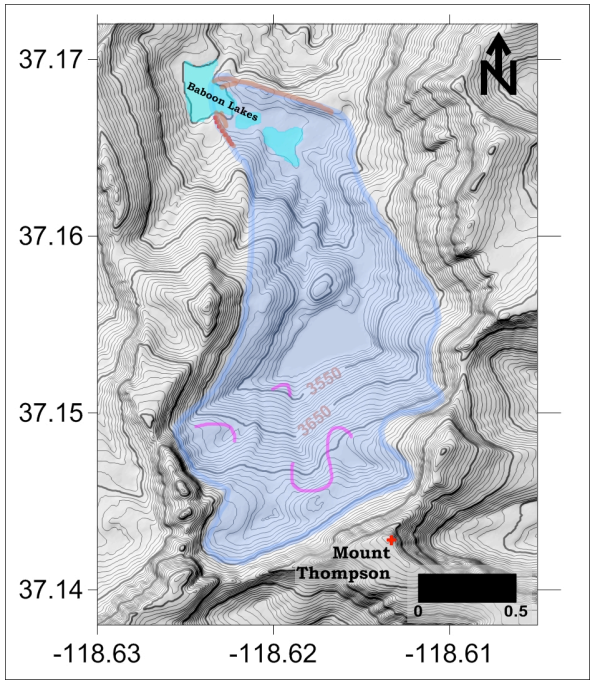

Figure B23. Location map for exposure dating in the Sierra Nevada.

Sampling sites for surface exposure dating (red circles), moraine crests (colored lines), and approximate glacier outlines (transparent, colored polygons) in the Sierra Nevada near Baboon Lakes. Brown line = SNV moraine; Magenta line = moraines as mapped by Clark and Gillespie (1997). Scale bar is in kilometers.

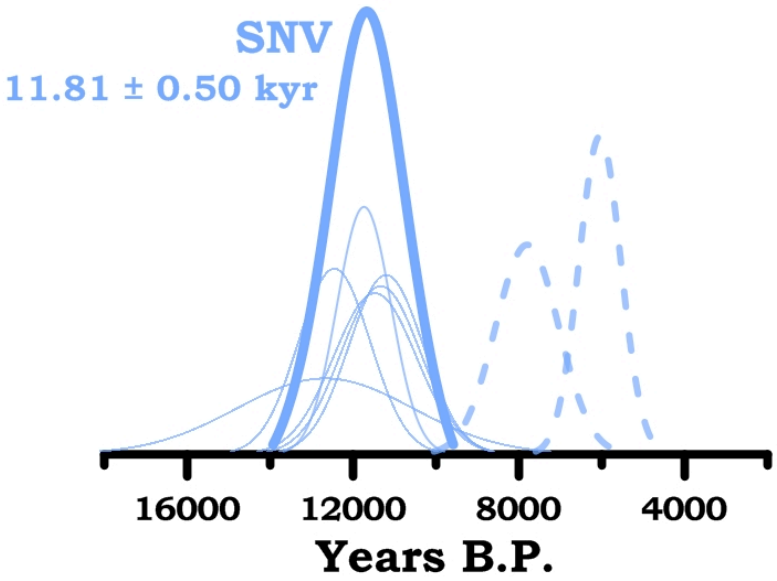

Figure B24. Probability density functions for the Sierra Nevada.

Probability density functions of individual (lines) and summed (bold line) surface exposure ages and mean age and standard error values from Table S4 (Lifton et al. scaling) for the Sierra Nevada near Baboon Lakes. Dashed lines are outlier as defined in text.

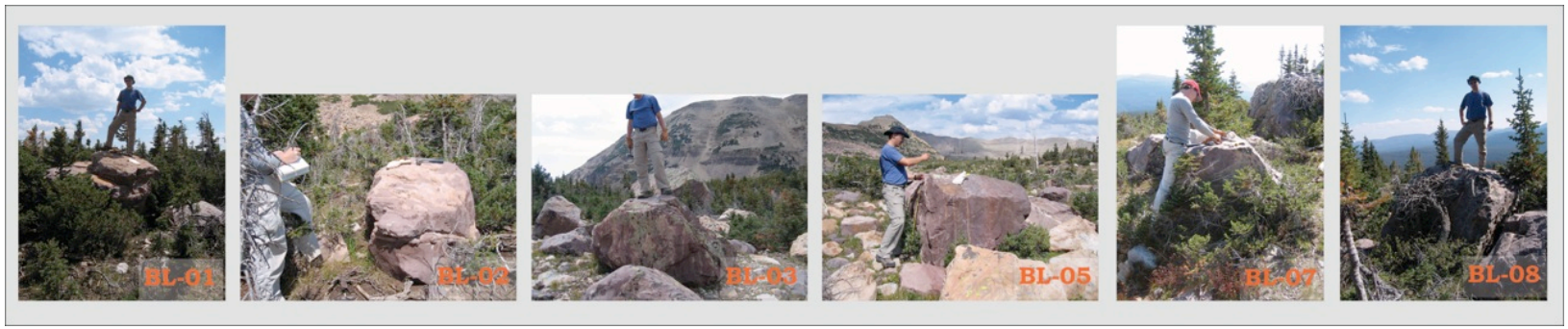

Figure B25. Photographs of individual boulders in the Uinta Mountains near Blue Lake.

Figure B26. Photographs of individual boulders in the Uinta Mountains near Deadhorse Lake.

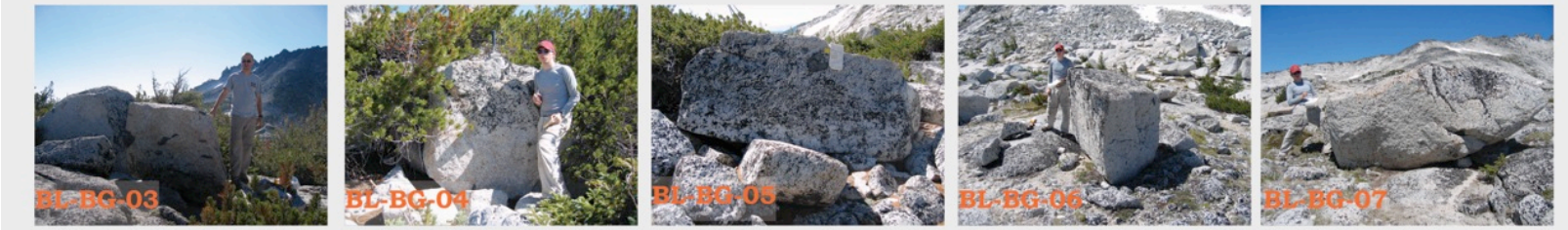

Figure B27. Photographs of individual boulders in the Cascade Range in the Enchantment Lakes Basin.

Figure B28. Photographs of individual boulders in the Colorado Front Range near Upper Chicago Lake (top row) and Triple Lakes (bottom two rows).

Figure B29. Photographs of individual boulders study in the Medicine Bow Mountains.

Figure B30. Photographs of individual boulders in the Sange de Cristo Mountains near Lake Katherine.

Figure B31. Photographs of individual boulders in the Sierra Nevada.

Figure B32. Photographs of individual boulders in the Tobacco Root Range.

Figure B33. Photographs of individual boulders in the South Snake Range in Great Basin National Park.

Figure B34. Photographs of individual boulders in the Wind River Range near Temple Lake (top row) and in the Stough Creek Drainage (bottom two rows).

B.5 References

Armour, J., Fawcett, P. J., and Geissman, J. W. (2002). 15 k.y. paleoclimatic and glacial record from northern New Mexico. *Geology* **30,** 723-726.

Balco, G., Briner, J., Finkel, R. C., Rayburn, J. A., Ridge, J. C., and Schaefer, J. M. (2009). Regional beryllium-10 production rate calibration for northeastern North America. *Quaternary Geochronology* **4,** 99-107.

Balco, G. A., Stone, J. O., Lifton, N. A., and Dunai, T. J. (2008). A complete and easily accessible means of calculating surface exposure ages or erosion rates from ^{10}Be and ^{26}Al measurements. *Quaternary Geochronology* **3,** 174-195.

Benedict, J. B. (1973). Chronology of cirque glaciation, Colorado Front Range. *Quaternary Research* **3,** 584-599.

Benson, L., Madole, R. F., Kubik, P., and McDonald, R. (2007). Surface-exposure ages of Front Range moraines that may have formed during the Younger Dryas, 8.2 cal ka, and Little Ice Age events. *Quaternary Science Review* **26,** 1638-1649.

Bilderback, E. L. (2004). "Timing and Paleoclimatic Significance of Latest Pleistocene and Holocene Cirque Glaciation in the Enchantment Lakes Basin, North Cascades, WA." Unpublished Masters thesis, Western Washington University.

Birman, J. H. (1964). Glacial Geology across the Crest of the Sierra Nevada, California. *In* "California. Geol. Soc. Amer. Special Paper n. 75." pp. 80.

Clark, D. H., and Gillespie, A. R. (1997). Timing and significance of late-glacial and Holocene cirque glaciation in the Sierra Nevada, California. *Quaternary International* **38-39,** 21-38.

Currey, D. R. (1974). Probable pre-Neoglacial age of the type Temple Lake moraine, Wyoming. *Arctic and Alpine Research* **6,** 293-300.

Curry, R. R. (1969). Holocene climatic and glacial history of the central Sierra Nevada, California. *In* "United States Contributions to Quaternary Research, Geological Society of America Special Paper 123." (S. A. Schumm, and W. C. Bradley, Eds.), pp. 1-47.

Dahms, D. E. (2002). Glacial stratigraphy of Stough Creek Basin, Wind River Range, Wyoming. *Geomorphology* **42,** 59-83.

Davis, P. T. (1988). Holocene Glacier Fluctuations in the American Cordillera. *Quaternary Science Reviews* **7,** 129-157.

Desilets, D., and Zreda, M. G. (2003). Spatial and temporal distribution of secondary cosmic-ray nucleon intensity and applications to in situ cosmogenic dating. *Earth and Planetary Science Letters* **206,** 21-42.

Desilets, D., Zreda, M. G., and Prabu, T. (2006). The energy dependence of cosmogenic nuclide scaling models: New measurments at low latitudes. *Earth and Planetary Science Letters* **246,** 265-276.

Dunai, T. J. (2000). Scaling factors for production rates of in situ produced cosmogenic nuclides: a critical reevaluation. *Earth and Planetary Science Letters* **176,** 157-169.

Dunai, T. J. (2001). Influence of secular variation of the geomagnetic field on the production rates of in situ produced cosmogenic nuclides. *Earth and Planetary Science Letters* **193,** 197-212.

Goehring, B. M. (2006). "^{10}Be Exposure Ages of Erratic Boulders in Southern Norway and Implications for the History of the Fennoscandian Ice Sheet." Unpublished Masters thesis, Oregon State University.

Gosse, J. C., Evenson, E. B., Klein, J., Lawn, B., and Middleton, R. (1995). Precise cosmogenic ^{10}Be measurements in western North America: Support for a global Younger Dryas cooling event. *Geology* **23,** 877-880.

Gosse, J. C., and Phillips, F. M. (2001). Terrestrial in situ cosmogenic nuclides: theory and application. *Quaternary Science Reviews* **20,** 1475-1560.

Hall, R. D., and Heiny, J. S. (1983). Glacial and postglacial physical stratigraphy and chronology, North Willow Creek and Catarct Creek drainage basin, eastern Tobacco Root Range, southwestern Montana, U.S.A. *Arctic and Alpine Research* **15,** 19-52.

Lal, D. (1991). Cosmic ray labeling of erosion surfaces: In-situ nuclide production rates and erosion models. *Earth and Planetary Science Letters* **104,** 424-439.

Licciardi, J. F. (2000). "Alpine Glacier and Pluvial Lake Records of Late Pleistocene Climate Variability in the Western United States." Unpublished Ph.D. thesis, Oregon State University.

Licciardi, J. M., Clark, P. U., Brook, E. J., Elmore, D., and Sharma, P. (2004). Variable responses of western U.S. glaciers during the last deglaciation. *Geology* **32,** 81-84.

Licciardi, J. M., and Pierce, K. L. (2008). Cosmogenic exposure-age chronologies of Pinedale and Bull Lake glaciations in greater Yellowstone and the Teton Range, U.S.A. *Quaternary Science Review* **27,** 814-831.

Lifton, N. A., Bieber, J. W., Clem, J. M., Duldig, M. L., Evenson, P., Humble, J. E., and Pyle, R. (2005). Addressing solar modulation and long-term uncertanties in scaling secondary cosmic rays for in situ comogenic nuclide applications. *Earth and Planetary Science Letters* **239,** 140-161.

Lifton, N. A., Caffee, M. W., Finkel, R., Schaefer, J. M., Stone, J., Goehring, B. M., Phillips, F., Oviatt, C. G., and Rood, D. H. (2009). A new estimate of the spallogenic production rate of in situ cosmogenic 10Be from Lake Bonneville shoreline features, Promontory Point, Utah. *In* "Geological Society of America Annual Meeting." pp. 229. Geological Society of America Abstracts with Programs, Portland.

Miller, C. D., and Birkeland, P. W. (1974). Probable pre-Neoglacial age of the type Temple Lake moraine, Wyoming: Discussion and additional relative-age data. *Arctic and Alpine Research* **6,** 301-306.

Moss, J. H. (1951). Late glacial advances in the southern Wind River Mountains, Wyoming. *American Journal of Science* **249,** 865-883.

Munroe, J. S. (2002). Timing of postglacial cirque reoccupation in the northern Uinta Mountains, northeastern Utah, USA. *Arctic Antarctic and Alpine Research* **34,** 38-48.

Osborn, G., and Bevis, K. (2001). Glaciation in the Great Basin of the Western United States. *Quaternary Science Reviews* **20,** 1377-1410.

Oviatt, C. G. (1977). Glacial Geology of the Lake Marie Area, Medicine Bow Mountains, Wyoming. *Contributions to Geology, University of Wyoming* **16,** 27-38.

Owen, L. A., Finkel, R. C., Minnich, R. A., and Perez, A. E. (2003). Extreme southwestern margin of late Quaternary glaciation in North America: Timing and controls. *Geology* **31,** 729-732.

Phillips, F. M., Zreda, M., Plummer, M. A., Elmore, D., and Clark, D. H. (2009). Glacial geology and chronology of Bishop Creek and vicinity, eastern Sierra Nevada, California. *Geological Society of America* **121,** 1013-1033.

Putnam, A. E., Schaefer, J. M., Barrell, D. J. A., Vandergoes, M., Denton, G. H., Kaplan, M. R., Finkel, R. C., Schwartz, R., Goehring, B. M., and Kelley, S. E. (2010). In situ cosmogenic 10Be production-rate calibration from the Southern Alps, New Zealand. *Quaternary Geochronology* **5,** 392-409.

Richmond, G. M. (1965). Glaciation of the Rocky Mountains. *In* "The Quaternary of the United States." (H. E. Wright Jr., and D. G. Frey, Eds.). Princeton University Press, Princeton.

Rinterknecht, V. R. (2003). "Cosmogenic 10Be Chronology for the Last Deglaciation of the Southern Scandinavian Ice Sheet." Unpublished Manuscripts thesis, Oregon State University.

Stone, J. O. (2000). Air pressure and cosmogenic isotope production. *Journal of Geophysical Research* **105,** 23,753 - 23,759.

Taylor, J. R. (1997). "An Introduction to Error Analysis." University Science Books, Sausalito.

Waitt, R. B., Yount, J. C., and Davis, P. T. (1982). Regional significance of an early Holocene moraine in Enchantment Lakes Basin, North Cascades Range, Washington. *Quaternary Research* **17,** 191-210.

Wesling, J. R. (1988). "Glacial chronology and soil development in Winsor Creek drainage basin, southernmost Sangre de Cristo Mountains." University of New Mexico.

Yount, J. C., Birkeland, P. W., and Burke, R. M. (1979). Glacial and periglacial deposits of the Mono Creek recesses, west-central Sierra Nevada, California: Measurements of age-dependent properties of deposits. *In* "Field guide to relative dating methods applied to glacial deposits in the third and fourth recesses and along the eastern Sierra Nevada, California, with supplementary notes on other Sierra Nevada localities. Field trip guidebook for the Friends of the Pleistocene, Pacific Cell." (R. M. Burke, and P. W. Birkeland, Eds.).

Zielinski, G. A., and Davis, P. T. (1987). Late Pleistocene age of the type Temple Lake moraine, Wind River range, Wyomong, USA. *Geographie Physique et Quaternaire,* **41,** 397-401.

Zreda, M. G., and Phillips, F. M. (1995). Insights into alpine moraine development from cosmogenic (super 36) Cl buildup dating. *Geomorphology* **14,** 149-156.

Appendix C – A Reconstruction of Holocene Temperature

C.1 Seasonal Bias

A commonly cited problem regarding paleoclimate data is whether the climate proxy of interest is biased toward a specific season (Mix, 2006; Leduc et al., 2010). To test this issue with our compiled temperature dataset, we compared different temperature proxies that were collected from the same site or from sites that are within 5°s of latitude and longitude (Figure C1 and C2). Given the chronologic and calibration uncertainties based on our Monte Carlo simulations, we do not find a strong temperature difference between proxies at common sites used in this study. The average difference in temperature through time between sites that are within a 5x5° grid and use different proxies to derive temperature is 1.6 ± 1.0°C (Figure C3). Comparing this to the average difference in temperature between sites that use the same temperature calibration, 2.1 ± 1.0°C, if a proxy based bias does exist it is within the error of the proxies themselves. We emphasize that we are not suggesting that proxy biases cannot exist, as has been and pointed out by co-authors of this paper this can certainly occur (Mix, 2006). However, we do argue that given the cumulative uncertainties in the temperature calibration and the chronology, it is very difficult to assess in Holocene temperature reconstructions at this point and is well within the uncertainty for the datasets we have selected.

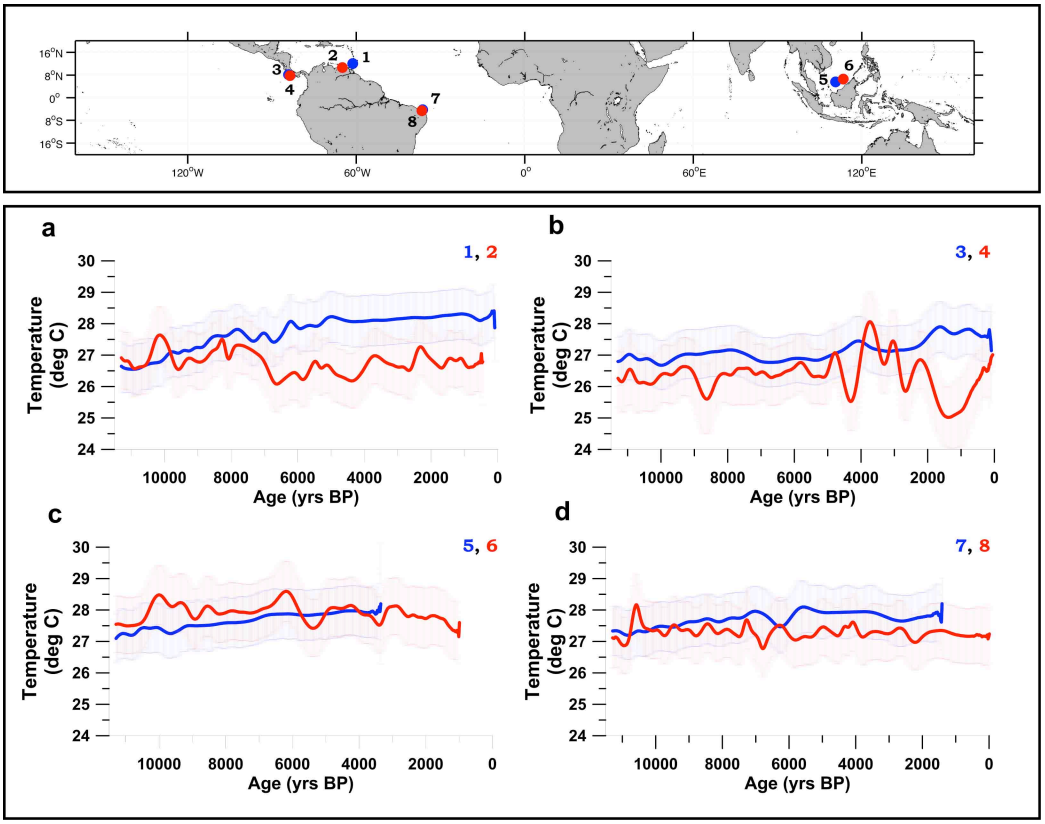

Figure C1: Temperature reconstructions at select sites where different proxy based reconstructions were used.

In each of these comparisons, the blue lines represent temperature reconstructions derived from alkenones ($U^{K'}_{37}$) and the red represent temperatures from planktonic foraminifera (Mg/Ca).

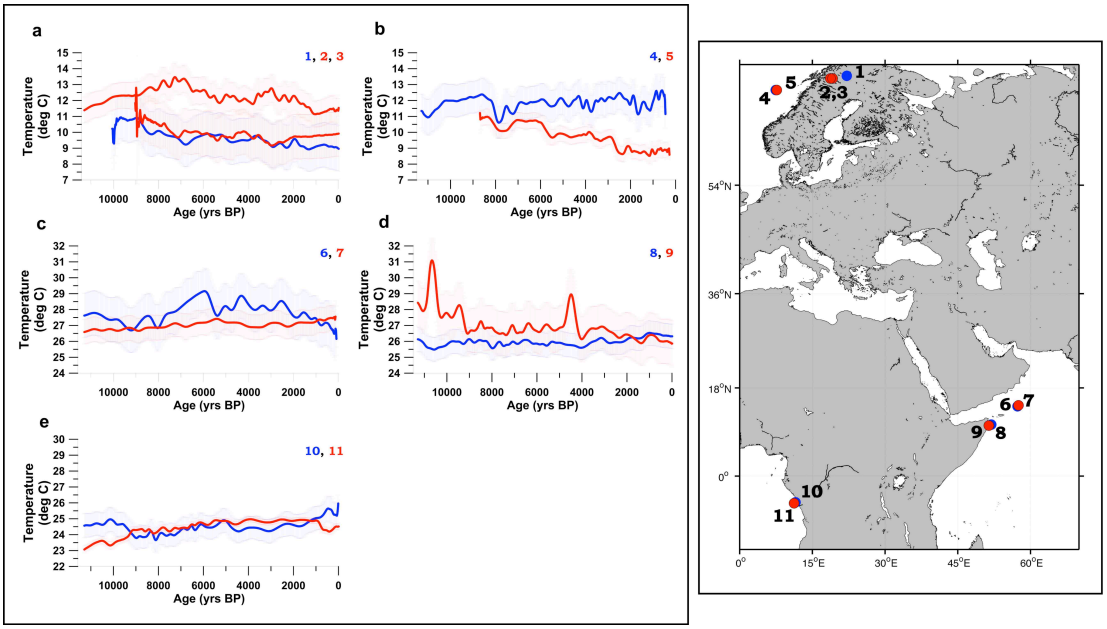

Figure C2: Temperature reconstructions at select sites where different proxy based reconstructions were used.

a, Pollen temperature reconstructions plotted with chronomid (red). **b,** Alkenones ($U^{K'}_{37}$) and Radiolara (red). **c-d,** Alkenones ($U^{K'}_{37}$) and TEX_{86} (red). **e,** Alkenones ($U^{K'}_{37}$) and branched tetraether membrane lipids (MBT) (red).

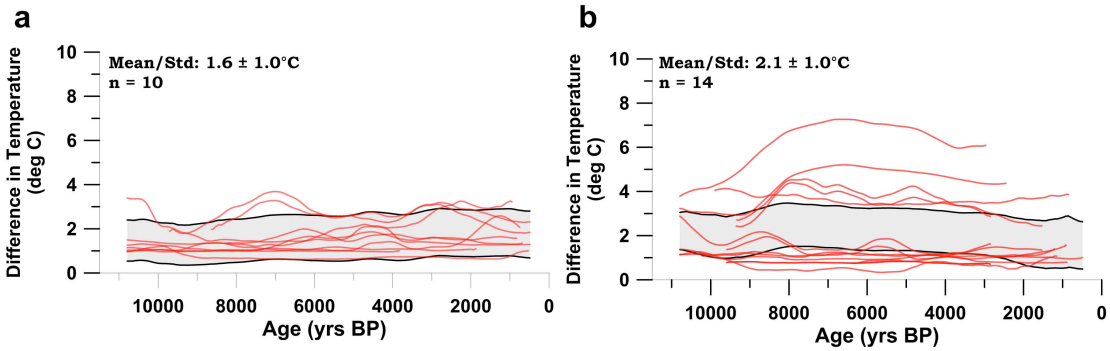

Figure C3: Average difference in absolute temperature between records within a 5x5° area.

a, Difference in absolute temperature through time for records using different proxy based temperature methods (red lines) with the mean and standard deviation for all ten records (grey bar). b, Difference in absolute temperature through time for records using the same proxy based temperature method (red lines) with the mean and standard deviation for all fourteen records (grey bar).

C.2 Data Selection Criteria

Though there likely exists several hundred Holocene temperature reconstructions from across the globe, we followed a very strict criterion for selecting dataset to add to our study. Our motivation was to use only the best data available that would enable us to address centennial and millennial variability by having good chronologic controls with relatively high sample resolution. When determining which datasets to include in our analysis, we restricted our selection to records with the following criteria:

1. Sampling resolutions better than ~400 yrs.
2. Spanning greater than ~6000 years of the Holocene and crossing the 4500 – 5500 yr B.P. reference period.
3. Chronologically derived age points from the site itself (i.e. not cross correlated or 'wiggle matched' chronologies). This includes layer counting as was done for most of the ice core chronologies.
4. Temperatures derived from an established proxy based method.
5. Obtainable from one of the many databases (PANGEA, NOAA-Paleoclimate) or provided directly by the original authors.
6. Datasets that included the original sampling depth and proxy measurement (i.e. not just time and temperature).

C.3 Global Temperature Reconstruction from Sparse Dataset

An obvious question regarding our temperature reconstruction is whether 73 globally distributed points can accurately represent the average global temperature through time. Because no observational data exists beyond the 1880s, we use the instrumental data from the NCEP-NCAR reanalysis (Kalnay et al., 1996) to test whether a sparse sampling of data can realistically represent the actual global average

temperatures. To do this we randomly selected surface air temperature points from the 1x1° grid boxes of the reanalysis data for each year through the 1948-2008 instrumental periods (Figure C4 and C5). We varied our experiment in three ways: the first was to select random grid points from the global temperature field for each year between 1948 and 2008. This was done 1000 times and in each of the 1000 randomized simulations the selections of the grid points did not change through time (i.e. identical grid points chosen for 1948, 1949,…., 2008). The second experiment was identical to the first, except we allowed the grid points to change with each time step (i.e. new grid points chosen for 1948, 1949, ...) producing a very similar result. In the third experiment we only selected from the grid boxes where our global temperature data was derived. From this analysis, we find that after selecting ~25 data points the correlation between the subset time series and the actual temperature time series from 1948-2008 is >0.80 and by 70 data points the correlation is greater than 0.90. This finding is reassuring and provides confidence that our relatively small dataset is providing a good approximation of the global average temperature.

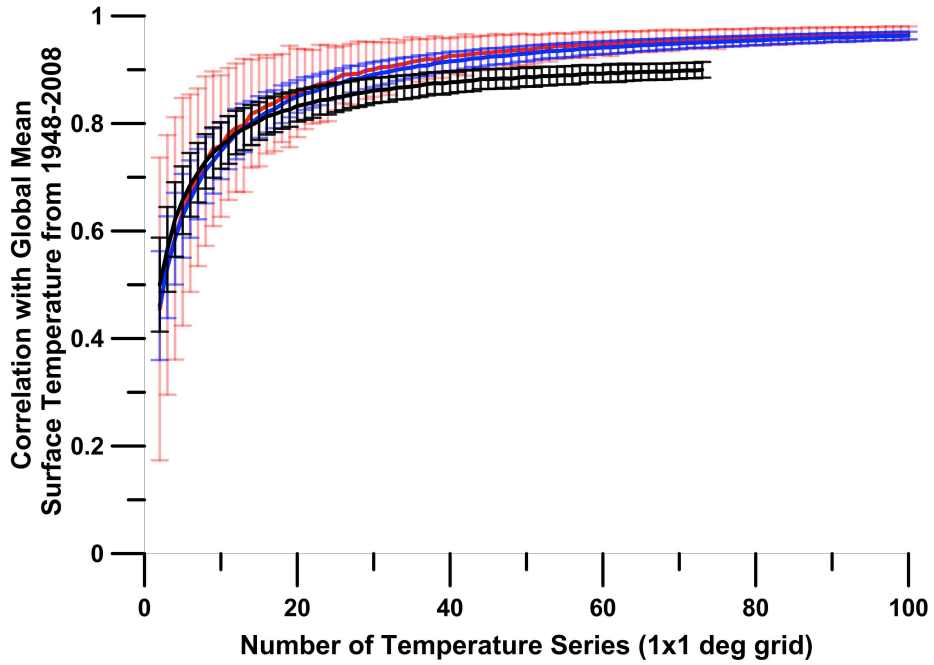

Figure C4: Correlations with global mean surface temperature.

Plotted is the mean (line) and 1σ uncertainty (error bar) of the 1000 simulations. The red line represents the experiment where the grid points did not change through time for each of the 1000 simulations, the blue is when they change for each time step, and the black is the experiment where only grid boxes from where our global temperature data was derived.

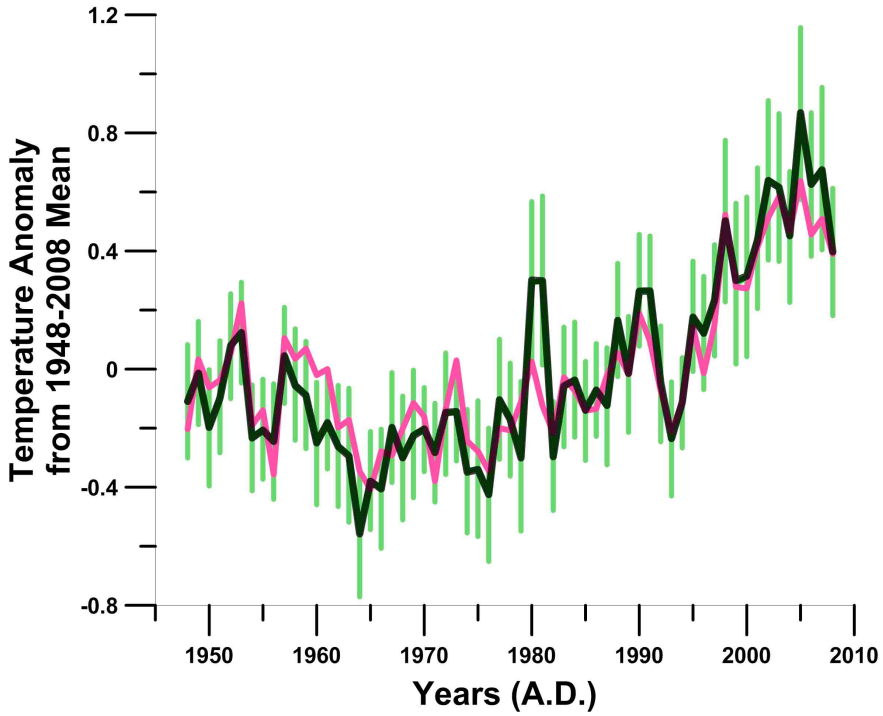

Figure C5: Time Series of Global Average Temperature Anomalies.
The black line is the global average temperature anomaly from the NCEP NCAR reanalysis for 1948 to 2008. The pink line is the average temperature anomaly from the 73 datapoints from where our global temperature stack is derived. The green line, which is indistinguishable from the black, represents the average temperature anomaly at 73 randomly selected sites across the globe and the 2σ error of 1000 realizations.

C.4 Uncertainty

Two sources of error contribute to the uncertainty associated with any given temperature reconstruction from paleoclimate data. The first is the uncertainty in the proxy to temperature calibration. To address this in our global temperature stack, we accounted for calibration error by applying the following methods for each of the various temperature proxies:

a. Mg/Ca from Planktonic Foraminifera – The general form of the Mg/Ca based temperature reconstruction is either described as an exponential or linear function.

$$Mg/Ca = (B \pm b) * exp((A \pm a) * T)$$

$$Mg/Ca = (B \pm b) * T - (A \pm a)$$

where: T=temperature

For each of the Mg/Ca based temperature measurements we applied the calibration that was originally used by the authors. The error was related to the original "A" and "B" coefficients and allowed to vary within its uncertainty ("a" and "b") following a random draw from a normal distribution.

b. $U^{K'}_{37}$ from Alkenones – For all alkenone records we applied the calibration of Müller et al. (1998) and their associated error.

$$U^{K'}_{37} = T*(0.033 \pm 0.0001) + (0.044 \pm 0.016)$$

c. TEX_{86} – For all TEX_{86} records we applied the original calibration suggested by the authors and the error from the global core top calibration of Kim et al.(Kim et al., 2008) (± 1.7°C).

d. Chronomids – For the chronomid temperature reconstructions we used the average root mean squared error (± 1.7°C) from six studies (Walker IR, 1997; Larocque, 2001; Bigler and Hall, 2002; Palmer SL, 2002; Rosenberg SM, 2004;

Barley et al., 2006) and treated it as the 1σ standard deviation for all of the temperature measurements.

e. Pollen – Pollen temperature error followed from Seppä et al. (2005) (± 1.0°C) and was treated as the 1σ uncertainty.

f. Ice Core – We conservatively assumed an ice temperature uncertainty of ±30%, which is well within or beyond other estimates.

g. All other Methods – The error from the remaining records (MBT, Radiolaria, Transfer Function Analysis) was derived from the original publication (Table C1) and treated as the 1σ temperature uncertainty.

The second source of error comes from the chronologic uncertainty associated with developing age models for each record. To account for this in our reconstruction, we perturbed the age control points (typically calibrated ^{14}C ages) within their uncertainties for each record using a Monte Carlo based approach, which is described in detail below. The majority of our age control points were based on radiocarbon dated materials. In order to compare the records appropriately, we recalibrated all of the radiocarbon dates with Calib 6.0.1 using INTCAL09 and its protocol (Reimer, 2009) for the site-specific locations and materials. Any reservoir ages used in the ocean datasets followed the original authors suggested values. The uncertainty between the age control points was modeled as a random walk, after Huybers and Wunch(Huybers and Wunch, 2004), where we applied a "jitter" value of 200. Chronologic error was assumed to be autocorrelated through time and was modeled as a first order autoregressive process with a coefficient of 0.999. For the ice core records, we applied a 2% error for the Antarctica sites and a 1% error for the Greenland site.

C.5 Monte Carlo Based Procedure and Description

To account for both the temperature calibration and chronologic uncertainties, we applied a Monte Carlo based approach that perturbed each of the records age models and calibrated temperatures 10,000 times following a random draw from a normal distribution based on the records uncertainty (Figure C6). Each of the calibrated temperatures was interpolated onto the new age models to render 10,000 realizations of the calibrated temperatures that incorporated both the uncertainty in the age model and the proxy-to-temperature calibration (Figure C6 a and C7). This was done for each record and compiled into a large three-dimensional matrix (Figure C6 b), and then averaged in the third dimension (i.e. dataset) and compressed into a single matrix representing 10,000 globally stacked temperature records (Figure C6 c, C8, and C9). The mean and standard deviation was then taken from the 10,000 simulated globally stacked temperatures (Figure C6 d) to produce our full interglacial time series.

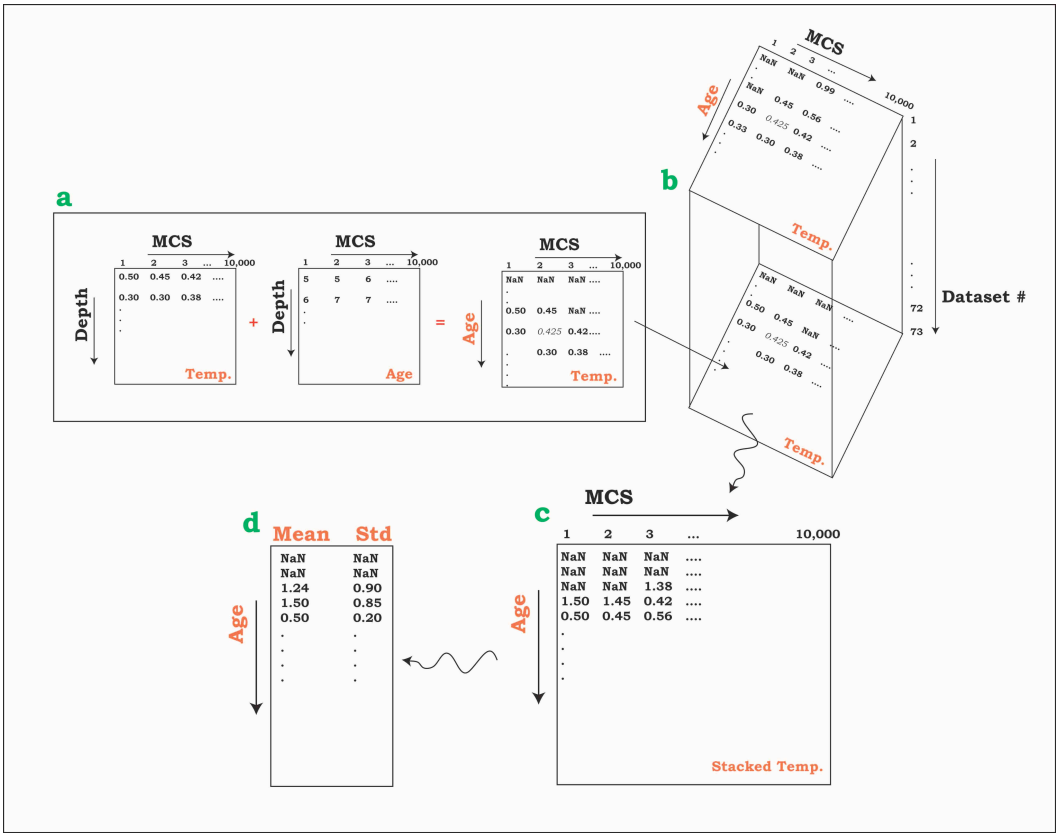

Figure C6: Diagram for helping visualize our Monte Carlo based procedure described in the supplemental text.

a, Combining perturbed temperature (Temp.) and age model values to form 10,000 simulated versions of each dataset. b, Three dimensional matrix of each of the 10,000 simulated datasets. c, 10,000 realizations of the globally stacked temperature record after compressing the three dimensions matrix by averaging the datasets. d, Mean and standard deviation (Std) of the 10,000 globally stacked temperature records.

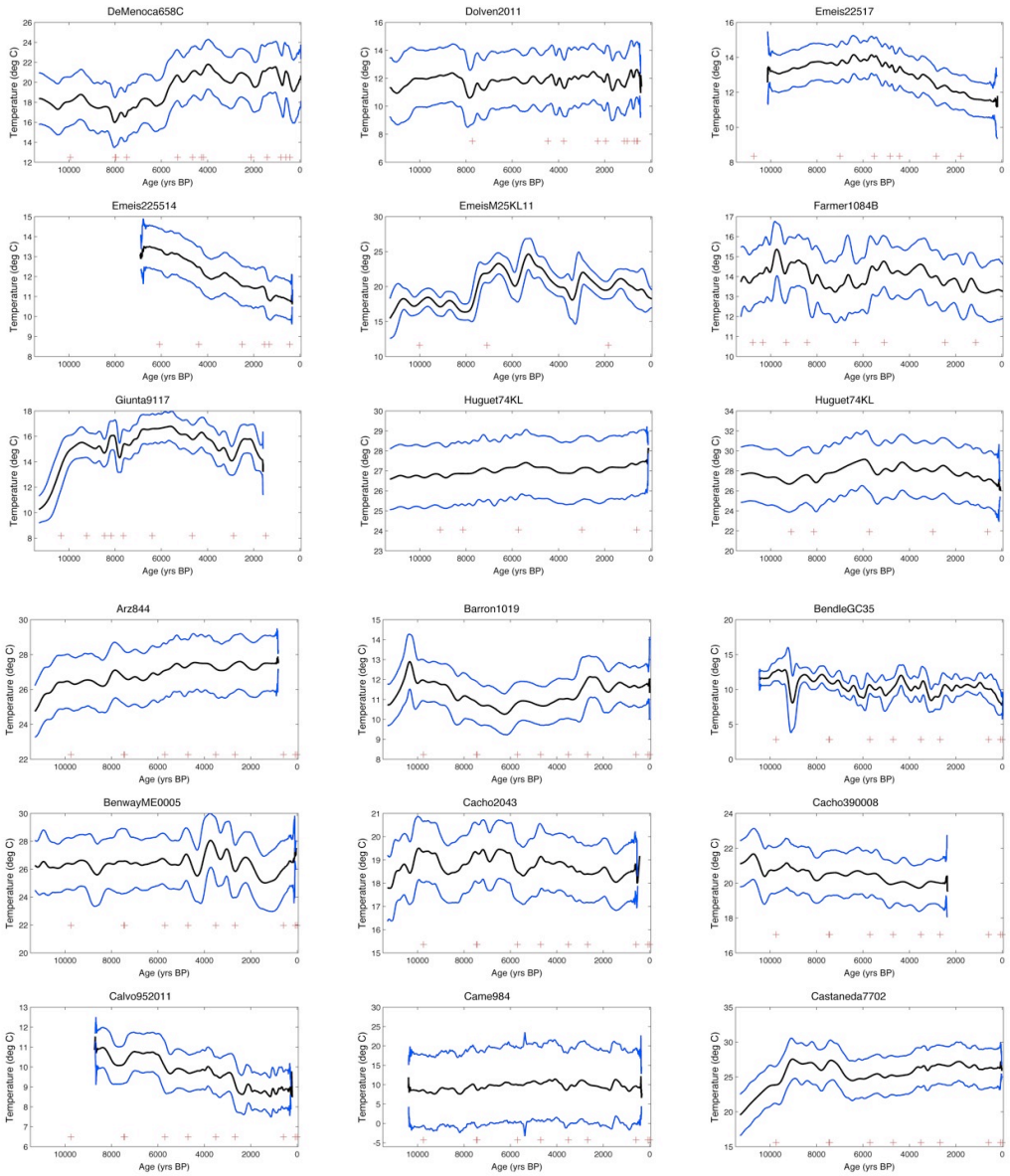
DeMenoca658C
Dolven2011
Emeis22517
Emeis225514
EmeisM25KL11
Farmer1084B
Giunta9117
Huguet74KL
Huguet74KL
Arz844
Barron1019
BendleGC35
BenwayME0005
Cacho2043
Cacho390008
Calvo952011
Came984
Castaneda7702
Temperature (deg C)
Age (yrs BP)

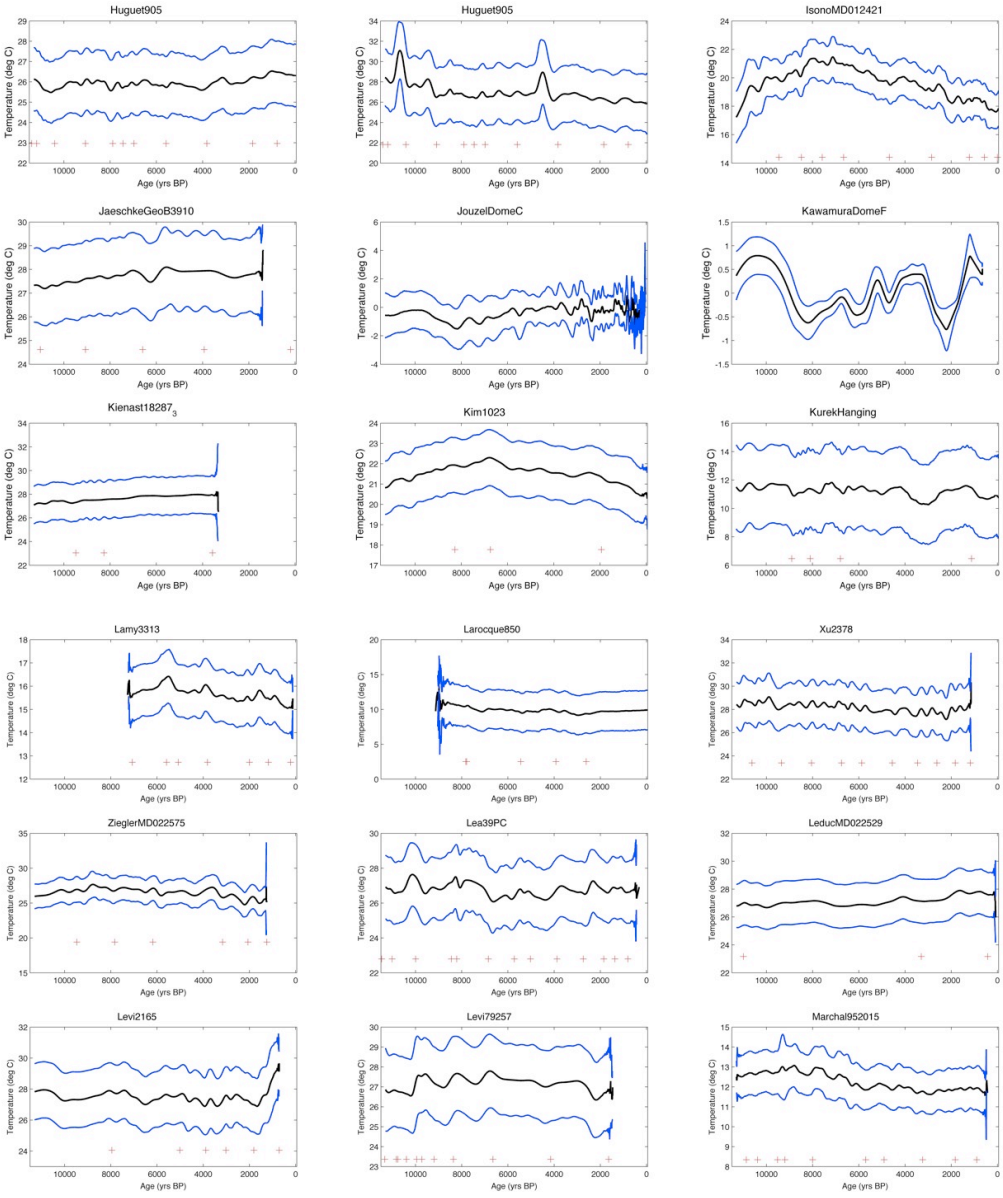
Huguet905
Huguet905
IsonoMD012421
JaeschkeGeoB3910
JouzelDomeC
KawamuraDomeF
Kienast18287$_3$
Kim1023
KurekHanging
Lamy3313
Larocque850
Xu2378
ZieglerMD022575
Lea39PC
LeducMD022529
Levi2165
Levi79257
Marchal952015
Temperature (deg C)
Age (yrs BP)

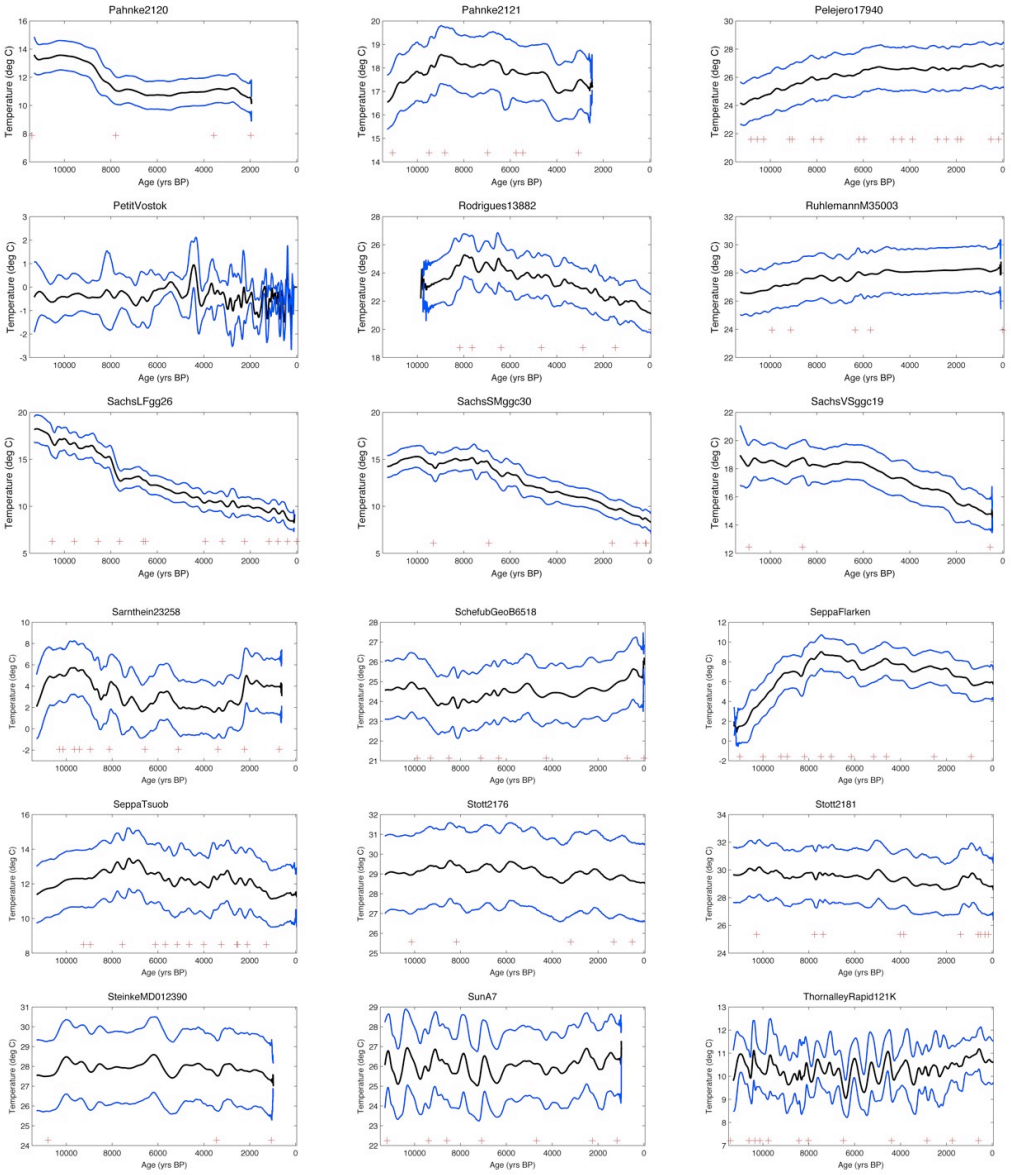
Pahnke2120
Pahnke2121
Pelejero17940
PetitVostok
Rodrigues13882
RuhlemannM35003
SachsLFgg26
SachsSMggc30
SachsVSggc19
Sarnthein23258
SchefubGeoB6518
SeppaFlarken
SeppaTsuob
Stott2176
Stott2181
SteinkeMD012390
SunA7
ThornalleyRapid121K
Temperature (deg C)
Age (yrs BP)

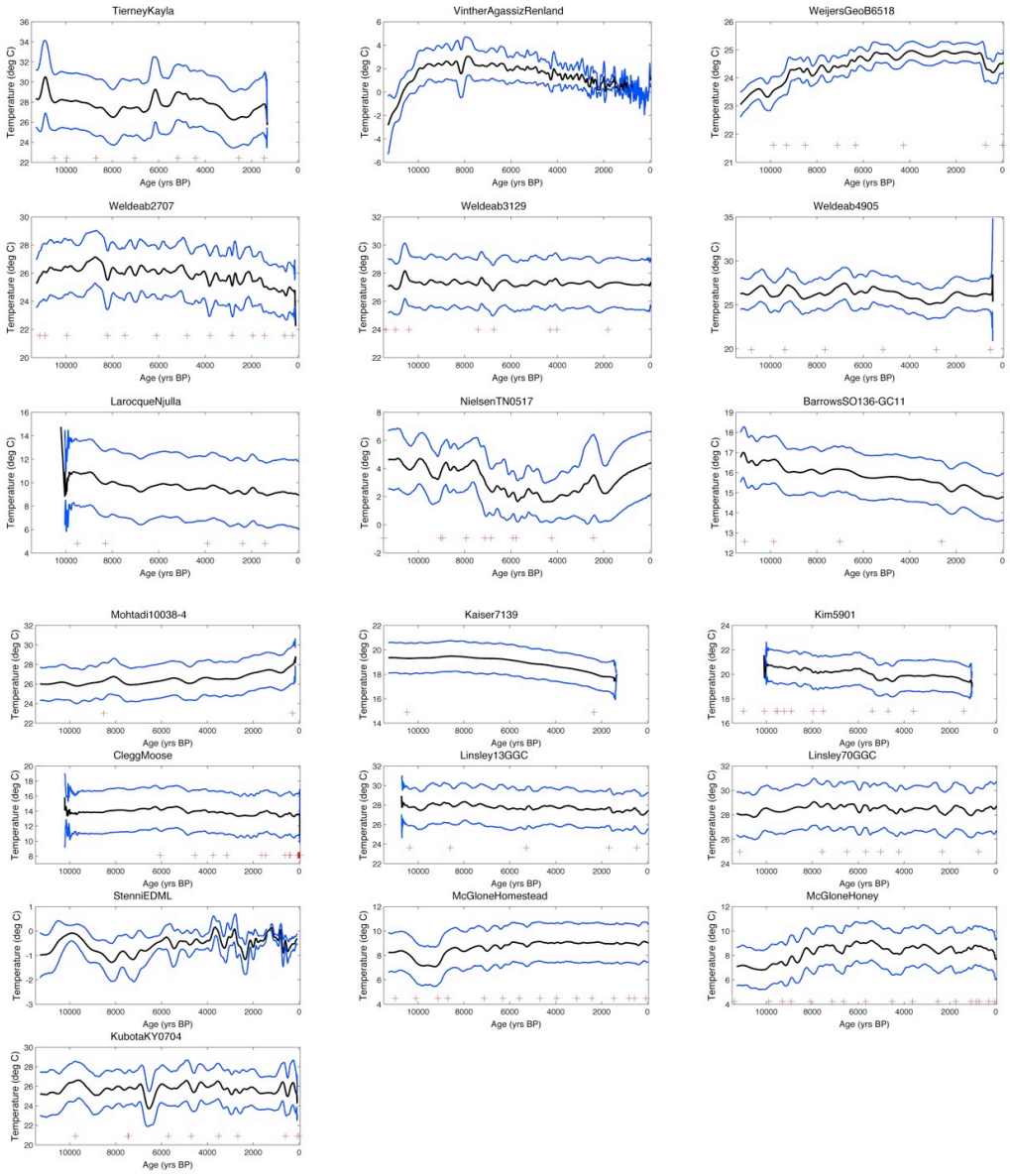

Figure C7: Time series of the mean and 2σ uncertainty band of every dataset used in this study.

The red crosses represent the age control points in the datasets.

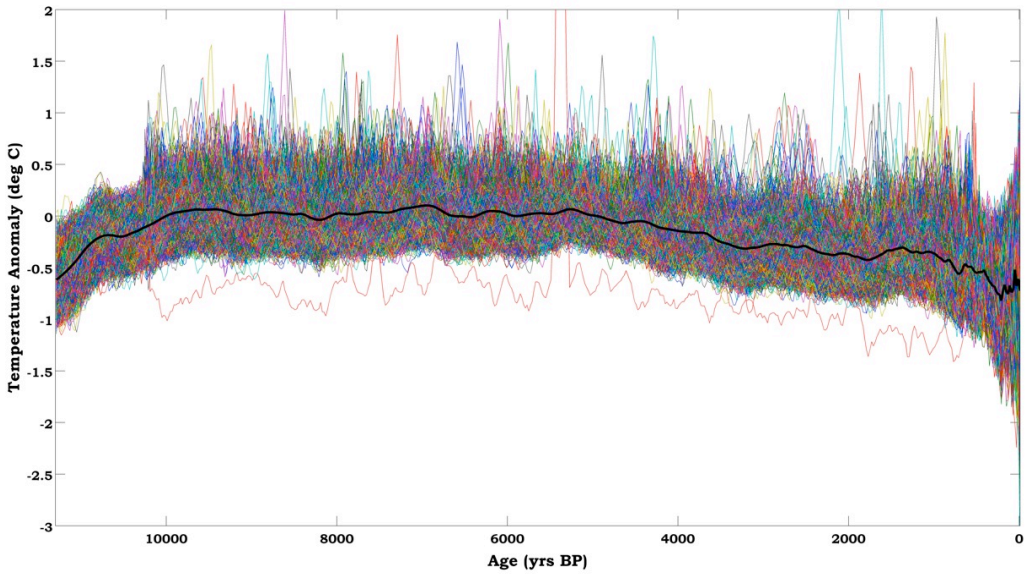

Figure C8: Monte Carlo simulations from all 73 proxy temperature records. All 10,000 realizations of the globally stacked time series (colored lines) and the mean (black line). Temperature anomaly is from the 4500-5500 yr B.P. mean.

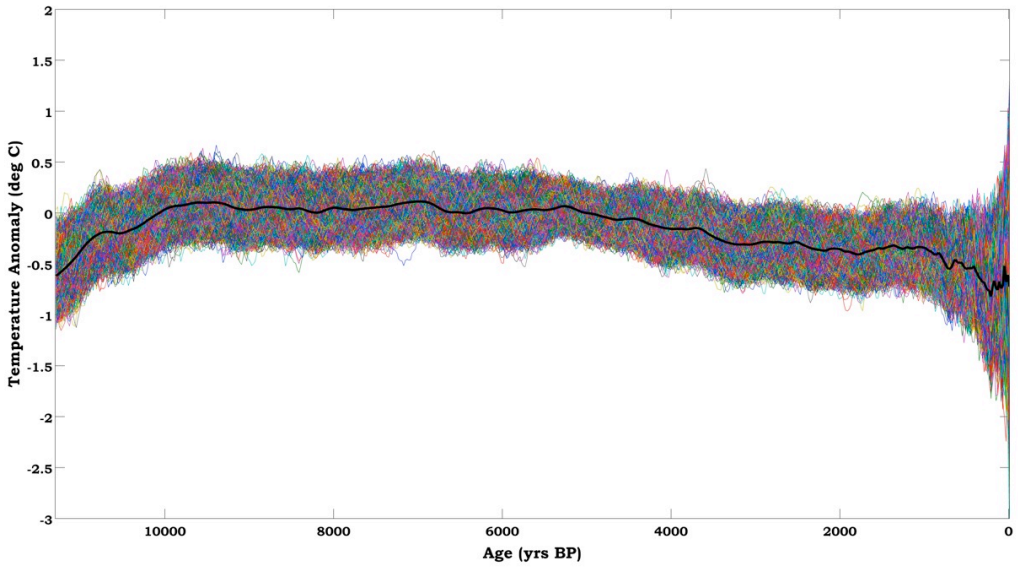

Figure C9: Monte Carlo simulations from 72 proxy temperature records. Another 10,000 realizations of our globally stacked time series (colored lines) and the mean (black line) where one record (Came et al., 2007) with very large temperature calibration error (von Langen et al., 2005) was removed. Note differences with Figure C8. The average difference in the mean and standard deviation between the two records is 0.01°C and 0.02°C, respectively.

Table C1. List of data sets used in the global temperature stack.

Core, Hole, Lake, Ice Core	Proxy	Temperature Calibration	Lat. (DD)	Long. (DD)	Elevation (m a.s.l.)	Reference	File Name
GeoB5844-2	UK'37	Müller	27.7	34.7	-963	(Arz et al., 2003)	Arz844
ODP-1019D	UK'37	Müller	41.7	-124.9	-980	(Barron et al., 2003)	Barron1019
SO136-GC11	UK'37	Müller	-43.5	167.9	-1556	(Barrows et al., 2007)	BarrowsSO136-GC11
JR51GC-35	UK'37	Müller	67.0	-18.0	-420	(Bendle and Rosell-Mele, 2007)	BendleGC35
ME005A-43JC	Mg/Ca	Anand	7.9	-83.6	-1368	(Benway et al., 2006a)	BenwayME0005A
MD95-2043	UK'37	Müller	36.1	-2.6	-1000	(Cacho et al.,	Cacho2043

						2001)	
M39-008	UK'37	Müller	39.4	-7.1	-576	(Cacho et al., 2001)	Cacho390008
MD95-2011	UK'37	Müller	67.0	7.6	-1048	(Calvo et al., 2002)	Calvo952011
ODP 984	Mg/Ca	von Langen	61.4	-24.1	-1648	(Came et al., 2007)	Came984
GeoB 7702-3	TEX86	Kim	31.7	34.1	-562	(Castañeda et al., 2010)	Castaneda7702
Moose Lake	Chironomids	Global Avg. RMSEP	61.4	-143.6	437	(Clegg et al., 2010)	CleggMoose
ODP 658C	Transfer Function	1.5°C error	20.8	-18.6	-2263	(deMenocal et al., 2000)	DeMenoca658C
Composite: MD95-2011 / HM79-4	Radiolara	1.2°C error	67.0	7.6	-	(Dolven et al., 2002)	Dolven2011
IOW225517	UK'37	Müller	57.7	7.1	-293	(Emeis et al.,	Emeis22517

						2003)	
IOW225514	UK'37	Müller	57.8	8.7	-420	(Emeis et al., 2003)	Emeis225514
M25/4-KL11	UK'37	Müller	36.7	17.7	-3376	(Emeis et al., 2003)	EmeisM25KL11
ODP 1084B	Mg/Ca	Mashiotta	-25.5	13.0	-1992	(Farmer et al., 2005)	Farmer1084B
AD91-17	UK'37	Müller	40.9	18.6	-844	(Giunta et al., 2001)	Giunta9117
74KL	UK'37	Müller	14.3	57.3	-3212	(Huguet et al., 2006)	Huguet74KL
74KL	TEX86	Schouten	14.3	57.3	-3212	(Huguet et al., 2006)	Huguet74KL
NIOP-905	UK'37	Müller	10.6	51.9	-1567	(Huguet et al., 2006)	Huguet905
NIOP-905	TEX86	Schouten	10.6	51.9	-1567	(Huguet et al., 2006)	Huguet905

Composite: MD01-2421 / KR02-06 St.A GC / KR02-06 St.A MC	UK'37	Müller	36.0	141.8	-2224	(Isono et al., 2010)	IsonoMD012421
GeoB 3910	UK'37	Müller	-4.2	-36.3	-2362	(Jaeschke et al., 2007)	JaeschkeGeoB3910
Dome C, Antarctica	IceCore	30% error	-75.1	123.4	3240	(Jouzel et al., 2007a)	JouzelDomeC
GeoB 7139-2	UK'37	Müller	-30.2	-72.0	-3270	(Kaiser et al., 2008)	Kaiser7139
Dome F, Antarctica	IceCore	30% error	-77.3	39.7	3810	(Kawamura et al., 2007)	KawamuraDomeF
18287-3	UK'37	Müller	5.7	110.7	-598	(Kienast et al., 2001)	Kienast18287_3
GeoB 1023-5	UK'37	Müller	-17.2	11.0	-1978	(Kim et al., 2002)	Kim1023

GeoB 5901-2	UK'37	Müller	36.4	-7.1	-574	(Kim et al., 2004)	Kim5901
MD98-2181	Mg/Ca	Anand	31.6	129.0	-2114	(Kubota et al., 2010)	KubotaKY0704
Hanging Lake	Chironomids	Global Avg. RMSEP	68.4	-138.4	500	(Kurek et al., 2009)	KurekHanging
GeoB 3313-1	UK'37	Müller	-41.0	-74.3	825	(Lamy et al., 2002)	Lamy3313
Lake 850	Chironomids	Global Avg. RMSEP	68.4	19.2	850	(Larocque and Hall, 2004)	Larocque850
Lake Nujulla	Chironomids	Global Avg. RMSEP	68.4	18.7	999	(Larocque and Hall, 2004)	LarocqueNjulla
PL07-39PC	Mg/Ca	Anand	10.7	-65.0	-790	(Lea et al., 2003)	Lea39PC
MD02-2529	UK'37	Müller	8.2	-84.1	-1619	(Leduc et al., 2007)	LeducMD022529
MD98-2165	Mg/Ca	Dekens	-9.7	118.3	-2100	(Levi et al.,	Levi2165

						2007)	
MD79-257	MAT	1.1°C error	-20.4	36.3	-1262	(Levi et al., 2007)	Levi79257
BJ8 13GGC	Mg/Ca	Anand	-7.4	115.2	-594	(Linsley et al., 2010)	Linsley13GGC
BJ8 70GGC	Mg/Ca	Anand	-3.6	119.4	-482	(Linsley et al., 2010)	Linsley70GGC
MD95-2015	UK'37	Müller	58.8	-26.0	-2630	(Marchal et al., 2002)	Marchal952015
Homestead Scarp	MAT	0.98°C error	-52.5	169.1	30	(McGlone et al., 2010)	McGloneHomestead
Mount Honey	MAT	0.98°C error	-52.5	169.1	120	(McGlone et al., 2010)	McGloneHoney
GeoB 10038-4	Mg/Ca	Anand	-5.9	103.3	-1819	(Mohtadi et al., 2010)	Mohtadi10038-4
TN05-17	Diatom MAT	0.75°C error	-50.0	6.0	-3700	(Nielsen et al., 2010)	NielsenTN0517

MD97-2120	UK'37	Müller	-45.5	174.9	-3290	(Pahnke and Sachs, 2006)	Pahnke2120
MD97-2121	UK'37	Müller	-40.4	178.0	-3014	(Pahnke and Sachs, 2006)	Pahnke2121
17940	UK'37	Müller	20.1	117.4	-1968	(Pelejero et al., 1999)	Pelejero17940
Vostok, Antarctica	IceCore	30% error	-78.5	108.0	3500	(Petit, 1999)	PetitVostok
D13822	UK'37	Müller	38.6	-9.5	-88	(Rodrigues et al., 2009)	Rodrigues13882
M35003-4	UK'37	Müller	12.1	-61.2	-1299	(Rühlemann et al., 1999)	RuhlemannM35003
OCE326-GGC26	UK'37	Müller	43.0	-55.0	-3975	(Sachs, 2007)	SachsLFgg26
OCE326-GGC30	UK'37	Müller	44.0	-63.0	-250	(Sachs, 2007)	SachsSMggc30
CH07-98-	UK'37	Müller	36.9	-74.6	-1049	(Sachs, 2007)	SachsVSggc19

GGC19							
GIK23258-2	Transfer Function	1.5°C error	75.0	14.0	-1768	(Sarnthein et al., 2003)	Sarnthein23258
GeoB 6518-1	UK'37	Müller	-5.6	11.2	-962	(Schefuß et al., 2005)	SchefubGeoB6518
Flarken Lake	Pollen	Seppa	58.6	13.7	108	(Seppä and Birks, 2001); (Seppä et al., 2005)	SeppaFlarken
Tsuolbmajavri Lake	Pollen	Seppa	68.7	22.1	526	(Seppä and Birks, 2001); (Seppä and Weckström, 1999)	SeppaTsuob
MD01-2390	Mg/Ca	Dekens	6.6	113.4	-1545	(Steinke et al., 2008)	SteinkeMD012390
EDML	IceCore	30% error	-75.0	0.1	2892	(Stenni et al.,	StenniEDML

						2010)	
MD98-2176	Mg/Ca	Anand	-5.0	133.4	-2382	(Stott et al., 2007)	Stott2176
MD98-2181	Mg/Ca	Anand	6.3	125.8	-2114	(Stott et al., 2007)	Stott2181
A7	Mg/Ca	Anand	27.8	127.0	-1262	(Sun et al., 2005)	SunA7
RAPID-12-1K	Mg/Ca	Thornalley	62.1	-17.8	-1938	(Thornalley et al., 2009)	ThornalleyRapid121K
NP04-KH3, -KH4	TEX86	Powers	-6.7	29.8	773	(Tierney et al., 2008)	TierneyKayla
Agassiz / Renland	IceCore	30% error	71.3/ 81.0	26.7 / -71	1730/ 2350	(Vinther et al., 2009)	VintherAgassizRenland
GeoB6518-1	MBT	0.2°C error	-5.6	11.2	-962	(Weijer et al., 2007)	WeijersGeoB6518
MD03-2707	Mg/Ca	Dekens	2.5	9.4	-1295	(Weldeab et al., 2007)	Weldeab2707

GeoB 3129	Mg/Ca	Anand	-4.6	-36.6	-830	(Weldeab et al., 2006)	Weldeab3129
GeoB 4905	Mg/Ca	Anand	2.5	9.4	-1328	(Weldeab et al., 2005)	Weldeab4905
MD01-2378	Mg/Ca	Anand	13.1	121.8	-1783	(Xu et al., 2008)	Xu2378
MD02-2575	Mg/Ca	Anand	29.0	-87.1	-847	(Ziegler et al., 2008)	ZieglerMD022575

C.6 References

Arz, H. W., Pätzold, J., and Müller, P. J. (2003). Influence of Northern Hemisphere climate and global sea level rise on the restricted Red Sea marine environment during termination I. *Paleoceanography* **18,** doi:10.1029/2002PA000864.

Barley, E. M., Walker, I. R., Kurek, J., Cwynar, L. C., Mathewes, R. W., Gajewski, K., and Finney, B. P. (2006). A northwest North American training set: distribution of freshwater midges in relation to air temperature and lake depth. *Journal of Paleolimnology* **36,** 295-314.

Barron, J. A., Heusser, L., Herbert, T., and Lyle, M. (2003). High resolution climatic evolution of coastal northern California during the past 16,000 years. *Paleoceanography* **18,** 20-1 to 20-14.

Barrows, T. T., Lehman, S. J., Fifield, L. K., and De Deckker, P. (2007). Absence of Cooling in New Zealand and the Adjacent Ocean During the Younger Dryas Chronozone. *Science* **318,** 86-89.

Bendle, J. A. P., and Rosell-Mele, A. (2007). High-resolution alkenone sea surface temperature variability on the North Icelandic Shelf: implications for Nordic Seas palaeoclimatic development during the Holocene. *The Holocene* **17,** 9-24.

Benway, H. M., Mix, A. C., Haley, B. A., and Klinkhammer, G. P. (2006). Eastern Pacific Warm Pool paleosalinity and climate variability: 0 – 30 kyr. *Paleoceanography* **21,** PA3008, doi:10.1029/2005PA001208.

Bigler, C., and Hall, R. I. (2002). Diatoms as indicators of climatic and limnological change in Swedish Lapland: a 100-lake calibration-set and its validation for paleoecological reconstructions. *Journal of Paleolimnology* **27,** 97-115.

Cacho, I., Grimalt, J. O., Canals, M., Sbaffi, L., Shackelton, N. J., Schonfeld, J., and Zahn, R. (2001). Variability of the western Mediterranean Sea surface temperature during the last 25,000 years and its connection with the Northern Hemisphere climatic changes. *Paleoceanography* **16,** 40-52.

Calvo, E., Grimalt, J., and Jansen, E. (2002). High resolution UK37 sea surface temperature reconstruction in the Norwegian Sea during the Holocene. *Quaternary Science Review* **21,** 1385-1394.

Came, R. E., Oppo, D. W., and McManus, J. F. (2007). Amplitude and timing of temperature and salinity variability in the subpolar North Atlantic over the past 10 k.y. *Geology* **35,** 315-318.

Castañeda, I. S., Schefuß, E., Pätzold, J., Damste, J. S. D., Weldeab, S., and Schouten, S. (2010). Millennial-scale sea surface temperature changes in the eastern Mediterranean (Nile River Delta region) over the last 27,000 years. *Paleoceanography* **25,** PA1208, doi:10.1029/2009PA001740.

Clegg, B. F., Clarke, G. H., Chipman, M. L., Chou, M., I.R., W., Tinner, W., and Hu, F. S. (2010). Six millennia of summer temperature variation based on midge analysis of lake sediments from Alaska. *Quaternary Science Review***,** doi:10.1016/j.quascirev.2010.08.001.

deMenocal, P., Ortiz, J., Guilderson, T., and Sarnthein, M. (2000). Coherent High- and Low-Latitude climate variability during the Holocene warm period. *Science* **288,** 2198-2202.

Dolven, J. K., Cortese, G., and Bjøklund, K. R. (2002). A high-resolution radiolarian-derived paleotemperature record for the Late Pleistocene-Holocene in the Norwegian Sea. *Paleoceanography* **17,** doi:10.1029/2002PA000780.

Emeis, K. C., Struck, U., Blanz, T., Kohly, A., and Woß, M. (2003). Salinity changes in the central Baltic Sea (NW Europe) over the last 10 000 years. *The Holocene* **13,** 411-421.

Farmer, E. C., deMendocal, P. B., and Marchitto, T. M. (2005). Holocene and deglacial ocean temperature variability in the Benguela upwelling region: Implications for low-latitude atmospheric circulation. *Paleoceanography* **20,** doi:10.1029/2004PA001049.

Giunta, S., Emeis, K. C., and Negri, A. (2001). Sea-surface temperature reconstruction of the last 16,000 years in the Eastern Mediterranean Sea. *Rivista Italiana di Paleontologia e Stratigrafia* **107,** 463-476.

Huguet, C., Kim, J.-H., Damsté, J. S. S., and Schouten, S. (2006). Reconstruction of sea surface temperature variations in the Arabian
Sea over the last 23 kyr using organic proxies (TEX86 and UK37). *Paleoceanography* **21,** doi:10.1029/2005PA001215.

Huybers, P., and Wunch, C. (2004). A depth-derived Pleistocene age model: Uncertainty estimates, sedimentation variability, and nonlinear climate change. *Paleoceanography* **19,** PA1028, doi:10.1029/2002PA000857.

Isono, G., Yamamoto, M., Irino, T., Oba, T., Murayama, M., Nakamura, T., and Kawahata, H. (2010). The 1500-year climate oscillation in the midlatitude North Pacific during the Holocene. *Geology* **37,** 591-594.

Jaeschke, A., Rühlemann, C., Arz, H., Heil, G., and Lohmann, G. (2007). Coupling of millennial-scale changes in sea surface temperature and precipitation off northeastern Brazil with high-latitude climate shifts during the last glacial period. *Paleoceanography* **22,** doi:10.1029/2006PA001391.

Jouzel, J., Masson-Delmotte, V., Cattani, O., Dreyfus, G., Falourd, S., Hoffmann, G., Minster, B., Nouet, J., Barnola, J. M., Chappellaz, J., Fischer, H., Gallet, J. C., Johnsen, S., Leuenberger, M., Loulergue, L., Luethi, D., Oerter, H., Parrenin, F., Raisbeck, G., Raynaud, D., Schilt, A., Schwander, J., Selmo, E., Souchez, R., Spahni, R., Stauffer, B., J. P. Steffensen, Stenni, B., Stocker, T. F., Tison, J. L., Werner, M., and Wolff, E. W. (2007). Orbital and Millennial Antarctic Climate Variability over the Past 800,000 Years. *Science* **317,** 793-796.

Kaiser, J., Schefuß, E., Lamy, F., Mohtadi, M., and Hebbeln, D. (2008). Glacial to Holocene changes in sea surface temperature and coastal vegetation in north central Chile: high versus low latitude forcing. *Quaternary Science Review* **27,** 2064-2075.

Kalnay, E., Kanamitsu, M., Kistler, R., Collins, W., Deaven, D., Gandin, L., Iredell, M., Saha, S., White, G., Woollen, J., Zhu, Y., Leetmaa, A., and Reynolds, R. (1996). The NCEP/NCAR 40-year Reanalysis Project. *Bulletin of the American Meteorological Society* **77,** 437-470.

Kawamura, K., Parrenin, F., Lisiecki, L., Uemura, R., Vimeux, F., Severinghaus, J. P., Hutterli, M. A., Nakazawa, T., Aoki, S., Jouzel, J., Raymo, M. E., Matsumoto, K., Nakata, H., Motoyama, H., Fujita, S., Goto-Azuma, K., Fujii, Y., and Watanabe, O. (2007). Northern Hemisphere forcing of climatic cycles in Antarctica over the past 360,000 years. *Nature* **448,** 912-916.

Kienast, M., Steinke, S., Stattegger, K., and Calvert, S. E. (2001). Synchronous Tropical South China Sea SST Change and Greenland Warming During Deglaciation. *Science* **291,** 2132-2134.

Kim, J.-H., Rimbu, N., Lorenz, S. J., Lohmann, G., Nam, S., Schouten, S., Rühlemann, C., and Schneider, R. R. (2004). North Pacific and North Atlantic sea-surface temperature variability during the Holocene. *Quaternary Science Review* **23,** 2141-2154.

Kim, J.-H., Schneider, R. R., Muller, P. J., and Wefer, G. (2002). Interhemispheric comparison of deglacial sea-surface temperature patterns in Atlantic eastern boundary currents. *Earth and Planetary Science Letters* **194,** 383-393.

Kim, J.-H., Schouten, S., Hopmans, E. C., Donner, B., and Sinninghe Damsté, J. S. (2008). Global sediment core-top calibration of the TEX86 paleothermometer in the ocean. *Geochimica et Cosmochimica Acta* **72,** 1154-1173.

Kubota, Y., Kimoto, K., Tada, R., Oda, H., Yokoyama, Y., and Matsuzaki, H. (2010). Variations of East Asian summer monsoon since the last deglaciation based on

Mg/Ca and oxygen isotope of planktic foraminifera in the northern East China Sea. *Paleoceanography* **25,** doi:10.1029/2009PA001891.

Kurek, J., Cwynar, L., and Vermaire, J. C. (2009). A late Quaternary paleotemperature record from Hanging Lake, northern Yukon Territory, eastern Beringia. *Quaternary Research* **72,** 246-257.

Lamy, F., Rühlemann, C., Hebbein, D., and Wefer, G. (2002). High- and low-latitude climate control on the position of the southern Peru-Chile Current during the Holocene. *Paleoceanography* **17,** 10.1029/2001PA000727.

Larocque, I. (2001). How many chironomid head capsules are enough? A statistical approach to determine sample size for palaeoclimatic reconstructions. *Paleogeography, Palaeoclimatology, Palaeoecology* **172,** 133-142.

Larocque, I., and Hall, R. I. (2004). Holocene temperature estimates and chironomid community composition in the Abisko Valley, northern Sweden. *Quaternary Science Review* **23,** 2453-2465.

Lea, D. W., Pak, D. K., Peterson, L. C., and Hughen, K. A. (2003). Sychroneity of Tropical and High-Latitude Atlantic Temperatures over the Last Glacial Termination. *Science* **301,** 1361-1364.

Leduc, G., Schneider, R., Kim, J.-H., and Lohmann, G. (2010). Holocene and Eemian sea surface temperature trends as revealed by alkenone and Mg/Ca paleothermometry. *Quaternary Science Review* **29,** 989-1004.

Leduc, G., Vidal, L., Tachikawa, K., Rostek, F., Sonzogni, C., Beaufort, L., and Bard, E. (2007). Moisture transport across Central America as a positive feedback on abrupt climatic changes. *Nature* **445,** 908-911.

Levi, C., Labeyrie, L., Bassinot, F., Guichard, F., Cortijo, E., Waelbroeck, C., Caillon, N., Duprat, J., de Garidel-Thoron, T., and Elderfield, H. (2007). Low-latitude hydrological cycle and rapid climate changes during the last deglaciation. *Geochemistry, Geophysics, and Geosystems* **8,** Q05N12, doi:10.1029/2006GC001514.

Linsley, B. K., Rosenthal, Y., and Oppo, D. W. (2010). Holocene evolution of the Indonesian throughflow and the western Pacific warm pool. *Nature Geoscience* **3,** 578-583.

Marchal, O., Cacho, I., Stocker, T. F., Grimalt, J. O., Calvo, E., Martrat, B., Shackleton, N., Vautravers, M., Cortijo, E., Kreveld, S. v., Andersson, C., Koç, N., Chapmanh, M., Sbaffii, L., Duplessy, J.-C., Sarnthein, M., Turon, J.-L., Duprat, J., and Jansen, E. (2002). Apparentlong-termcoolingoftheseasurfaceinthenortheast Atlantic and Mediterranean during the Holocene. *Quaternary Science Review* **21,** 455-483.

McGlone, M. S., Turney, C. S. M., Wilmshurst, J. M., Renwick, J., and Pahnke, K. (2010). Divergent trends in land and ocean temperature in the Southern Ocean over the past 18,000 years. *Nature Geoscience* **3,** 622-626.

Mix, A. (2006). Running hot and cold in the eastern equatorial Pacific. *Quaternary Science Reviews* **25,** 1147-1149.

Mohtadi, M., Steinke, S., Lückge, A., Groeneveld, J., and Hathorne, E. C. (2010). Glacial to Holocene surface hydrography of the tropical eastern Indian Ocean. *Earth and Planetary Science Letters* **292,** 89-97.

Müller, P. J., Kirst, G., Ruthland, G., von Storch, I., and Rosell-Melé, A. (1998). Calibration of the alkenone paleotemperature index UK'37 based on core-tops from the eastern South Atlantic and the global ocean (60N-60S). *Geochimica et Cosmochimica Acta* **62,** 1757-1772.

Nielsen, S. H. H., Koç, N., and Crosta, X. (2010). Holocene climate in the Atlantic sector of the Southern Ocean: Controlled by insolation or oceanic circulation? *Geology* **32,** 317-320.

Pahnke, K., and Sachs, J. P. (2006). Sea surface temperatures of southern midlatitudes 0 – 160 kyr B. P. *Paleoceanography* **21,** PA2003, doi:10.1029/2005PA001191.

Palmer SL, W. I., Heinrichs ML, Hebda R, Scudder G. (2002). Postglacial midge community change and Holocene palaeotemperature reconstructions near treeline, southern British Columbia (Canada). *Journal of Paleolimnology* **28,** 469-490.

Pelejero, C., Grimalt, J., Heilig, S., Kienast, M., and Wang, L. (1999). High resolution UK37 temperature reconstructions in the South China Sea over the past 220 kyr. *Paleoceanography* **14,** 224-231.

Petit, J. R. (1999). Climate and Atmospheric history of the past 420,000 years from the Vostok ice core, Antarctic. *Nature* **399,** 429-436.

Reimer, P. J., Baillie, M. G. L., Bard, E., Bayliss, A., Beck, J. W., Blackwell, P. G., Bronk Ramsey, C., Buck, C. E., Burr, G. S., Edwards, R. L., Friedrich, M., Grootes, P. M., Guilderson, T. P., Hajdas, I., Heaton, T. J., Hogg, A. G., Hughen, K. A., Kaiser, K. F., Kromer, B., McCormac, F. G., Manning, S. W., Reimer, R. W., Richards, D. A., Southon, J. R., Talamo, S., Turney, C. S. M., van der Plicht, J., and Weyhenmeyer, C.E. (2009). INTCAL 09 and MARINE09 radiocarbon age calibration curves, 0-50,000 years Cal BP. *Radiocarbon* **51,** 1111-1150.

Rodrigues, T., Grimalt, J. O., Abrantes, F. G., Flores, J. A., and Lebreiro, S. M. (2009). Holocene interdependences of changes in sea surface temperature, productivity, and fluvial inputs in the Iberian continental shelf (Tagus mud patch). *Geochemistry, Geophysics, and Geosystems* **10,** Q07U06, doi:10.1029/2008GC002367.

Rosenberg SM, W. I., Mathewes RW, Hallett DJ. (2004). Midge-inferred Holocene climate history of two subalpine lakes in southern British Columbia. *Holocene* **14,** 258-271.

Rühlemann, C., Mulitza, S., Muller, P. J., Wefer, G., and Zahn, R. (1999). Warming of the tropical Atlantic Ocean and slowdown of thermohaline circulation during the last deglaciation. *Nature* **402,** 511-514.

Sachs, J. P. (2007). Cooling of Northwest Atlantic slope waters during the Holocene. *Geophysical Research Letters* **34,** L03609, doi:10.1029/2006GL028495.

Sarnthein, M., Gersonde, R., Niebler, S., Pflaumann, U., Spielhagen, R. F., Thiede, J., Wefer, G., and Weinelt, M. (2003). Overview of Glacial Atlantic Ocean Mapping (GLAMAP 2000). *Paleoceanography* **18,** 10.1029/2002PA000769.

Schefuß, E., Schouten, S., and Schneider, R. R. (2005). Climatic controls on central African hydrology during the past 20,000 years. *Nature* **437,** 1003-1006.

Seppä, H., and Birks, H. J. B. (2001). July mean temperature and annual precipitation trends during the Holocene in the Fennoscandian tree-line area: pollen-based climate reconstructions. *The Holocene* **11,** 527-539.

Seppä, H., Hammarlund, D., and Antonsson, K. (2005). Low-frequency and high-frequency changes in temperature and effective humidity during the Holocene in south-central Sweden: implications for atmospheric and oceanic forcings of climate. *Climate Dynamics* **25,** 285-297.

Seppä, H., and Weckström, J. (1999). Holocene vegetational and limnological changes in the Fennoscandian tree-line area as documented by pollen and diatom records from Lake Tsuolbmajavri, Finland. *Ecoscience* **6,** 621-635.

Steinke, S., Kienast, M., Groeneveld, J., Lin, L.-C., Chen, M.-T., and Rendle-Bühring, R. (2008). Proxy dependence of the temporal pattern of deglacial warming in the tropical South China Sea: toward resolving seasonality. *Quaternary Science Review* **27,** 688-700.

Stenni, B., Masson-Delmotte, V., Selmo, E., Oerter, H., Meyer, H., Röthlisberger, R., Jouzel, J., Cattani, O., Falourd, S., Fischer, H., Hoffmann, G., Iacumin, P., Johnsen,

S. J., Minster, B., and Udisti, R. (2010). The deuterium excess records of EPICA Dome C and Dronning Maud Land ice cores (East Antarctica). *Quaternary Science Review* **29,** 146-159.

Stott, L., Timmerman, A., and Thunell, R. (2007). Southern hemisphere and deep-sea warming led deglacial atmospheric CO2 rise and tropical warming. *Science* **318,** 435-438.

Sun, Y., Oppo, D. W., Xiang, R., Liu, W., and Gao, S. (2005). Last deglaciation in the Okinawa Trough: Subtropical northwest Pacific link to Northern Hemisphere and tropical climate. *Paleoceanography* **20,** PA4005, doi:10.1029/2004PA001061.

Thornalley, D. J. R., Elderfield, H., and McCave, I. N. (2009). Holocene oscillations in temperature and salinity of the surface subpolar North Atlantic. *Nature* **457**.

Tierney, J. E., Russell, J. M., Huang, Y., Damste, J. S. D., Hopmans, E. C., and Cohen, A. S. (2008). Northern Hemisphere Controls on Tropical Southeast African Climate During the Past 60,000 Years. *Science* **322,** 252-255.

Vinther, B. M., Buchardt, S. L., Clausen, H. B., Dahl-Jensen, D., Johnsen, S. J., Fisher, D. A., Koerner, R. M., Raynaud, D., Lipenkov, V., Andersen, K. K., Blunier, T., Rasmussen, S. O., Steffensen, J. P., and Svensson, A. M. (2009). Holocene thinning of the Greenland ice sheet. *Nature* **461,** 385-388.

von Langen, P. J., Pak, D. K., Spero, H. J., and Lea, D. W. (2005). Effects of temperature on Mg/Ca in neogloboquadrinid shells determined by live culturing. *Geochemistry, Geophysics, and Geosystems* **6,** Q10P03, doi:10.1029/2005GC000989.

Walker IR, L. A., Cwynar LC, Lotter AF. (1997). An expanded surface-water palaeotemperature inference model for use with fossil midges from eastern Canada. *Journal of Paleolimnology* **18,** 165-178.

Weijer, J. W. H., Schefuß, E., Schouten, S., and Damste, J. S. D. (2007). Coupled Thermal and Hydrological Evolution of Tropical Africa over the Last Deglaciation. *Science* **315,** 1701-1704.

Weldeab, S., Lea, D. W., Schneider, R. R., and Andersen, N. (2007). 155,000 Years of West African Monsoon and Ocean Thermal Evolution. *Science* **316,** 1303-1307.

Weldeab, S., Schneider, R. R., and Kölling, M. (2006). Deglacial sea surface temperature and salinity increase in the western tropical Atlantic in synchrony with high latitude climate instabilities. *Earth and Planetary Science Letters* **241,** 699-706.

Weldeab, S., Schneider, R. R., Kölling, M., and Wefer, G. (2005). Holocene African droughts relate to eastern equatorial Atlantic cooling. *Geology* **33,** 981-984.

Xu, J., Holbourn, A., Kuhnt, W., Jian, Z., and Kawamura, H. (2008). Changes in the thermocline structure of the Indonesian outflow during Terminations I and II. *Earth and Planetary Science Letters* **273,** 152-162.

Ziegler, M., Nürnberg, D., Karas, C., Tiedemann, R., and Lourens, L. J. (2008). Persistent summer expansion of the Atlantic Warm Pool during glacial abrupt cold events. *Nature Geoscience* **1,** 601-605.

Bibliography

Adkins, J. F., McIntyre, K., and Schrag, D. P. (2002). The salinity, temperature, and $\delta^{18}O$ of the glacial deep ocean. *Science* **298,** 1769-1773.

Aharon, P. (2003). Meltwater flooding events in the Gulf of Mexico revisited: implications for rapid climate change during the last deglaciation. *Paleoceanography* **18,** doi:10.1029/2002PA0000840.

Alley, R. B., Anandakrishnan, S., Dupont, T. K., Parizek, B. R., and Pollard, D. (2007a). Effect of sedimentation on ice-sheet grounding-line stability. *Science* **315,** 1838-1841.

Alley, R. B., Berntsen, T., Bindoff, N. L., Chen, Z., Chidthaisong, A., Friedlingstein, P., Gregory, J. M., Hegerl, G. C., Heimann, M., Hewitson, B., Hoskins, B. J., Joos, F., Jouzel, J., Kattsov, V., Lohmann, U., Manning, M., Matsuno, T., Molina, M., Nicholls, N., Overpeck, J., Qin, D., Raga, G., Ramaswamy, V., Ren, J., Rusticucci, M., Solomon, S., Somerville, R., Stocker, T. F., Stott, P. A., Stouffer, R. J., Whetton, P., Wood, R. A., and Wratt, D. (2007b). Summary for Policymakers. *In* "Climate Change 2007: The Physical Science Basis. Contribution of Working Group I to the Fourth Assessment Report of the Intergovernmental Panel on Climate Change." (S. Solomon, D. Qin, M. Manning, Z. Chen, M. Marquis, K. B. Averyt, M. Tignor, and H. L. Miller, Eds.). Cambridge University Press, Cambridge.

Alvarez-Solas, J., Charbit, S., Ritz, C., Paillard, D., Ramstein, G., and Dumas, C. (2010). Links between ocean temperature and iceberg discharge during Heinrich events. *Nature Geoscience* **3,** 122-126.

Ammann, C. M., and Wahl, E. R. (2007). The importance of the geophysical context in statistical evaluations of climate reconstruction procedures. *Climate Change* **85,** 71-88.

Armour, J., Fawcett, P. J., and Geissman, J. W. (2002). 15 k.y. paleoclimatic and glacial record from northern New Mexico. *Geology* **30,** 723-726.

Arz, H. W., Pätzold, J., and Müller, P. J. (2003). Influence of Northern Hemisphere climate and global sea level rise on the restricted Red Sea marine environment during termination I. *Paleoceanography* **18,** doi:10.1029/2002PA000864.

Asmerom, Y., Polyak, V. J., and Burns, S. J. (2010). Variable winter moisture in the southwestern United States linked to rapid glacial climate shifts. *Nature Geoscience* **3,** 114-117.

Balco, G., Briner, J., Finkel, R. C., Rayburn, J. A., Ridge, J. C., and Schaefer, J. M. (2009). Regional beryllium-10 production rate calibration for northeastern North America. *Quaternary Geochronology* **4,** 99-107.

Balco, G. A., Stone, J. O., Lifton, N. A., and Dunai, T. J. (2008). A complete and easily accessible means of calculating surface exposure ages or erosion rates from ^{10}Be and ^{26}Al measurements. *Quaternary Geochronology* **3,** 174-195.

Barley, E. M., Walker, I. R., Kurek, J., Cwynar, L. C., Mathewes, R. W., Gajewski, K., and Finney, B. P. (2006). A northwest North American training set: distribution of freshwater midges in relation to air temperature and lake depth. *Journal of Paleolimnology* **36,** 295-314.

Barron, J. A., Heusser, L., Herbert, T., and Lyle, M. (2003). High resolution climatic evolution of coastal northern California during the past 16,000 years. *Paleoceanography* **18,** 20-1 to 20-14.

Barrows, T. T., Lehman, S. J., Fifield, L. K., and De Deckker, P. (2007). Absence of Cooling in New Zealand and the Adjacent Ocean During the Younger Dryas Chronozone. *Science* **318,** 86-89.

Bassett, S. E., Milne, G. A., Mitrovica, J. X., and Clark, P. U. (2005). Ice sheet and solid earth influences on far-field sea-level histories. *Science* **309,** 925-928.

Beckmann, A., and Haidvogel, D. B. (1993). Numerical simulation of flow around a tall isolated seamount. Part I: Problem formulation and model accuracy. *Journal of Physical Oceanography* **23,** 1736-1753.

Bendle, J. A. P., and Rosell-Mele, A. (2007). High-resolution alkenone sea surface temperature variability on the North Icelandic Shelf: implications for Nordic Seas palaeoclimatic development during the Holocene. *The Holocene* **17,** 9-24.

Benedict, J. B. (1973). Chronology of cirque glaciation, Colorado Front Range. *Quaternary Research* **3,** 584-599.

Benson, L., Madole, R. F., Kubik, P., and McDonald, R. (2007). Surface-exposure ages of Front Range moraines that may have formed during the Younger Dryas, 8.2 cal ka, and Little Ice Age events. *Quaternary Science Review* **26,** 1638-1649.

Benway, H. M., Mix, A. C., Haley, B. A., and Klinkhammer, G. P. (2006a). Eastern Pacific Warm Pool paleosalinity and climate variability: 0 – 30 kyr. *Paleoceanography* **21,** PA3008, doi:10.1029/2005PA001208.

Benway, H. M., Mix, A. C., Haley, B. A., and Klinkhammer, G. P. (2006b). Eastern Pacific Warm Pool paleosalinity and climate variability: 0-30 kyr. *Paleoceanography* **21**.

Bigler, C., and Hall, R. I. (2002). Diatoms as indicators of climatic and limnological change in Swedish Lapland: a 100-lake calibration-set and its validation for paleoecological reconstructions. *Journal of Paleolimnology* **27,** 97-115.

Bilderback, E. L. (2004). "Timing and Paleoclimatic Significance of Latest Pleistocene and Holocene Cirque Glaciation in the Enchantment Lakes Basin, North Cascades, WA." Unpublished Masters thesis, Western Washington University.

Birkeland, P. W. (1964). Pleistocene glaciation of the northern Sierra Nevada, north of Lake Tahoe, California. *Journal of Geology* **72**.

Birman, J. H. (1964). Glacial Geology across the Crest of the Sierra Nevada, California. *In* "California. Geol. Soc. Amer. Special Paper n. 75." pp. 80.

Blunier, T., and Brook, E. J. (2001). Timing of millennial-scale climate change in Antarctica and Greenland during the last glacial period. *Science* **291,** 109-112.

Bond, G. (1997). A pervasive millennial-scale cycle in North Atlantic Holocene and Glacial climates. *Science* **278,** 1257-1266.

Bond, G., Broecker, W., Johnsen, S., McManus, J., Labeyrie, L., Jouzel, J., and Bonani, G. (1993). Correlations between climate records from North Atlantic sediments and Greenland ice. *Nature* **365,** 143-147.

Bond, G. C., and Lotti, R. (1995). Iceberg discharges into the North Atlantic on millennial time scales during the last glaciation. *Science* **267,** 1005-1010.

Bradley, R. S., Hughes, M. K., and Diaz, H. F. (2003). Climate in Medieval Time. *Science* **302,** 404-405.

Brohan, P., Kennedy, J. J., Haris, I., Tett, S. F. B., and Jones, P. D. (2006). Uncertainty estimates in regional and global observed temperature changes: A new dataset from 1850. *Journal of Geophysical Research* **111,** D12106, doi:10.1029/2005JD006548

Brook, E. J., Kurz, M. D., Ackert, J. R. P., Denton, G. H., Brown, E. T., Raisbeck, G. M., and Yiou, F. (1993). Chronology of Taylor Glacier advances in Arena Valley, Antarctica, using *in situ* cosmogenic ^{3}He and ^{10}Be. *Quaternary Research* **39,** 11-23.

Burke, R. M., and Birkeland, P. W. (1983). Holocene Glaciation in the Mountain Ranges of the Western United States. *In* "Late Quaternary Environments of the United States." (H. E. Wright, Ed.), pp. 3-11. University of Minnesota Press, Minneapolis.

Cacho, I., Grimalt, J. O., Canals, M., Sbaffi, L., Shackelton, N. J., Schonfeld, J., and Zahn, R. (2001). Variability of the western Mediterranean Sea surface temperature during the last 25,000 years and its connection with the Northern Hemisphere climatic changes. *Paleoceanography* **16,** 40-52.

Calvo, E., Grimalt, J., and Jansen, E. (2002). High resolution UK37 sea surface temperature reconstruction in the Norwegian Sea during the Holocene. *Quaternary Science Review* **21,** 1385-1394.

Came, R. E., Oppo, D. W., and McManus, J. F. (2007). Amplitude and timing of temperature and salinity variability in the subpolar North Atlantic over the past 10 k.y. *Geology* **35,** 315-318.

Carlson, A. E. (2009). Geochemical constraints on the Laurentide Ice Sheet contribution to Meltwater Pulse 1A. *Quaternary Science Review* **28,** 1625-1630.

Castañeda, I. S., Schefuß, E., Pätzold, J., Damste, J. S. D., Weldeab, S., and Schouten, S. (2010). Millennial-scale sea surface temperature changes in the eastern Mediterranean (Nile River Delta region) over the last 27,000 years. *Paleoceanography* **25,** PA1208, doi:10.1029/2009PA001740.

Clague, J., Marcott, S. A., Menounos, B., Osborn, G., Novak, A. M., and Clark, P. U. (in preparation).

Clark, D. H., and Gillespie, A. R. (1997). Timing and significance of late-glacial and Holocene cirque glaciation in the Sierra Nevada, California. *Quaternary International* **38/39,** 21-38.

Clark, P. U., Dyke, A. S., Shakun, J. D., Carlson, A. E., Clark, J., Wohlfarth, B., Hostetler, S. W., Mitrovica, J. X., and McCabe, A. M. (2009). The Last Glacial Maximum. *Science* **325,** 710-714.

Clark, P. U., Hostetler, S. W., Pisias, N. G., Schmittner, A., and Meissner, K. J. (2007). Mechanisms for an ~7-kyrs climate and sea-level oscillation during Marine Isotope Stage 3. *In* "Ocean Circulation: Mechanisms and Impacts " (A. Schmittner, J. C. H. Chiang, and S. R. Hemming, Eds.), pp. 392. American Geophysical Union, Washington, DC.

Clark, P. U., McCabe, A. M., Mix, A. C., and Weaver, A. J. (2004). Rapid rise of sea level 19,000 years ago and its global implications. *Science* **304,** 1141-1144.

Clegg, B. F., Clarke, G. H., Chipman, M. L., Chou, M., I.R., W., Tinner, W., and Hu, F. S. (2010). Six millennia of summer temperature variation based on midge analysis

of lake sediments from Alaska. *Quaternary Science Review***,** doi:10.1016/j.quascirev.2010.08.001.

Crandell, D. R. (1969). Surficial geology of Mount Rainier National Park, Washington. *U.S. Geological Survey Bulletin 1288*.

Crowley, T. J. (1992). North Atlantic deep water cools the southern hemisphere. *Paleoceanography* **7,** 489-497.

Currey, D. R. (1974). Probable pre-Neoglacial age of the type Temple Lake moraine, Wyoming. *Arctic and Alpine Research* **6,** 293-300.

Curry, R. R. (1969). Holocene climatic and glacial history of the central Sierra Nevada, California. *In* "United States Contributions to Quaternary Research, Geological Society of America Special Paper 123." (S. A. Schumm, and W. C. Bradley, Eds.), pp. 1-47.

Dahms, D. E. (2002). Glacial stratigraphy of Stough Creek Basin, Wind River Range, Wyoming. *Geomorphology* **42,** 59-83.

Davis, P. T. (1988). Holocene Glacier Fluctuations in the American Cordillera. *Quaternary Science Reviews* **7,** 129-157.

deMenocal, P., Ortiz, J., Guilderson, T., and Sarnthein, M. (2000). Coherent High- and Low-Latitude climate variability during the Holocene warm period. *Science* **288,** 2198-2202.

Desilets, D., and Zreda, M. G. (2003). Spatial and temporal distribution of secondary cosmic-ray nucleon intensity and applications to in situ cosmogenic dating. *Earth and Planetary Science Letters* **206,** 21-42.

Desilets, D., Zreda, M. G., and Prabu, T. (2006). The energy dependence of cosmogenic nuclide scaling models: New measurments at low latitudes. *Earth and Planetary Science Letters* **246,** 265-276.

Dinniman, M. S., Klinck, J. M., and Smith, W. W., Jr. (2007). The influence of sea ice cover and icebergs on circulation and water mass formation in a numerical circulation model of the Ross Sea, Antarctica. *Journal of Geophysical Research* **112,** C11013. doi:10.1029/2006JC004036.

Dokken, T., and Jansen, E. (1999). Rapid changes in the mechanism of ocean convection during the last glacial period. *Nature* **401,** 458-461.

Dolven, J. K., Cortese, G., and Bjøklund, K. R. (2002). A high-resolution radiolarian-derived paleotemperature record for the Late Pleistocene-Holocene in the Norwegian Sea. *Paleoceanography* **17,** doi:10.1029/2002PA000780.

Dunai, T. J. (2000). Scaling factors for production rates of in situ produced cosmogenic nuclides: a critical reevaluation. *Earth and Planetary Science Letters* **176,** 157-169.

Dunai, T. J. (2001). Influence of secular variation of the geomagnetic field on the production rates of in situ produced cosmogenic nuclides. *Earth and Planetary Science Letters* **193,** 197-212.

Egbert, G. D., and Erofeeva, S. Y. (2004). Efficient inverse modeling of barotropic ocean tides. *Journal of Oceanic and Atmospheric Technology* **19,** 183-204.

Elderfield, H., Yu, J., Anand, P., Kiefer, K., and Nyland, B. (2006). Calibrations for benthic foraminiferal Mg/Ca paleothermometry and the carbonate ion hypothesis. *Earth and Planetary Science Letters* **250,** 633-649.

Emeis, K. C., Struck, U., Blanz, T., Kohly, A., and Woß, M. (2003). Salinity changes in the central Baltic Sea (NW Europe) over the last 10 000 years. *The Holocene* **13,** 411-421.

Esper, J., Cook, E. R., and Schweingruber, F. H. (2002). Low-Frequency Signals in Long Tree-Ring Chronologies for Reconstructing Past Temperature Variability. *Science* **295,** 2250-2253.

Farmer, E. C., deMendocal, P. B., and Marchitto, T. M. (2005). Holocene and deglacial ocean temperature variability in the Benguela upwelling region: Implications for low-latitude atmospheric circulation. *Paleoceanography* **20,** doi:10.1029/2004PA001049.

Giunta, S., Emeis, K. C., and Negri, A. (2001). Sea-surface temperature reconstruction of the last 16,000 years in the Eastern Mediterranean Sea. *Rivista Italiana di Paleontologia e Stratigrafia* **107,** 463-476.

Goehring, B. M. (2006). "^{10}Be Exposure Ages of Erratic Boulders in Southern Norway and Implications for the History of the Fennoscandian Ice Sheet." Unpublished Masters thesis, Oregon State University.

Gosse, J. C., Evenson, E. B., Klein, J., Lawn, B., and Middleton, R. (1995). Precise cosmogenic ^{10}Be measurements in western North America: Support for a global Younger Dryas cooling event. *Geology* **23,** 877-880.

Gosse, J. C., and Phillips, F. M. (2001). Terrestrial in situ cosmogenic nuclides: theory and application. *Quaternary Science Reviews* **20,** 1475-1560.

Gutjahr, M., Hoogakker, B. A. A., Frank, M., and McCave, I. N. (2010). Changes in North Atlantic Deep Water strength and bottom water masses during Marine Isotope Stage 3 (45-35 ka BP). *Quaternary Science Review* **29,** 2451-2461.

Haley, B. A., and Klinkhammer, G. P. (2002). Development of a flow-though system for cleaning and dissolving foraminiferal tests. *Chemical Geology* **185,** 51-69.

Hall, R. D., and Heiny, J. S. (1983). Glacial and postglacial physical stratigraphy and chronology, North Willow Creek and Catarct Creek drainage basin, eastern Tobacco Root Range, southwestern Montana, U.S.A. *Arctic and Alpine Research* **15,** 19-52.

Heinrich, H. (1988). Origin and consequences of cyclic ice rafting in the Northeast Atlantic ocean during the past 130,000 years. *Quaternary Research* **29,** 142-152.

Hendy, I., and Kennett, J. (2000). Dansgaard/Oeschger cycles and the California Current System; Planktonic foraminiferal response. *Paleoceanography* **15,** 30-42.

Hodell, D. A., and Curtis, J. H. (2008). Oxygen and carbon isotopes of detrital carbonate in North Atlantic Heinrich Events. *Marine Geology* **256,** 30-35.

Holland, D. M., and Jenkins, A. (1999). Modelling thermodynamic ice-ocean interactions at the base of an ice shelf. *Journal of Physical Oceanography* **29,** 1787-1800.

Huang, S. (2004). Merging information from different resources for new insights into climate change in the past and future. *Geophysical Research Letters* **31,** L13205, doi:10.1029/2004GL019781.

Hughen, K. A., Baillie, M. G. L., Bard, E., Beck, J. W., Bertrand, C. J. H., Blackwell, P. G., Buck, C. E., Burr, G. S., Cutler, K. B., Damon, P. E., Edwards, R. L.,

Fairbanks, R. G., Friedrich, M., Guilderson, T. P., Kromer, B., McCormac, G., Manning, S., Ramsey, C. B., Reimer, P. J., Reimer, R. W., Remmele, S., Southon, J. R., Stuiver, M., Talamo, S., Taylor, F. W., van der Plicht, J., and Weyhenmeyer, C. E. (2004). Marine04 marine radiocarbon age calibration, 0-26 cal kyr BP. *Radiocarbon* **46,** 1059-1086.

Huguet, C., Kim, J.-H., Damsté, J. S. S., and Schouten, S. (2006). Reconstruction of sea surface temperature variations in the Arabian
Sea over the last 23 kyr using organic proxies (TEX86 and UK37). *Paleoceanography* **21,** doi:10.1029/2005PA001215.

Hulbe, C. L. (1997). An ice shelf mechanism for Heinrich layer production. *Paleoceanography* **12,** 711-717.

Huybers, P., and Wunch, C. (2004). A depth-derived Pleistocene age model: Uncertainty estimates, sedimentation variability, and nonlinear climate change. *Paleoceanography* **19,** PA1028, doi:10.1029/2002PA000857.

Isono, G., Yamamoto, M., Irino, T., Oba, T., Murayama, M., Nakamura, T., and Kawahata, H. (2010). The 1500-year climate oscillation in the midlatitude North Pacific during the Holocene. *Geology* **37,** 591-594.

Jaeschke, A., Rühlemann, C., Arz, H., Heil, G., and Lohmann, G. (2007). Coupling of millennial-scale changes in sea surface temperature and precipitation off northeastern Brazil with high-latitude climate shifts during the last glacial period. *Paleoceanography* **22,** doi:10.1029/2006PA001391.

Jakobsson, M., Macnab, R., Mayer, L., Anderson, R., Edwards, M., Hatzky, J., Schenke, H. W., and Johnson, P. (2008). An improved bathymetric portrayal of the

Arctic Ocean: Implications for ocean modeling and geological, geophysical and oceanographic analyses. *Geophysical Research Letters* **35**.

Jansen, E., Overpeck, J., Briffa, K. R., Duplessy, J.-C., Joos, F., Masson-Delmotte, V., Olago, D., Otto-Bliesner, B. L., Peltier, W. R., Rahmstorf, S., Ramesh, R., Raynaud, D., Rind, D., Solomina, O., Villalba, R., and Zhang, D. (2007). Paleoclimate. *In* "Climate Change 2007: The Physical Science Basis. Contribution of Working Group I to the Fourth Assessment Report of the Intergovernmental Panel on Climate Change." (S. Solomon, D. Qin, M. Manning, Z. Chen, M. Marquis, K. B. Averyt, M. Tignor, and H. L. Miller, Eds.). Cambridge University Press, Cambridge.

Joughin, I., Smith, B. E., and Holland, D. M. (2010). Sensitivity of 21st century sea level to ocean-induced thinning of Pine Island Glacier, Antarctica. *Geophysical Research Letters* **37**.

Jouzel, J., Masson-Delmotte, V., Cattani, O., Dreyfus, G., Falourd, S., Hoffmann, G., Minster, B., Nouet, J., Barnola, J. M., Chappellaz, J., Fischer, H., Gallet, J. C., Johnsen, S., Leuenberger, M., Loulergue, L., Luethi, D., Oerter, H., Parrenin, F., Raisbeck, G., Raynaud, D., Schilt, A., Schwander, J., Selmo, E., Souchez, R., Spahni, R., Stauffer, B., J. P. Steffensen, Stenni, B., Stocker, T. F., Tison, J. L., Werner, M., and Wolff, E. W. (2007a). Orbital and Millennial Antarctic Climate Variability over the Past 800,000 Years. *Science* **317,** 793-796.

Jouzel, J., Masson-Delmotte, V., Cattani, O., Dreyfus, G., Falourd, S., Hoffmann, G., Minster, B., Nouet, J., Barnola, J. M., Chappellaz, J., Fischer, H., Gallet, J. C., Johnsen, S., Leuenberger, M., Loulergue, L., Luethi, D., Oerter, H., Parrenin, F., Raisbeck, G., Raynaud, D., Schilt, A., Schwander, J., Selmo, E., Souchez, R., Spahni, R., Stauffer, B., Steffensen, J. P., Stenni, B., Stocker, T. F., Tison, J. L., Werner, M.,

and Wolff, E. W. (2007b). Orbital and millennial Antarctic climate variability over the past 800,000 years. *Science* **317,** 793-796.

Kaiser, J., Schefuß, E., Lamy, F., Mohtadi, M., and Hebbeln, D. (2008). Glacial to Holocene changes in sea surface temperature and coastal vegetation in north central Chile: high versus low latitude forcing. *Quaternary Science Review* **27,** 2064-2075.

Kalnay, E., Kanamitsu, M., Kistler, R., Collins, W., Deaven, D., Gandin, L., Iredell, M., Saha, S., White, G., Woollen, J., Zhu, Y., Leetmaa, A., and Reynolds, R. (1996). The NCEP/NCAR 40-year Reanalysis Project. *Bulletin of the American Meteorological Society* **77,** 437-470.

Kawamura, K., Parrenin, F., Lisiecki, L., Uemura, R., Vimeux, F., Severinghaus, J. P., Hutterli, M. A., Nakazawa, T., Aoki, S., Jouzel, J., Raymo, M. E., Matsumoto, K., Nakata, H., Motoyama, H., Fujita, S., Goto-Azuma, K., Fujii, Y., and Watanabe, O. (2007). Northern Hemisphere forcing of climatic cycles in Antarctica over the past 360,000 years. *Nature* **448,** 912-916.

Kienast, M., Steinke, S., Stattegger, K., and Calvert, S. E. (2001). Synchronous Tropical South China Sea SST Change and Greenland Warming During Deglaciation. *Science* **291,** 2132-2134.

Kim, J.-H., Rimbu, N., Lorenz, S. J., Lohmann, G., Nam, S., Schouten, S., Rühlemann, C., and Schneider, R. R. (2004). North Pacific and North Atlantic sea-surface temperature variability during the Holocene. *Quaternary Science Review* **23,** 2141-2154.

Kim, J.-H., Schneider, R. R., Muller, P. J., and Wefer, G. (2002). Interhemispheric comparison of deglacial sea-surface temperature patterns in Atlantic eastern boundary currents. *Earth and Planetary Science Letters* **194,** 383-393.

Kim, J.-H., Schouten, S., Hopmans, E. C., Donner, B., and Sinninghe Damsté, J. S. (2008). Global sediment core-top calibration of the TEX86 paleothermometer in the ocean. *Geochimica et Cosmochimica Acta* **72,** 1154-1173.

Klinkhammer, G. P., Haley, B. A., Mix, A. C., Benway, H. M., and Cheseby, M. (2004). Evaluation of automatd flow-through time-resolved analysis of foraminifera for Mg/Ca paleothermometry. *Paleoceanography* **19,** PA4030, doi:10.1029/2004PA001050.

Kristjánsdóttir, G. B., Lea, D. W., Jennings, A. E., Pak, D. K., and Belanger, C. L. (2007). New spatial Mg/Ca-temperature calibrations for three Arctic, benthic foraminifera and reconstruction of north Iceland shelf temperature for the past 4000 years. *Geochemistry, Geophysics, and Geosystems* **8,** Q03P21, doi:10.1029/2006GC001425.

Kubota, Y., Kimoto, K., Tada, R., Oda, H., Yokoyama, Y., and Matsuzaki, H. (2010). Variations of East Asian summer monsoon since the last deglaciation based on Mg/Ca and oxygen isotope of planktic foraminifera in the northern East China Sea. *Paleoceanography* **25,** doi:10.1029/2009PA001891.

Kurek, J., Cwynar, L., and Vermaire, J. C. (2009). A late Quaternary paleotemperature record from Hanging Lake, northern Yukon Territory, eastern Beringia. *Quaternary Research* **72,** 246-257.

Lal, D. (1991). Cosmic ray labeling of erosion surfaces: In-situ nuclide production rates and erosion models. *Earth and Planetary Science Letters* **104,** 424-439.

Lamy, F., Rühlemann, C., Hebbein, D., and Wefer, G. (2002). High- and low-latitude climate control on the position of the southern Peru-Chile Current during the Holocene. *Paleoceanography* **17,** 10.1029/2001PA000727.

Larocque, I. (2001). How many chironomid head capsules are enough? A statistical approach to determine sample size for palaeoclimatic reconstructions. *Paleogeography, Palaeoclimatology, Palaeoecology* **172,** 133-142.

Larocque, I., and Hall, R. I. (2004). Holocene temperature estimates and chironomid community composition in the Abisko Valley, northern Sweden. *Quaternary Science Review* **23,** 2453-2465.

Laskar, J., Robutel, P., Joutel, F., Gastineau, M., Correia, A. C. M., and Levrard, B. (2004). A long term numerical solution for the insolation quantities of the Earth. *Astronomy and Astrophysics* **428,** 261-285.

Lea, D. W., Pak, D. K., Peterson, L. C., and Hughen, K. A. (2003). Sychroneity of Tropical and High-Latitude Atlantic Temperatures over the Last Glacial Termination. *Science* **301,** 1361-1364.

Lear, C. H., Rosenthal, Y., and Slowey, N. (2002). Benthic foraminifera Mg/Ca-paleothermometry: A revised core-top calibration. *Geochimica et Cosmochimica Acta.* **66,** 3375-3387.

Leduc, G., Schneider, R., Kim, J.-H., and Lohmann, G. (2010). Holocene and Eemian sea surface temperature trends as revealed by alkenone and Mg/Ca paleothermometry. *Quaternary Science Review* **29,** 989-1004.

Leduc, G., Vidal, L., Tachikawa, K., Rostek, F., Sonzogni, C., Beaufort, L., and Bard, E. (2007). Moisture transport across Central America as a positive feedback on abrupt climatic changes. *Nature* **445,** 908-911.

Lemieux-Dudon, B., Blayo, E., Petit, J.-R., Waelbroeck, C., Svensson, A., Ritz, C., Barnola, J.-M., Narcisi, B. M., and Parrenin, F. (2009). Consistent dating of Antarctica and Greenland ice cores. *Quaternary Science Review* **29,** 8-20.

Lemieux-Dudon, B., Blayo, E., Petit, J. R., Waelbroeck, C., Svensson, A., Ritz, C., Barnola, J. M., Narcisi, B. M., and Parrenin, F. (2010). Consistent dating for Antarctic and Greenland ice cores. *Quaternary Science Reviews* **29,** 8-20.

Levi, C., Labeyrie, L., Bassinot, F., Guichard, F., Cortijo, E., Waelbroeck, C., Caillon, N., Duprat, J., de Garidel-Thoron, T., and Elderfield, H. (2007). Low-latitude hydrological cycle and rapid climate changes during the last deglaciation. *Geochemistry, Geophysics, and Geosystems* **8,** Q05N12, doi:10.1029/2006GC001514.

Lewis, E., and Wallace, D. W. R. (1998). *CO2 system calculations, ORNL/CDIAC-105 (CO2SYS v.1.05)*.

Licciardi, J. F. (2000). "Alpine Glacier and Pluvial Lake Records of Late Pleistocene Climate Variability in the Western United States." Unpublished Ph.D. thesis, Oregon State University.

Licciardi, J. M. (2001). Chronology of latest Pleistocene lake-level fluctuations in the pluvial Lake Chewaucan basin, Oregon, USA. *Journal of Quaternary Science* **16,** 545-553.

Licciardi, J. M., Clark, P. U., Brook, E. J., Elmore, D., and Sharma, P. (2004). Variable responses of western U.S. glaciers during the last deglaciation. *Geology* **32,** 81-84.

Licciardi, J. M., and Pierce, K. L. (2008). Cosmogenic exposure-age chronologies of Pinedale and Bull Lake glaciations in greater Yellowstone and the Teton Range, U.S.A. *Quaternary Science Review* **27,** 814-831.

Licciardi, J. M., Schaefer, J. M., Taggart, J. R., and Lund, D. C. (2009). Holocene glacier fluctuations in the Peruvian Andes indicate northern climate linkage. *Science* **325,** 1677-1679.

Lifton, N. A., Bieber, J. W., Clem, J. M., Duldig, M. L., Evenson, P., Humble, J. E., and Pyle, R. (2005). Addressing solar modulation and long-term uncertanties in scaling secondary cosmic rays for in situ comogenic nuclide applications. *Earth and Planetary Science Letters* **239,** 140-161.

Lifton, N. A., Caffee, M. W., Finkel, R., Schaefer, J. M., Stone, J., Goehring, B. M., Phillips, F., Oviatt, C. G., and Rood, D. H. (2009). A new estimate of the spallogenic production rate of in situ cosmogenic 10Be from Lake Bonneville shoreline features, Promontory Point, Utah. *In* "Geological Society of America Annual Meeting." pp. 229. Geological Society of America Abstracts with Programs, Portland.

Linsley, B. K., Rosenthal, Y., and Oppo, D. W. (2010). Holocene evolution of the Indonesian throughflow and the western Pacific warm pool. *Nature Geoscience* **3,** 578-583.

Liu, Z., Otto-Bliesner, B. L., He, F., Brady, E. C., Tomas, R., Clark, P. U., Carlson, A. E., Lynch-Stieglitz, J., Curry, W., Brook, E. J., Erickson, D., Jacob, R., Kutzbach, J. E., and Cheng, J. (2009). Transient simulation of last deglaciation with a new mechanism for Bølling-Allerød warming. *Science* **325,** 310-314.

MacAyeal, D. R. (1993). Binge/purge oscillations of the Laurentide ice sheet as a cause of the North Atlantic's Heinrich events. *Paleoceanography* **8, No. 6,** 775-784.

MacDonald, G. M., Moser, K., Bloom, A. M., Porinchu, D. F., Potito, A. P., Wolfe, B. B., Edwards, T. W. D., Petel, A., Orme, A. R., and Orme, A. J. (2008). Evidence of temperature depression and hydrological variations in the eastern Sierra Nevada during the Younger Dryas stade. *Quaternary Research* **70,** 131-140.

Mangini, A., Godoy, J. M., Kowsmann, R., Santos, G. M., Ruckelshausen, M., Schroeder-Ritzrau, A., and Wacker, L. (2010). Deep sea corals off Brazil verify a poorly ventilated Southern Pacific Ocean during H2, H1 and the Younger Dryas. *Earth and Planetary Science Letters* **293,** 269-276.

Mann, M. E., Rutherford, S., Wahl, E., and Ammann, C. (2007). Robustness of proxy-based climate field reconstruction methods. *Journal of Geophysical Research* **112,** D12109, doi: 10.1029/2006JD008272.

Mann, M. E., Zhang, Z., Hughes, M. K., Bradley, R. S., Miller, S. K., Rutherford, S., and Ni, F. (2008). Proxy-based reconstructions of hemispheric and global surface temperature variations over the past two millennia. *Proceedings of the National Academy of Sciences* **105,** 13252-13257.

Manning, M. R., Petit, M., Easterling, D., Murphy, J., Patwardhan, A., Rogner, H.-H., Swart, R., and Yohe, G. (2004). *In* "IPCC Workshop on Describing Scientific Uncertainties in Climate Change to Support Analysis of Risk and of Options: Workshop report." Intergovernmental Panel on Climate Change, Geneva.

Marchal, O., Cacho, I., Stocker, T. F., Grimalt, J. O., Calvo, E., Martrat, B., Shackleton, N., Vautravers, M., Cortijo, E., Kreveld, S. v., Andersson, C., Koç, N., Chapmanh, M., Sbaffii, L., Duplessy, J.-C., Sarnthein, M., Turon, J.-L., Duprat, J., and Jansen, E. (2002). Apparentlong-termcoolingoftheseasurfaceinthenortheast

Atlantic and Mediterranean during the Holocene. *Quaternary Science Review* **21,** 455-483.

Marcott, S. A., Shakun, J. D., Clark, P. U., and Mix, A. C. (in review). Holocene Temperature Variations.

Matthes, F. E. (1929). Multiple glaciations in the Sierra Nevada. *Science* **70,** 75-76.

Matthes, F. E. (1942). Report of Committee on Glaciers, 1941-1942. *Amer. Geophys. Union Trans.* **23,** 374-392.

McGlone, M. S., Turney, C. S. M., Wilmshurst, J. M., Renwick, J., and Pahnke, K. (2010). Divergent trends in land and ocean temperature in the Southern Ocean over the past 18,000 years. *Nature Geoscience* **3,** 622-626.

McManus, J. F., Francois, R., Gherardi, J.-M., Keigwin, L. D., and Brown-Leger, S. (2004). Collapse and rapid resumption of Atlantic meridional criculation linked to deglacial climate changes. *Nature* **428,** 834-837.

Meehl, G. A., Stocker, T. F., Collins, W. D., Friedlingstein, P., Gaye, A. T., Gregory, J. M., Kitoch, A., Knutti, R., Murphy, J. M., Noda, A., Raper, S. C. B., Watterson, I. G., Weaver, A. J., and Zhao, Z.-C. (2007). Global Climate Projections. *In* "Climate Change 2007: The Physical Science Basis. Contribution of Working Group I to the Fourth Assessment Report of the Intergovernmental Panel on Climate Change." (S. Solomon, D. Qin, M. Manning, Z. Chen, M. Marquis, K. B. Averyt, M. Tignor, and H. L. Miller, Eds.). Cambridge University Press, Cambridge.

Meese, D. A. (1997). The Greenland Ice Sheet Project 2 depth-age scale: Methods and results. *J. Geophys. Res.* **102,** 26411-26423.

Meland, M. Y., Dokken, T. M., Jansen, E., and Hevrøy, K. (2008). Water mass properties and exchange between the Nordic seas and the northern North Atlantic during the period 23-6 ka: Benthic oxygen isotopic evidence. *Paleoceanography* **23,** PA1210, doi:10.1029/2007PA001416.

Mellor, G. L., and Yamada, T. (1982). Development of a turbulence closure model for geophysical fluid problems. *Reviews of Geophysics and Space Physics* **20,** 851-875.

Miller, C. D., and Birkeland, P. W. (1974). Probable pre-Neoglacial age of the type Temple Lake moraine, Wyoming: Discussion and additional relative-age data. *Arctic and Alpine Research* **6,** 301-306.

Mix, A. (2006). Running hot and cold in the eastern equatorial Pacific. *Quaternary Science Reviews* **25,** 1147-1149.

Moberg, A., Sonechkin, D. M., Holmgren, K., Datsenko, N. M., Karlén, W., and Laureitzen, S. E. (2005). Highly variable Northern Hemisphere temperatures reconstructed from low- and high-resolution proxy data. *Nature* **433,** 613-617.

Mohtadi, M., Steinke, S., Lückge, A., Groeneveld, J., and Hathorne, E. C. (2010). Glacial to Holocene surface hydrography of the tropical eastern Indian Ocean. *Earth and Planetary Science Letters* **292,** 89-97.

Monnin, E., Indermuhle, A., Dallenbach, A., Fluckiger, J., Stauffer, B., and Stocker, T. F. (2001). Atmospheric CO2 concentrations over the last glacial termination. *Science* **291,** 112-114.

Moss, J. H. (1951). Late glacial advances in the southern Wind River Mountains, Wyoming. *American Journal of Science* **249,** 865-883.

Moss, R., and Schneider, S. (2000). Uncertainties, in Guidance Papers on the Cross Cutting Issues of the Third Assessment Reprot of the IPCC. *In* "Intergovernmental Panel on Climate Change (IPCC)." (R. Pachauri, T. Taniguchi, and K. Tanaka, Eds.), Geneva.

Müller, P. J., Kirst, G., Ruthland, G., von Storch, I., and Rosell-Melé, A. (1998). Calibration of the alkenone paleotemperature index UK'37 based on core-tops from the eastern South Atlantic and the global ocean (60N-60S). *Geochimica et Cosmochimica Acta* **62,** 1757-1772.

Munroe, J. S. (2002). Timing of postglacial cirque reoccupation in the northern Uinta Mountains, northeastern Utah, USA. *Arctic Antarctic and Alpine Research* **34,** 38-48.

NGRIPmembers. (2004). High-resolution record of Northern Hemisphere climate extending into the last interglacial period. *Nature* **431,** 147-151.

Nielsen, S. H. H., Koç, N., and Crosta, X. (2010). Holocene climate in the Atlantic sector of the Southern Ocean: Controlled by insolation or oceanic circulation? *Geology* **32,** 317-320.

O'Neil, J. R., Clayton, R. N., and Mayeda, T. K. (1969). Oxygen isotope fractionation in divalent metal carbonates. *Journal of Chemical Physics* **51,** 5547-5558.

Osborn, G., and Bevis, K. (2001). Glaciation in the Great Basin of the Western United States. *Quaternary Science Reviews* **20,** 1377-1410.

Oviatt, C. G. (1977). Glacial Geology of the Lake Marie Area, Medicine Bow Mountains, Wyoming. *Contributions to Geology, University of Wyoming* **16,** 27-38.

Owen, L. A., Finkel, R. C., Minnich, R. A., and Perez, A. E. (2003). Extreme southwestern margin of late Quaternary glaciation in North America: Timing and controls. *Geology* **31,** 729-732.

Padman, L., Howard, S. L., Orsi, A., and Muench, R. D. (2009). Tides of the northwestern Ross Sea and their impact on dense outflows of Antarctic Bottom Water. *Deep Sea Research, Part II* **56,** 818-834.

Pahnke, K., and Sachs, J. P. (2006). Sea surface temperatures of southern midlatitudes 0 – 160 kyr B. P. *Paleoceanography* **21,** PA2003, doi:10.1029/2005PA001191.

Palmer SL, W. I., Heinrichs ML, Hebda R, Scudder G. (2002). Postglacial midge community change and Holocene palaeotemperature reconstructions near treeline, southern British Columbia (Canada). *Journal of Paleolimnology* **28,** 469-490.

Pelejero, C., Grimalt, J., Heilig, S., Kienast, M., and Wang, L. (1999). High resolution UK37 temperature reconstructions in the South China Sea over the past 220 kyr. *Paleoceanography* **14,** 224-231.

Petit, J. R. (1999). Climate and Atmospheric history of the past 420,000 years from the Vostok ice core, Antarctic. *Nature* **399,** 429-436.

Phillips, F. M., Zreda, M., Plummer, M. A., Elmore, D., and Clark, D. H. (2009). Glacial geology and chronology of Bishop Creek and vicinity, eastern Sierra Nevada, California. *Geological Society of America* **121,** 1013-1033.

Porter, S. C., and Denton, G. H. (1967). Chronology of Neoglaciation in the North American Cordillera. *Amer. Jour. of Sci* **265,** 177-210.

Putnam, A. E., Schaefer, J. M., Barrell, D. J. A., Vandergoes, M., Denton, G. H., Kaplan, M. R., Finkel, R. C., Schwartz, R., Goehring, B. M., and Kelley, S. E. (2010). In situ cosmogenic 10Be production-rate calibration from the Southern Alps, New Zealand. *Quaternary Geochronology* **5,** 392-409.

Quillman, U., Marchitto, T. M., Andrews, J. T., Jennings, A. E., and Dean, W. E. (2008). *38th International Arctic Workshop, Abstracts and Programs*.

Rasmussen, T. L., Oppo, D. W., Thomsen, E., and Lehman, S. J. (2003). Deep sea records from the southeast Labrador Sea: Ocean circulation changes and ice-rafting events during the last 160,000 years. *Paleoceanography* **18,** doi:10.1029/2001PA000736.

Rasmussen, T. L., and Thomsen, E. (2004). The role of the North Atlantic Drift in the millennial timescale glacial climate fluctuations. *Palaeogeography Palaeoclimatology Palaeoecology* **210,** 101-116.

Rasmussen, T. L., Thomsen, E., van Weering, T. C. E., and Labeyrie, L. (1996). Rapid changes in surface and deep water conditions at the Faeroe Margin during the last 58,000 years. *Paleoceanography* **11,** 757-772.

Reimer, P. J., Baillie, M. G. L., Bard, E., Bayliss, A., Beck, J. W., Blackwell, P. G., Bronk Ramsey, C., Buck, C. E., Burr, G. S., Edwards, R. L., Friedrich, M., Grootes, P. M., Guilderson, T. P., Hajdas, I., Heaton, T. J., Hogg, A. G., Hughen, K. A., Kaiser, K. F., Kromer, B., McCormac, F. G., Manning, S. W., Reimer, R. W., Richards, D. A., Southon, J. R., Talamo, S., Turney, C. S. M., van der Plicht, J., and Weyhenmeyer, C.E. (2009). INTCAL 09 and MARINE09 radiocarbon age calibration curves, 0-50,000 years Cal BP. *Radiocarbon* **51,** 1111-1150.

Remenda, V. H., Cherry, J. A., and Edwards, T. W. D. (1994). Isotopic composition of old ground water from Lake Agassiz: implications for Late Pleistocene climate. *Science* **266,** 1975-1978.

Richmond, G. M. (1960). Glaciation of the east slope of Rocky Mountain National Park, Colorado. *Geological Society of America Bulletin* **71,** 1371-1382.

Richmond, G. M. (1965). Glaciation of the Rocky Mountains. *In* "The Quaternary of the United States." (H. E. Wright Jr., and D. G. Frey, Eds.). Princeton University Press, Princeton.

Rignot, E., Casassa, G., P., G., Krabill, W., Rivera, A., and Thomas, A. (2004). Accelerated ice discharge from the Antarctic Peninsula following the collapse of Larsen B ice shelf. *Geophysical Research Letters* **31,** doi:10.1029/2004GL020697.

Rignot, E., and Jacobs, S. S. (2002). Rapid bottom melting widespread near Antarctic Ice Sheet grounding lines. *Science* **296,** 220-2023.

Rinterknecht, V. R. (2003). "Cosmogenic 10Be Chronology for the Last Deglaciation of the Southern Scandinavian Ice Sheet." Unpublished Manuscripts thesis, Oregon State University.

Robinson, L. F., Adkins, J. F., Keigwin, L. D., Southon, J., Fernandez, D. P., Wang, S.-L., and Scheirer, D. S. (2005). Radiocarbon variability in the Western Northt Atlantic during the last deglaciation. *Science* **310,** 1469-1473.

Rodrigues, T., Grimalt, J. O., Abrantes, F. G., Flores, J. A., and Lebreiro, S. M. (2009). Holocene interdependences of changes in sea surface temperature, productivity, and fluvial inputs in the Iberian continental shelf (Tagus mud patch).

Geochemistry, Geophysics, and Geosystems **10,** Q07U06, doi:10.1029/2008GC002367.

Rosenberg SM, W. I., Mathewes RW, Hallett DJ. (2004). Midge-inferred Holocene climate history of two subalpine lakes in southern British Columbia. *Holocene* **14,** 258-271.

Rühlemann, C., Mulitza, S., Lohmann, G., Paul, A., Prange, M., and Wefer, G. (2004). Intermediate depth warming in the tropical Atlantic related to weakened thermohaline circulation: Combining paleoclimate data and modeling results for the last deglaciation. *Paleoceanography* **19,** doi:10.1029/2003PA000948.

Ruhlemann, C., Mulitza, S., Muller, P. J., Wefer, G., and Zahn, R. (1999). Warming of the tropical Atlantic Ocean and slowdown of thermohaline circulation during the last deglaciation. *Nature* **402,** 511-514.

Rühlemann, C., Mulitza, S., Muller, P. J., Wefer, G., and Zahn, R. (1999). Warming of the tropical Atlantic Ocean and slowdown of thermohaline circulation during the last deglaciation. *Nature* **402,** 511-514.

Sachs, J. P. (2007). Cooling of Northwest Atlantic slope waters during the Holocene. *Geophysical Research Letters* **34,** L03609, doi:10.1029/2006GL028495.

Sarnthein, M., Gersonde, R., Niebler, S., Pflaumann, U., Spielhagen, R. F., Thiede, J., Wefer, G., and Weinelt, M. (2003). Overview of Glacial Atlantic Ocean Mapping (GLAMAP 2000). *Paleoceanography* **18,** 10.1029/2002PA000769.

Schaefer, J. M., Denton, G. H., Barrell, D. J. A., Ivy-Ochs, S., Kubik, P. W., Andersen, B. G., Phillips, F. M., Lowell, T. V., and Schluchter, C. (2006). Near-

Synchronous Interhemispheric Termination of the Last Glacial Maximum in Mid-Latitudes. *Science* **312,** 1510-1513.

Schaefer, J. M., Denton, G. H., Kaplan, M., Putnam, A., Finkel, R. C., Barrell, D. J. A., Andersen, B. G., Schwartz, R., Mackintosh, A., Chinn, T., and Schluchter, C. (2009). High-frequency Holocene glacier fluctuations in New Zealand differ from the northern signature. *Science* **324,** 622-625.

Schefuß, E., Schouten, S., and Schneider, R. R. (2005). Climatic controls on central African hydrology during the past 20,000 years. *Nature* **437,** 1003-1006.

Schneider, T. (2001). Analysis of incomplete climate data: Estimation of mean values and covariance matrices and imputation of missing values. *Journal of Climate* **14,** 853-871.

Schrag, D. P., Adkins, J. F., McIntyre, K., Alexander, J. L., Hodell, D. A., Charles, C. D., and McManus, J. F. (2002). The oxygen isotopic composition of seawater during the Last Glacial Maximum. *Quaternary Science Reviews* **21,** 331-342.

Seppä, H., and Birks, H. J. B. (2001). July mean temperature and annual precipitation trends during the Holocene in the Fennoscandian tree-line area: pollen-based climate reconstructions. *The Holocene* **11,** 527-539.

Seppä, H., Hammarlund, D., and Antonsson, K. (2005). Low-frequency and high-frequency changes in temperature and effective humidity during the Holocene in south-central Sweden: implications for atmospheric and oceanic forcings of climate. *Climate Dynamics* **25,** 285-297.

Seppä, H., and Weckström, J. (1999). Holocene vegetational and limnological changes in the Fennoscandian tree-line area as documented by pollen and diatom records from Lake Tsuolbmajavri, Finland. *Ecoscience* **6,** 621-635.

Shaffer, G., Olsen, S. M., and Bjerrum, C. J. (2004). Ocean subsurface warming as a mechanism for coupling Dansgaard-Oeschger climate cycles and ice-rafting events. *Geophysical Research Letters* **31,** L24202, doi:10.1029/2004GL020968.

Shakun, J. D., Clark, P. U., He, F., Liu, Z., Otto-Bleisner, B., Marcott, S. A., Mix, A. C., Schmittner, A., and Bard, E. (in review). CO2 forcing of global climate during the last deglaciation.

Shchepetkin, A. F., and McWilliams, J. C. (2003). A method for computing horizontal pressure-gradient force in an oceanic model with a nonaligned vertical coordinate. *Journal of Geophysical Research* **108(C3),** 3090, doi:10.1029/2001JC001047.

Shchepetkin, A. F., and McWilliams, J. C. (2005). The Regional Oceanic Modeling System (ROMS): a split explicit, free-surface, topography-following-coordinate oceanic model. *Ocean Modelling* **9,** 347-404.

Smith, W. H. F., and Sandwell, D. T. (1997). Global sea floor topography from satellite altimetry and ship depth soundings. *Science* **277,** 1956-1962.

Solomon, S., Qin, D., Manning, M., Chen, Z., Marquis, M., Averyt, K. B., Tignor, M., and Miller, H. L. (2007). Contribution of Working Group II to the Fourth Assessment Report of the Intergovernmental Panel on Climate Change, 2007. *In* "Contribution of Working Group II to the Fourth Assessment Report of the Intergovernmental Panel on Climate Change, 2007." Cambridge University Press, New York.

Steinke, S., Kienast, M., Groeneveld, J., Lin, L.-C., Chen, M.-T., and Rendle-Bühring, R. (2008). Proxy dependence of the temporal pattern of deglacial warming in the tropical South China Sea: toward resolving seasonality. *Quaternary Science Review* **27,** 688-700.

Stenni, B., Masson-Delmotte, V., Selmo, E., Oerter, H., Meyer, H., Röthlisberger, R., Jouzel, J., Cattani, O., Falourd, S., Fischer, H., Hoffmann, G., Iacumin, P., Johnsen, S. J., Minster, B., and Udisti, R. (2010). The deuterium excess records of EPICA Dome C and Dronning Maud Land ice cores (East Antarctica). *Quaternary Science Review* **29,** 146-159.

Stone, J. O. (2000). Air pressure and cosmogenic isotope production. *Journal of Geophysical Research* **105,** 23,753 - 23,759.

Stoner, J. S., Channell, J. E. T., Hillaire-Marcel, C., and Kissel, C. (2000). Geomagnetic paleointensity and environmental record from Labrador Sea core MD95-2024: global marine sediment and ice core chronostratigraphy for the last 110 kyr. *Earth and Planetary Science Letters* **183,** 161-177.

Stott, L., Timmerman, A., and Thunell, R. (2007). Southern hemisphere and deep-sea warming led deglacial atmospheric CO2 rise and tropical warming. *Science* **318,** 435-438.

Stuiver, M., and Grootes, P. M. (2000). GISP2 oxygen isotope ratios. *Quaternary Research* **53,** 277-284.

Sun, Y., Oppo, D. W., Xiang, R., Liu, W., and Gao, S. (2005). Last deglaciation in the Okinawa Trough: Subtropical northwest Pacific link to Northern Hemisphere and tropical climate. *Paleoceanography* **20,** PA4005, doi:10.1029/2004PA001061.

Taylor, J. R. (1997). "An Introduction to Error Analysis." University Science Books, Sausalito.

Thornalley, D. J. R., Elderfield, H., and McCave, I. N. (2009). Holocene oscillations in temperature and salinity of the surface subpolar North Atlantic. *Nature* **457**.

Tierney, J. E., Russell, J. M., Huang, Y., Damste, J. S. D., Hopmans, E. C., and Cohen, A. S. (2008). Northern Hemisphere Controls on Tropical Southeast African Climate During the Past 60,000 Years. *Science* **322,** 252-255.

Vinther, B. M., Buchardt, S. L., Clausen, H. B., Dahl-Jensen, D., Johnsen, S. J., Fisher, D. A., Koerner, R. M., Raynaud, D., Lipenkov, V., Andersen, K. K., Blunier, T., Rasmussen, S. O., Steffensen, J. P., and Svensson, A. M. (2009). Holocene thinning of the Greenland ice sheet. *Nature* **461,** 385-388.

von Langen, P. J., Pak, D. K., Spero, H. J., and Lea, D. W. (2005). Effects of temperature on Mg/Ca in neogloboquadrinid shells determined by live culturing. *Geochemistry, Geophysics, and Geosystems* **6,** Q10P03, doi:10.1029/2005GC000989.

von Storch, H., Zorita, E., Jone, J. M., Dimitriev, Y., González-Rouco, F., and Tett, S. F. B. (2004). Reconstructing past climate from noisy data. *Science* **306,** 679-682.

Wagner, J. D. M., Cole, J. E., Beck, J. W., Patchett, P. J., Henderson, G. M., and Barnett, H. R. (2010). Moisture variability in the southwestern United States linked to abrupt glacial climate change. *Nature Geoscience* **3,** 110-113.

Wahl, E. R., and Ammann, C. M. (2007). Robustness of the Mann, Bradley, Hughes reconstruction of Northern Hemisphere surface temperatures: Examination of criticisms based on the nature and processing of proxy climate evidence. *Climate Change* **85,** 33-69.

Wahl, E. R., Ritson, D. M., and Ammann, C. M. (2006). Comment on "Reconstructing Past Climate from Noisy Data". *Science* **312,** 529b.

Waitt, R. B., Yount, J. C., and Davis, P. T. (1982). Regional significance of an early Holocene moraine in Enchantment Lakes Basin, North Cascades Range, Washington. *Quaternary Research* **17,** 191-210.

Walker IR, L. A., Cwynar LC, Lotter AF. (1997). An expanded surface-water palaeotemperature inference model for use with fossil midges from eastern Canada. *Journal of Paleolimnology* **18,** 165-178.

Weijer, J. W. H., Schefuß, E., Schouten, S., and Damste, J. S. D. (2007). Coupled Thermal and Hydrological Evolution of Tropical Africa over the Last Deglaciation. *Science* **315,** 1701-1704.

Weldeab, S., Lea, D. W., Schneider, R. R., and Andersen, N. (2007). 155,000 Years of West African Monsoon and Ocean Thermal Evolution. *Science* **316,** 1303-1307.

Weldeab, S., Schneider, R. R., and Kölling, M. (2006). Deglacial sea surface temperature and salinity increase in the western tropical Atlantic in synchrony with high latitude climate instabilities. *Earth and Planetary Science Letters* **241,** 699-706.

Weldeab, S., Schneider, R. R., Kölling, M., and Wefer, G. (2005). Holocene African droughts relate to eastern equatorial Atlantic cooling. *Geology* **33,** 981-984.

Wesling, J. R. (1988). "Glacial chronology and soil development in Winsor Creek drainage basin, southernmost Sangre de Cristo Mountains." University of New Mexico.

Whitlock, C., and Bartlein, P. J. (1997). Vegetation and climate change in northwest America during the past 125 kyr. *Nature* **388,** 57-61.

WOCE. (2002). World Ocean Circulation Experiment, Global Data, Version 3.0. WOCE International Project Office, Southampton, UK.

Xu, J., Holbourn, A., Kuhnt, W., Jian, Z., and Kawamura, H. (2008). Changes in the thermocline structure of the Indonesian outflow during Terminations I and II. *Earth and Planetary Science Letters* **273,** 152-162.

Yount, J. C., Birkeland, P. W., and Burke, R. M. (1979). Glacial and periglacial deposits of the Mono Creek recesses, west-central Sierra Nevada, California: Measurements of age-dependent properties of deposits. *In* "Field guide to relative dating methods applied to glacial deposits in the third and fourth recesses and along the eastern Sierra Nevada, California, with supplementary notes on other Sierra Nevada localities. Field trip guidebook for the Friends of the Pleistocene, Pacific Cell." (R. M. Burke, and P. W. Birkeland, Eds.).

Yu, J., Elderfield, H., and Pitrowski, A. M. (2008). Seawater carbonate ion-δ13C systematics and application to glacial-interglacial North Atlantic ocean circulation. *Earth and Planetary Science Letters* **271,** 209-220.

Zahn, R., Schönfeld, J., Kudrass, H.-R., Park, M.-H., Erlenkeuser, H., and Grootes, P. M. (1997). Thermohaline instability in the North Atlantic during meltwater events: Stable isotope and ice-rafted detritus records from core SO75-26KL, Portugues margin. *Paleoceanography* **12,** 696-710.

Ziegler, M., Nürnberg, D., Karas, C., Tiedemann, R., and Lourens, L. J. (2008). Persistent summer expansion of the Atlantic Warm Pool during glacial abrupt cold events. *Nature Geoscience* **1,** 601-605.

Zielinski, G. A., and Davis, P. T. (1987). Late Pleistocene age of the type Temple Lake moraine, Wind River range, Wyomong, USA. *Geographie Physique et Quaternaire,* **41,** 397-401.

Zreda, M. G., and Phillips, F. M. (1995). Insights into alpine moraine development from cosmogenic (super 36) Cl buildup dating. *Geomorphology* **14,** 149-156.